The effect of precipitation techniques on bioadhesive microparticle characteristics

A thesis presented in fulfilment of the requirements for the degree of Doctor of Philosophy

by

Issraa Rasheed Abed Al-Rahman Al-Obaidi

2011

University of Strathclyde

UK

Strathclyde Institute of Pharmacy and Biomedical Sciences

Declaration

Dedication

I would like to dedicate this work to my husband Issam, without his love, support and continuous patience; this project would not have been completed successfully.

And to my two kids Dema and Amen

Also to my mother for her love, care and moral encouragement all these years of my Ph.D. study and to my sisters (Asmaa, Thanaa and Wifaq) and brothers (Ahmad and Mohamed Al-amin) for their encouragement

Finally this thesis is dedicated to the memory of my father,
Who did his best for me to spread my experience and pushed me toward the successful life. For all his love, kindness, encouragement and support throughout my life.

Acknowledgement

Many thanks to the following people who helped me during my Ph.D study. It is to them that I owe my deepest appreciation.

Dr Fiona McInnes whose encouragement, supervision and support (as a sister) throughout my study enabled me to develop an understanding in research.

Prof. Howard Stevens whose supervision and experience improved my knowledge.

Anne Goudie and Steve Steer for excellent technical help.

My colleagues; Heba Mansour, Vivekanand Bhardwaj, Mohamed Abdulridha, Yasmine, Manal Al saadi, Michelle Mathie, Jennifer law, Lisa McIntosh, for making SIPBS 218 a great place to work.

My sponsor Iraqi government for the financial support.

Abbreviations

AUC	Area under curve
α-lactose	Alpha lactose
ATR	Attenuated total reflectance
CA	Calcitonin acetate
CP	Cefditoren pivoxil
DCM	Drug coated microcrystal
DSC	Differential scanning calorimetry
DTPA	Diethyl enetriamine penta acetic acid
DVS	Dynamic vapour sorption
D_2O	Deuterium oxide
DS	Dropping method using Silverson mixer
DW	Distilled water
FT/IR	Fourier transform infrared
f_2	Similarity factor
HPC	Hydroxypropyl cellulose
HPMC K100LV	Hydroxypropyl methylcellulose (grade K100LV)
IPA	Isopropyl alcohol
$K_2 SO_4$	Potassium sulphate
LP	Leuprolide
MCC	Mucociliary clearance
M.C.S	Maximum crystal size
MH	Metformin HCl
M.P	Melting point
NMR	Nuclear magnetic resonance
^{1}H-NMR	Proton-Nuclear magnetic resonance
^{13}C-NMR	Carbon-Nuclear magnetic resonance
Na-Diclofenac	Diclofenac sodium
NDM	Non-dropping method using magnetic stirrer
NDS	Non-dropping method using Silverson mixer
PEG	Poly ethylene glycol
PCMC	Protein coated microcrystal
RH	Relative humidity
rpm	Round per minute
SEM	Scanning electron microscopy
Tg	Glass transition temperature
TA	Texture analyser
TGA	Thermo-gravimetric analysis
VH	Verapamil HCl
UV	Ultraviolet spectrophotometry
U and L	Upper and lower layer
XRPD	X-ray powder diffraction

Abstract

A solvent precipitation technique was developed for preparing bioadhesive HPMC microparticles for nasal delivery. Aqueous gels of lactose:HPMC (1:1) were used as a model formulation, added to a precipitating solvent, and the effect of processing parameters such as stirring speed (1000-2000 rpm), needle gauge (19g, 21g and 23g), and dropping rate (5 ml/hour and 10 ml /hour) were studied. The optimal particle size required for nasal delivery (less than 100 μm) was obtained using a stirring speed of 8000 rpm, a temperature of 4°C, a dropping rate of 10 ml/ hour, using a 23g needle.

Verapamil hydrochloride (VH) and metformin hydrochloride (MH) were investigated as model drugs using the optimised processes. The resultant VH:HPMC (1:1) microparticles achieved a maximum drug loading of only 8.7%, and precipitation of MH:HPMC microparticles in IPA achieved a similar loading. However, MH:HPMC microparticles with a drug loading of 45-53% were obtained with precipitation in acetone. This correlated with the relative solubilities of MH in IPA and acetone.

In-vitro assessment of adhesion properties of the microparticles showed that the process of precipitation greatly increased the adhesiveness in comparison with HPMC powder alone, due to the formation of a continuous HPMC matrix. MH:HPMC (1:1) microparticles precipitated in acetone provided the optimal combination of adhesive properties and sustained release of drug, and the reasons for this were further investigated using microparticles precipitated from HPMC alone.

Bioadhesive performance was found to be dependent on the dehydrated state of the polymer following precipitation, with the most dehydrated formulations showing greater adhesive performance. Dehydration of the aqueous gel was found to be most efficient when the gel was added dropwise to highly agitated acetone.

The optimal MH:HPMC (1:1) microparticle formulation was found to be stable following storage under stressed conditions, as a result of dehydration during the precipitation technique.

Publications

- Aqueous-organic microparticle precipitation method resulting in polymorphism of α-lactose monohydrate, Journal of Pharmacy and Pharmacology, volume 62, Number 10, 2010.

- Sustained release HPMC microparticles for nasal delivery, prepared by a co-precipitation technique**,** Journal of Pharmacy and Pharmacology, volume 62, Number 10, 2010.

- Aqueous-organic microparticle precipitation method resulting in polymorphism of α-lactose monohydrate, AAPS Annual Meeting and Exposition, November 14-18, 2010 in New Orleans, LA.

- Sustained release HPMC microparticles for nasal delivery, prepared by a co-precipitation technique, AAPS Annual Meeting and Exposition, November 14-18, 2010 in New Orleans, LA.

- Sustained release from HPMC/metformin microparticles for nasal delivery, manufactured using an aqueous-organic precipitation technique, PharmSciFair 2011, 13-17 June in Prague, Czech Republic.

- Two different organic solvents to produce sustained release HPMC microparticles for nasal delivery using co-precipitation technique, PharmSciFair 2011, 13-17 June in Prague, Czech Republic.

Table of Contents

Chapter 1

General introduction

1.0 Introduction

There are many drugs which cannot be administered orally due to metabolism by enzymatic activity or degradation in stomach acid, while other drugs suffer from extensive hepatic first pass metabolism. Absorption via the nasal route is directly to systemic circulation, has low enzymatic activity, high blood perfusion and a large surface area for drug absorption (Lansley & Martin 2001), and thus offers a viable alternative to the oral route. The main drawback of this route is the mucociliary clearance (MCC) that clears the drug from the nasal cavity within 21 minutes (Arora et al 2002). Most commercially available nasal formulations are in the form of sprays or drops, which will suffer from this rapid clearance from the nose. Bioadhesive polymers may be a solution to this problem, by increasing the contact time between formulation and nasal mucosa and decreasing the MCC.

This chapter describes the anatomy of the nasal cavity, advantages and disadvantages of the route, factors which are important in nasal absorption and bioadhesion, and methods which have been utilised to study adhesive formulations.

1.1 The nasal route

The nasal cavity is considered to be an attractive route of systemic drug absorption because of its considerable surface area of approximately 160 cm^2 (Lansley & Martin 2001), which is large due to the presence of numerous microvilli (Arora et al 2002). A high rate of blood perfusion provides rapid absorption to the systemic circulation and subsequent onset of action. Also, the low metabolic activity of nasal cavity in comparison to the gastrointestinal tract makes this route an attractive option for delivery of protein and peptide compounds (Lansley & Martin 2001). As a

consequence of these benefits, drugs administered nasally may often be administered in a lower dose than orally, with a resultant reduction in the extent of side effects (Vyas et al 2006).

Other researchers have suggested that the olfactory region of the nose can be used to bypass the blood brain barrier, reducing the therapeutic dose required in order to treat conditions such as Parkinson's and Alzheimer's diseases, and thereby minimising the side effects of such treatments (Kao et al 2000).

1.2 Nasal anatomy

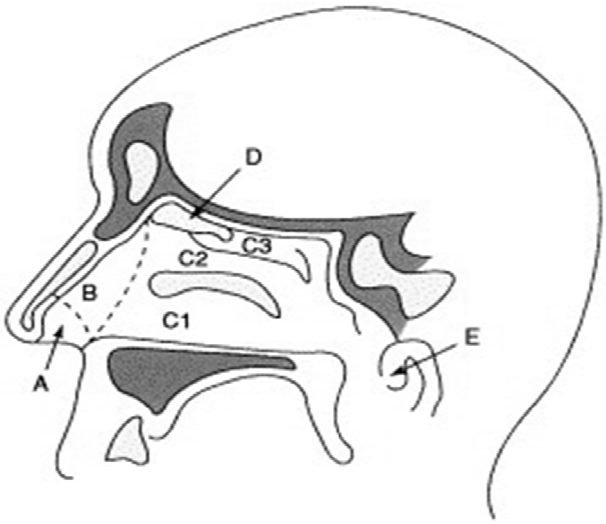

The nasal vestibule (a),
Atrium (b),
Respiratory region:
Inferior turbinate (c1),
Middle turbinate (c2)
Superior turbinate (c3),
The olfactory region (d)
Nasopharynx (e)

Figure 1.1 Schematic of a sagittal section of human nose, reproduced from Ugwoke et al (2001).

The nasal cavity consists of two symmetrical sides which are separated by the nasal septum and extend posteriorly to the nasopharynx. The nasal passage, which runs from the nasal vestibule, to the nasopharynx, has a length of approximately 12-14cm (Chien 1992), and is shown in Figure 1.1. The most anterior part of the nasal cavity,

the nasal vestibule, opens to the face through the nostrils (Ugwoke et al 2005). This vestibule is rich with hairs (vibrissae), and the mucosa is composed of stratified squamous and keratinized epithelium, with sebaceous glands. Due to this nature, it is very resistant to dehydration, can resist noxious environmental substances and limits the permeation of substances (Arora et al 2002; Ugwoke et al 2005).

The atrium is an intermediate region between the vestibule and the respiratory region. It is the narrowest region of the nasal cavity. It consists of a transitional epithelial cell, with stratified squamous cells anteriorly and pseudo-stratified columnar cells with microvilli posteriorly. It is poorly permeable as it has a small surface area and as a result of the stratified cells which are present anteriorly (Arora et al 2002; Wermeling & Miller 2003).

The respiratory region, which includes the nasal turbinates, occupies the major part of the nasal cavity. It divides it into three sections comprising the superior nasal turbinate at the top, the middle nasal turbinate, and the inferior turbinate. These folds provide the nasal cavity with a very high surface area compared with its small volume (Ugwoke et al 2001).

The presence of the turbinates creates a turbulent airflow through the nasal passages which ensures a better contact between the inhaled air and the mucosal surface (Illum 2003), and plays an important role in the humidification and temperature regulation of inspired air, a primary function of the human nose. Figure 1.2 shows the general structure of the pseudo-stratified nasal mucosa in the respiratory region.

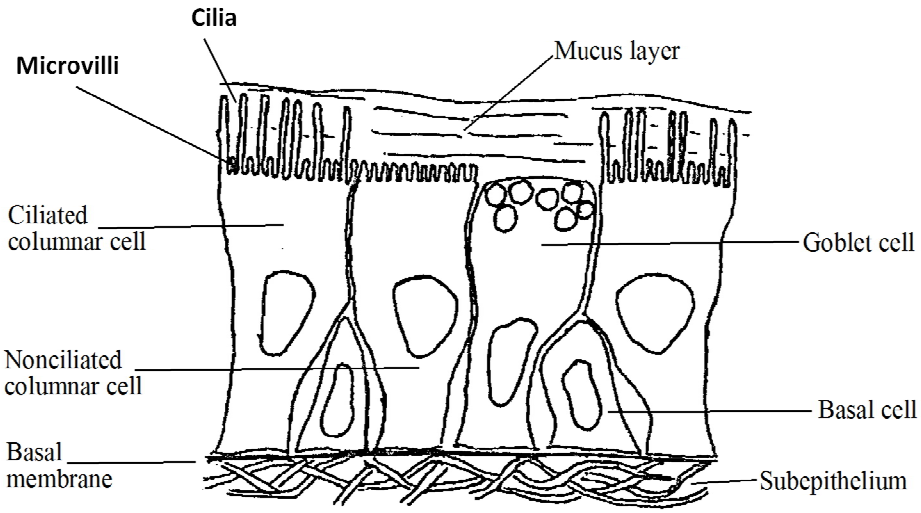

Figure 1.2 Respiratory regions (nasal turbinate mucosa), modified from Mathison et al (1998).

Columnar epithelial cells interspersed with goblet cells, seromucus ducts, and the openings of sub-epithelial seromucus glands cover the respiratory region (the turbinates), resulting in this region producing more nasal secretions than other areas (Arora et al 2002). Furthermore, many of these cells possess actively beating cilia with microvilli. Each ciliated cell contains about 100 cilia, while both ciliated and non-ciliated cells possess about 300 microvilli each (Ugwoke et al 2005).

The olfactory region is situated above the superior nasal turbinate (Figure 1.1), and possesses specialised ciliated olfactory nerve cells for smell perception.

The last part of nasal cavity is the nasopharynx, it consists of two types of cells; pseudo-stratified columnar epithelium in the upper part and stratified squamous cells in the lower part. The nasal cavity drains to this area.

1.2.1 Nervous system of nasal cavity

The autonomic nervous system controls the blood supply and secretions of the nose through α-adrenergic control. Thus, it provides the blood required for heating and humidification of inspired air (Ugwoke et al 2001).

1.2.2 Nasal secretion and the mucous layer

The sub-mucosal glands secrete high quantities of nasal mucus. These glands consist of mucus cells secreting the mucus gel, and serous cells producing a watery fluid. Seromucus glands in the human nose have been estimated to number 100,000 (Tos 1983). Mucus secretion is a complex mixture of many substances and consists of about 95% water, 2% mucin, 1% salts, 1% of other proteins such as albumin, immunoglobulin, lysozyme and lactoferrin, and <1% lipids (Kaliner et al 1984).

This mucus layer, which is approximately 5 μm thick, is made of two layers, a lower sol layer (periciliary layer) and an upper gel layer (Hinchcliffe & Illum 1999; Ugwoke et al 2001). The low viscosity periciliary layer is formed by epithelial cell exudates as it is immediately adjacent to the epithelial surface. The gel layer is secreted by goblet cells, and contains mucins, which are glycoproteins of high molecular mass (2000-4000 Kilo Daltons) (Marttin et al 1998; Ugwoke et al 2001).

The nasal mucus has many benefits; it protects the nasal mucosa, has water-holding capacity, exhibits surface electrical activity, acts as adhesive and transports particulate matter towards the nasopharynx (Ugwoke et al 2005).

1.3 Nasal absorption

There are many physiological and formulation factors that can affect nasal absorption, such as pH, molecular weight, drug solubility and administration device. Another factor may be the enzymatic degradation of drugs particularly peptides and proteins within the lumen of the nasal cavity or across the epithelial barrier, although

the activity here is much lower than that of the gut (Hussain et al 1985; Jorgensen & Bechgaard 1994).

A drug can be absorbed systemically by crossing the epithelial membrane via one or a combination of the pathways shown in Figure 1.3; the transcellular route, the paracellular route, carrier-mediated transport, absorption through transcytosis and intercellular tight junction. Transcellular passive diffusion is especially suited for small lipophilic molecules, while the paracellular pathway is suitable for small hydrophilic molecules (Ugwoke et al 2001; Illum 2003).

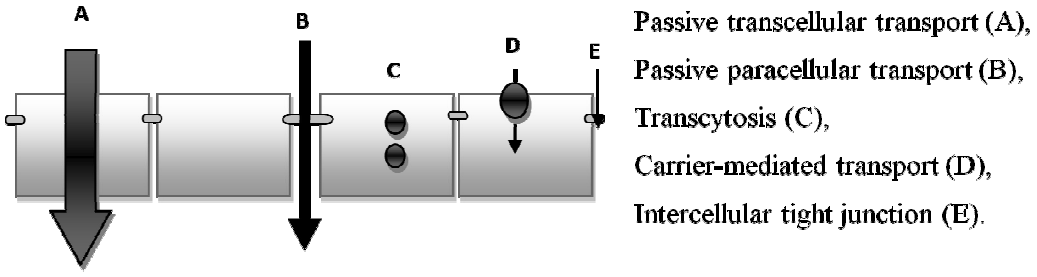

Figure 1.3 Drug transport pathways across the epithelium, modified from Ugwoke et al (2001).

1.3.1 Hydrophilicity/lipophilicity

Most hydrophilic drugs (molecular weight <1000 Daltons) are able to penetrate the nasal epithelium, through the aqueous channels of the membrane (Jadhav et al 2007), while large hydrophilic molecules such as peptides and proteins achieve poor bioavailability of less than 10% and 5% respectively (Illum 2003). As molecular weight increases, absorption via aqueous channels in the nasal mucosa decreases.

Lipophilic drugs are generally well absorbed from the nasal cavity via the transcellular route due to the partition coefficient facilitating partitioning into the lipid cell membrane, with the bioavailability often matching that obtained following

intravenous injection (Thomas & Ahsan 2008). For example, nasal administration of fentanyl and propranolol can achieve up to 80% and 100% bioavailability respectively by crossing the biological membranes via the transcellular route (Hussain et al 1980; Striebel et al 1993).

1.3.2 Effect of pH

According to the pH partition theory, an ionised drug is absorbed through the nasal mucosa to a lower extent than the unionised species. The nasal absorption of weak electrolytes was found to be highly dependent on their degree of ionisation (Hirai et al 1981). The absorption rate of aminopyrine increases in alkaline pH when the unionised form is predominant (Hirai et al 1981), also scopolamine, a basic drug with a pKa of 7.6 (Lattin & Fifer 2002), showed dramatically increased plasma concentrations with an increase in the pH of a nasal formulation (Ahmed et al 2000).

1.3.3 Osmolarity

Ohwaki and co-authors reported that maximum absorption of secretin in rats was achieved at a sodium chloride concentration of 0.462 M, because of shrinkage of the nasal epithelial mucosa at that salt concentration (Ohwaki et al 1987). On the other hand, a hypo-osmotic insulin mucoadhesive gel delivered nasally in rats produced a pronounced decrease in plasma glucose levels in comparison with a hyper or iso-tonic gel (Pereswetoff & Edman 1995).

1.3.4 Polymorphism

Dissolution rate and solubility of drugs, and consequently their absorption through biological membranes, are affected by polymorphism. As a result, it has been reported that it is desirable to ensure the polymorphic stability and purity of drugs for nasal powders and/or suspensions (Jadhav et al 2007).

1.3.5 Biochemical metabolism

Nasal administration of drugs avoids hepatic first pass metabolism, but the nasal mucosa still acts as an enzymatic barrier to the delivery of many drugs. This type of metabolism is called pseudo first pass metabolism (Arora et al 2002). Cytochrome P450 can oxidize many nasal decongestants and anaesthetics (Sarkar 1992), and insulin, calcitonin and other peptide drugs are degraded by peptidase and protease enzymes (Lansley & Martin 2001). Enzymatic activity can be locally inhibited to improve the bioavailability of drugs that are subject to enzymatic degradation. This has been established for some mucoadhesive polymers such as carbopol 934P and polycarbophil that inhibit the proteolytic enzyme trypsin, which can thus increase the stability of co-administered peptides (Luessen et al 1994).

1.3.6 Mucociliary clearance

Mucociliary clearance (MCC) is a defence mechanism of the nasal cavity that clears mucous and substances adhering to the nasal mucosa (bacteria, allergens, viruses, toxins etc.), and drains them into the nasopharynx for eventual discharge into the gastrointestinal tract. Whenever a drug is nasally administered, it is cleared from the nasal cavity in approximately 21 min by MCC (Marttin et al 1998; Arora et al 2002). Particles can become trapped within the upper gel layer of the nasal mucous. The tips of the cilia on the mucosal surface contact the bottom of this gel layer, and during the process of MCC they propel the gel layer towards the nasopharynx, where the particles are swallowed for destruction in the gastrointestinal tract. The lower sol layer remains stationary during this process, and allows the cilia to return to their original position following a full beat (Marttin et al 1998; Hinchcliffe & Illum 1999). The cilia propel the mucus at a beat frequency of about 10 Hz towards the nasopharynx. The mucus turnover is about 15-30 min (Hinchcliffe & Illum 1999). Wermeling and Miller reported that a cilia beat frequency of approximately 10-13 Hz results in the movement of mucus at a rate of approximately 5-6 mm/min, and therefore clearance of particles from the nose within 20 minutes (Wermeling & Miller 2003).

The extent of the effect of MCC on drug absorption may vary depending on the site of drug deposition. Ciliated epithelium is present in the middle and posterior parts of the turbinates, while in the anterior region of the nasal cavity, there is little or no ciliary epithelium. Therefore a drug deposited in the posterior part of the nose is cleared faster than a drug deposited in the anterior site of the nasal cavity (Thomas & Ahsan 2008).

1.4 Bioadhesion

Bioadhesion is an expression used for sticking a substrate to a biological tissue, while mucoadhesion described the process of attaching to the mucous layer of a tissue (Wermeling & Miller 2003; Keely et al 2005). Bioadhesive polymers are used to overcome the rapid mucociliary clearance of drug formulations from nasal cavity by increasing the time of adhesion to the nasal mucosa. In this process, firstly the bioadhesive agent and membrane (mucus layer) are required to come in contact with each other, and subsequently the chains of the adhesive agent penetrate into the mucosal chains (glycoprotein network of mucosal mucin). This reduces the rate of clearance of the formulation by the MCC, with a resultant increase in the residence time within the nasal cavity, and consequently enhancement of drug absorption and duration of action (Wermeling & Miller 2003). The adhesion of polymers is affected by one or combination of different factors, such as polymer related factors and environmental related factors (Ugwoke et al 2005).

1.4.1 Polymer molecular weight

The adhesion of polymer to nasal mucosa can be affected by its molecular mass. Smart and co-authors reported that the bioadhesion of sodium carboxy methylcellulose produced at 78600 Daltons and can be increased by increasing the molecular weight (Smart et al 1984). On the other hand, some polymers have a specific molecular weight designed to produce optimal bio- or mucoadhesion, above that they will lose this phenomenon or remain the same.

This work was reported by Ugwoke and co-authors, they found that the bioadhesive power of dextran with molecular weights of 19,500,000 Daltons produced similar bioadhesive strength to those with a molecular weight of 200,000 Daltons such as polyethylene glycol (PEG), suggesting that the helical structure of dextran shielded some moieties of the polymer that required for entanglement and adhesion with mucus layer in comparison to the linear structure of PEG (Ugwoke et al 2001). The bioadhesiveness of polyethylene oxide increased with an increase in molecular weight up to 4000 000 Daltons (Ugwoke et al 2001). It is suggested that the length of free chain is important to increase the bioadhesion. So the linear structure of polymer results in prolonged binding of polymer to the biological surface (Dondeti et al 1996; Ugwoke et al 2001).

1.4.2 Hydration and swelling

Bioadhesive polymers such as cellulose derivatives, carbopol, starch, gelatine, pectin, chitosan, poloxamer, PVP, sodium alginate, carrageenan and xanthan gum, all have differing ability to absorb water and swell, as the rate and extent of water uptake depends on the type and number of hydrophilic functional groups present in the polymer structure (Dondeti et al 1996). The mechanism involves the attachment of a dry polymer to the wet mucus (Andrews et al 2009), following which water transfers to swell the polymer and allow flexibility and movement of the polymers chains, and subsequent interaction with the mucin chains on the surface of the tissue. The penetration of water into the polymer structure will loosen the cross linked chains, producing a flexible and relaxed polymer that easily binds and penetrates the mucosa. The more rapidly the polymer is hydrated, the more rapid the onset of this process of diffusion and formation of bonds at the interface will be, and consequently faster initiation of the bioadhesion process will take place. However, excessive hydration or swelling can be detrimental to performance, and lead to a decrease in the bioadhesion (Mortazavi & Smart 1993; Dondeti et al 1996).

Mucoadhesive strength has been found to decrease with an increase in density of cross-linking within the polymer. This is thought to be a result of a decrease in the

flexibility and mobility of the polymer chain, reducing its ability to diffuse or penetrate into the nasal mucosa (Park & Robinson 1987).

1.4.3 Bonding

A strong interaction of hydrophilic polymer with nasal mucin is created due to hydrogen bond forming groups as hydroxyl and carboxyl moieties. The adhesion of a polymer to a biological tissue is strongly dependant on secondary chemical bonds such as Vander Waals, hydrogen, hydrophilic and electrostatic forces (Robinson et al 1987).

1.4.4 Viscosity

Increasing the viscosity of a bioadhesive polymer has been shown to increase the contact time between the drug and the nasal mucosa thereby increasing the time for permeation (Jadhav et al 2007) . However, increasing the viscosity of formulation will decrease the penetration rate of the drug into the mucus, and may influence the surface area over which the drug can spread on the nasal mucosa for absorption (Zaki et al 2006; Furubayashi et al 2007; McInnes et al 2007b).

It was found that high viscosities decrease bioadhesion as a result of a decrease in the mobility of polymer chain, and consequently less interpenetration of the polymer with the glycoprotein network of mucosal mucin (Dondeti et al 1996). McInnes and co-workers found that the preparation of a lyophilised nasal insert of insulin with 2% HPMC achieved extended nasal residence *in-vivo*, indicating an optimum combination of rapid adhesion without over hydration, while higher concentrations of 3% HPMC showed no spreading and was usually cleared from nasal mucosa within 90 min by mucociliary clearance (McInnes et al 2007b).

1.4.5 Physiological factors

With time, mucus production reduces the mucoadhesion bond strength, allowing the upturn of MCC to normal clearance rates and removing the formulation from its adhesion site. Pathological conditions of upper respiratory tract such as asthma, deviation of nasal septum, allergic rhinitis, common cold and chronic sinusitis can all affect bioadhesion due to their effect on MCC rate, ciliary beating and/or mucus rheology (Wanner et al 1996; Houtmeyers et al 1999). Such diseases that increase the MCC rate will reduce the contact time of the drug with the absorptive nasal mucosa. Nasal hyper-secretion also dilutes a nasally administered drug solution, leading to reduce concentration gradient, with a possible influence on absorption (Ugwoke et al 2001).

1.5 Bioadhesive polymers and formulations

Hydroxypropyl methylcellulose (HPMC) is a non-ionic cellulose ether polymer. The hydration rate of HPMC depends on the nature of the constituents, such as the molecular structure and the degree of substitution (hydroxypropoxyl and methoxyl). Particularly, the hydration rate of HPMC increases with an increase in the hydroxypropoxyl content. The viscosity of HPMC aqueous solution can be increased by increasing its average molecular weight (MW) or concentration (Rowe et al 2003a).

HPMC is widely used in pharmaceutical formulations. Its use in the oral field has been extensively studied. Melia and co-workers studied the behaviour of the HPMC gel layer, more accurately described as a hydrated gelatinous entangled polymer chain network, using confocal fluorescence microscopy (Pygall et al 2008). The earliest images revealed an initial phase of water entrance into the tablet pore network, followed by the progressive formation of a coherent gel layer by outward columnar swelling and coalescence of hydrated HPMC particles within a few minutes. The slowing of gel layer growth within 1 to 2 min, suggests the rapid development of an effective diffusion barrier that inhibited water ingress (Pygall et al

2009; Williams et al 2009). Earlier studies by Rajabi-Siahboomin used NMR to investigate the hydration processes of different grades of HPMC as part of a tablet formulation (Rajabi-Siahboomi et al 1996).

The same group studied drug release kinetics in hydrophilic HPMC matrices by incorporating pH modifying agents, as well as soluble and insoluble excipients in the matrix. The inclusion of sodium citrate in HPMC E4M and K4M matrix tablets accelerated the release of the weak acid model drug, felbinac. They suggested that citrate salt may produce an osmotic effect (hofmeister effect) promoting the interaction of HPMC with water. Therefore, in addition to altering drug solubility, a buffering agent may also influence polymer swelling, dissolution and the structure of the hydrated polymer network, which are key factors in HPMC matrix gel layer retardation of drug release (Pygall et al 2009). HPMC preparations containing a high concentration of soluble sugar (lactose) enhanced the rate of growth of hydrated layer whereas a water insoluble excipient, such as microcrystalline cellulose resulted in disruption of the hydrated layer and disintegration of the underlying matrix (Pygall et al 2008).

Ghimire and co-workers studied the effect of HPMC concentration on the *in-vitro* erosion profile of matrix tablets. HPMC tablets with a concentration of 20% (w/w) HPMC showed faster erosion profile than those containing 40% (w/w) HPMC. The higher HPMC concentration afforded greater strength to the gel layer that formed upon hydration. This made the gel layer more resistant to dilution as well as to erosion *in-vivo* (Ghimire et al 2010).

HPMC has also been proposed as a bioadhesive polymer for nasal delivery systems to overcome MCC (Dyvik & Graffner 1992). In 1988, Pennington and co-workers administered three concentrations of HPMC nasal spray solutions with a viscosity of 36, 120 and 430 $mm^2.s^{-1}$ to eight healthy subjects. The clearance rates decreased with increasing solution viscosity, the half-times being 1.0, 1.7 and 2.2 h respectively (Pennington et al 1988).

McInnes and co-workers formulated HPMC as a bioadhesive nasal insert in a concentration of 2% to prolong the nasal mucosal absorption of nicotine in sheep by

increasing its residence time in nose for 2-3 hours and decreasing MCC (McInnes et al 2000). HPMC was formulated with insulin as a nasal gel to prolong the contact time between insulin and the absorptive sites in the nasal cavity, and was found to directly enhance the absorption through the nasal mucosa (Souza et al 2005). A similar result was obtained by Kuotsu & Bandyopadhyay (2007) with oxytocin using the same polymer.

Bertram and Bodmeier (2006) later prepared in situ gelling bioadhesive nasal inserts using different hydrophilic polymers (carrageenan, Carbopol, chitosan, HPMC K15M and E5, sodium alginate, sodium carboxymethyl cellulose, polyvinyl pyrrolidone 90, and xanthan gum) to extend the *in-vitro* release of oxymetazoline HCl. The drug release decreased with increasing polymer content and increased drug loading of the insert.

Another study reported the preparation of a nasal spray of a dried powder mixture of bioadhesive polymers such as starch and carbopol 974P with insulin for lowering glucose blood levels. This formulation was tested in rabbits, and it was found that a single administration of insulin in the dry powder bioadhesive formulations produced a highly viscous bioadhesive in the nasal cavity, as a consequence of hydration in contact with mucosa and resultant reduction in mucociliary clearance (Callens et al 2003). Conversely, McInnes et al (2007b) found that following administration of insulin containing HPMC nasal insert formulations in man, no appreciable absorption was detected.

Suzuki and Makino evaluated nasal powder formulations of leuprolide (LP) and calcitonin acetate (CA) peptides using hydroxypropyl cellulose (HPC) in rabbits. The highest plasma concentration of LP and CA was obtained at concentrations of 25% and 10-20% of hydroxypropyl cellulose respectively. They suggested these results were a result of HPC polymer increasing the retention of drugs on the nasal mucosa due to its gel-forming property (Suzuki & Makino 1999).

Shahiwala and co-workers studied the *in-vivo* bioavailability of levonorgestrel administered nasally in rats using unformulated drug and mucoadhesive formulations. Mucoadhesive agents such as chitosan and carpobol 934P produced a

threefold increase in the drug bioavailability from 29.93% to 101.70% and 99.42%, with a significantly improved plasma half life from 7.0 hours to 55.7 hours and 52.9 hours, respectively. Pharmacokinetic studies indicated that the dosing interval can be reduced to once every 2 days without changing the dose (0.5%) (Shahiwala & Misra 2004).

1.6 *In-vitro* measurement of bioadhesion

Many researchers have reported *in-vitro* methods to assess the bioadhesion and clearance of polymer from an artificial nasal mucosa.

1.6.1 Polymer platform attachment

The device consists of a glass plate which is loaded with the polymer and suspended from a microbalance (Figure 1.4). The polymer-coated plate was then slowly dipped into a beaker of mucus surrounded by a water bath to keep constant body temperature (37°C). The work requires to detach the various polymer-coated glass slides from the mucus media and then be related to one another to compare their adhesiveness (Smart et al 1984).

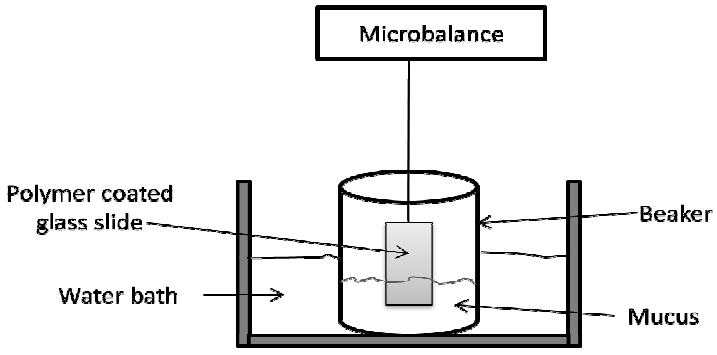

Figure 1.4 *In-vitro* bioadhesive measurement using polymer coated glass slide immersed in mucus medium, modified from Smart et al (1984).

1.6.2 Shear stress measurement

The shear stress measures the force required for a bioadhesive polymer to slide with respect to the mucus layer in a direction parallel to their plane of contact (Kamath & Park 1994). The equipment consists of two coated glass slides with polymer and a film of mucus. Mucus forms a thin film between the two polymer coated slides, and the test measures the force required to separate the two surfaces.

1.6.3 Agar plate-disintegration apparatus

Nakamura and co-authors used an agar plate of 7 cm in diameter (1.5% w/v), onto which the sample was sprayed from a distance of 5 cm. After 5 minutes, the plate was connected to a disintegration apparatus and moved up and down in phosphate buffer pH 7.2 at 37°C (Figure 1.5). The residence time of the sample to the agar was observed by eye (Nakamura et al 1996).

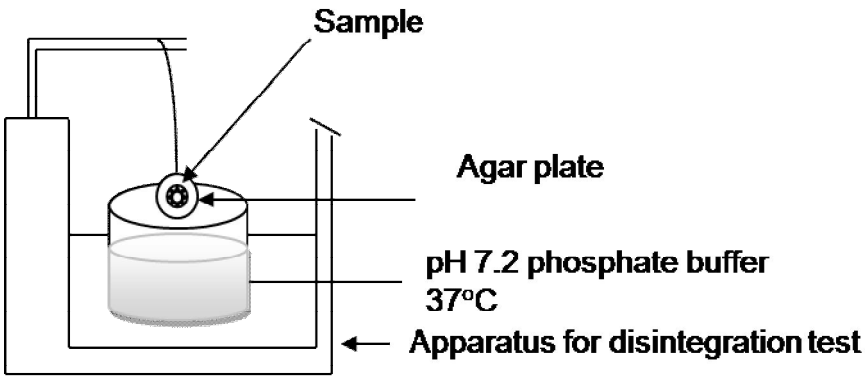

Figure 1.5 Apparatus used for measurement of residence time of polymers, modified from Nakamura et al (1996).

1.6.4 Mucin-agar plate

A tilted agar plate method was developed by McInnes et al (2001), and was later modified by Bertram and Bodmeier (2006), who prepared a plate containing 100g of a 1% agar-2% mucin solution in phosphate buffer pH 6.0. The dynamic adhesion of nasal inserts was tested by locating them on the top of the surface of the mucin-agar plate. Then the plate was then tilted vertically to allow the nasal formulations to move downwards across the plate as a result of gravity. The distance travelled by samples in cm as a function of time was measured.

McInnes and co-workers studied the adhesion dynamic of 1%, 2% and 3% HPMC lyophilised discs using agar plates as shown in Figure 1.6 (McInnes et al 2001).

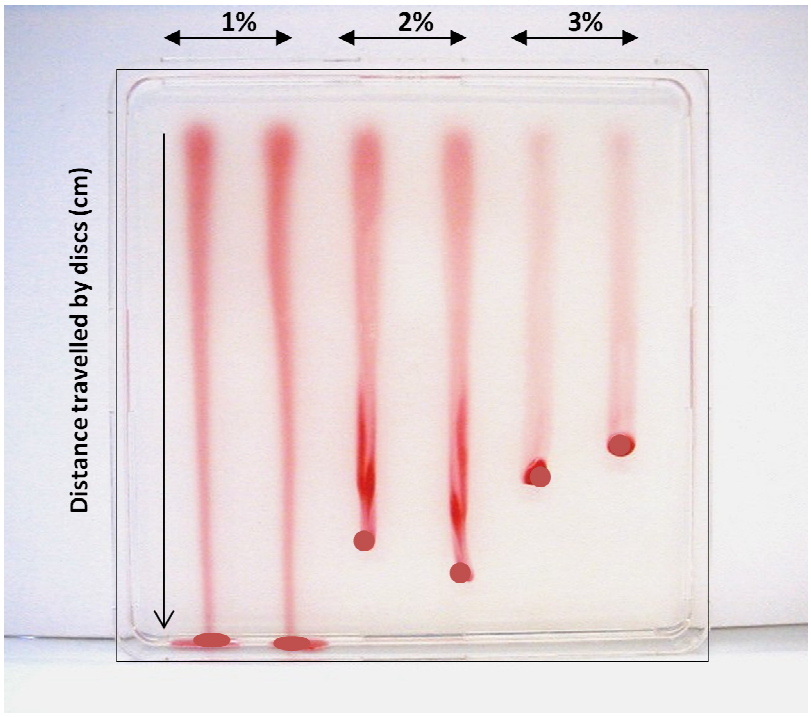

Figure 1.6 Dynamic adhesion of different concentrations of lyophilised HPMC discs (1%-3%), using agar method, modified from McInnes et al (2001).

The lyophilised discs were stained with red dye for clarity. As the concentration of HPMC increases, its dynamic adhesion increases as a result of increasing the viscosity of in situ gel formulations.

1.6.5 Texture analyser

The texture analyser (TA) can be used to measure the force required to detach a formulation from a biological or artificial tissue through breaking the adhesion bond between substrate and tested formulation (Jones et al 1997). The technique involves attaching the substance to the end of the TA probe, which is then lowered at a defined rate until the tested substance contacts the surface of adhesion media. The probe then holds this substance with a defined force, for a defined period of time, and at a set rate, measuring the force required to do that. McInnes and co-workers proposed a new method for the measurement of adhesion force as shown in Figure 1.7. The device was designed to hydrate lyophilised HPMC K4MP discs and form an adhesive gel on the surface of the agar, while the remaining portion would be rigid enough to enable the formulation to be pulled along the surface of the agar, mimicking movement on the nasal surface, and allowing the TA probe to measure the force required to do this (McInnes et al 2007a).

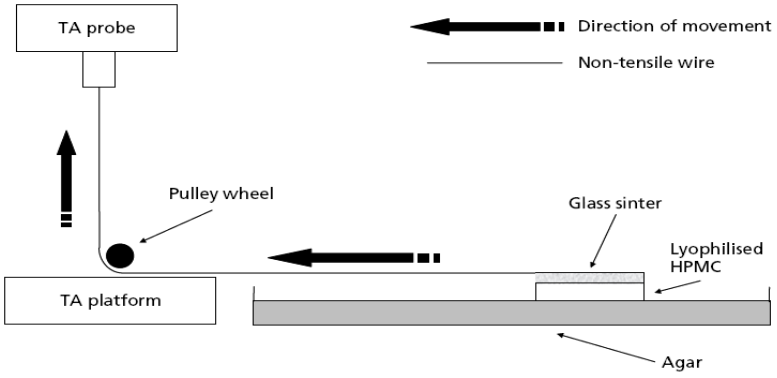

Figure 1.7 Mechanism of sliding test using texture analyser, reproduced from McInnes et al (2007a).

1.7 *In-vivo* measurement of bioadhesion

The technique of gamma scintigraphy has been used to study the intensity and nasal distribution after administration of radiolabelled formulations, allowing the deposition and residence time to be investigated (Illum et al 1987; Pennington et al 1988; McInnes et al 2007b).

Figure 1.8 shows a schematic diagram of gamma-scintigraphy camera. Gamma emission from the source is filtered by a parallel-hole collimator, and then absorbed by sodium iodide crystals. This stimulates the release of photons with distinctive wavelengths which are detected by photomultiplier tubes and converted to an electronic image (Pennington et al 1988).

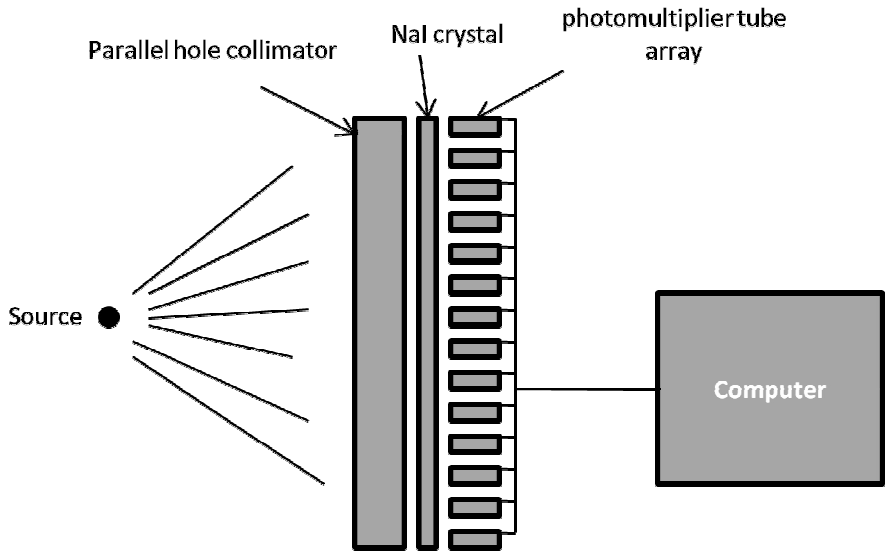

Figure 1.8 Schematic diagram of gamma-camera, modified from Webb et al (2002). Gamma radiation is emitted from the source, filtered by the collimator, absorbed by NaI crystals which release photons. Photomultiplier tubes detect these emissions and convert to an electronic image.

In a study reported by Pennington and co-authors, HPMC nasal spray solutions were radio-labelled with technetium-99m DTPA and given to healthy subjects. The sites of deposition and the rates of clearance from the nasal cavity were monitored using a gamma camera (Pennington et al 1988).

Illum and co-authors investigated the clearance of the technetium-99m labelled microsphere systems from the nasal cavity of human volunteers as compared to nasal powder and nasal spray systems, using gamma scintigraphy (Illum et al 1987). Also McInnes et al (2007a) reported the clearance of a nasal insert from the nasal cavity of volunteers using gamma scintigraphy.

1.8 Particulate drug delivery systems

Particulates have been used for many routes of administration such as oral (Remunan-Lopez et al 1998; Takka & Acarturk 1999; Greimel et al 2007; Zhang et al 2011), pulmonary (Fu et al 2002; Amidi et al 2007; Sivadas et al 2008), parenteral (Huo et al 2005; Harsha et al 2009) and nasal (Illum et al 1987; Lim et al 2002; Leitner et al 2004; Krauland et al 2006).

Particle size and shape are important factors that play an essential role in controlling nasal drug absorption and bioavailability, as when administered nasally, different sizes of particle will deposit in a different part of the respiratory tract. Droplets or particles with a size of <10 μm will be deposited in the upper respiratory tract, while those <0.5 μm will be exhaled (Arora et al 2002). In the nasal cavity, a particle size of greater than 50 μm has been shown to provide a favourable pattern of distribution in the nose (Wermeling & Miller 2003).

Linked to the advantages of bioadhesive polymers, controlled release particle formulations have been studied throughout the literature as a method to produce bioadhesive particulate drug delivery systems such as microparticles, with the aim of prolonging the contact of drug particles with the nasal mucosa and facilitating absorption.

1.8.1 Microparticulate drug delivery systems

Microparticles are attractive as carriers for sustained, systemic and localised release of drug molecules (Hou et al 2008), to adjust the drug concentration released with time in the nasal cavity, enhancing the therapeutic efficacy of the compound (Siepmann & Siepmann 2006). Many physical and chemical variables can be involved in the control of drug release, and it is therefore important to optimise the design of the system with respect to composition, dimensions, and preparation procedure (Siepmann & Siepmann 2006). The drug can be dissolved in the polymer matrix in form of a solid solution, suspended in the form of a solid dispersion, or may be adsorbed to the particle surface (Zimmer & Kreuter 1995).

1.8.1.1 Microspheres /microcapsules

Microspheres and microcapsules can control drug release kinetics through control of the shape and size of the particles. Microspheres are small solid particulate carriers containing dispersed drug particles either in solution or crystalline form (Dandagi et al 2006). Microparticles have been manufactured from natural and synthetic polymers such as albumin, gelatine, starch, ethyl cellulose, polylactic acid, poly cyanoacrylate and poly hydroxybutyrate (Dandagi et al 2006).

Microcapsules differ from microspheres in having a barrier membrane surrounding a solid or liquid core (Jain 2008). Microencapsulation methods involve solvent evaporation/ extraction, phase separation (coacervation), spray drying, ionotropic gelation/ polyelectrolyte complexation, interfacial polymerisation and supercritical fluid precipitation (Yeo et al 2001). These systems are able to provide particle sizes of about 50-100 μm in diameter, which is small enough to be administered as a nasal formulation (De Ascentiis et al 1996; Ranade & Hollinger 1996; Jain 2008).

Astra (1997) reported the use of starch and dextran as building materials for microspheres for delivery of large molecular weight water soluble proteins and peptides. The delivery mechanism involved absorption of water to the matrix of the sphere, swelling and formation of gel, while a further mechanism of absorption

enhancement was thought to be a result of the microspheres exerting a direct effect on the nasal mucosa by opening the tight junctions between the epithelial cells.

Bjork & Edman (1990) reported that the use of degradable starch microspheres to deliver insulin nasally in rats produced a rapid *in-vivo* decrease of plasma glucose, suggesting the microspheres adhered to the mucous membrane and start to swell, drawing water from the mucus and the underlying epithelial cells. This dehydration might induce reversible shrinking of the epithelial cells and widening of the tight junctions, thereby enhancing the transport of insulin.

The effect of drug to polymer ratio (core:coat ratio) on the release profile of gentamicin sulfate from HPMC microspheres was studied by Hascicek and co-workers (Hascicek et al 2003), who found that a 4:1 ratio produced faster release of gentamicin in comparison to 1:2. This suggested that as the polymer concentration increases, release of drug slows.

Other bioadhesive microspheres composed from carbomer and hyaluronan esters have been used to prolong the retention time of gentamicin, insulin and desmopressin within the nasal cavity. The clearance half-life of microspheres can be 3–4 hours, in comparison with 15 minutes for a simple solution. Improved bioavailabilities have been seen for those drugs using a mechanism of temporary widening of the tight junctions of cultured cells (Lansley & Martin 2001).

1.8.1.2 Precipitation technique to produce microparticles

Preparation of protein coated microcrystals (PCMCs) has been reported as a method of obtaining stable-state biomolecule formulations, and engineering drug particles for a wide range of delivery options, particularly pulmonary (Kreiner et al 2001; Kreiner et al 2005). The preparation of PCMC involves dissolution of the appropriate crystal-forming carrier together with the given bio-molecule in an aqueous solution. Rapid dehydration of the two components is facilitated by the addition drop wise of the aqueous solution with vigorous mixing into a water miscible organic solvent, resulting in the immediate formation of the PCMC with the bio-molecule

immobilized on the surface of the crystalline core carrier (via a crystal-lattice mediated self-assembly process) (Kreiner & Parker 2005; Murdan et al 2005) as illustrated in Figure 1.9.

Figure 1.9 Process of preparing drug coated microcrystals (DCM) by dropping an aqueous mixture of drug and carrier in to a water miscible precipitating agent, modified from Murugesan et al (2005).

The prepared microcrystals may be stored as a suspension or alternatively filtered/ centrifuged, rinsed with solvent and air dried to form a fine free- flowing powder (Ross et al 2002; Kreiner et al 2005). The technique has been applied to a wide range of biomolecules, from small peptides to large proteins including plasmids, insulin, lysozyme, cytochrome-c, adenosine deaminase, hyaluronidase, α-1-antitrypsin, glucose oxidase, proteases and lipases, DNA and RNA (oligonucleotides and plasmids) (Kreiner et al 2005), IgG, lactate dehydrogenase and catalase (Kreiner & Parker 2005), vaccines for tetanus and diphtheria (Murdan et al 2005).

Different types of carrier can be used such as sugar, salt or amino acid. A primary requirement of the carrier is that it should have high solubility in water and slight solubility in the precipitating water-miscible organic solvent (Kreiner et al 2001).

The precipitation process may be influenced by additives such as polymers, which may affect the rates of nucleation and growth to different extents, depending upon the nature of the surface and structures of the adsorbed molecules. Katzhendler et al (1998) reported that molecules such as HPMC may be adsorbed upon all crystal faces reducing the rate of crystallisation to zero, or upon selective faces leading to a change in morphology of the developing solids. HPMC shows surface activity (Chang & Gray 1978), and it can be adsorbed onto the newly created surface of the precipitated drug to lower the interfacial tension. In this way, the precipitated drug is stabilised against crystal growth by the adsorbed polymer (Reekmans 1998). Rasenack and co-workers prepared micro-sized anti-inflammatory steroid particles for pulmonary use (beclomethasone-17, 21-dipropionate, budessonide and triamcinolone acetonide) by solvent change process that precipitated and stabilised the drug in a small particle size by the use of HPMC (Rasenack et al 2003).

Ross and co-workers (Ross et al 2002) found that as the rate of droplet addition decreased and stirring speed increased, the resultant particle size decreased, suggesting that greater dispersion of the aqueous solution in the precipitating solvent resulted in a more rapid dehydration of the particles and hence a smaller particle size. Furthermore, delivery of smaller aqueous solution droplets into the organic solvent produced smaller particles. Particle morphology, size and biomolecule payload could therefore be controlled by choosing appropriate conditions of dehydration (Ross et al 2004).

Cooling temperature of precipitating solvent affects the crystal size distribution and habit. von Bonsdorff-Nikander and co-workers, found that at low temperature 0°C, the particles were small and even in shape and length while increased temperature (50°C) led to uneven shapes and sizes (Figure 1.10) (von Bonsdorff-Nikander et al 2003).

It is important to keep the temperature constant over the precipitation technique to obtain microparticles of high compositional uniformity, in which the particle shape remains unchanged during growth. This can be done by lowering the temperature of the solution (Garcia et al 1999; Tiwary 2007).

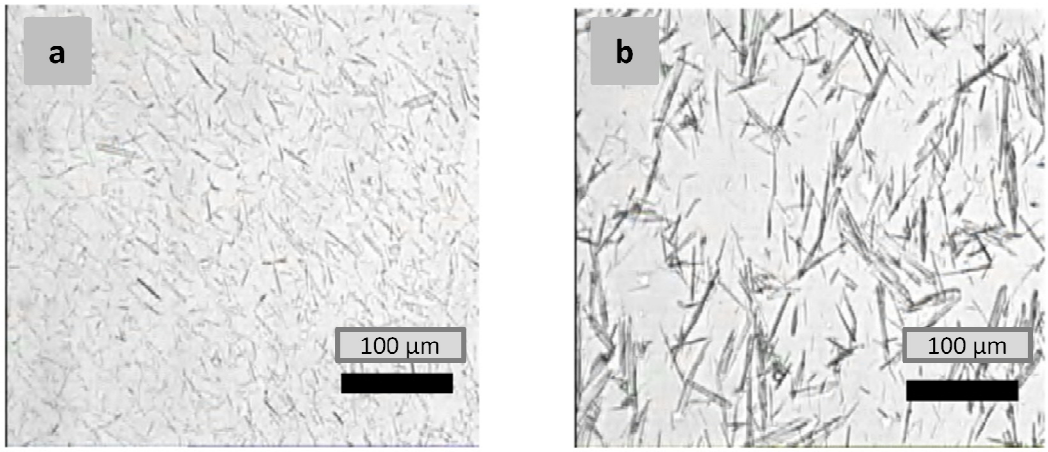

Figure 1.10 Microscopy pictures of β-sitosterol suspensions prepared by cooling at a) 0°C (immersed in ice) and b) 50°C, reproduced from von Bonsdorff-Nikander et al (2003).

1.9 Conclusion

- Wide ranging reports in the literature show that the nasal route is a promising site for achieving enhanced systemic absorption of drugs. It provides a large surface area and consequently small doses may possibly be used, with a related reduction in side effects.

- Bioadhesives provide a means of enhancing local and systemic drug effects, by prolonging the residence time of dosage form at the nasal mucosal site.

- Microparticulate drug delivery systems with control of the shape and size of particles can improve bioavailability and stability.

- Co-precipitation techniques have not been widely reported and the intriguing prospect of forming a drug-polymer particle with bioadhesive properties therefore forms the hypothesis for the studies described in this thesis.

Objectives

In order to investigate the hypothesis, the following studies will be carried out:

- Formulation of HPMC microparticles using co-precipitation technique loaded with water soluble model compounds, eg lactose or drug models such as verapamil hydrochloride or metformin hydrochloride, using isopropyl alcohol and acetone as precipitating agents.

- *In-vitro* dynamic adhesion tests will be developed, in order to consider the effect formulation variables have on adhesion.

- Examination of the hydration process of the dried microparticles formulations, and their effect on bioadhesive properties.

- Investigations of the physical properties of the HPMC microparticle formulations, to assess factors which may affect the hydration and/or bioadhesive behaviour.

- *In-vitro* release studies of drug microparticle formulations.

- Accelerated stability studies to investigate the effect of precipitation technique on the prepared microparticles using stress conditions of high temperature and humidity.

Chapter 2

General Methods

2.1 Introduction

This chapter describes these analytical techniques and how they will be utilised in this thesis, and also the general experimental methodology used.

2.1.1 Light microscopy (Optical microscopy)

Visible light is used in optical or light microscopy instruments to produce a magnified image of a sample (Rawlins 1992). There are two important microscopic components, the condenser which is located under the stage and allows light pass through the sample, and the objective lens which collects the light diffracted by the sample, forming a magnified image. Optical microscopy is also called compound light microscopy because a magnified image is produced by the combination of its objective and eyepiece lenses. Optical microscopy can provide molecular information about a sample when an anisotropic material is viewed between crossed polars, producing polarised light (Rawlins 1992; Vaughan 1993).

Light is a beam of electromagnetic vibration that vibrates in different directions. When this light is passed through a polarised filter, it will be filtered out in one direction (plane polarised) as shown in Figure 2.1.

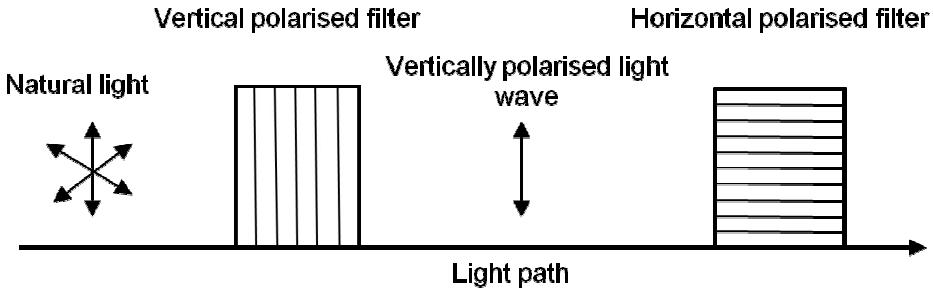

Figure 2.1 Diagram of plane polarised light, modified from Oldfield (1994). Natural light is filtered out in one direction (plane polarised) after passing through polarised filters.

This microscope can be used to differentiate between isotropic and anisotropic substances. When an isotropic substance is placed between crossed polars, it doesn't affect the vibration of the polarised light from the polariser because its refractive index is the same in all directions. Therefore isotropic materials cannot be seen under polarised light microscopy and darkness is produced. These materials include all amorphous solids. Most types of crystals however, are anisotropic (Chayen 1983; West 1984; Oldfield 1994).

2.1.2 Scanning Electron microscopy (SEM)

SEM is different from light microscopy in that an electron beam is used instead of light. In addition, it provides a higher magnification and superior resolution of images. The surface of the sample is scanned by a primary electron beam. Different types of signals are generated such as X-rays, backscattered electrons and secondary electrons as shown in Figure 2.2.

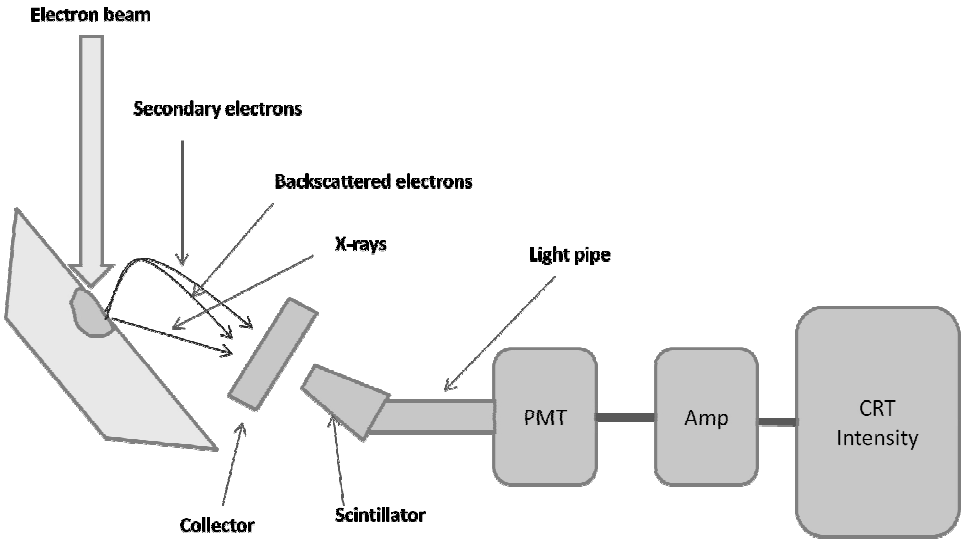

Figure 2.2 Diagram of SEM, modified from Goldstein et al (2003). Scanning the surface of the sample with the primary electron beam generates different types of signals which are detected and converted to an image.

Secondary electrons can be displayed as an image in which the detector system converts the signals created from different points on the sample with different intensities to an image on the viewing screen (Brittain et al 1991; Goldstein et al 2003).

Coating of the sample before scanning is an important step to overcome the effect of charging resulting from electron bombardment. Metal coating such as gold is widely used for SEM imaging. However other types of metals can be used instead such as aluminium, silver and copper when the gold metal interacts strongly with electrons as a result of its high atomic number. Coating with these metals can be achieved by vacuum evaporation, using a wire basket made of tungsten or boat made from molybdenum sheet, heated by passing a large electric current. Sometimes sputter coating may be used instead, in which gold and gold-palladium are used as metal coating for samples of irregular shape (Reed 2005).

2.1.3 Laser diffraction for particle size measurement

Laser diffraction is widely used for particle sizing using helium-neon (He-Ne) as a source of laser light. The Malvern Mastersizer 2000 is laser diffraction instrument used to analyse particle ranging from 0.02-2000 μm. The technique is based on the principle that particles are passed through a focused laser beam, which will scatter the light at an angle that is inversely related to particle size. Series of detectors are set up to identify the wide range of angles resulting from different sizes of particles. Consequently, these detected signals will produce data showing particle size as illustrated in Figure 2.3.

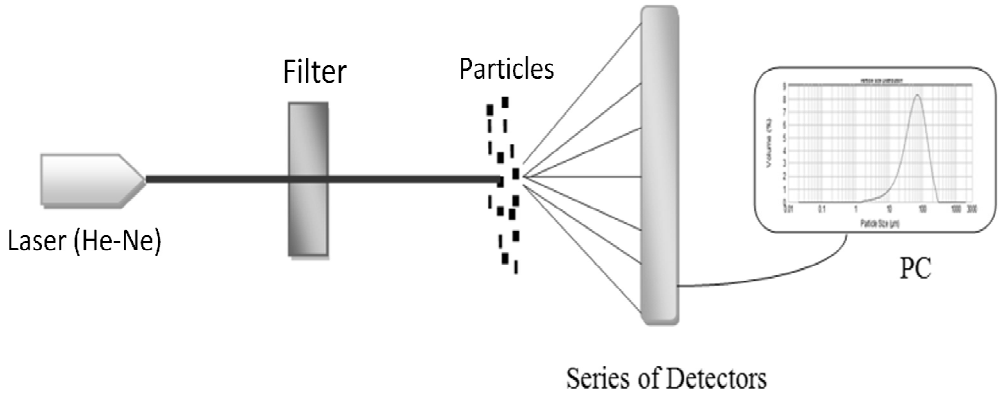

Figure 2.3 Principles of laser diffraction. Particles passed through a focused laser beam generate scattered light at an angle that is inversely related to particle size. The detectors identify these angles as signals to produce data.

2.1.4 Zeta potential measurement

The zetasizer is used for many purposes such as measuring particle size, molecular weight and zeta potential of particles in liquid form such as suspensions (Malvern 2004). The liquid layer surrounding the particle has two regions, an inner part, in

which the ions are strongly bound to the particle, and an external region which the ions are less strongly bound (the diffuse layer). Within this layer there is an estimated boundary in which any ions will move with the particle when it moves in the liquid, but any ions outside the boundary will stay where they are. This layer is called the slipping plane, and the zeta potential is the potential which exists in the slipping plane between the particle surface and the dispersing liquid, which varies according to the distance from the particle surface as shown in Figure 2.4.

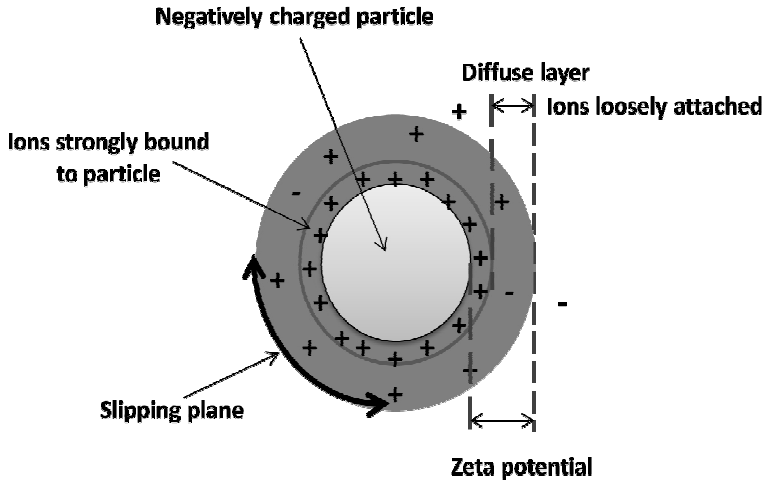

Figure 2.4 Definition of zeta potential, modified from Malvern (2004). The zeta potential is the potential which exists in the slipping plane between the particle surface and the dispersing liquid.

The mechanism of zeta potential measurement involves creation of a net charge at the particle surface when an electric field is applied. This will affect the arrangement of ions in the surrounding region of its interface with the liquid, resulting in an increase in the concentration of oppositely charged ions (counter ion) (Malvern 2004). Any factor which affects the solid/liquid interface can affect the zeta potential value, such as pH of the medium and addition of additives. When an alkali substance is added to the suspension the pH of the medium will change, and a negative charge will dominate and its zeta potential value will change as consequence (Ofir et al

2007). It was reported that addition of HPMC to a suspension of cefditoren pivoxil (CP) affected the magnitude of its zeta potential through adsorption of the polymer to the surface of CP (Yokoi et al 2005).

2.1.5 Nuclear magnetic resonance spectroscopy (NMR)

NMR is a technique that investigates a molecule at the atomic level, and provides information concerning the environment of that atom (Watson 1999).

Many atomic nuclei with a positive charge such as ^{1}H and ^{13}C isotopes spin on an axis of rotation. The spinning of these atoms are oriented randomly in the absence of an external magnetic field but in the presence of a magnetic field, they will orient specifically and generate a small magnetic dipole as shown in Figure 2.5. The technique of application of a magnetic field to detect this is called (^{1}H-NMR) and (^{13}C-NMR) respectively.

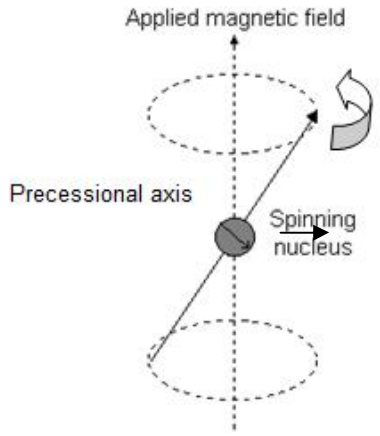

Figure 2.5 Spinning nucleus in a magnetic field, modified from Khandpur (2006). Nucleus will orient specifically and generate a small magnetic dipole.

The magnetic fields of spinning nuclei will line up either parallel or vertical to the external field. The electromagnetic radiation or field supplies energy of an appropriate frequency to be absorbed by a nucleus which is known as a resonance that causes the nuclei to change its orientation of spinning, into for example anti-parallel state (flip) (Priestle & Paris 1996).

NMR measurement is achieved by dissolving the solid sample in a solvent that doesn't itself give a signal, which is then transferred into an NMR tube (made from borosilicate glass) as shown in Figure 2.6.

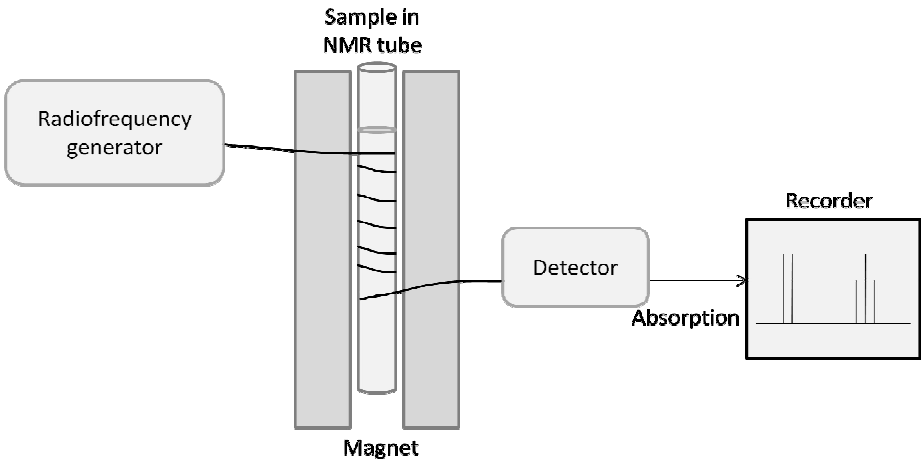

Figure 2.6 NMR measurement, modified from Watson (1999). The tube containing liquid sample is placed in the magnet where the sample will absorb the radiation generated by the instrument. The detector detects the absorption as a signal.

Then the tube is placed in the magnet. A radiofrequency radiation is generated by the instrument and then absorbed by the sample. The detector will detect the absorption and the recorder will show a signal. Since each atom is surrounded by different electrons, different shield signals will be created, and information will be obtained about each atom in a molecule as a consequence (Watson 1999).

The solvent used for ^{1}H-NMR analysis depends on the property of the sample. Water is strongly protic which means it contains protons (^{1}H). As a result the proton signal created from a water soluble compound is usually lower than the proton signal created from water. In order to detect the ^{1}H signal of the analysed compound, different approaches can be used. Deuterium oxide (D_2O) can be used as an alternative solvent, as the proton of water is exchanged with deuterium. Pre-saturation is another technique for solvent signal suppression, in which a low power resonance frequency irradiation is directed at the sample. Another approach is the use of pulsed field gradient technology that provides spectra of compounds with a suppressed signal of water with the use of pre-saturation methods (Keeler et al 1994; Wishart 2005).

2.1.6 X-ray powder diffraction (XRPD)

X-rays are short wavelength and high energy electromagnetic radiation. They are generated when a beam of high velocity electrons from a heated filament focus at an angle (θ) onto a series of latticed planes (layered structure), parallel to a crystal face and separated by distance (d), in a sealed diffraction tube as shown in Figure 2.7. These rays are diffracted because crystalline solids are created from a relatively simple group of components (atoms and atomic groupings) repeated at regular intervals in three dimensions, and X-ray wavelengths are the same order of magnitude as the spacing of atom centres (Beckett & Stenlake 1988; Suryanarayana & Norton 1998).

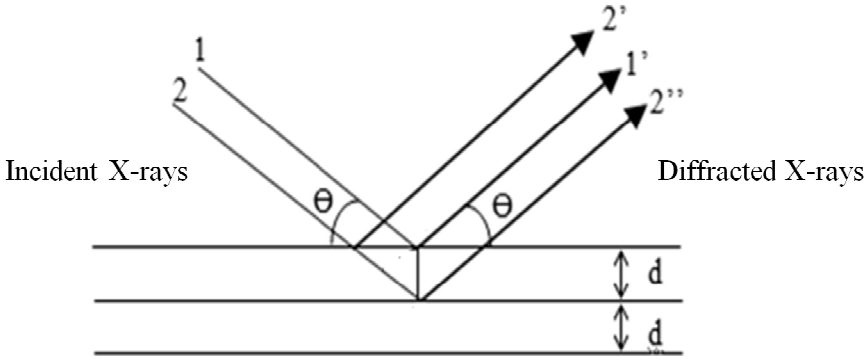

Figure 2.7 Diffraction of X-rays beam on the different planes parallel to a crystal surface, modified from Beckett & Stenlake (1988).

Measurement of X-ray diffraction is achieved by using the Bragg law or equation (Equation 2.1), in which θ is the X-ray incidence angle (Bragg angle), λ is the wavelength of the characteristics X-rays and d is the lattice spacing of the crystal. Each crystalline material has a characteristic atomic structure, so it will diffract X-rays in a unique characteristic pattern.

Bragg law; $\sin\theta = n\lambda/2d$ [Equation 2.1]

X-rays diffraction is an important characterisation apparatus in pharmaceutical science. It can identify different forms of crystalline and amorphous material, which may give information about the dissolution rate and subsequent bioavailability of the compounds (Cunningham 2004).

2.1.7 Fourier transform infrared spectroscopy (FT/IR)

In general, an infrared absorption spectra results from a change in the vibrational energy of the ground state of a molecule, accompanied by a change in dipole moment

of that molecule. Molecular vibrations are classified into stretching and bending vibrations. The former involves changes in the bond length when the atoms are connected by a spring vibrating with a particular frequency. Figure 2.8 shows the symmetric and asymmetric types of that vibration.

Figure 2.8 Symmetric and asymmetric stretching vibrations of water molecule, modified from Stuart (2004).

Bending or deformation vibrations result when the molecule is cut by a plane through the hydrogen atoms and carbon atom. There are two types of bending vibrations; in-plane and out-of-plane bending as shown in Figure 2.9.

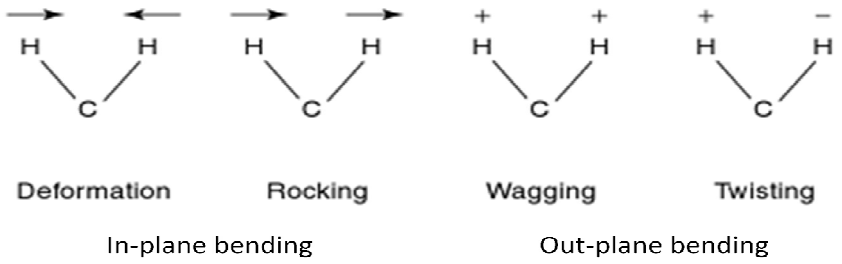

Figure 2.9 In-plane (deformation and rocking) and out-plane (wagging and twisting) bending vibrations, modified from Stuart (2004).
(+) Atom moves above the plane and (-) atom moves below the plane.

Stretching or bending of bonds involving atoms in widely separated groups of the periodic table and will lead to peaks. Vibrations of bonds such as C-C and N=N will give weak peaks which also result from a small change in the dipole moment of molecule vibrations (Stuart 2004). These vibrations are represented as wave-numbers in cm^{-1}. Any change in these numbers can give an idea about chemical changes in the compound.

Fourier-transform infrared (FT/IR) spectrum is produced from the interference of the radiation between two beams to yield a signal produced as a function of the change of path length between the two beams. In other words, it makes the use of all frequencies emitted from the source simultaneously and therefore provides an immediate increase in the signal to noise ratio. The basic components of the instrument are summarised in Figure 2.10. IR data can be obtained either in the mid-infrared (400-4000 cm^{-1}) or near-infrared (4000-14,000 cm^{-1}) regions depending on the requirement of study (Brittain et al 1991).

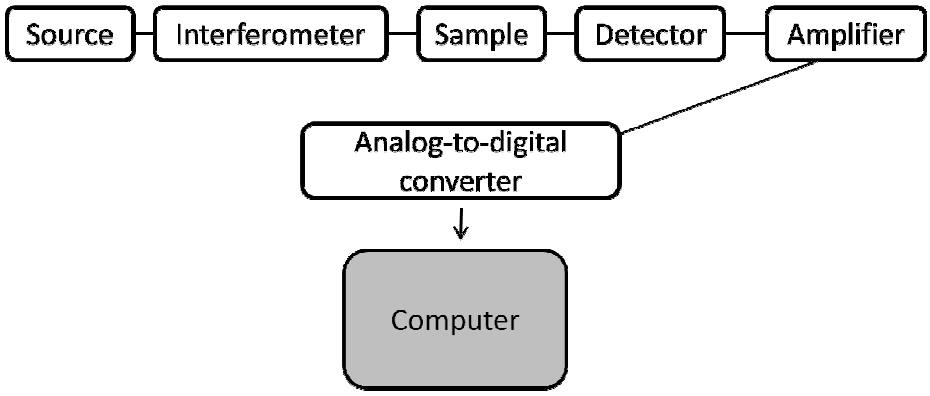

Figure 2.10 Basic components of FT/IR spectroscopy, modified from Stuart (2004).

2.1.8 Differential scanning calorimetry (DSC)

DSC can provide a quantitative measurement of heat of reaction, by assessing the energy input into a substance (in comparison to a reference) as a function of temperature, as the samples are subjected to a controlled temperature programme (Ford & Timmins 1989). As most phase transitions are accompanied by a change in heat resulting from a chemical reaction, melting, absorption or mixing, DSC is used to detect these events and characterise the sample (Giron 1998). When a sample is submitted for a standard DSC analysis, a few milligrams of the sample are weighed and sealed in an aluminium pan and placed in the instrument. The pan is then heated at a pre-determined rate. The amount of power required to heat the sample to a particular temperature is measured in relation to the reference pan. The resulting plot is the heat flow against temperature, which can give information about melting, crystallisation and glass transition temperature in samples as shown in Figure 2.11 (Ford & Timmins 1989).

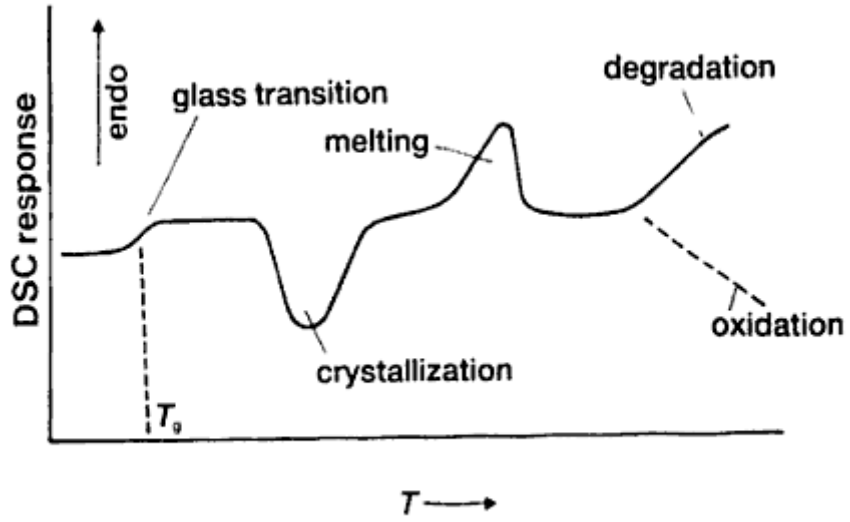

Figure 2.11 DSC curve of a typical organic polymer, reproduced from Brown (2001).

2.1.9 Thermo-gravimetric analysis (TGA)

TGA is a widely used thermo-analytical method. It detects the change in mass of a sample while a controlled temperature programme is applied (Ford & Timmins 1989). Figure 2.12 shows a schematic diagram of TGA.

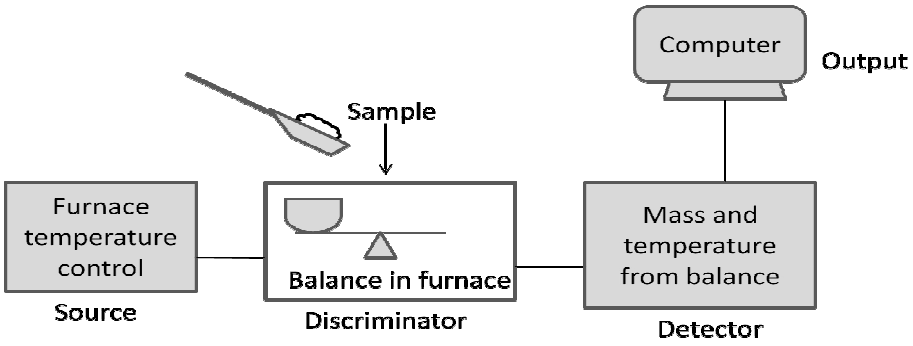

Figure 2.12 Schematic diagram of TGA, modified from McMahon (2007). Any change in the mass of the sample with heating can be detected by the microbalance located in the furnace.

The most important parts are the furnace and balance. A sample is placed into a TGA pan attached to a sensitive microbalance. The sample holder portion of the TGA balance is placed into the furnace. The balance allows the measurement of any changes in the weight of the sample under the influence of the changing temperature (Ford & Timmins 1989; McMahon 2007). TGA is useful for determining sample purity and water content (moisture level less than 0.5% can be detected), carbonate and organic content, oxidation- reduction reactions, decomposition reactions, quantitative separation of the main components in multi-component mixtures, kinetic study and accelerated aging tests (Patnaik & Dean 2004; McMahon 2007).

2.1.10 *In-vitro* dynamic adhesion

Nasal mucus consists of mucin glycoproteins, proteins, lipids, inorganic salts and water in which the latter is more than 95% of its weight (Mortazavi & Smart 1993). Mucin glycoproteins are an important structure in the mucus gel, providing gel-like cohesive and adhesive properties of the mucus and permitting close contact between the polymer of the formulation and the mucosal surface by allowing the chain sections of the polymer to interact and tangle with the glycoprotein of the mucus. This entanglement has an important role in the bioadhesion, changing the properties of the mucous layer and reducing the rate of mucociliary clearance of the formulation (Nakamura et al 1999; Lee et al 2000).

Agar is a polysaccharide of D-galactose and 3, 6-anhydro-L-galactose with a few variations, and it has low ester sulphate content. Agar can form a strong or rigid gel hydrocolloid through its double helical structure. These helices aggregate to form three dimensional networks, holding the water molecules within the agar (Glicksman 1987; Lahaye & Rochas 1991; Fuchigami et al 2006). Water availability is an important factor in the performance of bioadhesive systems, as the adhesion of the polymer depends on its ability to absorb water from mucosal surface, in order to swell and produce the gel structure which facilitates the polymer binding to the mucus.

Therefore, using a mucin-agar plate as an artificial model of nasal mucosa has been proposed as a simple method of assessing bioadhesion. This technique was used previously with agar alone (McInnes et al 2001) or mucin-agar combinations (Bertram & Bodmeier 2006).

2.1.11 Dynamic vapour sorption (DVS)

Vapour sorption measurement was first reported by Strickland, in which pharmaceutical powders were weighed and stored in desiccators containing different saturated salt solutions of defined relative humidity, and the weight of the sample measured regularly until equilibrium was obtained (Strickland 1962). Later a fully

automated, sensitive and rapid system was developed which is called Dynamic Vapour Sorption (DVS) (Figure 2.13). The apparatus consists of microbalance, which allows a sample to be weighed during exposure to controlled temperature and humidity conditions by placing the sample in a chamber (Levoguer & Williams 1997). Regulation of humidity (relative humidity) can be obtained by mixing a specific ratio of air saturated with 100% relative humidity generated by a vapour humidifier, and dry air.

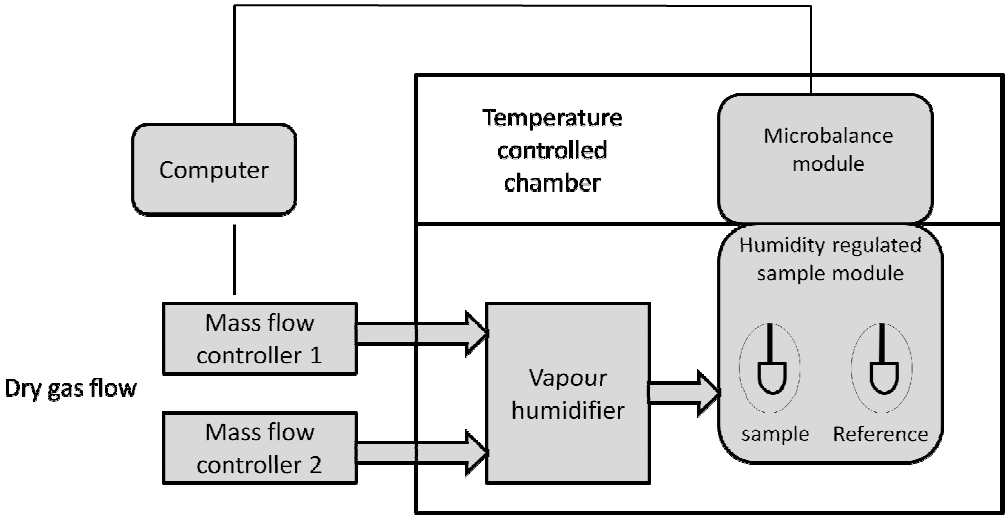

Figure 2.13 Dynamic vapour sorption (DVS) apparatus, modified from Surface Measurement Systems website. The sample is placed in the sample pan connected to a microbalance, and subjected to a controlled temperature and humidity environment. The change in mass of the sample with time as a function of relative humidity can then be recorded.

Moisture sorption behaviour is obtained from the equilibrium moisture uptake (shown in Figure 2.14) at each relative humidity (RH). The duration of the experiment depends on the nature of moisture uptake of the sample, in which its outer surface absorbs water faster than the bulk which is slower because of vapour diffusion within (Reutzel-Edens & Newman 2006). This technique can be used to distinguish between amorphous and crystalline forms of drugs.

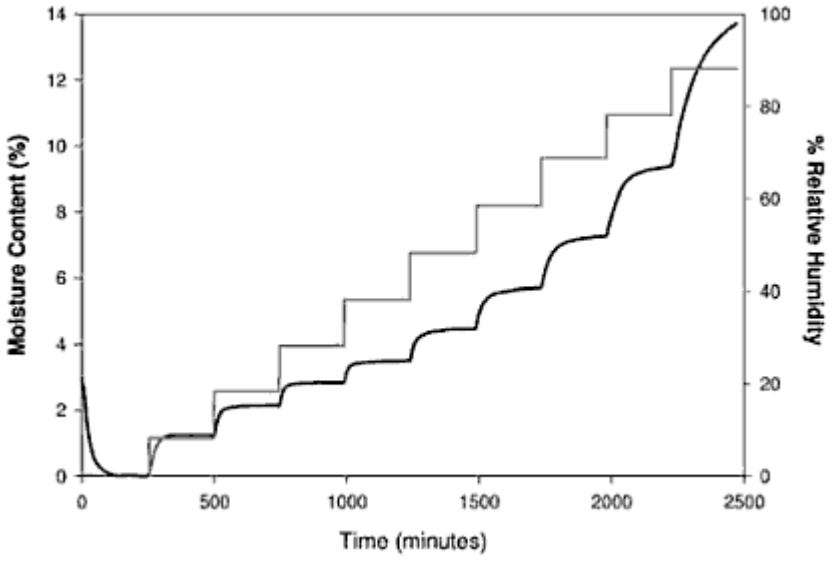

Figure 2.14 Sorption kinetics of microcrystalline cellulose, showing the extent and rate of water uptake, reproduced from Reutzel-Edens & Newman (2006).

2.1.12 Ultraviolet spectrophotometry (UV)

Absorption of light by a substance in a solution, in both UV (200-400 nm) and visible (400-800 nm) regions of the electromagnetic spectrum, excites the electronic transition in a molecule (vibrational and rotational transitions). This is depicted in Figure 2.15, which shows that the intensity of a light beam may be reduced when passed through a transparent cell containing a solution of an absorbing substance, by reflecting at the cell faces, absorbance by molecules and scattering by particles. This effect is described in Lambert's law as shown in Equation 2.2.

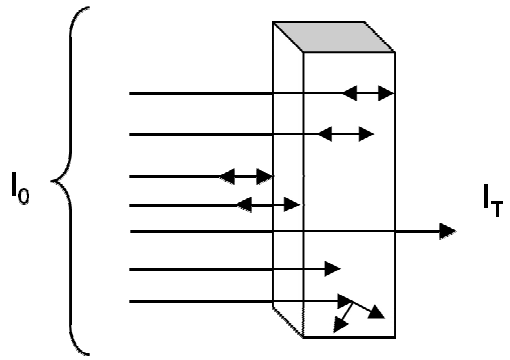

Figure 2.15 Mechanism of light transition through a cell containing an absorbing substance. The intensity of the light beam reduces as a result of light reflecting at the cell faces, absorbance by molecules and scattering by particles.

$$\text{Ln } I_0/ I_T = kc \qquad \text{[Equation 2.2]}$$

On conversion to a logarithm, the equation becomes:

$$\text{Log } I_0/ I_T = kc/ 2.303 \qquad \text{[Equation 2.3]}$$

In which I_0 is the original intensity on the cell, I_T is reduced intensity transmitted from the cell, K represents proportionality constant and c is the concentration.

Beer's law defines the absorbance as the exponential reduction in intensity of a beam of monochromatic radiation with an increasing the number of absorbing molecules. Therefore the absorbance is proportional to the concentration.

The Beer-Lambert law (Equation 2.4) is a combination of both definitions. Therefore, the molar absorptivity of a substance in solution at a specified wavelength is the absorbance at that wavelength of a 1 mol/l solution in a 1 cm cell, and can be used for quantitative measurement of absorptivity of drugs. When the value of ε is

less than 100, those drugs are weakly absorbing, and those with ε value higher than 1000 are intensely absorbing.

$$A = \log I_0 / I_T = \varepsilon b c \qquad \text{[Equation 2.4]}$$

In which A is the absorbance, ε is molar absorptivity in mol/cm, b represents cell path length in cm (1 cm) and c is the concentration in moles/ l.

2.1.13 Franz-cell diffusion apparatus

The Franz cell diffusion apparatus in Figure 2.16 (Shah et al 1989) can used to study the *in-vitro* diffusion or release profile of a drug from a formulation across a membrane, under conditions which imitate those of the nasal cavity.

Figure 2.16 Franz-cell diffusion apparatus.

Figure 2.17 illustrates the principal components of the cell. The diffusion segment consists of receptor and donor compartments, separated by a diffusible membrane, for example filter paper of excised tissue, which is kept in contact with the surface of the dissolution medium (20 millilitre) contained within the receptor compartment. This allows the membrane to be wetted sufficiently and the formulation to be hydrated in a similar manner to the moist mucosa of the nasal cavity, without immersing the tested dosage in the dissolution medium. The receptor compartment is constantly agitated with a magnetic stirrer, and the dissolution system is maintained at 37°C using a water bath. Solubilised drug will subsequently diffuse out of the formulation, and through the membrane to the receptor compartment. Samples are withdrawn at predetermined intervals from a sampling port on the side of receptor compartment and analysed for drug content.

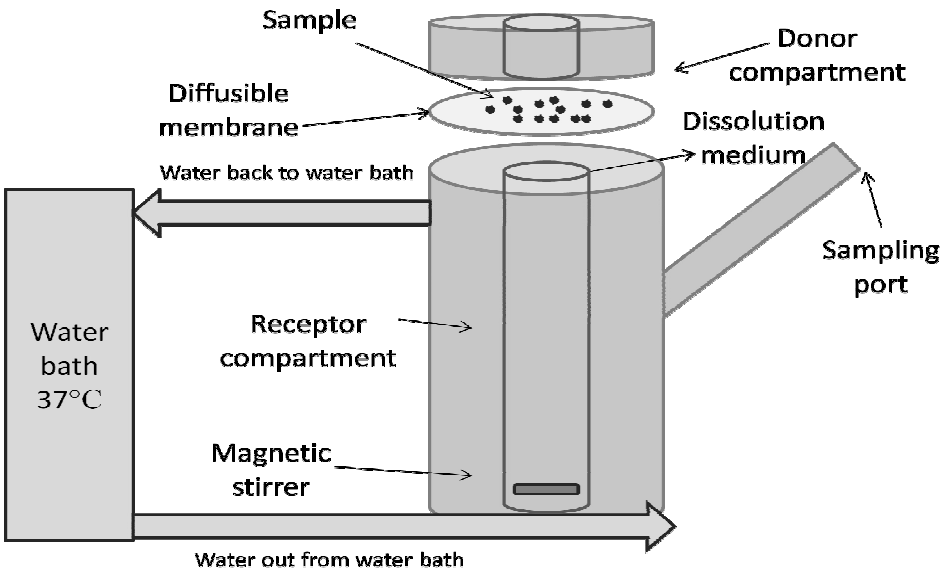

Figure 2.17 Principal components of Franz-cell diffusion cell. The sample is placed on the wetted diffusion membrane which contacts the surface of the dissolution medium (20 millilitre) contained within the receptor compartment.

2.1.13.1 Statistical comparison of dissolution profiles

Drug release profiles can be compared statistically using Fit factors. This procedure is called pair-wise and is discussed as the difference factor (f_1) and the similarity factor (f_2) (Moore & Flanner 1996; Pillay & Fassihi 1998; Costa & Sousa Lobo 2001).

f_1 measures the percent error between two curves over all times points as shown in Equation 2.5.

$$f_1 = \left\{ \frac{\sum_{t=1}^{n} w_t |R_t - T_t|}{\sum_{t=1}^{n} w_t R_t} \right\} \times 100\% \qquad \text{[Equation 2.5]}$$

Where n is sampling number, and R and T are the percentage of drug dissolved of the reference and test products at each time point t respectively.

The percent error (f_1) is zero when the test and reference profiles are identical and increases proportionally with dissimilarity between the two profiles.

The similarity factor f_2 is a logarithmic reciprocal transformation of the sum of squared errors and is a measurement of the similarity in the percentage dissolution between the two curves (Equation 2.6)

$$f_2 = 50 \log \left\{ \left[1 + \frac{1}{n} \Sigma w_t (R_t - T_t)^2 \right]^{-0.5} \times 100 \right\} \qquad \text{[Equation 2.6]}$$

Where n is the number of time points, w_t is an optional weight factor, R is the reference assay at time point t, and T is the test assay at time point t.

An f_2 value between 50 and 100 suggests that the dissolution profiles are similar. An f_2 value of 100 suggests that the test and reference profiles are identical, and as the value becomes smaller, the dissimilarity between release profiles increases (Anderson et al 1998; Pillay & Fassihi 1998).

2.2 Materials

2.2.1 Chemicals

α- lactose monohydrate (BN. 038K0112)	Sigma-Aldrich, Dorset, UK.
Metformin hydrochloride (BN. 120988)	Alpharma Pharmaceuticals Inc., Piscataway, USA.
Verapamil hydrochloride (BN. 118839)	Alpharma Pharmaceuticals Inc., Piscataway, USA.
Hydroxypropyl methylcellulose (K100LV premium, BN. KK08012N21)	Dow Chemicals Ltd, Michigan, USA.
Sodium diclofenac	Sigma Chemical Co., St. Louis, USA.
Porcine stomach mucin type II	Sigma-Aldrich, Dorset, UK.
Agar-Agar, Ultrapure granulated	Merck, Germany.
Sodium chloride	Sigma-Aldrich, Dorset, UK.
Sodium nitrite, 99.5%	Sigma-Aldrich, Dorset, UK.
Potassium carbonate	Sigma-Aldrich, Dorset, UK.
Potassium chloride	Fisher scientific, Leicestershire, UK.

2.2.2 Solvents

Isopropyl alcohol	Sigma-Aldrich, Dorset, UK.
Acetone	Sigma-Aldrich, Dorset, UK.
Deuterium oxide	Sigma- Aldrich Co., St. Louis, USA.
Distilled water	Lab water distillation system, SIPBS, Glasgow, UK.

2.3 Apparatus

2.3.1 Manufacture

Electrical stirrer (SS10)	Stuart scientific, Staffordshire, UK.
Magnetic stirrer	BibbySterilin Ltd, Staffordshire, UK.
Silverson SL 2T mixer (motor 1/10HP)	Silverson, Waterside, UK.
Syringe pump	Cole-Parmer, London, UK.
Shaker	Fisher Scientific, Leicestershire, UK.
Vac-oven (OV-11)	Medline scientific limited, Oxfordshire, UK.

Balances	Mettler Toledo AG 135 and Sartorius Laboratory, Giessen, Germany.
Buchner funnel	Sigma-Aldrich, Dorset, UK.
Eppendorf centrifuge tubes 1.5 ml	Eppendorf AG, Hamburg, Germany.
Centrifuge apparatus	Hermle labortechnik, Wehingen, Germany.
Needles of 19, 21 and 23g	BD syringes, Franklin Lakes, USA.
Disposable syringe 10 ml	BD Plastipak syringes, Franklin Lakes, USA.

2.3.2 Analysis

Polarised light microscope (Polyvar®)	Reichert-Jung, Arnsberg, Germany.
Microscope slides (76x 26 mm;1.0-1.2 mm thick)	VWR International Ltd., Poole, UK.
Mastersizer2000	Malvern instruments Ltd., Worcestershire, UK.
Zetasizer, nano series, Nano-ZS	Malvern instruments Ltd., Worcestershire, UK.
Clear disposable zeta cell (DTS 1060C)	Malvern instruments Ltd., Worcestershire, UK.
Differential scanning calorimeter (DSC822^e Model; TA controller TC15)	Mettler-Toledo Ltd., Leicester, UK.
Aluminium lid sealer	Mettler-Toledo Ltd., Leicester, UK.
Lid-pan sealing press	Mettler-Toledo Ltd., Leicester, UK.
Thermal Gravimetric analysis (TGA/SDTA851^e)	Mettler-Toledo Ltd., Leicester, UK.
Fourier transform infrared spectrophotometer (Jasco FT/IR -4200)	Jasco Ltd., Essex, UK.
Scanning electron microscope	JSEM, Tokyo, Japan.
Nuclear magnetic resonance (ECX-400MHz)	Jeol, Tokyo, Japan.
X-ray powder diffraction (Bruker-AXS D8)	Bruker AXS GmBH, Karlsruhe, Germany.
UV spectrophotometer	Helios Alpha or UV1,Rochester,USA
Agar culture plates (NUNC, 25 x 25cm)	VRW International Ltd., Poole, UK.
Franz-cell diffusion apparatus	Perme Gear, Hellertown, USA.
Cellulose nitrate Filter Paper (0.45µm)	Whatman, VRW, Leicestershire, UK.
Filter Paper (Grade 1, 42.5mm)	Whatman, VRW, Leicestershire, UK.
UV quartz spectrophotometer microcells of path length 1cm	Whatman, VRW, Leicestershire, UK.
Dynamic vapour sorption apparatus	Surface Measurement System, SMS Ltd., Alperton, UK.
Para film M	Pechiney Plastic Packaging, Menasha, USA.

2.4 PC software

DSC and TGA software (Star^e system)	Mettler-Toledo Ltd., Leicester, UK.
FT/IR software (CM6 1XN)	Jasco Ltd., Essex, UK.
Polarised light microscopy software (Leutron Vision V1.95.002)	Reichert-Jung, Arnsberg, Germany.
SEM software (Image Slave)	Meeco-Dindema, Sydney, Australia.
X-ray software (EVA 9.0.0.2)	Socabim, Karlsruhe, Germany.
Zetasizer software (Nano Series V 5)	Malvern Instruments Ltd., Worcestershire, UK.
Mastersizer 2000 software (V 5.4)	Malvern Instruments Ltd., Worcestershire, UK.
DVS software	Surface Measurement System, SMS Ltd., Alperton, UK.
Graph Pad Prism (Statistical analysis software V 5.04)	GraphPad Software, Inc., La Jolla, USA.
Minitab 15 (Statistical analysis software)	Minitab Ltd., Coventry, UK.

2.5 Methods

2.5.1 Solubility of lactose

Determination of the solubility of lactose was performed manually without UV spectrophotometry since there is no λ_{max} for lactose between 200-400nm.

Different concentrations of lactose in distilled water (1-30% w/w**)** were prepared, and flasks were sealed and shaken for 3-4 days (50 rpm) in a controlled shaker at a constant temperature of 25 ±0.5°C. The solubility of lactose in each flask was determined by filtering the solution, drying the filtrate and then weighing the dried precipitate. The amount of lactose dissolved was calculated by subtracting the weight obtained after filtration and drying from the initial weight of lactose added. The same method was used to determine lactose solubility in IPA and acetone.

2.5.2 Determination of λ_{max}, Standard calibration curve and solubility of metformin HCl and verapamil HCl

Saturated solutions of metformin hydrochloride (MH) and verapamil hydrochloride (VH) in different solvents at 37 ±0.5°C were prepared to determine the λ_{max} and solubility of these drugs. The solvents used were distilled water, acetone and isopropyl alcohol (IPA). A UV spectrophotometer was used to scan these solutions to identify the λ_{max}.

Different concentrations (0.0001, 0.0005, 0.001, 0.0015 and 0.002 % w/v for MH and 0.0025, 0.005, 0.0075, 0.01, 0.0125 and 0.015 % w/v for VH) of each drug solution were prepared using volumetric flasks and their absorption at the λ_{max} of each drug at a particular concentration was plotted to obtain a standard curve.

The solubility of each drug was calculated after diluting their saturated solution. The absorbance at the λ_{max} determined was obtained, and the concentration determined according to the standard curve.

2.5.3 Preparation of microparticles

Microparticles were precipitated using different types of stirring equipment.

2.5.3.1 Preparation of microparticles using mechanical stirrer

Aqueous solutions of lactose with HPMC (alone and in combination), were prepared in different concentrations (1-20% w/w for lactose alone, and 1-10% w/w for HPMC alone and lactose:HPMC (1:1)). Solutions were dropped via a needle (19-23 gauge) in a controlled manner using a syringe pump at 5 or 10 ml/hour, into 200 ml of the precipitating agent (IPA), and agitated at 1000 or 2000 rpm using an electrical stirrer (Stuart stirrer), as shown in Figure 2.18. The beaker used for preparation was covered with Parafilm in order to prevent evaporation of the precipitating agent. The resultant precipitate was collected by filtration using a Buchner funnel, while the filtrate was left in a fume hood for two days until dry. Where required for analysis, some batches were left as a suspension. The precipitates and suspensions of all formulations were stored in tightly sealed vials until use.

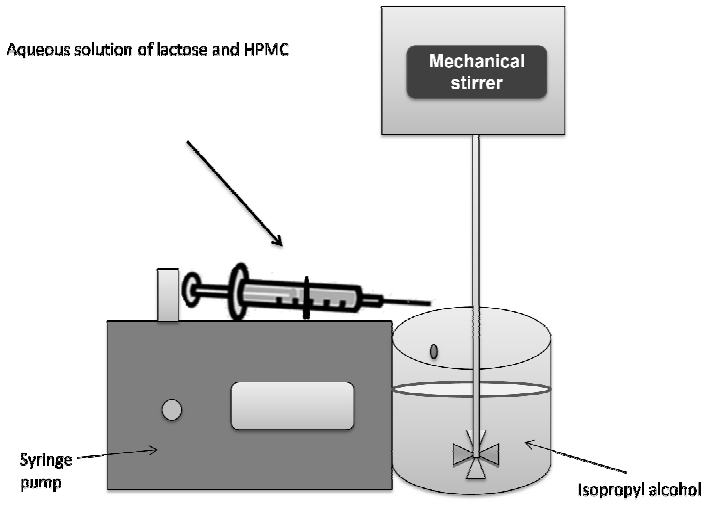

Figure 2.18 Preparation of lactose:HPMC (1:1) microparticles using mechanical stirrer (Stuart stirrer).

2.5.3.2 Preparation of microparticles using high shear mixer

The high shear mixer consists of an electrical stirrer and mesh as shown in Figure 2.19. It has a stirring speed of up to 9000 rpm in comparison to Stuart stirrer which can only achieve 2000 rpm. This equipment was used during initial precipitation experiments with lactose:HPMC (1:1) to optimise the required stirring rate and preparation conditions to be used later for MH:HPMC and VH:HPMC (1:1) formulations.

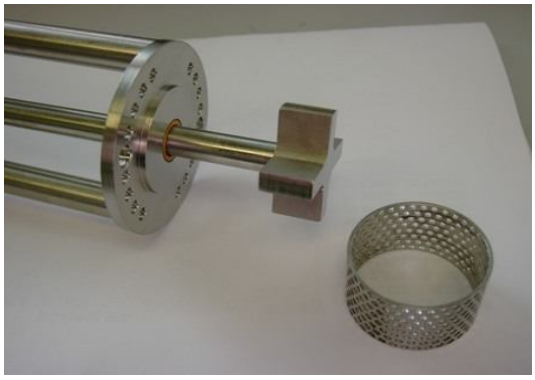

Figure 2.19 Electrical stirrer and mesh of Silverson SL 2T mixer.

Different parameters were varied to prepare lactose:HPMC microparticles, such as temperature of precipitation media (25 ±0.5°C and icy bath at 4 ±0.5°C), stirring speed (7500 and 8000 rpm) and different precipitating solvents (IPA and acetone). The final technique, as shown in Figure 2.20, involved the preparation of aqueous gels of HPMC alone and in combination with lactose, MH or VH in concentrations of 3% and 4% w/w (1:1).

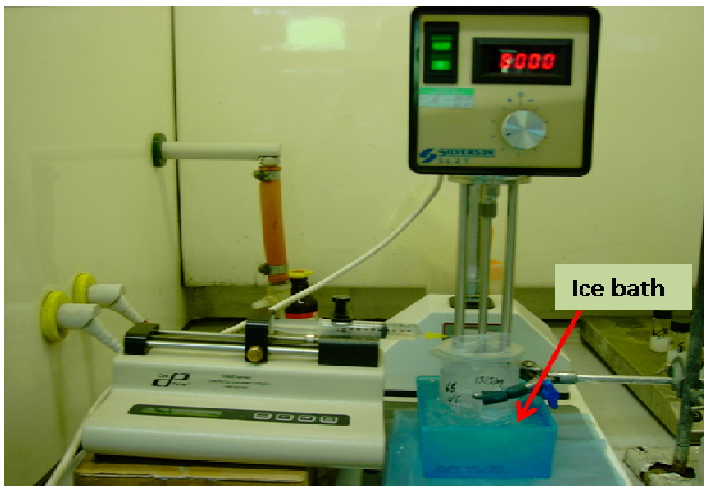

Figure 2.20 Preparation of drug:polymer microparticles using high shear mixer (Silverson SL 2T).

The gels were dropped in a controlled manner using a 23g needle and 10 ml/hr dropping rate into the precipitating agent (200 ml of IPA or acetone), agitated using an 8000 rpm stirring speed to obtain microparticles. The beaker used for preparation was covered with Parafilm, as mentioned previously, in order to prevent evaporation of the precipitating agent. Microparticles were collected by filtration for acetone and centrifugation for IPA. Following filtration or centrifugation, the samples were left in a fume hood until dry before being placed in a vacuum oven for 6 hours to evaporate any residual solvent that have been entrapped within the formulations.

2.5.4 Physiochemical properties of prepared microparticles

Different analytical techniques mentioned in the introduction of this chapter were utilised to study the physiochemical features of prepared microparticles.

2.5.4.1 Determination of percent yield and drug content of microparticle

MH and VH content of microparticles prepared using the technique described in Section 2.5.3.2 was determined by weighing 5 mg of each formulation, dissolving in 20 ml distilled water, and then measuring the absorbance of each drug (VH and MH) using UV spectrophotometry at 278 nm and 233 nm respectively.

Percent yield and drug content of microparticle of VH and MH formulations prepared were calculated as follows:

% Yield = Actual dried weight of microparticles gained / theoretical weight× 100

[Equation 2.7]

Drug content in microparticles (%) = Actual drug content/theoretical drug content×100

[Equation 2.8]

According to the calculated drug content of the prepared microparticles using previous equation, the physical mixture formulations of drug with polymer were prepared manually. The powders of unprocessed drug and polymer were mixed physically using mortar and pestle in ratio similar to the calculated ratios of drug:polymer microparticles.

2.5.4.2 Manual measurement of maximum size of prepared microparticles

Light and polarised light microscopy was used to assess the morphology of prepared microparticles. A drop from microparticle suspensions of lactose alone and in combination with HPMC (before drying step) were examined on a slide under the microscope (n=3). Four scales as shown in Figure 2.21 were obtained, which

represented the magnification of objective lenses of optical microscope. These scales were used to measure manually the length of the microparticles.

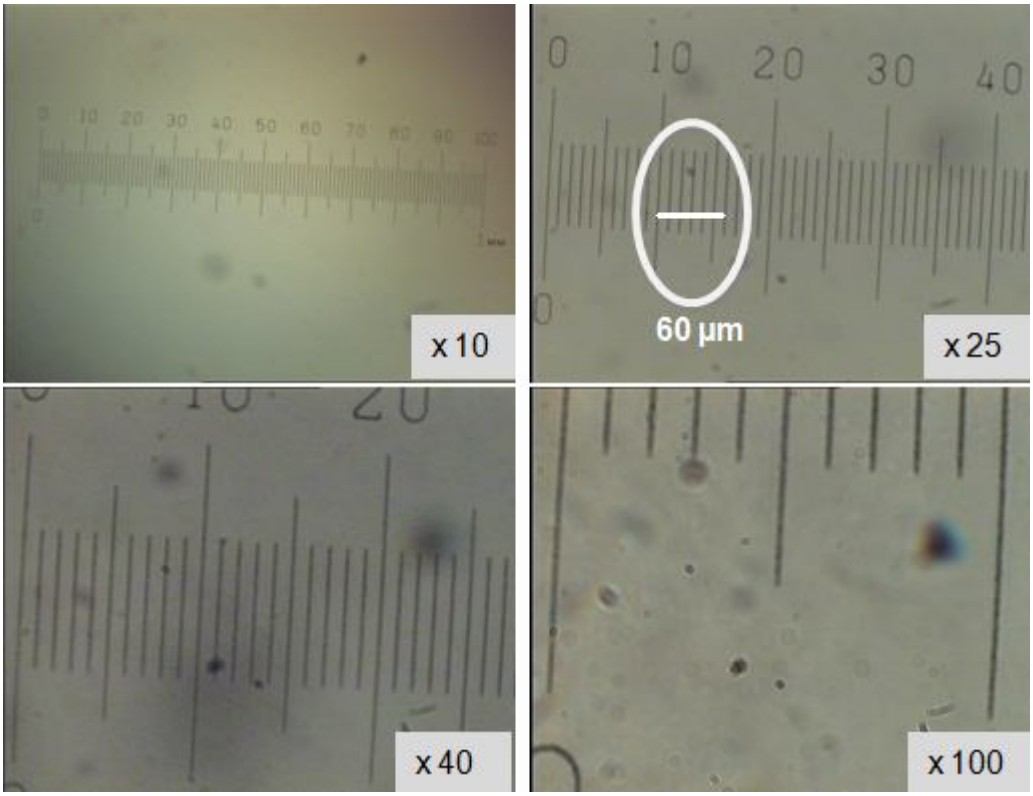

Figure 2.21 Scales used to measure maximum length microparticle size with light microscopy, n=3.

2.5.4.3 Measurement of mean microparticle size using laser diffraction

The mean size of prepared microparticles in suspension form was obtained by laser diffraction. A small volume of the suspension for analysis was added, and mean microparticle size measurement was obtained using the analysis software (n=3).

2.5.4.4 Scanning electron microscopy (SEM)

The morphology of prepared microparticles (clumps) and fine powder of unprocessed components were studied using SEM. Solid samples were prepared by spreading on 10 mm aluminium stubs with double sided copper tape. Then, the samples were coated with gold using a sputter coating system (Polaron SC 515). These samples were imaged in the SEM using different levels of magnification.

2.5.4.5 Zeta potential measurement

A zeta cell as shown in Figure 2.22, was used for zeta potential measurement. The sample was in suspension form, and a small volume (900 μL) of suspension diluted (1:20) with a dispersant solvent (IPA) was used for this analysis. All air bubbles were removed from the cell after filling. The refractive index and viscosity of IPA were determined before starting which were 1.39 and 2.320 cP, since the software of zeta potential measurement required this information.

Figure 2.22 DTS 1060C- clear disposable zeta cell was used for zeta potential measurement.

2.5.4.6 Nuclear magnetic resonance spectroscopy (^{1}H-NMR)

^{1}H-NMR was used to identify any chemical changes in the processed formulations. 20 mg of solid samples were weighed and left in water-vacuum desiccators overnight to extract any moisture. Later, they were dissolved in 1.5 ml of deuterium oxide (D_2O) and left sealed overnight to complete their dissolution. The solutions were transferred into NMR tubes to be analysed using the NMR apparatus. A pre-saturation method of single pulse was used for the analysis.

This technique was also used to estimate the percentage of lactose and HPMC in some formulations in relative to diclofenac as an internal standard. 1 mg of diclofenac was added to 10 mg of microparticles which was then dissolved in 750 µL of D_2O. These prepared samples were analysed using the same settings as previously described.

2.5.4.7 Fourier transform infrared spectroscopy (FT/IR)

Solid sample in a small amount (2-5 mg), was placed on the prism surface where it was compressed by a plunger and analysed from 650 cm^{-1}- 4000 cm^{-1} wave numbers, using attenuated total reflectance (ATR).

2.5.4.8 X-ray powder diffraction (XRPD)

The diffractometer was configured in Bragg-Brentano geometry, in which solid samples were placed in 0.7 mm borosilicate capillaries. The radiation source was monochromatic copper, and data were collected over a 2 theta range of 4-40° at a power of 50 mA and 40 kV. A step size of 0.017 degree was used.

2.5.4.9 Differential scanning calorimetry (DSC)

The Mettler Toledo DSC 822e system (based on the heat flux principle) was used. The system consists of a TA controller (TC 15) and a measuring cell (DSC 822e module) that was cooled under a purge of nitrogen at a flow rate of 50 ml/min

Aluminium pans (40 µl) were weighed before addition of the solid sample. The samples in weights of 2-5mg were evaluated. The lid of the pan was pierced using a pin to allow gas exchange during the heating program. The pan covered with pierced lid was hermetically sealed, and then placed in the DSC apparatus for analysis.

Different heating programmes were used according to the physical property of the material or drug used:

- The heating programme used for lactose:HPMC (1:1) microparticles, lactose microparticles, HPMC microparticles and their unprocessed components was 15-240°C at a 10°C/ min heating rate.

- For solid samples of VH:HPMC and MH:HPMC (1:1) microparticles, their physical mixture and unprocessed components of both model drugs the heating programme was 15-200°C and 15-270°C for VH and MH formulations respectively using a 10°C/ min heating rate.

- To calculate the glass transition temperature (Tg) for all solid samples of HPMC microparticles formulations and their unprocessed components, samples were exposed to a heating rate of 15-125°C at 10°C/min and then held for 10 minutes at 125°C to allow evolution of the moisture contained within the sample, to avoid mistake of the glass transition temperature (Tg). Following this, the sample was quenched cooled to -40°C and held at this temperature for 5 minutes before heating to 250°C using a 20°C / min heating rate (Okhamafe & York 1985).

2.5.4.10 Thermo-gravimetric analysis

Solid samples weighing 2-10 mg were loaded into an uncovered aluminium pan. A heating programme of 25-240°C at a rate of 10°C/min was used. The TGA curves of weight lost with heating were obtained for the samples

2.5.4.11 *In-vitro* dynamic adhesion

An artificial nasal mucosa was prepared using a concentration of 1% agar and 2% mucin w/v. The agar solution was prepared using a magnetic stirrer and heater, while mucin was continuously stirred to dissolve. The agar solution was left to cool down to 50°C before adding mucin (with stirring), then the mixture was rapidly poured into plates of 25×25cm to settle down and congeal for 1 hour. Following this, the plates were wrapped very well and stored in the fridge at 4°C overnight to be used later for dynamic adhesion measurement.

30 g of the solid sample was placed at the top of the plates. Then, a force of 0.05 N (supplied by aluminium discs) was applied to each sample for 60 seconds. All plates were wrapped with cling film to prevent any change in the humidity of the adhesion medium environment for the duration of the experiment. The plates were tilted to an angle of 80° and the samples allowed to slide down the plate, representing the direction of movement within the nasal cavity. The distance travelled by the samples with time was measured and used as an indication of extent of bioadhesion as shown in Figure 2.23.

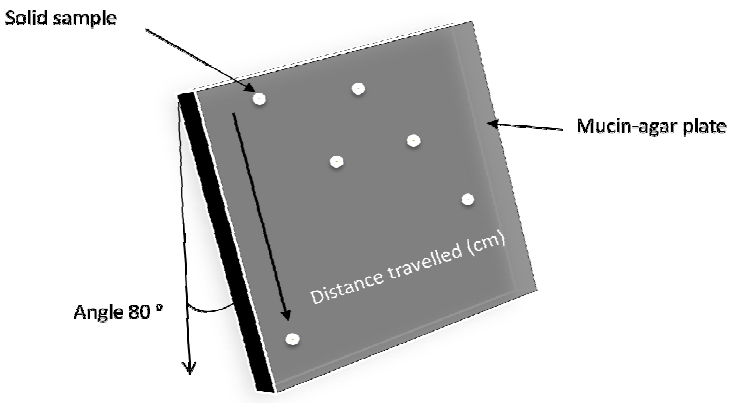

Figure 2.23 *In-vitro* dynamic adhesion test using mucin-agar plate. The distance travelled by the sample with time was measured as a function of the extent of bioadhesion.

2.5.4.12 Dynamic vapour sorption (DVS)

Solid samples weighing 8-10 mg were loaded on to the pan and the programme was set to control the humidity at 0% RH, followed by increasing RH in 10% increments to 95%. The RH was then decreased through the same steps, and the temperature maintained at 25 ±0.5°C throughout the cycle. A sorption/desorption profile was obtained from the DVS measurement percentage of mass increase (in relation to the dry weight) at 95% RH was calculated to assess the amount of humidity sorption by the sample.

2.5.4.13 Water uptake

Two methods were used to study water uptake of solid microparticles and unprocessed HPMC.

1. A saturated salt method, which involved storing solid samples at different humidities for 16 days. This was done by preparing saturated salts solutions at 25 ±0.5°C to represent three different relative humidities; potassium

carbonate, 43% RH , sodium nitrite, 65% RH and potassium chloride 85 %RH (Greenspan 1977).These salts were left in desiccators for two days before storage of samples in order to saturate the desiccators with the appropriate relative humidity.

2. A simple water uptake method was used to measure the percentage of water absorbed with time. Sponges were placed in 25 cm x 25 cm plates, and 250 ml water (the same volume of water in mucin-agar media) was added to wet the sponges. 30 mg of solid samples were placed on wetted filter paper on top of the sponges. Initial weight of both sample and wetted filter paper was recorded, and then weighed every 15 minutes to calculate the mass increase with time. The area under the curve (AUC) of uptake vs time was calculated to quantify the amount of water uptake with time.

2.5.4.14 Drug release

Drug release data was obtained for MH from MH:HPMC (1:1) microparticles in comparison to corresponding physical mixtures and MH powder, in weights equivalent to 1mg MH (according to drug content in the microparticles). A Franz-cell diffusion apparatus (explained in detail in Section 2.1.13) was used, in which distilled water (20 ml) was used as a dissolution medium in the receptor compartment, maintained at 37 ± 0.5°C, from which 0.5 ml samples were withdrawn at regular intervals, and substituted rapidly with fresh media. Samples were analysed for MH content using UV spectrophotometry at 233nm.

2.5.4.15 Statistical analysis

In the case of changing one factor of bioadhesion on different formulations, a one way ANOVA was used to identify statistically significant differences among the means of three samples or more. A T-test was used for two samples of equal variances, to analyse the significant differences among formulations by changing one

factor. These two tests were used for all analytical studies in this work. The differences were significant when the probability was $P \leq 0.05$.

The similarity factor (*f2*) was used to analyse the degree of similarity of the release profiles of MH formulations using the Equations 2.6 (Section 2.1.13.1). The dissimilarity was significant when $f2 < 50$ (Anderson et al 1998; Liu & Fassihi 2009).

Chapter 3

Developing aqueous-organic co-precipitation techniques for the preparation of bioadhesive microparticles using lactose as a model drug

3.1 Introduction

A significant amount of published work has been concerned with the use of solvent precipitation techniques for water insoluble or poorly soluble drugs, thus affording drug crystals with particular physiochemical properties to improve drug solubility, dissolution and bioavailability (Mishra et al 2003; Nokhodchi et al 2003; Adhiyaman & Basu 2006; Douroumis & Fahr 2007). Others have also employed this technique to increase the stability of vaccines or bioavailability of water soluble compounds such as small peptides and large proteins (Kreiner et al 2005; Kreiner & Parker 2005).

Solvent precipitation techniques result in the formation of different crystal forms and habits of drugs, and therefore different melting points, crystal size, shape, solubility and dissolution may be produced (Adhiyaman & Basu 2006). This is known as polymorphism. Lactose has four polymorphs, α-lactose monohydrate, β-lactose, stable anhydrous α-lactose and unstable hygroscopic anhydrous α-lactose (Kirk et al 2007). The common commercially available form is the α-monohydrate form, which originates from the milk of mammals (Rowe et al 2003b). Figure 3.1 shows the structure of lactose.

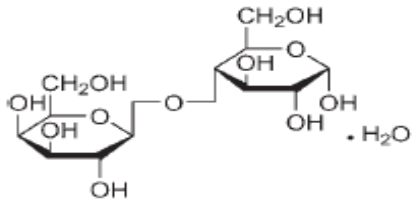

Figure 3.1 Chemical structure of lactose monohydrate, reproduced from Rowe et al (2003b).

Polymorphism can be identified by several analytical techniques. The phenomenon of lactose crystallisation and re-crystallisation after addition of different concentrations of acetone by SEM, DSC and XRPD was studied by Larhrib et al (2003). Using FT/IR, Kirk et al (2007) found that different crystal forms of lactose such as β-lactose (Lβ), stable anhydrous α-lactose (Lα-S) and unstable hygroscopic anhydrous α-lactose (LαH) could be identified using the IR region between 950-800cm^{-1}. Gustafsson used solid state NMR to study the amorphous component in the processed lactose (Gustafsson et al 1998).

In this chapter lactose was used as a water soluble model drug and HPMC was used as a bioadhesive support during the precipitation process, in which an aqueous solution of lactose and HPMC was precipitated using either IPA or acetone as a precipitating agent. The physical state of lactose within the precipitated lactose:HPMC (1:1) microparticles was investigated.

3.2 Materials and methods

The materials used in this chapter were α-lactose monohydrate, HPMC, IPA, and acetone, which were discussed in Section 2.2.

3.2.1 Determination the solubility of lactose

The solubility of lactose in water, IPA and acetone were determined using the technique described in Section 2.5.1.

3.2.2 The effect of formulation and processing variables on microparticle formation using mechanical stirrer

The effect of different processing parameters on the formation and physical properties of lactose and HPMC microparticles (alone and in combination) were studied using IPA and the preparation methods described in Section 2.5.3.1. The factors studied are summarised in Table 3.1.

Table 3.1 Processing parameters used for microparticle formation with IPA.

Formulation	Concentration of lactose (%w/w)	Concentration of HPMC (%w/w)	Stirring speed (rpm)	Needle gauge (g)	Dropping rate (ml/hr)
1	2	0	1500	23	10
2	4	0	1500	23	10
3	6	0	1500	23	10
4	8	0	1500	23	10
5	10	0	1500	23	10
6	12	0	1500	23	10
7	14	0	1500	23	10
8	16	0	1500	23	10
9	18	0	1500	23	10
10	20	0	1500	23	10
11	5	5	1000	19	10
12	5	5	1000	21	10
13	5	5	1000	23	10
14	5	5	1500	19	10
15	5	5	1500	21	10
16	5	5	1500	23	10
17	5	5	2000	19	10
18	5	5	2000	21	10
19	5	5	2000	23	10
20	5	5	2000	23	5
21	5	0	2000	23	10
22	0	5	2000	23	10
23	7.5	7.5	1000	19	10
24	7.5	7.5	1000	21	10
25	7.5	7.5	1000	23	10
26	7.5	7.5	1500	19	10
27	7.5	7.5	1500	21	10
28	7.5	7.5	1500	23	10
29	7.5	7.5	2000	19	10
30	7.5	7.5	2000	21	10
31	7.5	7.5	2000	23	10
32	7.5	0	2000	23	10
33	0	7.5	2000	23	10
34	10	10	1000	19	10
35	10	10	1000	21	10
36	10	10	1000	23	10
37	10	10	1500	19	10
38	10	10	1500	21	10
39	10	10	1500	23	10
40	10	10	2000	19	10
41	10	10	2000	21	10
42	10	10	2000	23	10
43	10	0	2000	23	10
44	0	10	2000	23	10
45	1	0	2000	23	10
46	2	0	2000	23	10
47	3	0	2000	23	10
48	4	0	2000	23	10
49	0	1	2000	23	10
50	0	2	2000	23	10
51	0	3	2000	23	10
52	0	4	2000	23	10
53	1	1	2000	23	10
54	2	2	2000	23	10
55	3	3	2000	23	10
56	4	4	2000	23	10

The effect of increasing concentration of lactose on microparticle morphology (shape and size) was studied in formulations 1-10 (Table 3.1), using light microscopy as discussed in Section 2.5.4.2 (at a constant stirring speed of 1500rpm). Three batches of lactose:HPMC (1:1) at a concentration of 5%, 7.5% and 10% w/w (formulations 19, 31 and 42) were studied to determine the effect of HPMC on the morphology of these combination microparticles in comparison to lactose only microparticles (formulations 21, 32 and 43, at a constant stirring speed of 2000rpm).

The effect of stirring speed (1000, 1500 and 2000 rpm), needle gauge (19g, 21g and 23g), lactose and HPMC concentrations (5%, 7.5% an 10%), and addition rate (5 and 10 ml/hour) on microparticle size and shape was also studied (formulations 11-42) using light microscopy (Section 2.5.4.2) and laser diffraction (Section 2.5.4.3).

3.2.3 Effect of stirring speed and temperature on lactose:HPMC microparticles using high shear mixer

Lactose:HPMC (1:1) microparticles prepared using a Silverson mixer (Section 2.5.3.2) were used to study the effect of three processing variables on their formation as shown in Table 3.2. The effect of stirring speed (7500 and 8000 rpm), temperature (25°C and 4°C ±0.5°C), precipitating agent (IPA and acetone), and lactose and HPMC (1:1) concentrations (3-5%) on particle size of lactose:HPMC microparticles was studied using laser diffraction (Section 2.5.4.3).

Table 3.2 Processing variables used for lactose:HPMC (1:1) formulations prepared using high shear mixer.

Formulation	Lactose concentration (%w/w)	HPMC concentration (%w/w)	Stirring speed (rpm)	Temperature (±0.5°C)	Precipitating agent
57	3	3	7500	25	IPA
58	4	4	7500	25	IPA
59	5	5	7500	25	IPA
60	3	3	7500	4	IPA
61	4	4	7500	4	IPA
62	3	3	7500	4	Acetone
63	4	4	7500	4	Acetone
64	3	3	8000	4	IPA
65	4	4	8000	4	IPA
66	3	3	8000	4	Acetone
67	4	4	8000	4	Acetone

3.2.4 Physiochemical properties of lactose:HPMC microparticles

The zeta potential of a diluted sample from the precipitation process, in concentrations of 1-10%w/w, was examined (n=3) to determine the physical interaction between lactose and HPMC (formulations 19, 31, 42 and 53-56) and compared with microparticles of lactose alone (formulations 21, 32, 43 and 45-48) and HPMC alone (formulations 22, 33, 44 and 49-52) as described in Section 2.5.4.5.

^{1}H-NMR was used to calculate the percentage of lactose and HPMC in formulation 19. The NMR spectrum of formulations 21 and 22 was obtained to investigate the presence of amorphous material. The method of analysis was explained in detail in Section 2.5.4.6.

Solid samples of HPMC (powder) were analysed using XRPD (Section 2.5.4.8), to determine the amorphous or crystalline content of HPMC.

DSC and FT/IR analysis of unprocessed materials, lactose only microparticles (formulations 21, 45-48), HPMC only microparticles (formulation 22) and different concentrations of lactose:HPMC (1:1) microparticles (formulations 19, 53-56) was performed using the methods outlined in Sections 2.5.4.9 and 2.5.4.7, to study lactose polymorphism and the effect of IPA on the resultant microparticles.

3.3 Results and discussion

3.3.1 Lactose solubility

It was found that concentrations of 1-20% w/w of lactose were soluble in distilled water (DW), producing a clear solution at 25 ±0.5°C. Above this concentration, undissolved lactose remained. This is in agreement with previous observations by Machado et al (2000). Lactose was found to be practically insoluble in both IPA and acetone.

According to the literatures, HPMC is insoluble in IPA and practically insoluble in acetone, but has certain solubility in aqueous-organic solutions (Rowe et al 2003a; Yamashita et al 2003). Therefore, it is expected that as the ratio of organic solvent in the mixture increases, HPMC solubility in that mixture decreases. Based on this information, a 1:20 volume ratio of DW:solvent (IPA or acetone) was used to prepare lactose, HPMC and lactose:HPMC (1:1) microparticles.

3.3.2 Lactose microparticle suspensions

Images obtained for formulation 1 using brightfield and polarised light microscopy confirmed crystalline structure in unprocessed lactose material and following precipitation, as shown in Figure 3.2. It appeared that the maximum crystal size of lactose became smaller and finer (90μm) following precipitation with IPA. A similar observation was described by Kreiner and co-authors for protein coated microcrystals (Kreiner et al 2001; Kreiner et al 2005).

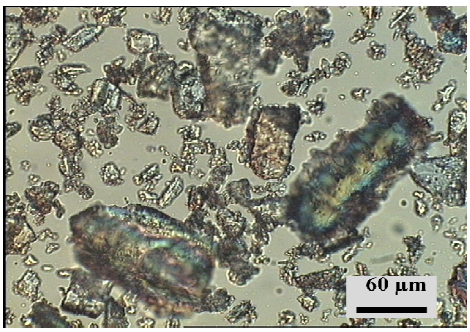

(a) Maximum particle size 200 µm

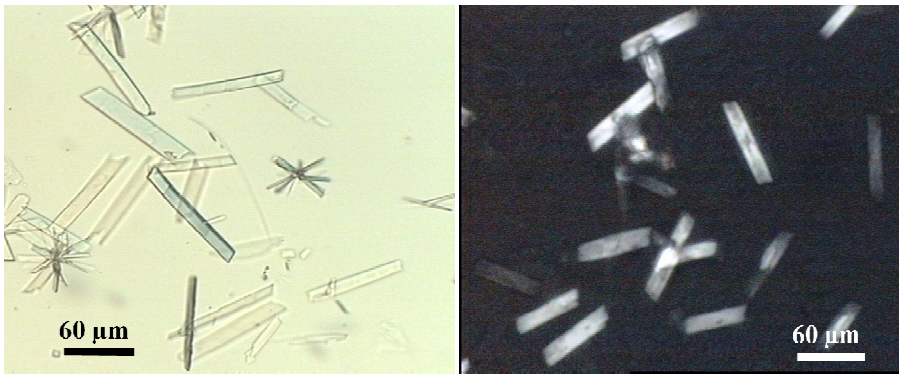

(b) Maximum crystal size 90 µm

Figure 3.2 Photomicrographs of (a) lactose powder and (b) precipitated lactose (formulation 1). The maximum size (length) of lactose microcrystals became smaller and finer following precipitation with IPA.

It was found that as the concentration of lactose increased, maximum resultant microcrystal size decreased (as determined by light microscopy, Figure 3.3) and aggregated forms appeared as shown in Figure 3.4, particularly at high concentrations. A similar result was obtained by Yudin and co-workers, who found that increasing nitrate solution concentration, lead to a decrease in the size of the crystals in the precipitate. This is in agreement with commonly accepted views of crystal formation from solutions (Yudin et al 1974). In order to initiate nucleation and promote a high growth rate, a high degree of super saturation is required (Pechkova & Nicolini 2003). In the current work, as the concentration of lactose solution increased, rapid nucleation and growth rate occurred.

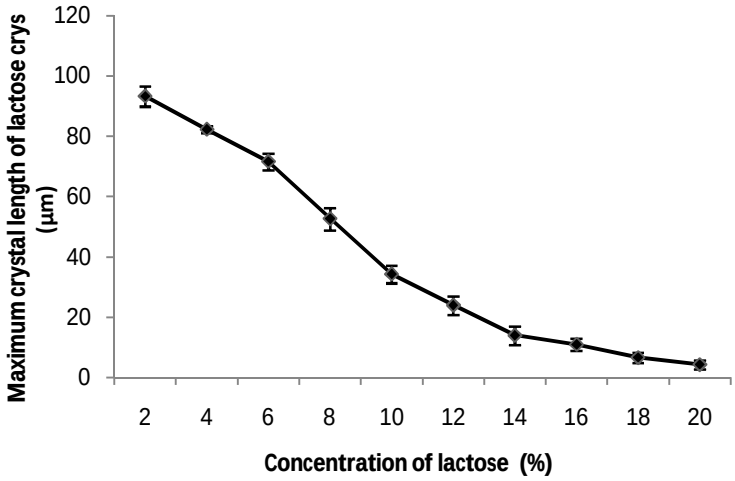

Figure 3.3 Effect of increasing concentration of lactose (formulations 1-10) on the maximum size (length) of lactose crystals using light microscopy, n=3. As the concentration of lactose increased, a smaller crystal size was obtained.

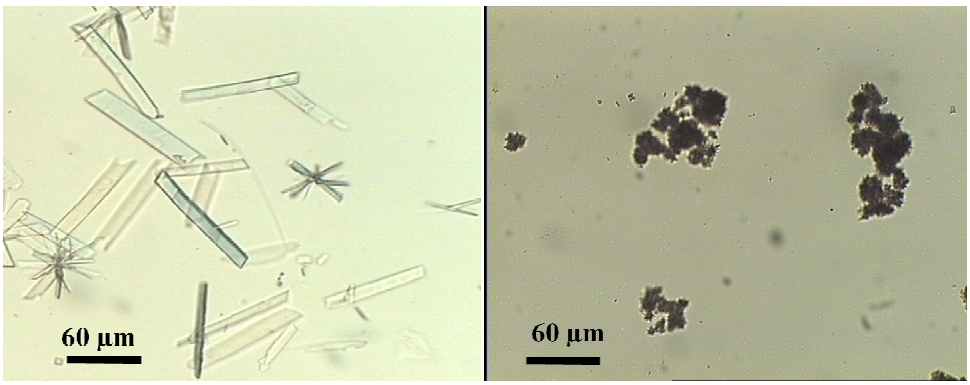

(a) Maximum crystal length 90 µm (b) Maximum crystal length 2 µm

Figure 3.4 Lactose microcrystals a) formulation 1 (2% w/w lactose) and b) formulation 10 (20% w/w lactose), using light microscopy. At high concentrations (20% lactose [formulation 10]), aggregates of lactose crystals appeared.

3.3.3 Effect of HPMC on lactose microparticle suspensions

Following the previous Section (3.3.2), where formulations of lactose alone were considered, combinations of lactose:HPMC (1:1) were studied. In some instances, two distinct layers were observed during the precipitation. A lower layer (L) consisted of large white particle aggregates, while the upper layer (U) contained fine suspended particles. At concentrations of 1-3% a homogenous suspension of precipitated particles was obtained. However, above this concentration (4%, 5%, 7.5% and 10% w/w), two layers were observed, with increasing concentration of lactose:HPMC (1:1) resulting in a higher proportion of material in the lower layer. It is suggested that this results from the higher viscosity gels inhibiting discrete droplet formation during the addition process, permitting the development of larger domains of viscous material that resisted solvent penetration.

The material in the upper layer was considered for further analysis. Figure 3.5 summarises the difference in microcrystal morphology of precipitated material from the upper layers at concentrations of 5%, 7.5% and 10% w/w of lactose alone (formulations 21, 32 and 43 respectively) and lactose:HPMC (1:1) (formulations 19, 31 and 42 respectively).

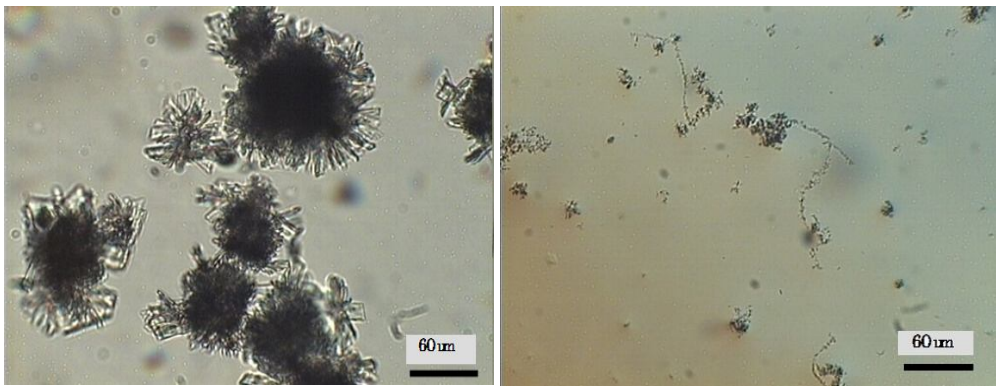

a) 5% lactose (M.C.S* 60µm) b) 5% lactose:HPMC (1:1) (M.C.S 2µm)

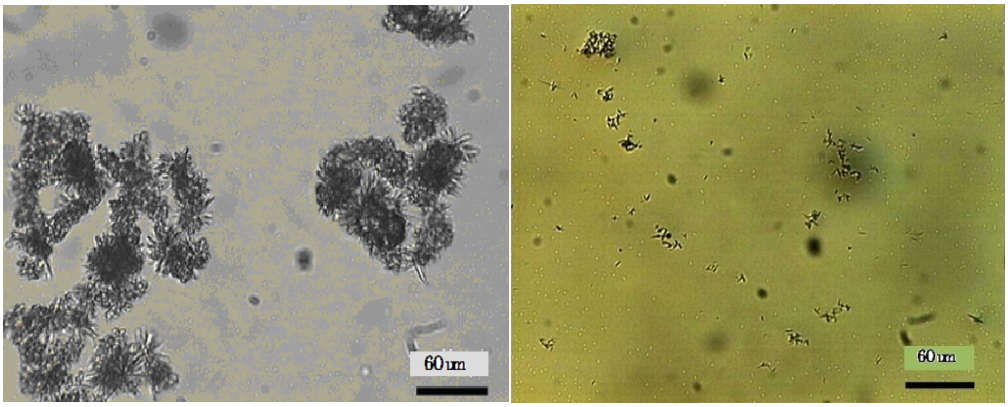

c) 7.5% lactose (M.C.S 20µm) d) 7.5% lactose:HPMC (1:1) (M.C.S 4.3µm)

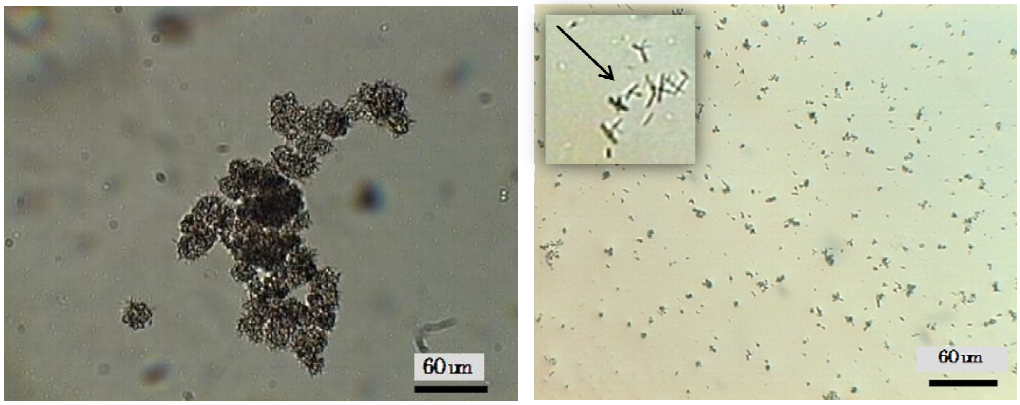

e) 10% lactose (M.C.S 12µm) f) 10% lactose:HPMC (1:1) (M.C.S 4.5 µm)

Figure 3.5 Photomicrographs showing a), c) and e) lactose microcrystals alone (formulations 21, 32 and 43) and b), d) and f) lactose:HPMC (1:1) (formulations 19, 31 and 42), using 2000 rpm stirring speed, 23 g of needle gauge and 10 ml/ hour dropping rate.

*Maximum crystal size (M.C.S)

It appeared that the presence of HPMC prevented the large particle aggregation observed with lactose alone and resulted in a dispersion of more uniform microparticles. This finding is confirmed by reports in the literature that HPMC possesses surface activity (Chang & Gray 1978; Brogly et al 2010), suggesting HPMC may interact with precipitated lactose to lower the interfacial tension and modify crystal growth.

Zeta potential measurements are conventionally performed in an aqueous environment. We have applied the technique to the suspensions resulting from the dropping process which are composed of DW:IPA (1:20). Data obtained from microparticle suspensions of lactose alone, HPMC alone and lactose:HPMC are shown in Figure 3.6.

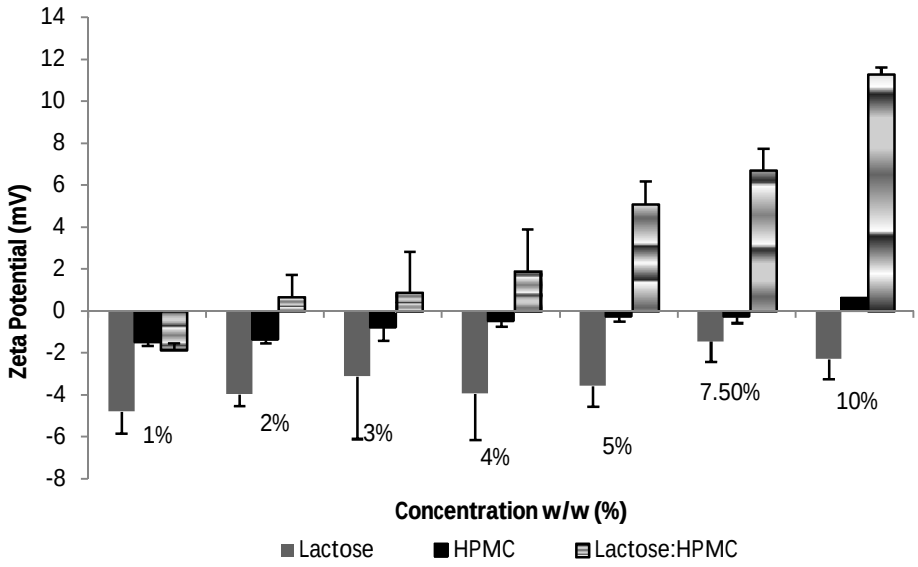

Figure 3.6 Zeta potential measurement of 1-10%w/w microparticle suspensions of lactose formulations (45-48, 21, 32 and 43), HPMC blank formulations (49-52, 22, 33 and 44) and lactose:HPMC (1:1) formulations (53-56, 19, 31 and 42), using 2000 rpm stirring speed, 23g of needle guage and 10 ml/ hour dropping rate, n=3. The zeta potential of lactose:HPMC (1:1) microparticles increased as the concentration of the mixture increased.

The zeta potential values of HPMC and lactose microparticles were negative in the essentially non-aqueous environment, however the zeta potential of lactose:HPMC microparticles increased from -1.85mV ± 0.31 to 11.3mV ± 0.33 as the concentration of the mixture increased (1-10% w/w). The data suggest that particles prepared from the combination of lactose:HPMC (1:1) behave differently from particles of lactose or HPMC alone, although the reason for this is unclear due to the non-aqueous environment.

3.3.4 Effect of processing factors

Figure 3.7 shows the effect of stirring speed (1000-2000rpm) on the particle size of lactose:HPMC (1:1) formulations (5%, 7.5% and 10%), dropped into IPA using a 23g needle. The microparticles became finer with a more needle like structure as the speed increased, suggesting that the rate of crystal growth was modified (Chang & Gray 1978; Reekmans 1998), due to more efficient dispersion of the aqueous phase into the IPA. Li et al (2007) suggested that greater stirring speeds intensified the micro-mixing between multi-phases, enhancing mass transfer and the rate of diffusion between the phases, resulting in homogenous super saturation in a very short time. Thus rapid nucleation resulted in formation of smaller microparticles during precipitation.

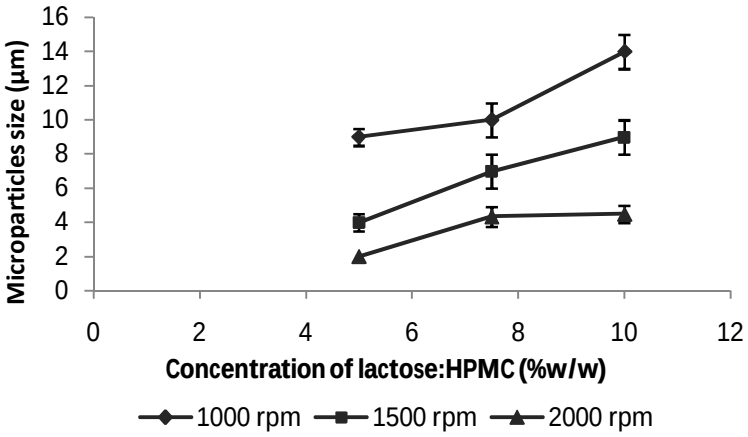

Figure 3.7 Effect of stirring speed on three concentrations of lactose:HPMC (1:1) microparticle formulations using needle gauge of 23g; formulations 13, 25 and 36 (5%, 7.5% and 10% w/w lactose:HPMC respectively) at 1000 rpm stirring speed, formulations 16, 28 and 39 (5%, 7.5% and 10% w/w lactose:HPMC respectively) at 1500 rpm stirring speed and formulations 19, 31 and 42 (5%, 7.5% and 10% w/w lactose:HPMC respectively) at 2000 rpm stirring speed , n=3.

The effect of using different needle gauges on the maximum size of lactose:HPMC (1:1) microparticles, with a fixed stirring speed (1000 rpm), is shown in Figure 3.8. A smaller gauge produced smaller crystals, as a result of the smaller drop volume. However, as the concentration increased, viscosity factors overcame this effect and larger drops were formed. Consequently a non significant effect on microparticle size was produced.

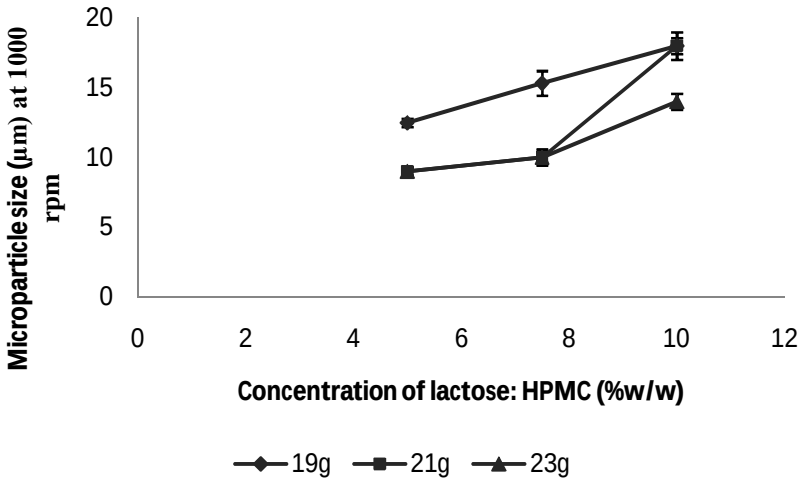

Figure 3.8 Effect of needle gauge on the size of lactose:HPMC (1:1) microparticle formulations using 1000 rpm stirring speed; formulations 11, 23 and 34 (5%, 7.5% and 10% lactose:HPMC), using needle gauge of 19 g, formulations 12, 24 and 35 (5%, 7.5% and 10% lactose:HPMC), using needle gauge of 21 g and formulations 13, 25 and 36 (5%, 7.5% and 10% lactose:HPMC), using needle gauge of 23 g, n=3.

Laser diffraction was employed to determine the effect of addition rate (5 or 10 ml/hour) on particle size for a 5% lactose:HPMC (1:1) formulation, at a fixed stirring speed and needle gauge (2000rpm and 23g respectively). The results are illustrated in Figure 3.9. The mean size of particles produced by a dropping rate of 5 ml/hour was 11.833 ±0.3 µm, while the mean particle size produced by a dropping rate of 10 ml/hour was 15.782 ±1.6 µm. The slower the dropping rate of 5 ml/hour gave more opportunity for nucleation to occur, thereby producing particles with finer size. In both cases, polydispersity was observed.

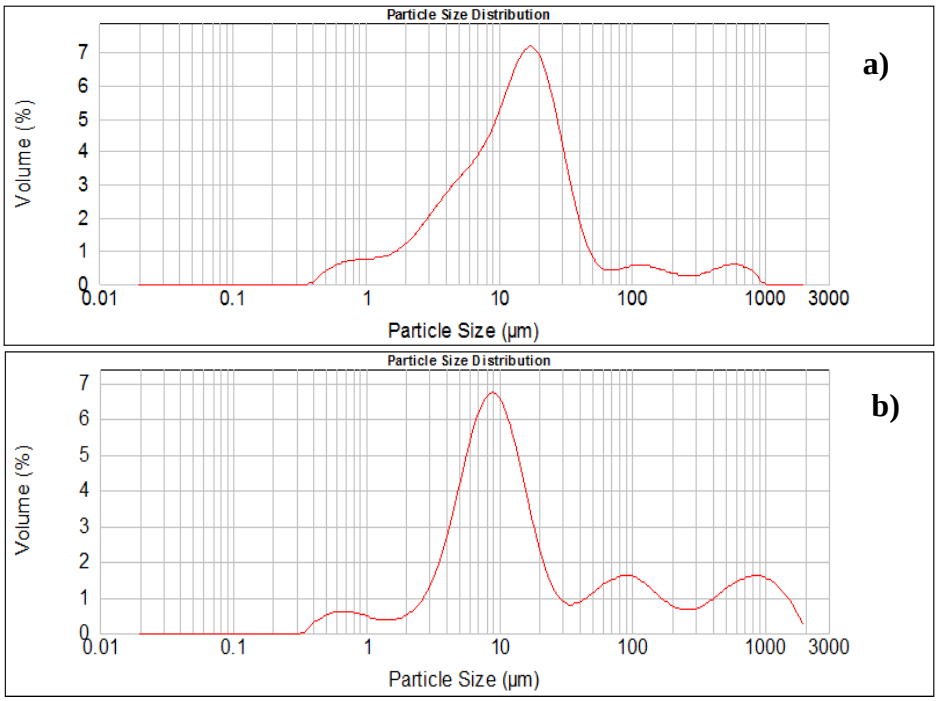

Figure 3.9 Effect of dropping rate on the mean size of 5% lactose:HPMC (1:1) microparticle of a) formulation 19 and b) formulation 20, using 10 ml/hr and 5 ml/hr dropping rate respectively with a needle gauge of 23 g and 2000 rpm stirring speed, n=3.

To summarise the outcomes of the processing variables, it was found that conditions used for formulation 19 (i.e. lactose:HPMC (1:1) at a concentration of 5%, 2000 rpm stirring speed, 23g needle and 10 ml/hour dropping rate), produced an acceptable microparticle product in the upper layer. However, a significant proportion of material was recovered from the lower layer. Therefore, further studies employed collection of both upper and lower precipitates by filtration, as described in Section 2.5.3.1.

3.3.5 Characterisation of dried lactose:HPMC microparticles

Combined precipitates (upper and lower) from formulations 19, 31 and 42 were collected by filtration (as described in Section 2.5.3.1), and following drying are

shown in Figure 3.10. As the concentration increased, the nature of the precipitate changed from aggregated particles to thread like agglomerates, reflecting the viscosity effect of the polymer and lack of dispersion in the IPA, as discussed previously (Section 3.3.3.).

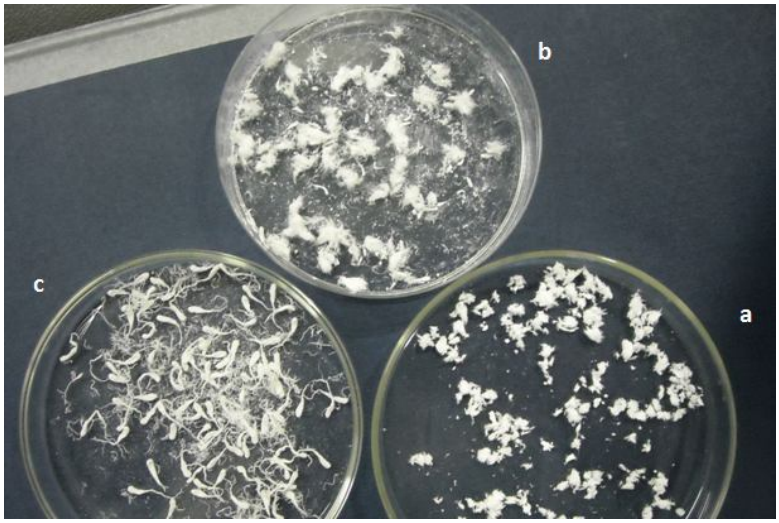

Figure 3.10 The final microparticle products of a) 5% lactose:HPMC (1:1) (formulation 19), b) 7.5% lactose:HPMC (1:1) (formulation 31) and c) 10% lactose:HPMC (1:1) (formulation 42), using 2000 rpm stirring speed, needle gauge of 23 g and 10 ml /hr dropping rate. As the concentration of HPMC increased, the nature of the precipitate changed from aggregated particles to thread like agglomerates.

3.3.5.1 Nuclear magnetic resonance spectroscopy (^{1}H-NMR)

In order to investigate the characteristics of precipitates from the upper and lower layers independently, the two layers were collected and dried, according to the methods described in Section 2.5.3.1. NMR was used to calculate the percentage of lactose and HPMC in the two layers and the spectra relative to diclofenac as an internal standard are shown in Figure 3.11, together with the spectra for pure lactose and HPMC. The peaks of α and β-galactose of lactose and HPMC are identified.

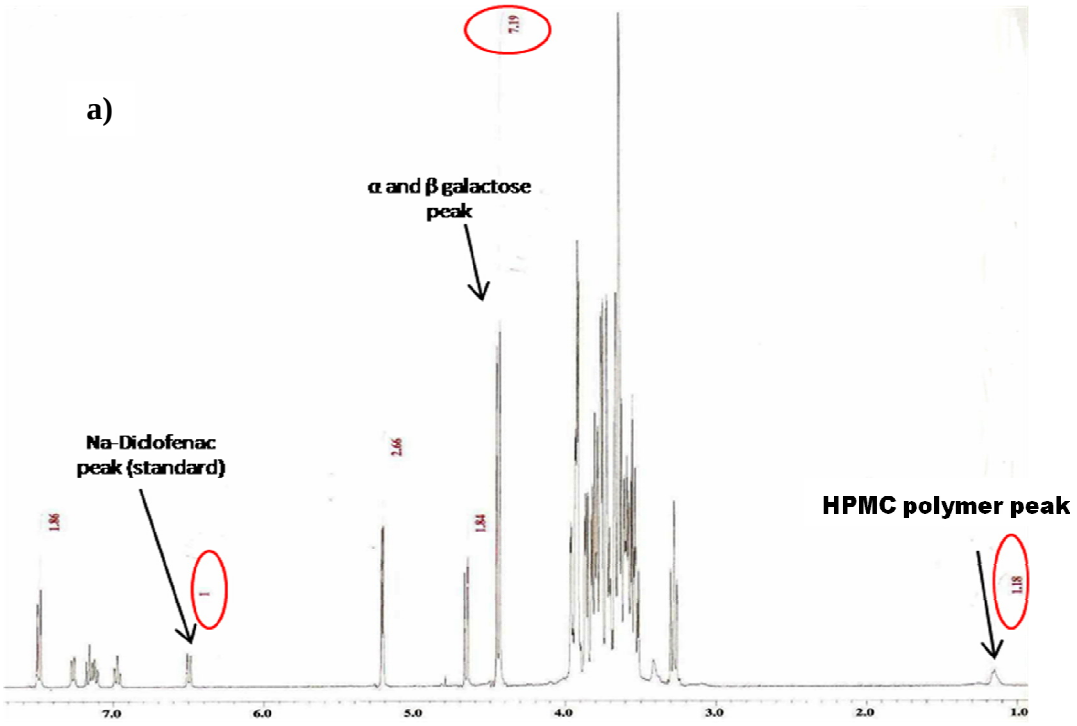
a)
α and β galactose peak
Na-Diclofenac peak (standard)
HPMC polymer peak
7.19
2.66
1.86
1.84
1
1.18
7.0
6.0
5.0
4.0
3.0
2.0
1.0

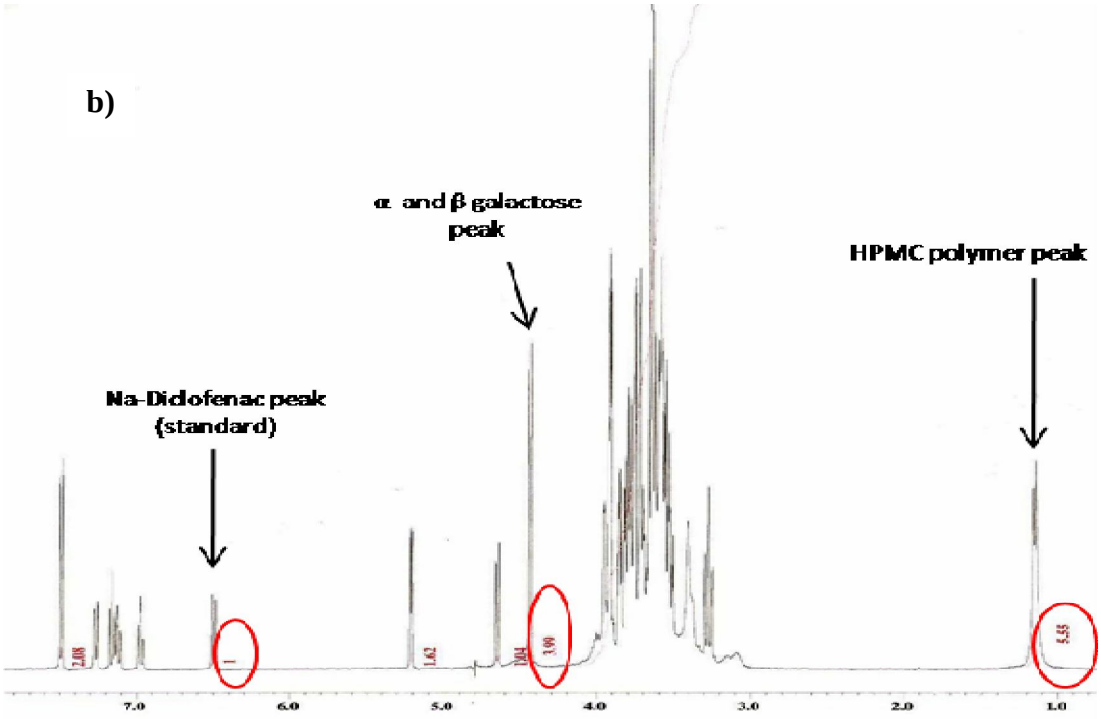
b)
α and β galactose peak
HPMC polymer peak
Na-Diclofenac peak (standard)
2.08
1
1.62
1.04
3.00
5.83
7.0
6.0
5.0
4.0
3.0
2.0
1.0

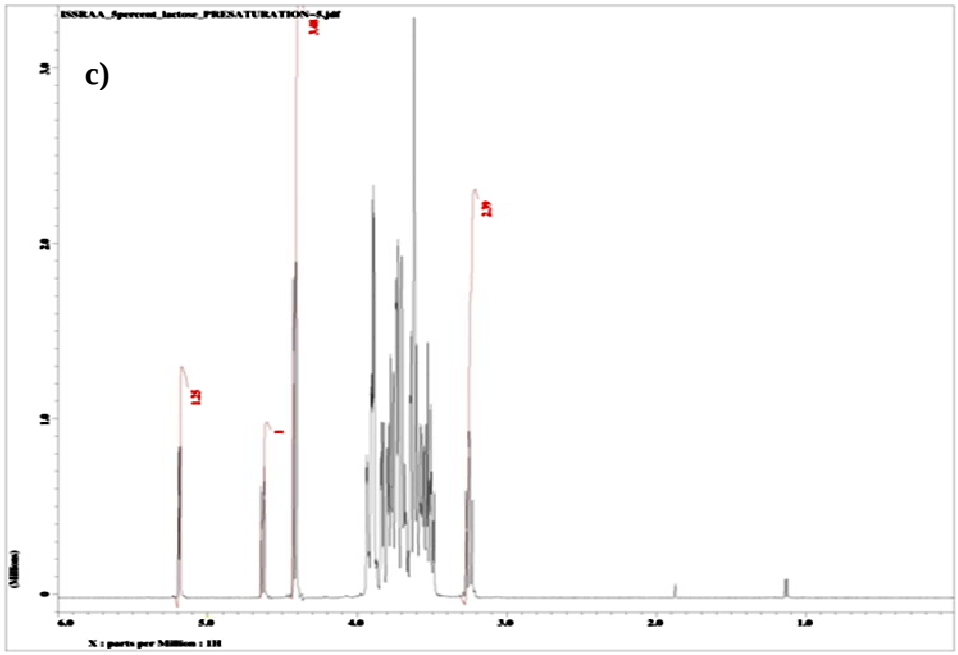

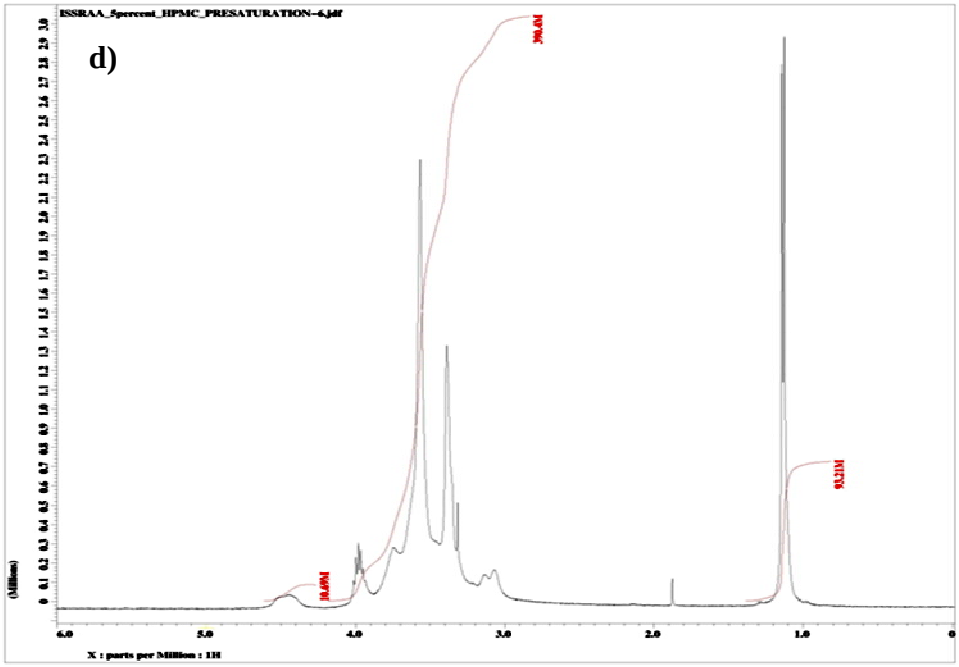

Figure 3.11 ^{1}H-NMR spectrum of formulation 19 (5%lactose:HPMC 1:1) a) upper and b) lower layer, relative to a diclofenac standard, c) pure lactose and d) pure HPMC.

The calculated percentage content of lactose and HPMC in the upper and lower layers is shown in Table 3.3.

Table 3.3 Percent of lactose and HPMC in the upper and lower layer of formulation 19 (5% lactose:HPMC 1:1).

Layer of formulation 19	Percent of lactose (%)	Percent of HPMC (%)
Upper	64.31	17.53
Lower	35.68	82.46

It is noted that HPMC has broad peak between 3-4 ppm in comparison to lactose (Figure 3.11c and d), and microparticles in the lower layer of formulation 19 have a widened peak in comparison to those of the upper layer. That confirmed the calculations obtained previously in which HPMC predominated in the lower layer. The distribution of lactose in each layer was not uniform, even though a 1:1 ratio of lactose and HPMC was used as an initial concentration of the aqueous gel before precipitation in IPA. This suggests that the low shearing efficiency of the mechanical stirrer to the viscous drops of lactose:HPMC gel in IPA precipitated aggregations of thick HPMC associated with some lactose in the lower layer in comparison to fine particles in the upper layer.

3.3.5.2 Fourier transform infrared spectroscopy

Figure 3.12 shows the infrared spectrum of HPMC, formulations 22 (5% HPMC), 19U (5% lactose:HPMC upper layer), 19L (5% lactose:HPMC lower layer), 21 (5% lactose) and lactose. A comparison of the spectra for HPMC and formulation 22 (Figure 3.12a and b respectively), shows that the process of precipitation in IPA did not affect the spectra. Similarly, there were no changes in the spectrum of processed 5% lactose compared to the unprocessed material (Figure 3.12e and f).

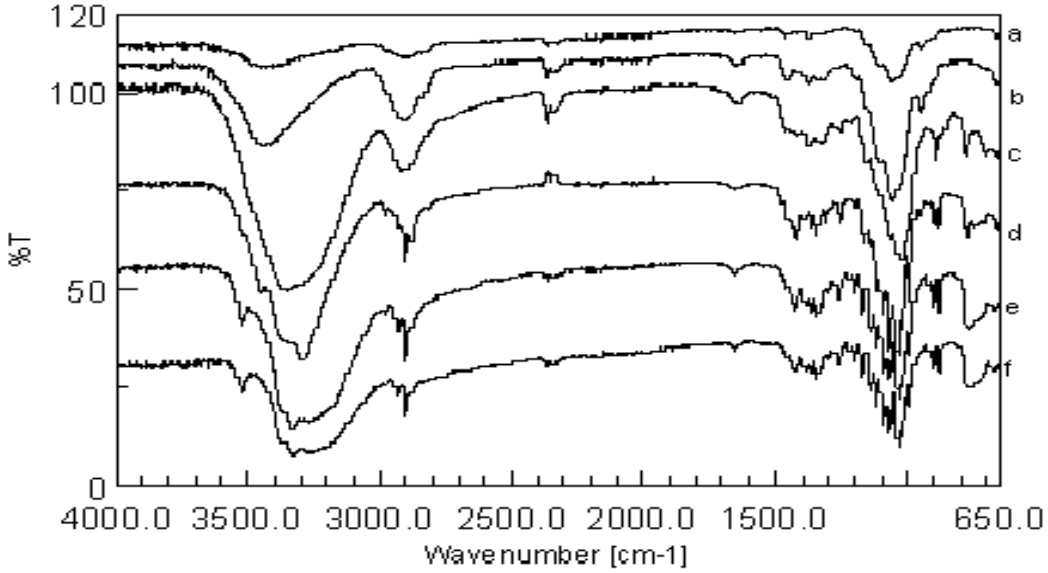

Figure 3.12 FT/IR Spectrums of a) HPMC, b) formulation 22 (5% HPMC), c) formulation 19U (5% lactose:HPMC 1:1), d) formulation 19L (5% lactose:HPMC 1:1), e) formulation 21 (5% lactose) and f) lactose. The formulations were prepared using 2000 rpm stirring speed, needle gauge of 23 g and 10 ml/hr dropping rate.

However, it is noted from the lactose only spectra (Figure 3.12e and f) that there are vibrations present at approximately 3524cm^{-1} that are not observed within the upper and lower layers of formulation 19 as shown in Figure 3.12c and d respectively. This is attributed to free O-H vibrations from water molecules in the monohydrate of lactose. This suggests the formation of the anhydrous form of lactose in formulation 19, when processed in the presence of HPMC polymer. The high content of O-H groups in HPMC produces a possible mechanism to explain this effect. Hydrogen bonding may occur between the HPMC and lactose at the site where water molecules would interact with lactose in the hydrate form. Thus the anhydrous form of lactose is produced for both layers. This interaction may occur at different sites on HPMC molecules which contain hydroxyl groups as well as oxygen groups as shown in Figure 3.13a. Also, lactose molecules have the same functional groups (Figure 3.13b) as HPMC.

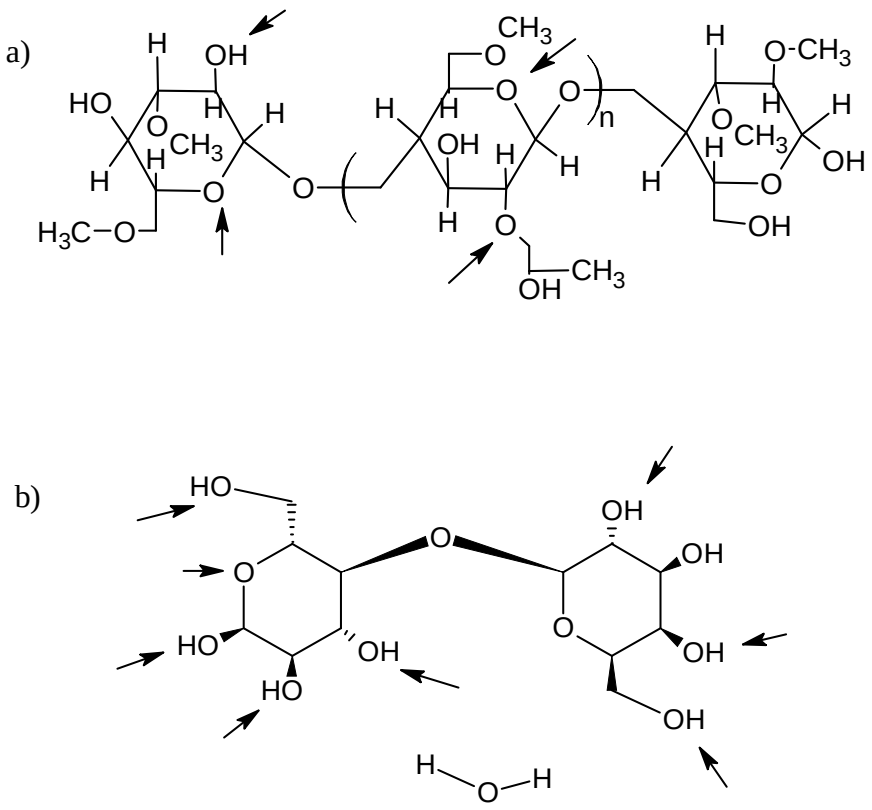

Figure 3.13 Possible sites of interaction between a) HPMC and b) lactose. Any hydroxyl and oxygen groups in the cellulose ring of HPMC (indicated by arrows) may interact with lactose.

This similarity in structure can enhance solute-polymer interaction (Katzhendler et al 1998), as observed in the region of absorbance between 3000- 3600 cm^{-1}, which is a diagnostic area of water molecules and H-bonding.

A more detailed examination of selected spectra above is shown in Figure 3.14, focussing on the vibrations ranging from 980-781 cm^{-1}.

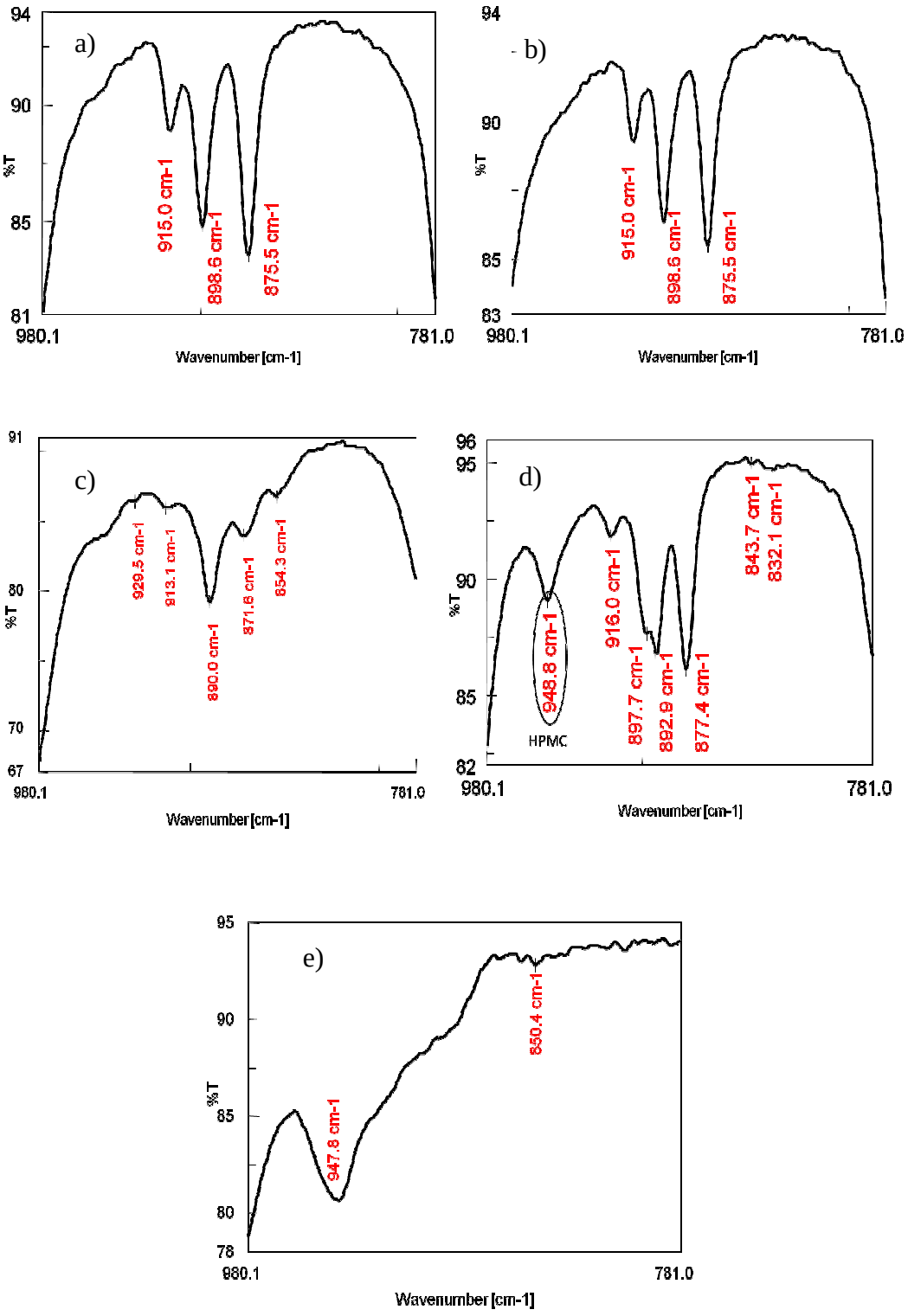

Figure 3.14 FT/IR spectra of different formulations in the region between 980- 780 cm $^{-1}$; a) Lactose, b) formulation 21 (5% lactose), c) formulation 19U (5% lactose:HPMC), d) formulation 19L (5% lactose:HPMC) and e) formulation 22 (5% HPMC).

According to Kirk et al (2007), the region ranging from 980-781 cm^{-1} can be an indicative part of the spectrum for polymorphism of lactose, relating to stretching and twisting of the C-H bond. In the studies shown in Figure 3.14a and b above, three vibrations appeared at 915 cm^{-1}, 898.6 cm^{-1}, 875.5cm^{-1}, while for the upper layer of formulation 19 in Figure 3.14c ; 929.5 cm^{-1}, 913.1 cm^{-1}, 890 cm^{-1}, 871.6 cm^{-1} and 854.3 cm^{-1}, which are reported to be related to anhydrous stable α-lactose (Kirk et al 2007). For the lower layer of formulation 19 in Figure 3.14d; 948.8 cm^{-1}, 916 cm^{-1}, 892.9 cm^{-1}, 877.4 cm^{-1}, 843.7 cm^{-1} and 832.1 cm^{-1}, were observed. Kirk suggested that a mixture of anhydrous β- and unstable α-lactose should show; 948 cm^{-1}, 892 cm^{-1}, 877 cm^{-1} and 833 cm^{-1} and the latter; 913 cm^{-1}, 892 cm^{-1}, 874 cm^{-1} and 855 cm^{-1} wave numbers (Kirk et al 2007), similar to those found in our studies. However, further analysis is required to confirm this finding suggesting lactose polymorphism as a result of processing.

The spectrum of the lower layer of formulation 19 has a predominant peak of HPMC at 947 cm^{-1} when compared with the spectrum of formulation 22 (5% HPMC) as shown in Figure 3.14d and e respectively . This result was in agreement with NMR finding that HPMC concentrated in the lower layer rather than the upper layer of formulation 19.

It was therefore hypothesised that processing lactose with HPMC polymer produced polymorphisms of lactose. In order to confirm this, the FT/IR spectrum of lactose:HPMC (1:1) microparticle formulations 53-55 (1%, 2%, 3%, which produced a single layer), and the lower layers of formulations 56 and 19 (4% and 5% w/w respectively) were investigated, to attempt to determine the concentration of HPMC required to induce polymorphism of lactose. Figure 3.15 demonstrates the spectra of these samples.

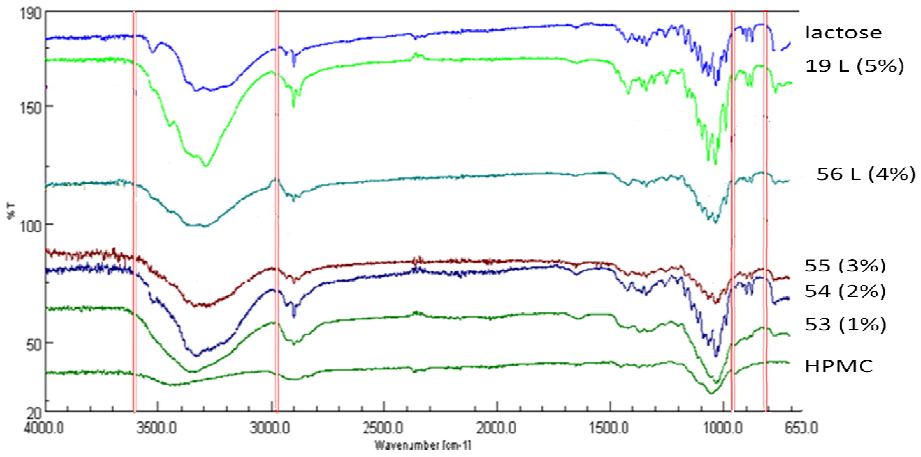

Figure 3.15 FT/IR spectra of different concentrations of lactose:HPMC (1:1) microparticles; formulation 19 (5% lactose:HPMC), formulation 56 (4% lactose:HPMC), formulation 55 (3% lactose:HPMC), formulation 54 (2% lactose:HPMC) and formulation 53 (1% lactose:HPMC), using 2000 rpm stirring speed, needle gauge of 23g and 10 ml/hr dropping rate.

The area between 3000-3600 cm^{-1} and 980-780 cm^{-1} are indicative for hydrogen bonding and polymorphism respectively as mentioned previously. It was found that as the concentration of HPMC increased, the hydrate form of lactose decreased, as demonstrated by the disappearance of the peak at 3524 cm^{-1}, due to HPMC polymer interacting with lactose by hydrogen bonding, modifying the crystal habit. The 980-780 cm^{-1} region for the above spectra, are shown in detail in Figure 3.16.

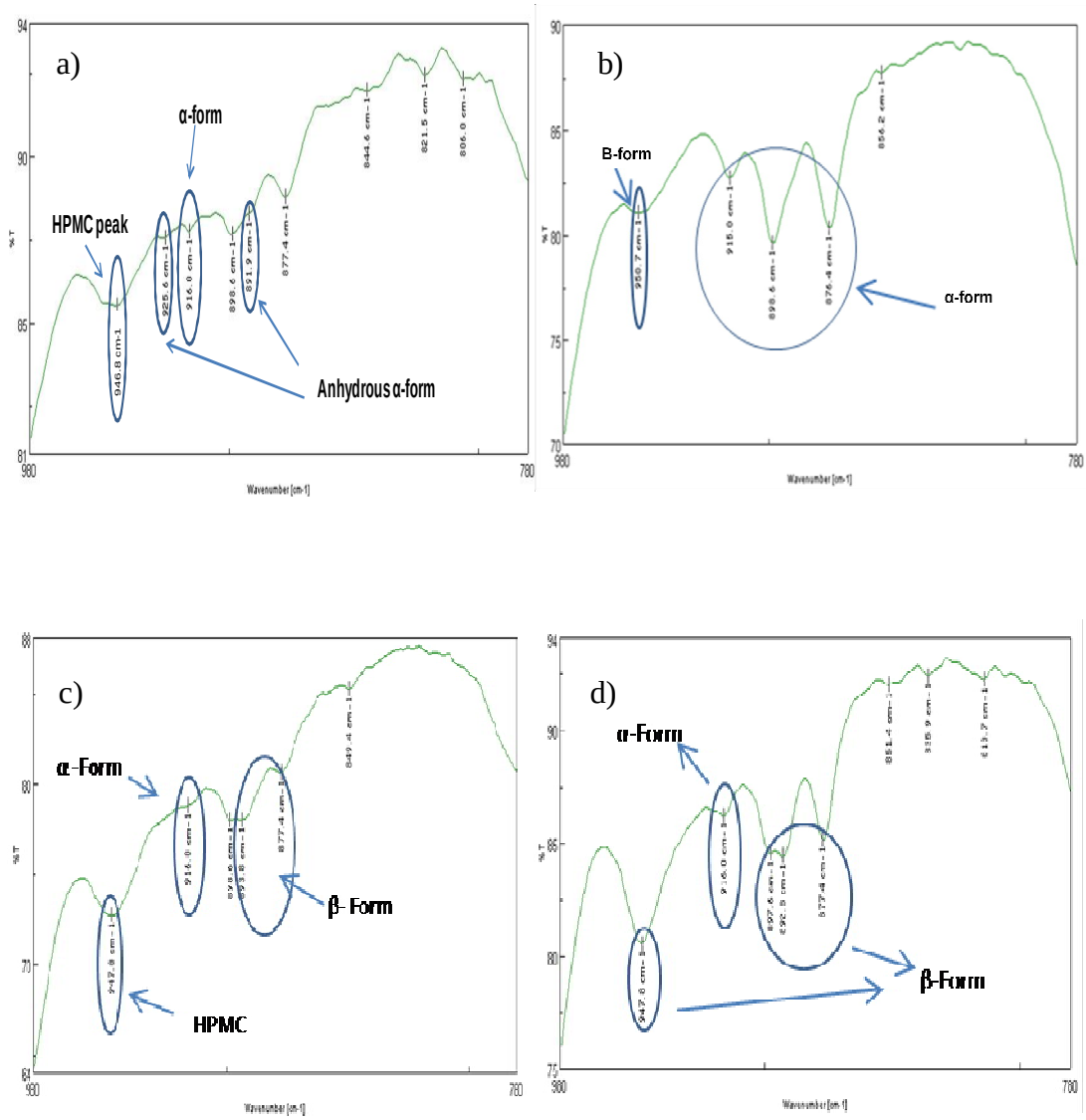

Figure 3.16 FT/IR spectra of a) formulation 53 (1% lactose:HPMC), b) formulation 54 (2% lactose:HPMC), c) formulation 55 (3% lactose:HPMC) and d) formulation 56L (4% lactose:HPMC) (with tentative peak assignments based on literature data on lactose alone), using 2000 rpm stirring speed, needle gauge of 23g and 10 ml/hr dropping rate.

Figure 3.16a shows that 1% lactose:HPMC (1:1) microparticles demonstrated a peak at 947 cm^{-1}, previously assigned to HPMC in Figure 3.14e, and peaks at 891 cm^{-1} and 926 cm^{-1}, previously assigned to anhydrous stable α-lactose. Figure 3.16b shows clear peaks assigned to α-lactose monohydrate at 915 cm^{-1}, 899 cm^{-1} and 876 cm^{-1}

and one peak assigned to the β-form at 950 cm^{-1}. At the 3% concentration (formulation 55), the peak assigned to the β-form starts to predominate over the α-form (Figure 3.16c). For formulation 56 L (4% lactose:HPMC), the peak assigned to the β-form also dominated compared to the peak assigned to the α-form as shown in Figure 3.16d. The 5% lactose:HPMC (formulation 19 L) showed peaks assigned to the predominate β-form of lactose as previously discussed (Figure 3.14d). This finding that as the concentration of HPMC increased the incidence of the β-form of lactose also increased.

Itoh and co-workers used IR spectra to differentiate between unstable anhydrous α-lactose and stable α-lactose hydrate using the region of spectrum; 800-1000 cm^{-1}, 1200-1400 cm^{-1} and 2700-3600 cm^{-1} (Itoh et al 1977). Another study used the region of 800-1000 cm^{-1} only as a main diagnostic area of lactose polymorphism (Kirk et al 2007). Crisp found that one distinct difference between the spectrum of α-lactose monohydrate and the anhydrous polymorphs are the vibrational bands at 1650 cm^{-1} and 3500 cm^{-1}. These stretches are indicative of the free water molecules within the lattice (Crisp et al 2010).

Another series of studies were performed on lactose in the absence of HPMC, to determine whether the concentration of lactose in the dropping solution might influence the resultant polymorphism. The FT/IR spectrums of lactose microparticles formed from 1%, 2%, 3%, 4% and 5% lactose solutions (formulations 45-48 and 21) are shown in Figure 3.17, and compared with lactose powder.

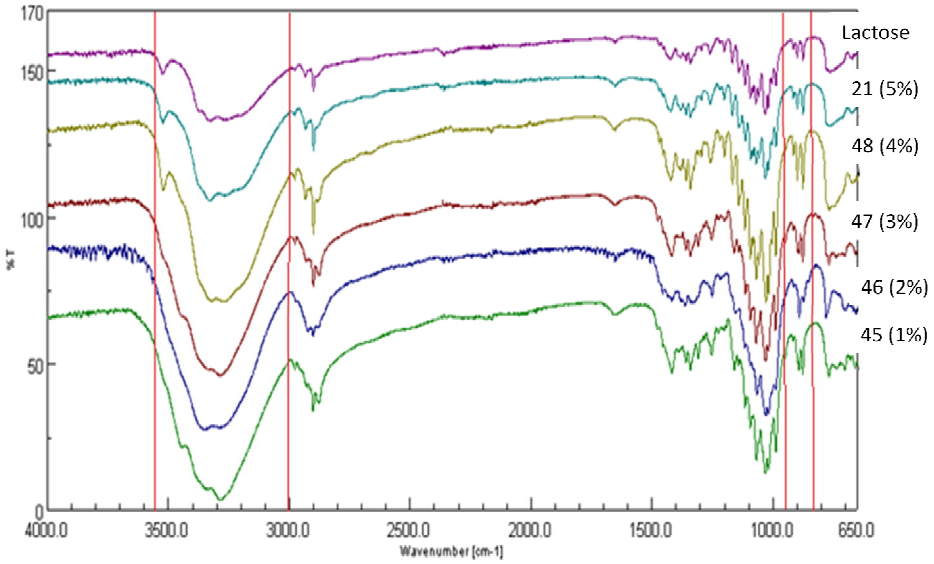

Figure 3.17 FT/IR spectra of different concentrations of lactose microcrystals, compared with lactose powder; formulation 21 (5% lactose), formulation 48 (4% lactose), formulation 47 (3% lactose), formulation 46 (2% lactose) and formulation 45 (1% lactose), using 2000 rpm stirring speed, needle gauge of 23g and 10 ml/hr dropping rate.

The region between 3000-3600 cm^{-1} in Figure 3.17, demonstrates that as the concentration of lactose increases, the presence of the α-lactose monohydrate peak predominates, possibly due to the solvate effect of IPA at lower concentrations of lactose. The wave numbers in the region 980-780 cm^{-1} are examined in detail in Figure 3.18.

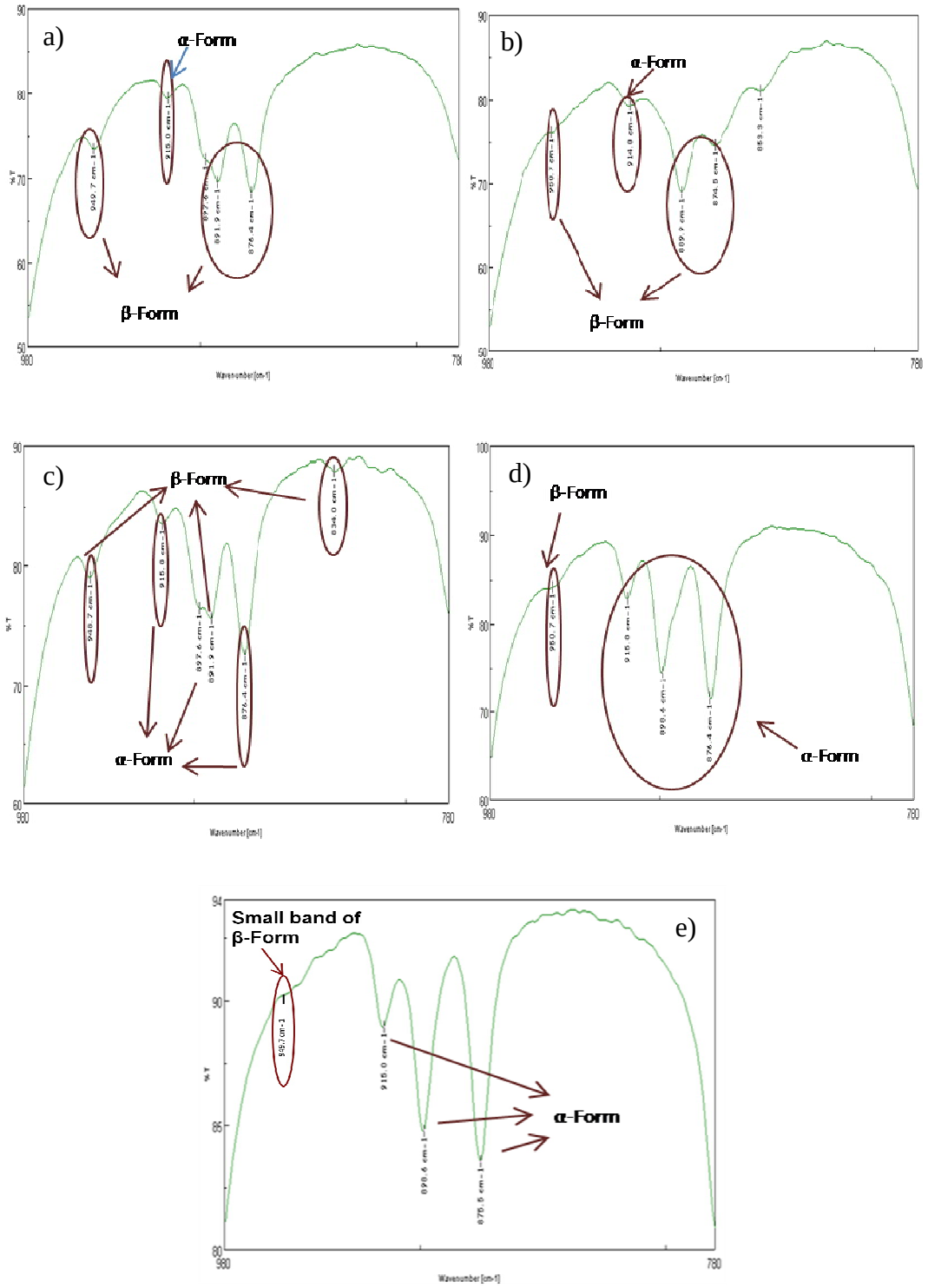

Figure 3.18 FT/IR spectra of different concentrations of precipitated lactose; a) formulation 45 (1% lactose), b) formulation 46 (2% lactose), c) formulation 47 (3% lactose), d) formulation 48 (4% lactose) and e) formulation 21 (5% lactose), using 2000 rpm stirring speed, needle gauge of 23g and 10 ml/hr dropping rate.

As the concentration of lactose decreased, the peaks assigned to the anhydrous β-form dominated in comparison to those assigned to the α-form (Figure 3.18). This could be due to the lower lactose concentration treated with large volume of IPA, as many literature reports show the effect of solvent on incidence of polymorphism (Blagden et al 1998; Maruyama & Ooshima 2000, 2001).

3.3.5.3 Differential scanning calorimetry

The formulations previously investigated using FT/IR were further examined using DSC. The thermograms are shown in Figure 3.19.

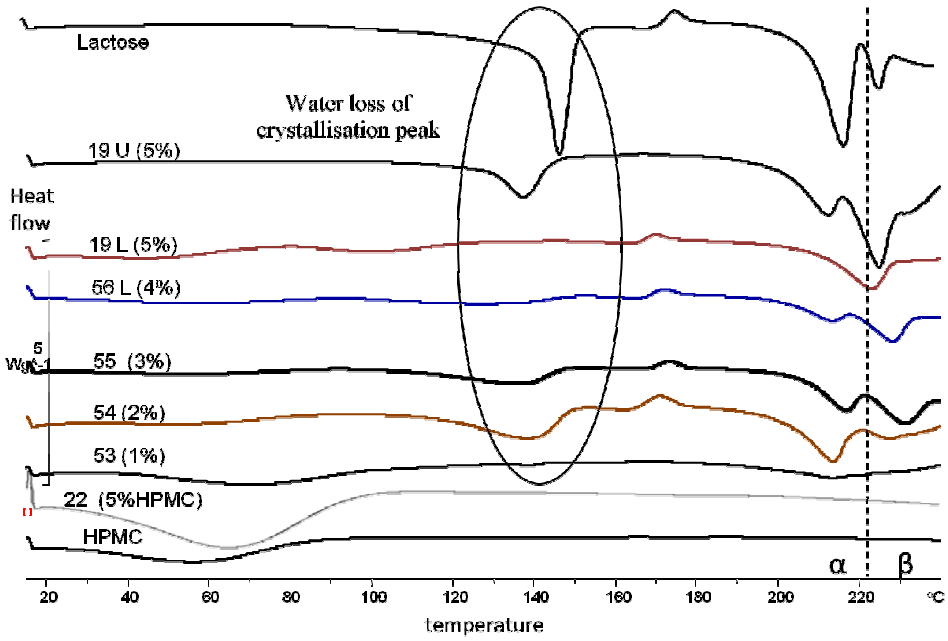

Figure 3.19 DSC thermograms of lactose, lactose:HPMC (1:1) microparticle formulations 19 U, 19 L, 56 L, 55, 54 and 53, HPMC microparticle formulation 22 and HPMC. The formulations were precipitated by IPA, using 2000 rpm stirring speed, needle gauge of 23g and 10 ml/hr dropping rate.

For HPMC, there is an endothermic broad peak between 20-80°C (or below 100°C) without any other endo- or exothermic peaks, suggesting it is an amorphous polymer (Katzhendler et al 1998). For lactose, there is a sharp endothermic peak at 148°C (594.27 mJ) which represents the loss of water of crystallisation (Ross 1978; Gombas et al 2002). Another endothermic peak at 170°C and an exothermic peak at 180°C are observed for lactose, which indicates formation of the unstable form of anhydrous lactose above 160°C, followed by melting of this form at 170°C and conversion into crystalline α/ β mixed crystals at above 180°C (as described by Lerk et al (1984)). These then melted at 217°C and 226°C respectively (Drapier-Beche et al 1999). The endothermic peaks at 148°C are further assessed in Table 3.4.

Table 3.4 Integration the endothermic peak of water of crystallisation of lactose in different concentrations of lactose:HPMC (1:1) microparticle formulations (prepared using 2000 rpm stirring speed, needle gauge of 23g and 10 ml/hr dropping rate) in comparison to lactose.

Formulation	Concentration (%)		Integration the endothermic peak of water of crystallisation (mJ)
	Lactose	HPMC	
Lactose	-	-	594.27
5% lactose:HPMC (19 U)	5	5	410.50
5% lactose:HPMC (19 L)	5	5	Not detected
4% lactose:HPMC (56 L)	4	4	62.03
3% lactose:HPMC (55)	3	3	139.94
2% lactose:HPMC (54)	2	2	180.79
1% lactose:HPMC (53)	1	1	2.38

The endothermic peak for water loss of crystallisation of the upper layer of formulation 19 (410.5 mJ), was reduced and at a lower temperature in comparison to lactose alone (Table 3.4), and absent in the lower layer. This suggests that there was some α-lactose monohydrate in the upper layer but none in the lower layer. Further support for this hypothesis is derived from the observation of an endothermic peak at 215°C, which is close to the melting point of non hygroscopic (stable) anhydrous α-lactose reported by Drapier-Beche et al (1999). Subsequently, the anhydrous α-

lactose converted to the β-form, resulting in an endothermic melt at 228°C, close to the value reported by Drapier-Beche et al (1999). The slight variation from literature values is attributed to the presence of HPMC in our samples. It is suggested that the lower layer of formulation 19 contains a mixture of a small amount of unstable (hygroscopic) anhydrous lactose and the β-form. The unstable hygroscopic α-form can be identified from the broad endothermic peak of dehydration between 80-120°C. The other endothermic peak at 165°C in formulation 19L is associated with the conversion of unstable to stable form of anhydrous β-lactose which is melted at 225°C. This is less than the melting point of pure β-lactose form due to the presence of HPMC possibly acting as a plasticiser and decreasing the lactose melting point.

For other formulations 56L, 55, and 54 (4%, 3% and 2% lactose:HPMC (1:1) respectively), the relationship between concentration and endothermic peak of water loss of crystallisation is complex. At the lowest concentration (1%), no endothermic peak was observed for water loss, however at 2-3%, a significant peak was observed. At higher concentrations, the peak progressively disappeared, with a corresponding increase in the presence of a peak above 220°C, corresponding to the β-form. The thermogram for the 1% formulation suggested that lactose was present as an anhydrous α-form that melted at 215°C.

Therefore these findings are in agreement with those of the IR results, supporting the hypothesis that there is an interaction between lactose and HPMC as a result of their structural compatibility, leading to hydrogen bonding as discussed previously. This permitted HPMC to modify the structure of lactose and produce different polymorphs.

Thermograms for lactose alone at different concentrations are shown in Figure 3.20.

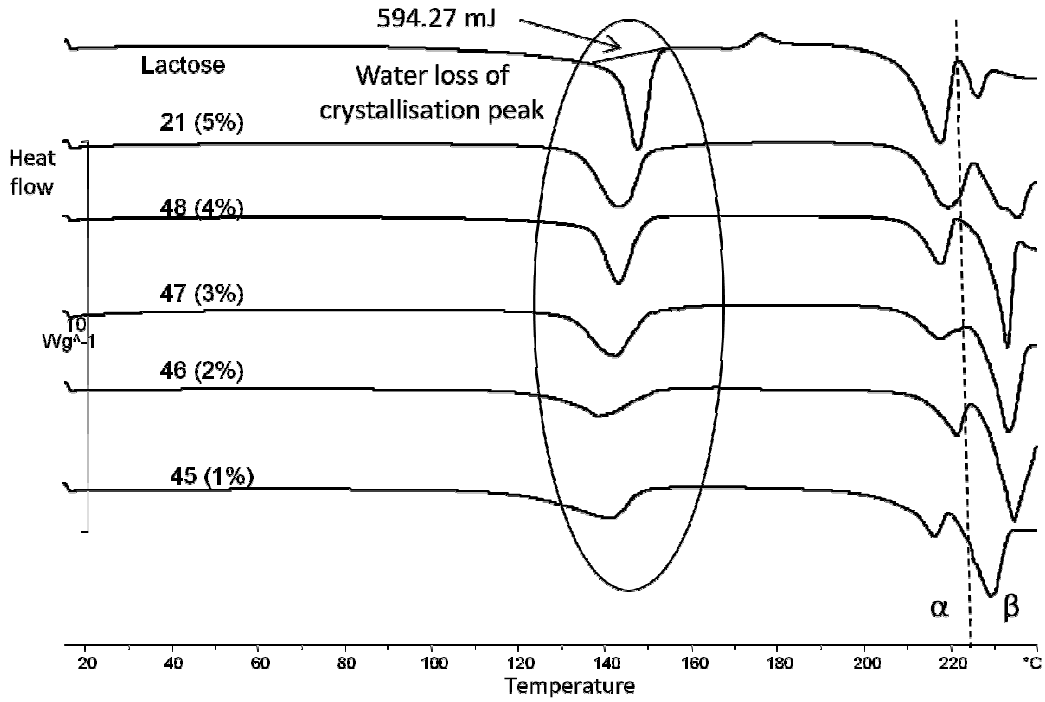

Figure 3.20 DSC thermograms of lactose powder and microparticles precipitated from different concentrations of lactose solution; formulation 21 (5% lactose), formulation 48 (4% lactose), formulation 47 (3% lactose), formulation 46 (2% lactose) and formulation 45 (1% lactose), using 2000 rpm stirring speed, needle gauge of 23g and 10 ml/hr dropping rate.

Precipitation into IPA at low lactose concentration results predominantly in the β-form, however as the lactose concentration increases, the presence of the monohydrate increases. The thermograms for all precipitated forms show melting endotherms of both α and β-lactose. Processing lactose resulted in a shift of the endothermic peak of water loss from 148°C to 142°C. The observed melting point of β-lactose varied between 233 and 237°C, in accordance with literature values (Lerk et al 1984; Larhrib et al 2003).

Quantification of the energy of the water loss of crystallisation peak for formulations 48, 47, 46 and 45 are shown in Figure 21, and increases with concentration.

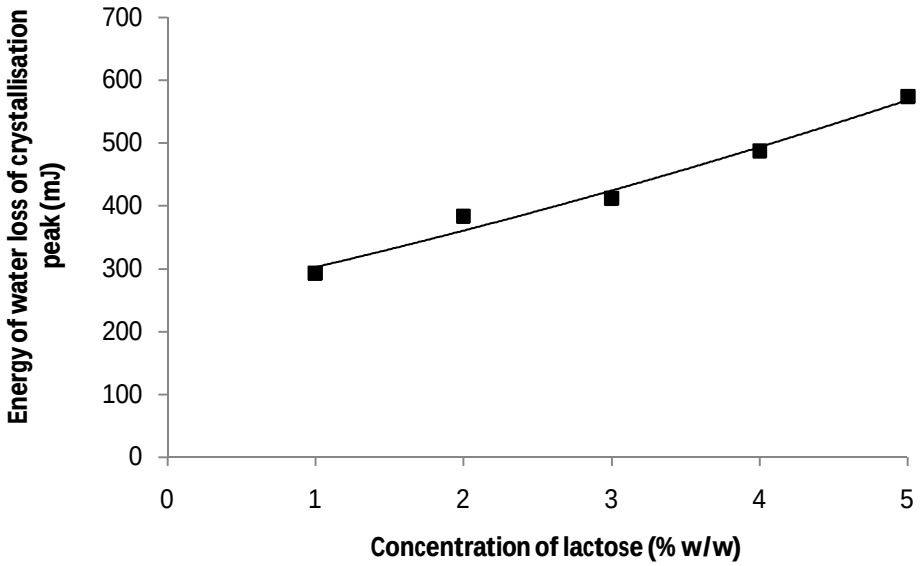

Figure 3.21 Integration the endothermic peak of water of crystallisation of lactose in different concentrations of lactose microparticle formulations 45-48. The energy of the water loss of crystallisation peak increased as the concentration of lactose increased.

3.3.6 Lactose:HPMC microparticles prepared by high shear mixer

It appeared that a mechanical stirrer (Stuart stirrer) produced two layers of lactose:HPMC aggregates and particles. To overcome this disadvantage a mixer with a higher shearing rate (Silverson SL 2T) was employed. Using this method, only one layer was visible in the suspension of lactose:HPMC (1:1) microparticle for formulations 57-67, using 7500-8000 rpm stirring speed and needle gauge of 23 g and 10 ml/ hr dropping rate (preparation explained in detail in Section 2.5.3.2).

3.3.6.1 Effect of stirring speed and temperature on lactose:HPMC microparticles precipitated by IPA or acetone using high shear mixer

Table 3.5 summarises the effect of stirring speed, temperature and precipitating agent (IPA and acetone) on the particle size of three concentrations of lactose:HPMC (1:1)

microparticles (3-5%), evaluated using laser diffraction. An acceptable microparticle size for nasal administration of less than 100µm was obtained under the conditions used.

Table 3.5 Mean microparticle size of lactose:HPMC (1:1) microparticles prepared by high shear Silverson SL2T mixer using different preparation conditions, n=3.

Formulation	Stirring speed (rpm)	Temperature used (± 0.5°C)	Precipitating agent	Mean microparticle size (µm), n=3
3% lactose:HPMC (57)	7500	25	IPA	79.90 ±11.1
4% lactose:HPMC (58)	7500	25	IPA	65.30 ±8.6
5% lactose:HPMC (59)	7500	25	IPA	81.38 ±1.9
3% lactose:HPMC (60)	7500	4	IPA	42.04 ±1.4
4% lactose:HPMC (61)	7500	4	IPA	48.92 ±5.1
3% lactose:HPMC (62)	7500	4	Acetone	31.18 ±8.2
4% lactose:HPMC (63)	7500	4	Acetone	34.54 ±9.1
3% lactose:HPMC (64)	8000	4	IPA	42.15 ±16.2
4% lactose:HPMC (65)	8000	4	IPA	27.91 ±0.1
3% lactose:HPMC (66)	8000	4	Acetone	11.90 ±1.8
4% lactose:HPMC (67)	8000	4	Acetone	21.25 ±11.3

Decreasing the temperature of the precipitating solvent (4°C) generally produced smaller microparticles, which is in agreement with data reported on another system (von Bonsdorff-Nikander et al 2003).

Acetone consistently produced a smaller microparticle size than with IPA. Acetone is a water miscible solvent but does not contain an OH group (aprotic), and we suggest that the water in the lactose:HPMC solution is rapidly taken up by the acetone, with the resultant formation of microparticles. However, with IPA it is suggested that the OH group of IPA may form an H-bond with HPMC and lactose in the presence of water, inhibiting the removal of water from the hydrophilic polymer, resulting in a slower process and larger particles.

3.4 Conclusion

- α-lactose monohydrate was used as a model compound to optimise the manufacturing conditions of bioadhesive HPMC microparticles for nasal delivery. The preparation technique involved the precipitation of aqueous gels of lactose:HPMC (1:1) into a precipitating agent (1:20 DW:IPA or acetone).

- Different processing parameters were evaluated, such as effect of stirring speed (1000-2000 rpm), needle gauge (19g, 21g and 23g), and dropping rate (5 ml/hour and 10 ml /hour), to control the mean particle size.

- Two layers of precipitate (upper and lower) were obtained with a low shear stirrer when the concentration of HPMC increased above 3% w/w. The presence of HPMC resulted in a smaller particle size (upper layer) in comparison to only lactose microparticles. The precipitate contained unequal proportions of lactose and HPMC in each layer (evident by NMR results), despite a lactose:HPMC ratio of 1:1 being used as the initial aqueous gel (before processing in the precipitating agent).

- FT/IR spectra and DSC thermograms of 1-5% w/w lactose:HPMC (1:1) formulations precipitated in IPA showed lactose polymorphism as a result of HPMC concentration changing the habit of lactose crystals by H-bonding. At 1% lactose:HPMC, anhydrous α-lactose was obtained, while at 2-3% lactose:HPMC, a mixture of α- and β-lactose was observed. Whereas at 4 and 5% concentrations, the α- form progressively disappeared, with a corresponding increase in the presence of a β-form.

- In the absence of HPMC, particles precipitated from lower lactose concentrations (1-4%) in IPA resulted predominantly in the β-form of lactose, however as the lactose concentration increased, the presence of the monohydrate also increased.

- A high shearing rate eliminated the problem of two layers. Effect of stirring speed 7500-8000 rpm, temperature of the precipitating media (4°C and 25°C ±0.5°C) and precipitating agents (IPA and acetone) were studied on three concentrations; 3%, 4% and 5% w/w lactose:HPMC (1:1). The optimal particle size required for nasal delivery (less than 100µm) was obtained using a stirring speed of 8000 rpm, a temperature of 4°C, a dropping rate of 10 ml/ hour, using a 23g needle.

- Future chapters will consider the replacement of lactose with drug molecules (verapamil HCl and metformin HCl) using the optimised processing methods.

Chapter 4

Preparation and evaluation of microparticles containing verapamil

4.1 Introduction

Verapamil hydrochloride (VH) is a phenyl alkyl amine ($C_{27}H_{38}N_2O_4$.HCl) with the chemical name; alpha-(3-((2-(3, 4-Dimethoxyphenyl) ethyl) methylamino) propyl) 3,4-dimethoxy-alpha-(1-methylethyl)-benzenacetonitrile hydrochloride. The molecular weight is 491.07. Figure 4.1 shows the chemical structure of VH.

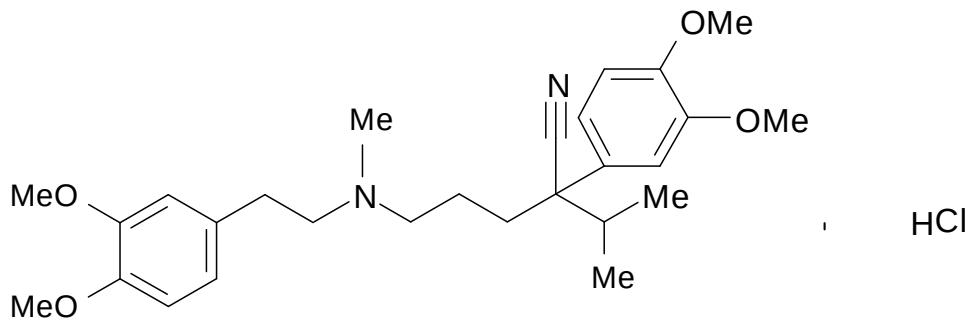

Figure 4.1 Chemical structure of verapamil HCl (VH).

It is an almost white crystalline powder with a melting point of 146-150°C and a pKa of 8.6. Its solution (1% in water) is yellow, viscous and oily. It shows UV absorption at 278nm. It is soluble in water (83mg/ml), chloroform and methanol, partially soluble in acetone and insoluble in diethyl ether (Yoshida et al 2010).

VH has calcium channel blocking action and is used in the treatment of angina, hypertension and tachyarrhythmia. It is rapidly and completely absorbed after oral administration (90%) but undergoes an extensive hepatic and intestinal first-pass

metabolism, resulting in a low extent of absolute oral bioavailability (22%) in humans (Nunes et al 2009; Iliger et al 2010; Yoshida et al 2010). It has a short half-life of 4±1.5 hours (Sahoo et al 2009), and therefore frequent and high doses are required to achieve a therapeutic effect, resulting in increased side effects.

Many trials have been reported in the literature to improve the bioavailability of VH using the oral route, such as sustained release tablets using different ratios of Eudragit:VH (Sahoo et al 2009), free floating microspheres of cellulose acetate, acrycoat S100 and Eudragit S100 loaded with VH (Tanwar et al 2007), and carrageenan beads to control the release of VH (Sipahigil & Dortunc 2001). However, the main drawback of oral route is first pass hepatic metabolism which overcome the advantages of these formulations.

The nasal route of administration is non-invasive and has low enzymatic activity making it a promising alternative route for systemic absorption of drugs. Therefore other researchers have investigated mucoadhesive VH microspheres for nasal administration, using gelatine and chitosan as carriers (Iliger et al 2010).

In order to formulate VH into a dosage form, the drug component will be processed through different steps that may change its physiochemical properties and consequently its bioavailability. For example Kilicarslan and Baykara (2003) reported preparation of VH as controlled release microspheres, and were able to modify the particle size, surface characteristics and dissolution rate of VH of microspheres through variation of drug/polymer ratio. These microspheres were prepared using a solvent evaporation technique and Eudragit RS 100 as a coat.

Yoshida and co-workers used TGA, DSC, FT/IR, liquid chromatography and XRPD to evaluate the physiochemical properties of VH such as polymorphism, stability, purity, and formulation compatibility among others (Yoshida et al 2010). Nunes and co-authors focused only on the thermal behaviour of VH using TGA and DSC to study its properties and compatibility with additives such as hydroxypropyl methylcellulose and polyvinyl pyrrolidone. It was found that there was no interaction between VH and the excipients when mixed physically (Nunes et al 2009). SEM has been widely used to assess the morphology of VH in dosage forms, and its

incorporation into the polymer matrix as microspheres (Sipahigil & Dortunc 2001; Kilicarslan & Baykara 2003; Iliger et al 2010).

In this chapter bioadhesive microparticles of VH:HPMC were prepared using the optimised aqueous organic co-precipitation technique (Chapter 3), in an attempt to improve bioavailability of VH and overcome side effects resulting from high and frequent doses of oral formulations. Different analytical techniques were employed to study the physiochemical properties of VH in microparticle formulations, such as SEM, DVS, FT/IR, XRPD and DSC.

4.2 Materials and methods

The drug and materials used in this chapter were VH, HPMC, IPA and acetone, which were detailed in Section 2.2.

4.2.1 Determination VH solubility

The solubility of VH in distilled water, IPA and acetone was determined using the technique described in Section 2.5.2. The standard UV calibration curve of VH in distilled water was obtained using the method mentioned in the same Section 2.5.2.

4.2.2 Preparation of blank HPMC microparticles

Blank 3% and 4% HPMC (w/w) microparticles were prepared using the technique mentioned in Section 2.5.3.2. Briefly, this method used a high shear mixer with 8000 rpm stirring speed and a temperature of 4 ±0.5°C in the precipitation media (IPA or acetone). Table 4.1 summarises these formulations.

Table 4.1 Composition and process parameters of HPMC blank microparticles.

Formulation	HPMC concentration (%w/w)	Temperature (± 0.5°C)	Stirring speed (rpm)	Precipitating agent
68	3	4	8000	IPA
69	4	4	8000	IPA
70	3	4	8000	Acetone
71	4	4	8000	Acetone

4.2.3 Preparation of VH:HPMC microparticles

VH:HPMC (1:1) microparticles were prepared using the technique described in Section 2.5.3.2. Table 4.2 summarises these formulations.

Table 4.2 Composition and process parameters of VH:HPMC (1:1) microparticles.

Formulation	VH concentration (%w/w)	HPMC concentration (%w/w)	Temperature (± 0.5°C)	Stirring speed (rpm)	Precipitating agent
72	3	3	4	8000	IPA
73	4	4	4	8000	IPA
74	3	3	4	8000	Acetone
75	4	4	4	8000	Acetone

4.2.4 Determination of percent yield and verapamil content of microparticles

Percent yield and verapamil content of the formulations in Table 4.2 were determined using the methods mentioned in Section 2.5.4.1. According to the calculated VH content of microparticle, physical mixtures of VH:HPMC were prepared in the same ratios (Section 2.5.4.1). Table 4.3 summarises these formulations.

Table 4.3 Formulation numbers of VH:HPMC physical mixtures and their equivalent microparticle formulations.

Physical mixture formulations	VH:HPMC microparticles
76	72
77	73
78	74
79	75

4.2.5 Physiochemical properties of VH:HPMC microparticles

4.2.5.1 Measurement of mean microparticle size

The mean size of microparticles of the formulations detailed in Table 4.2 was assessed using the laser diffraction technique discussed in Section 2.5.4.3.

4.2.5.2 Scanning Electron microscopy

The SEM technique described in Section 2.5.4.4 was used to obtain images for the formulations in Table 4.1 (formulations 69 and 71), Table 4.2 and their unprocessed components.

4.2.5.3 X-ray powder diffraction

Solid samples of VH:HPMC (1:1) microparticles (formulations detailed in Table 4.2), in comparison to their unprocessed components and physical mixtures (formulations 76-79) were analysed using XRPD as described in Section 2.5.4.8, to determine amorphous or crystalline content.

4.2.5.4 Differential scanning calorimetry

DSC analysis of blank HPMC microparticles (formulations 68-71), VH:HPMC (1:1) microparticles (formulations 72-75), their physical mixtures (formulations 76-79), and their unprocessed components was performed using the method outlined in Section 2.5.4.9, to determine the effect of processing on the melting point of VH.

4.2.5.5 Fourier transform infrared spectroscopy

The VH:HPMC (1:1) solid microparticle formulations and their unprocessed components were analysed using the FT/IR technique described in Section 2.5.4.7.

4.2.5.6 *In-vitro* Dynamic adhesion

In-vitro bioadhesion of all formulations in Tables 4.1 and 4.2, formulation 76 (Table 4.3) and HPMC alone were studied using mucin-agar plates. The preparation of adhesion media and the samples for this test were described in Section 2.5.4.11. The effect of precipitating agents (IPA and acetone), concentration of HPMC, VH loading, contact time (1 minute or 15 seconds), compression in to discs (using punch and die with 4 kg compression force) and temperature of the adhesion environment (for compressed discs at ambient laboratory temperature and 37 ±0.5°C) were assessed using the techniques mentioned in the same Section 2.5.4.11.

4.2.5.7 Dynamic vapour sorption

Vapour sorption of VH:HPMC (1:1) microparticle formulations (72-75) and HPMC alone were measured using the technique mentioned in Section 2.5.4.12.

4.3 Results and discussion

4.3.1 Determination of VH solubility and UV absorbance

It was found that this drug has sparingly solubility (USP solubility definition) in isopropyl alcohol (IPA) and acetone (1g /83 ml and 1g /33 ml respectively). Figure 4.2 shows the standard curve of UV absorption in distilled water using λ 278 nm.

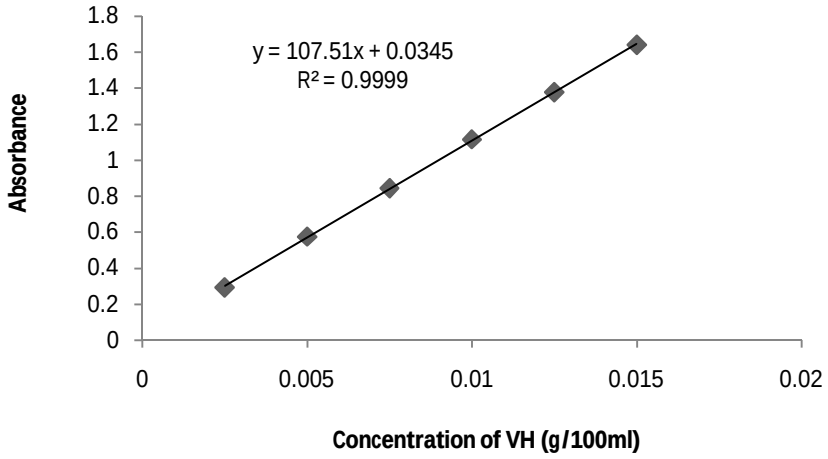

Figure 4.2 Standard calibration curve of verapamil HCl (VH) determined in distilled water at 278 nm with a 1 cm cell path length, using UV spectrophotometry.

4.3.2 Particle size and physiochemical properties of VH:HPMC microparticles

VH:HPMC (1:1) microparticles showed an acceptable particle size range, as shown in Table 4.4. The required microparticle size for nasal administration should be lower than 100µm (De Ascentiis et al 1996; Wermeling & Miller 2003). Low yield and verapamil content were obtained because of sparingly solubility of VH in IPA (formulations 72 and 73) and acetone (formulation 74 and 75). The slightly lower

loading efficiency of formulations 74 and 75 reflects the slightly higher solubility of VH in acetone when compared to IPA.

Table 4.4 Particle size, yield and verapamil content of VH:HPMC (1:1) microparticles, n=3.

Formulation	Mean size of microparticles (μm)	% Yield	Verapamil content (%)
3% VH:HPMC precipitated by IPA (72)	39.53 ±0.38	36.5 ±4.6	8.7 ±4.9
4% VH:HPMC precipitated by IPA (73)	43.33 ±18.38	39.0 ±9.9	6.1 ±2.1
3% VH:HPMC precipitated by acetone (74)	44.84 ±8.61	40.6 ±1.9	2.0 ±0.1
4% VH:HPMC precipitated by acetone (75)	47.74 ±0.04	39.8 ±1.1	2.3 ±2.7

This may result from the sparingly solubility of VH in the precipitating agents, causing partitioning of drug into the solvent, and consequently lower availability of VH for precipitation with HPMC from the aqueous mixture. It is also known that a saturated system is required to produce nucleation and crystallisation of a drug, therefore the effect of this partitioning in reducing the concentration of VH in the aqueous solution would also be expected to reduce the quantity of precipitated crystalline VH (Tiwary 2007). However this requires further study to confirm the presence or absence of VH crystals in the microparticles, which will be achieved in XRPD (Section 4.3.2.2) and DSC (Section 4.3.2.3) studies.

4.3.2.1 Scanning electron microscopy

The SEM images in Figure 4.3a and b show the morphology of HPMC and VH respectively. Figure 4.3c and d show blank formulations of HPMC precipitated using IPA (formulation 69) and acetone (formulation 71), and it is evident that dissolution and subsequent precipitation results in loss of particulate identity and formation of a more continuous surface. At 4% VH:HPMC (1:1) the surfaces of the microparticles

(Figure 4.3f and h, IPA and acetone respectively) appeared to be less regular with evidence of smaller particles on the surface. Such features were less clearly defined for the 3% formulation (Figure 4.3e and g).

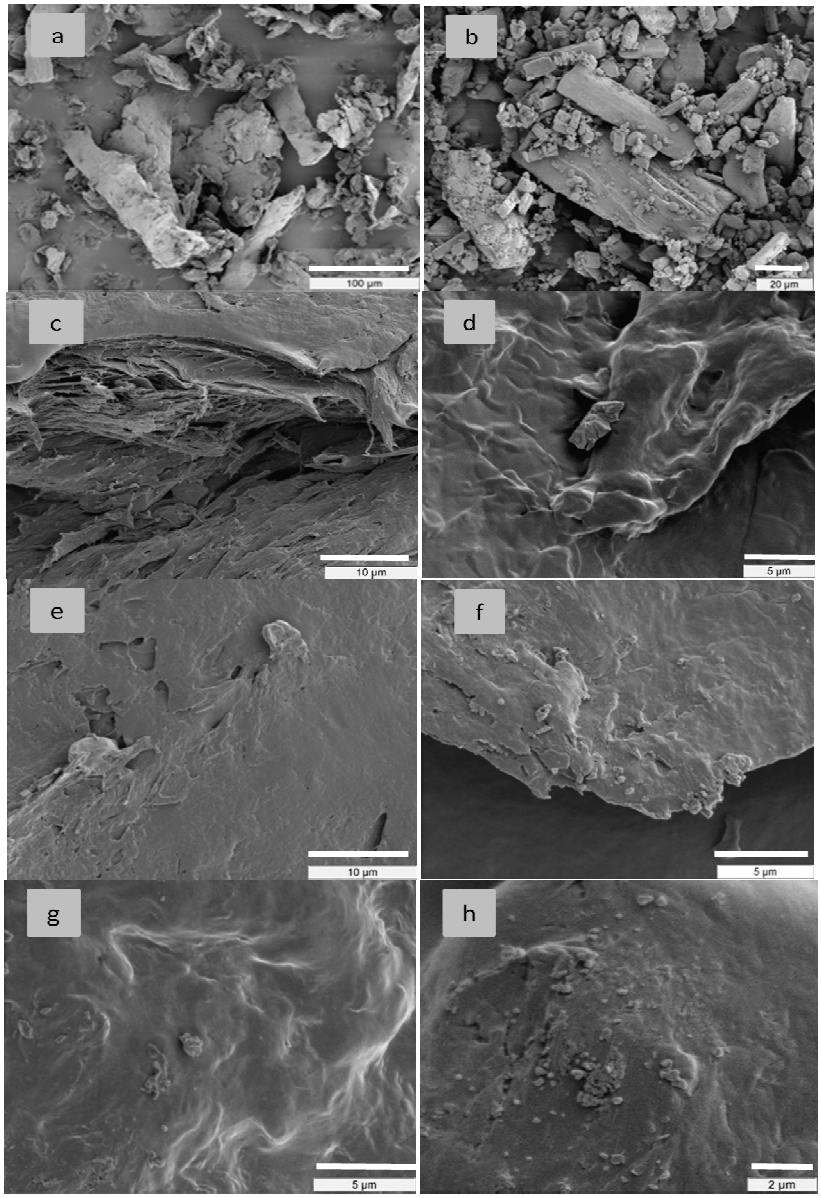

Figure 4.3 SEM images of a) HPMC, b) VH, c) formulation 69 (4% HPMC precipitated by IPA), d) formulation 71 (4% HPMC precipitated by acetone), e) formulation 72 (3% VH:HPMC precipitated by IPA), f) formulation 73 (4% VH:HPMC precipitated by IPA), g) formulation 74 (3% VH:HPMC precipitated by acetone) and h) formulation 75 (4% VH:HPMC precipitated by acetone).

4.3.2.2 X-ray diffraction powder analysis

Figure 4.4 shows the sharp peaks of x-ray spectrum of VH due to the crystalline form of unprocessed drug. While no sharp peaks appeared for VH:HPMC (1:1) microparticle formulations specially formulations 74 and 75 (precipitated by acetone), suggesting amorphous microparticles resulted from the co-precipitation technique. Formulation 72 (3% VH:HPMC (1:1) microparticles precipitated by IPA) showed just one small peak. This absence of crystalline verapamil, was in agreement with the SEM images (Section 4.3.2.1). However, physical mixtures of VH and HPMC containing equivalent amounts of VH:HPMC to the IPA microparticles (formulations 76 and 77), revealed the characteristic (small) peaks of VH, while at the lower concentrations equivalent to acetone microparticles (formulations 78 and 79), no peaks were evident due to the low concentration of drug.

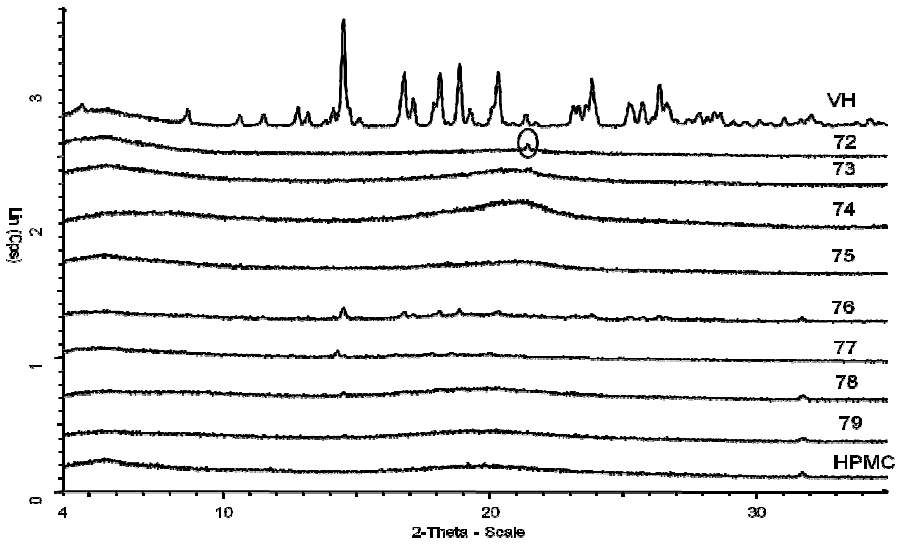

Figure 4.4 XRPD spectra of VH, formulation 72 (3% VH:HPMC precipitated by IPA), formulation 73 (4% VH:HPMC precipitated by IPA), formulation 74 (3% VH:HPMC precipitated by acetone) and formulation 75 (4% VH:HPMC precipitated by acetone), their physical mixtures; formulation 76 (physical mixture of formulation 72), formulation 77 (physical mixture of formulation 73), formulation 78 (physical mixture of formulation 74), formulation 79 (physical mixture of formulation 75) and HPMC.

4.3.2.3 Differential scanning calorimetry

Figures 4.5 and 4.6 show DSC thermograms for microparticles precipitated from IPA and acetone respectively, in comparison to verapamil and corresponding physical mixtures of verapamil and HPMC. The endothermic peak (melting point) of VH (Figure 4.5) was observed at 147°C, but was absent in IPA precipitated formulations 72 and 73. However the corresponding physical mixtures (76 and 77) show a small endothermic peak corresponding to the low content of VH in these physical mixtures. All formulations in Figure 4.5 displayed an endothermic peak between 30-110°C which corresponds to HPMC polymer.

Similar effects were observed in Figure 4.6, here IPA was replaced by acetone, although in this case it was not possible to detect the endothermic verapamil peak in the physical mixtures, because of the low drug content.

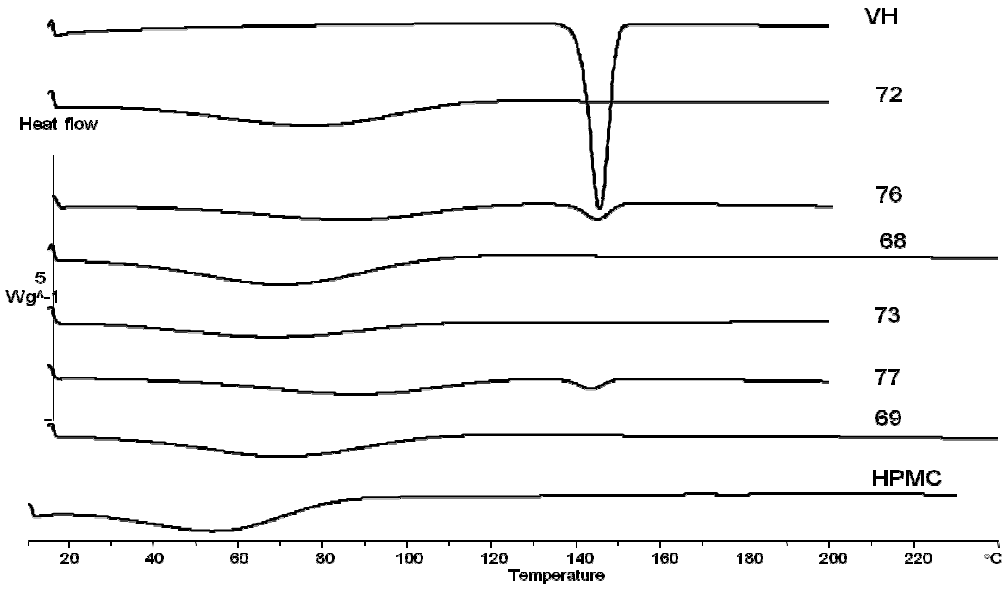

Figure 4.5 DSC thermograms of VH, formulation 72 (3% VH:HPMC precipitated by IPA), formulation 76 (physical mixture of formulation 72), formulation 68 (blank 3% HPMC precipitated by IPA), formulation 73 (4% VH:HPMC precipitated by IPA), formulation 77 (physical mixture of formulation 73), formulation 69 (blank 4% HPMC precipitated by IPA) and HPMC.

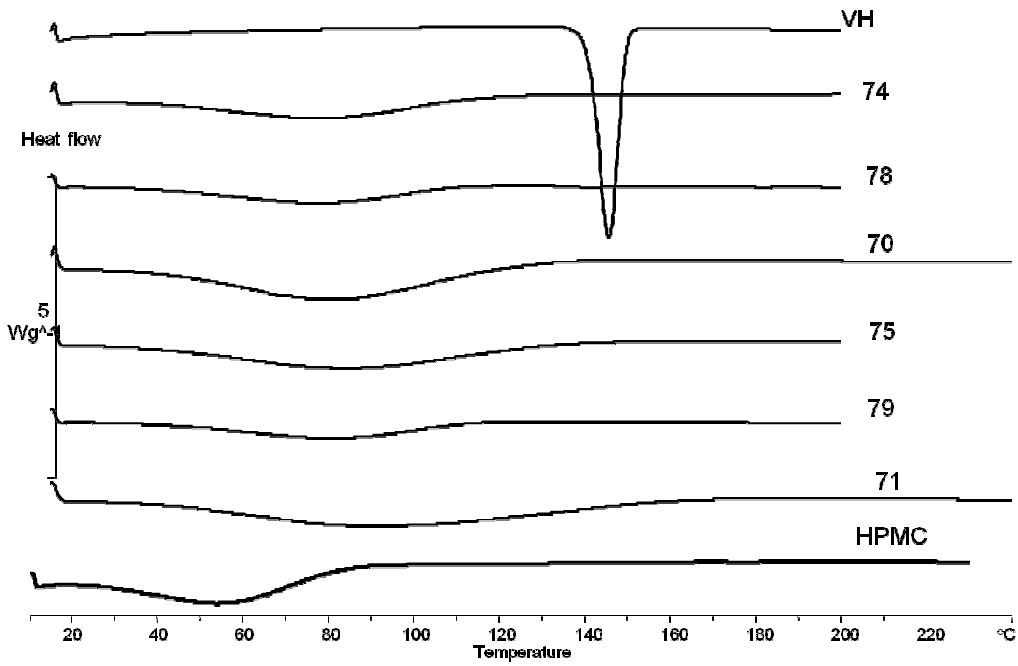

Figure 4.6 DSC thermograms of VH, formulation 74 (3% VH:HPMC precipitated by acetone), formulation 78 (physical mixture of formulation 74), formulation 70 (blank 3% HPMC precipitated by acetone), formulation 75 (4% VH:HPMC precipitated by acetone), formulation 79 (physical mixture of formulation 75), formulation 71 (blank 4% HPMC precipitated by acetone) and HPMC.

These DSC results therefore confirmed the data obtained from SEM and XRPD, whereby processing VH into microparticles using precipitation technique caused the formation of amorphous VH in the microparticles. These analyses were further complicated by the low drug contents of the precipitated and physical mixtures studied.

4.3.2.4 Fourier transform infrared spectroscopy

The spectrum of VH shown in Figure 4.7 shows the characteristic peaks in the region of 1600-1100 cm^{-1} and 3000-2750 cm^{-1}. HPMC shows characteristic peaks between 3700cm^{-1}- 2700cm^{-1}.

The precipitated materials from IPA and acetone were essentially similar, and showed the broad HPMC peak between 3700cm^{-1}- 2700cm^{-1}, however the peaks attributed to verapamil were all reduced in intensity, due to the low verapamil content in the samples.

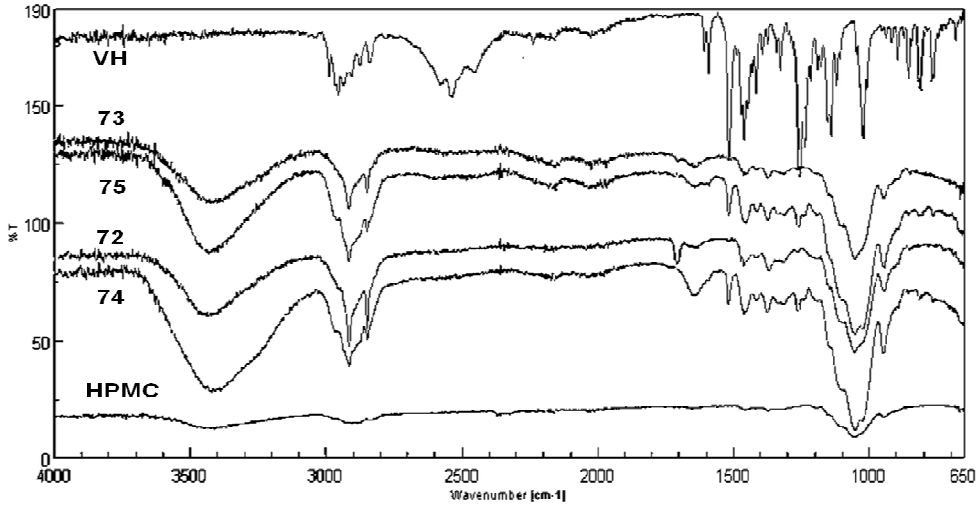

Figure 4.7 FT/IR spectra of VH, formulation 73 (4%VH:HPMC precipitated by IPA), formulation 75 (4% VH:HPMC precipitated by acetone), formulation 72 (3% VH:HPMC precipitated by IPA), formulation 74 (3% VH:HPMC precipitated by acetone) and HPMC.

4.3.2.5 *In-vitro* dynamic adhesion

The results of *in-vitro* adhesion tests on powder samples, using the mucin-agar plate method described in Section 2.5.4.11, are shown in Figure 4.8

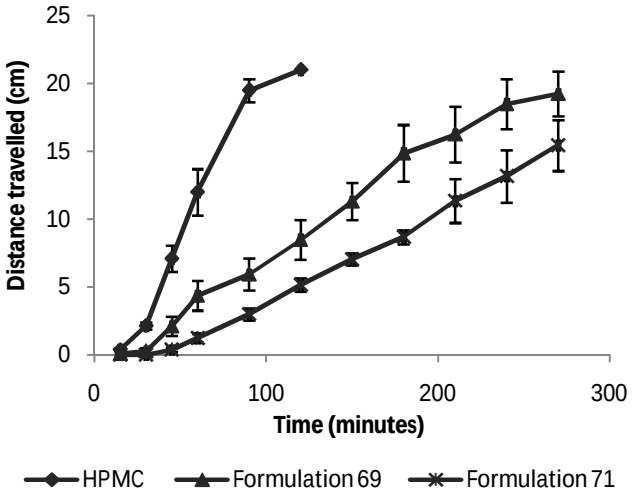

Figure 4.8 The dynamic adhesion profiles of blank 4% HPMC microparticle formulations (69 precipitated by IPA and 71 precipitated by acetone) in comparison to unprocessed HPMC, n=6. A significant increase in the dynamic adhesion of formulations 69 and 71 was observed when compared to unprocessed HPMC powder.

The bioadhesion of unprocessed HPMC polymer was significantly less than for precipitated HPMC microparticles using either IPA (formulation 69) or acetone (formulation 71) as precipitating agents. The unprocessed HPMC, in the form of discrete particles readily hydrated and flowed on the tilted plate, while the microparticle formulations were in the form of a more continuous material and with the characteristics of a matrix, rather than discrete particles.

The chemical structure of HPMC was previously shown in Figure 3.13a, and has many sites for H-bonding that may result in rapid hydration and sliding on the adhesion media (Andrews et al 2009). Observations are complicated by the fact that as the formulation hydrates, its mass increases as a result of water uptake, leading to greater gravitational effects.

HPMC microparticles precipitated by IPA moved more rapidly down the mucin-agar surface in comparison to microparticle formulations precipitated by acetone. The latter persisted longer on the plate indicating that their adhesion was better than

former formulations. The possible effects of differences in the surfaces of the material precipitated from IPA and acetone will be discussed in later chapters. It remains clear that the dynamic adhesion results showed more rapid hydration and gelling of IPA precipitated microparticles when compared with acetone precipitated microparticles. The incidence of water uptake of these two formulations will also be discussed in a later chapter.

Figure 4.9a and b illustrates the effect of HPMC concentration on the adhesion profile of blank HPMC microparticle formulations precipitated by IPA and acetone respectively.

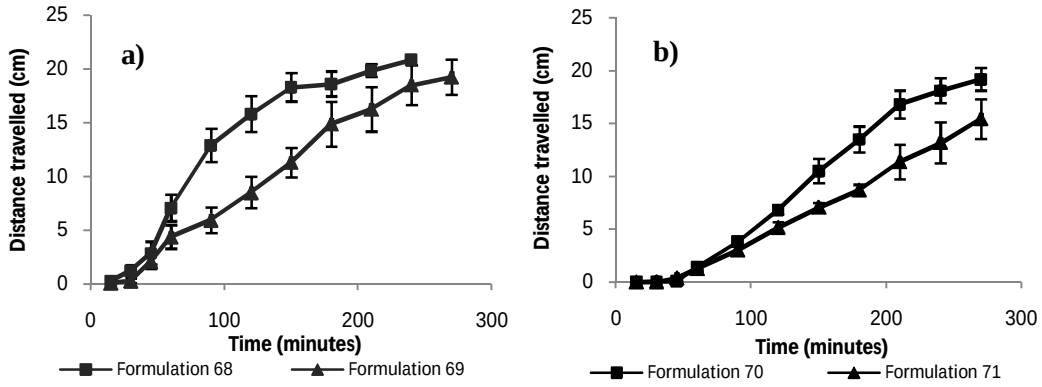

Figure 4.9 Adhesion profiles of a) blank 3% HPMC microparticles (formulation 68) and blank 4% HPMC microparticles (formulation 69) precipitated by IPA, and b) blank 3% HPMC microparticles (formulation 70) and blank 4% HPMC microparticles (formulation 71) precipitated by acetone, n=6. The *in-vitro* adhesion dynamic of blank HPMC formulations increased as the concentration of HPMC increased.

As the concentration of polymer increased, the *in-vitro* adhesion increased for both IPA and acetone formulations, suggesting the development of a viscous *in-situ* HPMC gel. In addition, the mean distance travelled at 120 minutes for 3% and 4% HPMC microparticles was 15.8 ±1.6 cm, 8.5 ±1.4 cm and 6.8 ±0.4 cm, 5.1 ±0.3 cm

for IPA and acetone formulations respectively ($P \leq 0.05$), using T-test for two samples of equal variances.

Figure 4.10 shows the *in-vitro* adhesion for VH:HPMC (1:1) microparticles precipitated from IPA and acetone, in comparison to blank HPMC microparticles. It was observed that although concentration of HPMC (with or with drug) had an effect on bioadhesion, the presence of the drug did not have any significant effect on bioadhesion. This was again presumed to be due to the low content of drug in these preparations.

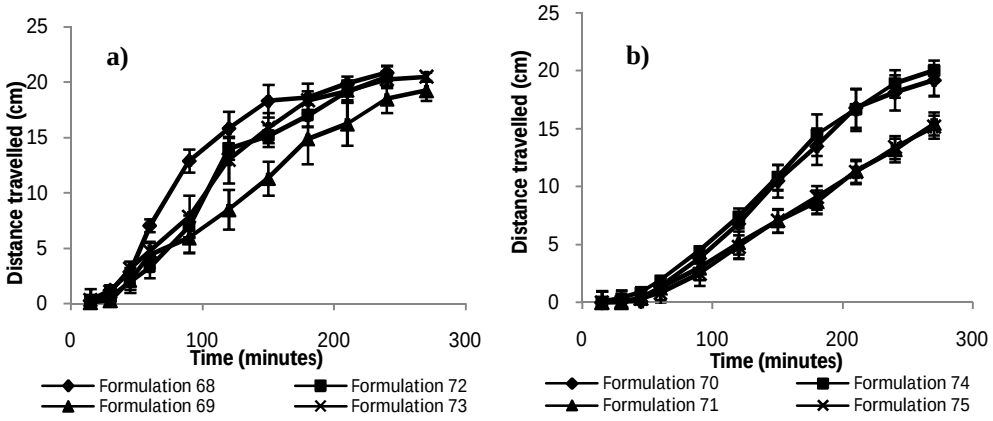

Figure 4.10 Effect of drug loading on the adhesion profile of, a) blank formulation 68 (3%HPMC), formulation 72 (3% VH:HPMC), formulation 69 (4%HPMC) and formulation 73 (4%VH:HPMC) precipitated by IPA and b) formulation 70 (3%HPMC), formulation 74 (3%VH:HPMC), blank formulation 71 (4%HPMC) and formulation 75 (4%VH:HPMC) precipitated by acetone. n=6. No significant differences were observed between blank HPMC and VH:HPMC microparticles.

The bioadhesion of the physical mixture of VH and HPMC in comparison to HPMC alone is shown in Figure 4.11.

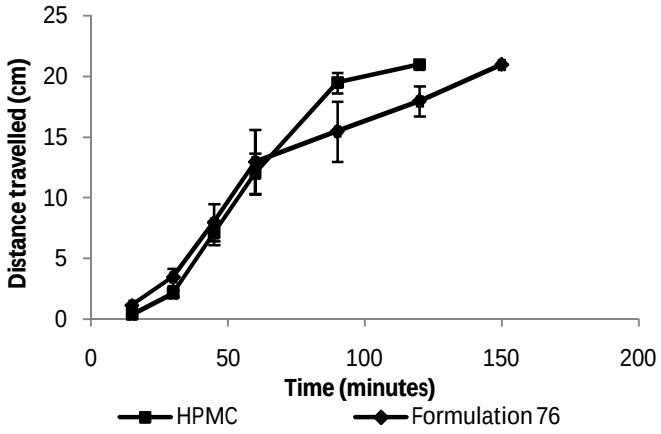

Figure 4.11 The adhesion profile of the physical mixture of VH:HPMC (formulation 76) and HPMC, n=5. Physically mixed VH with HPMC powder produced no significant effect on its dynamic adhesion profile in comparison to that of HPMC powder alone.

No significant differences were found between HPMC and the physical mixture with verapamil.

The technique of the bioadhesion test procedure was studied in a study reported in Figure 4.12 in which the contact times of the applied weight to the sample of 15 seconds and 1 minute were investigated.

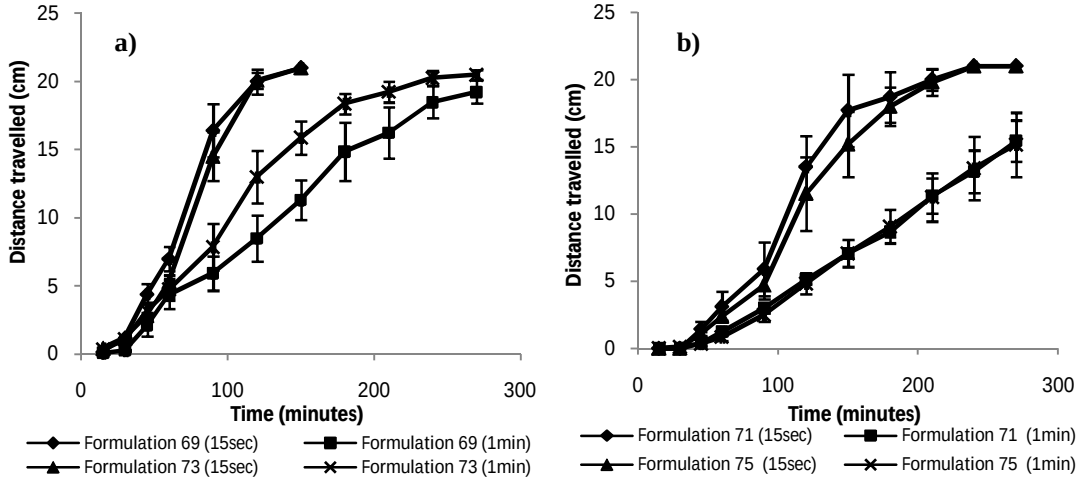

Figure 4.12 Effect of pressing time (15 seconds and 1 minute) on the dynamic adhesion of a) formulation 69 (4% HPMC) and formulation 73 (4%VH:HPMC) microparticles precipitated by IPA and b) formulation 71 (4% HPMC) and formulation 75 (4%VH:HPMC) microparticles precipitated by acetone, n=6. A significant increase in the dynamic adhesion of the formulations was observed when the contact time increased from 15 seconds to 1 minute.

It was found that bioadhesion of the samples was more effective when the samples pressed with a force of 0.05 N for 1 minute rather than 15 seconds. It is suggested that this permitted a more effective contact between the samples and the mucin-agar support which then resulted in a more effective hydration of samples. The hydration permitted the formulation to wet, swell and adhere to the base (Nakamura et al 1999; Lee et al 2000; Andrews et al 2009). In addition, statistical comparison of the effect of compression on 3% w/w blank HPMC and VH:HPMC (1:1) microparticle formulations is shown in Table 4.5 below, using T-test for two samples of equal variances.

Table 4.5 Statistical analysis the effect of the contact time (15 seconds and 1 minute) on the dynamic adhesion of 3% w/w formulations.

Composition	Mean of the distance travelled at 120 minutes (cm)		Statistical T-test analysis (Probability)*
	15 seconds	1 minutes	
3% HPMC precipitated by IPA (68)	18.5 ±1.5	15.8±1.6	0.05
3% HPMC precipitated by acetone (70)	16.4±1.5	6.8±0.4	0.0001
3% VH:HPMC precipitated by IPA (72)	19.7±1.1	14.0±1.2	0.04
3% VH:HPMC precipitated by acetone (74)	10.7±2.5	7.4±0.7	0.03

* The differences were significant when the probability was $P \leq 0.05$.

A further modification to the test procedure was then introduced. The previous assessments of bioadhesion were achieved on the microparticle formulations, VH and HPMC components, and their physical mixtures as powder form. It was thought that the surface area of these formulations might produce variations in the results of their adhesion to mucin-agar media. Therefore the effect of compression these formulation into discs was studied in order to control their surface area.

When the adhesion profiles of a VH:HPMC physical mixture (formulation 76) and compressed disc of the same formulation were compared, it was found that the adhesion profile of the disc was decreased, as shown in Figure 4.13. The mean distance travelled down the mucin-agar plate by uncompressed and discs of formulation 76 at 90 minutes was 15.6 ±2.6 cm and 21 ±0.0 cm (total distance of the disc is 21cm) respectively ($P \leq 0.05$), suggesting that compression reduced the porosity, impeding ingress of water required to form an adhesive bond.

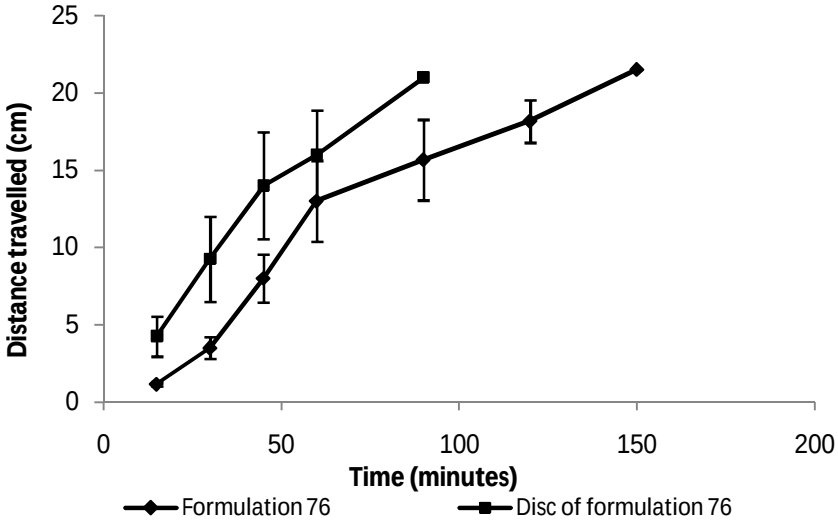

Figure 4.13 Effect of compressing a physical mixture (formulation 76) into discs on their dynamic adhesion in comparison to uncompressed formulation, n=3. Compression of formulation 76 into a disc resulted in a decrease in the dynamic adhesion of this formulation to mucin-agar medium.

Statistical comparison of the effect of compression on dynamic adhesion of microparticle formulations is shown in Table 4.6 below, using T-test for two samples of equal variances.

Table 4.6 Effect of compression of the 4% w/w microparticle formulations into discs on their dynamic adhesion in comparison to uncompressed formulations, n=6.

Composition	**Mean of the distance travelled at 120 minutes (cm)**		**Statistical T-test analysis (Probability)***
	uncompressed	**Discs**	
4% HPMC precipitated by IPA (69)	8.5 ±1.4	17.1 ±1.6	0.02
4% HPMC precipitated by acetone (71)	5.1 ±0.3	11.1 ±1.8	0.03
4% VH:HPMC precipitated by IPA (73)	13 ±2.1	17.6 ±2.8	0.06
4% VH:HPMC precipitated by acetone (75)	4.8 ±0.7	21 ±0.0	0.00005

* The differences were significant when the probability was $P \leq 0.05$.

The previous experiments were conducted at ambient laboratory temperature, variability in which may have had an effect on the viscosity of the hydrated gels. In order to eliminate this variability, and also to simulate the temperature conditions in the nose, the adhesion tests were repeated with compressed discs at a controlled temperature of 37 ±0.5°C.

It was found that performing adhesion tests at 37°C caused a pronounced decrease in their dynamic adhesion in comparison to laboratory temperature as shown in Table 4.7. The viscosity of HPMC is known to decrease with increasing temperature (to a temperature less than 60°C) (Shenoy 1999; Brogly et al 2010), and as viscosity is thought to affect bioadhesion, this may also explain the decrease in the observed *in-vitro* bioadhesion.

Table 4.7 Effect of two temperatures, ambient laboratory temperature and 37°C on the dynamic adhesion profiles of some microparticle formulations, n=6.

Composition	Mean of the distance travelled at 60 minutes		Statistical analysis (Probability) *
	ambient laboratory temperature	37°C	
4% HPMC precipitated by IPA (69)	7.7 ± 2.0	15.5 ±3.0	0.06
4% HPMC precipitated by acetone (71)	2.8 ±0.2	21 ±0.0	0.00003
4% VH:HPMC precipitated by IPA (73)	14.6 ±1.0	21 ±0.0	0.055
4% VH:HPMC precipitated by acetone (75)	3.1 ±1.3	15.5 ±3.1	0.04

* The differences were significant when the probability was $P \leq 0.05$.

4.3.2.6 Dynamic vapour sorption

DVS curves were obtained for HPMC and all VH:HPMC (1:1) microparticle formulations (72-75). Figure 4.14 shows the DVS curve of HPMC as an example of a profile obtained.

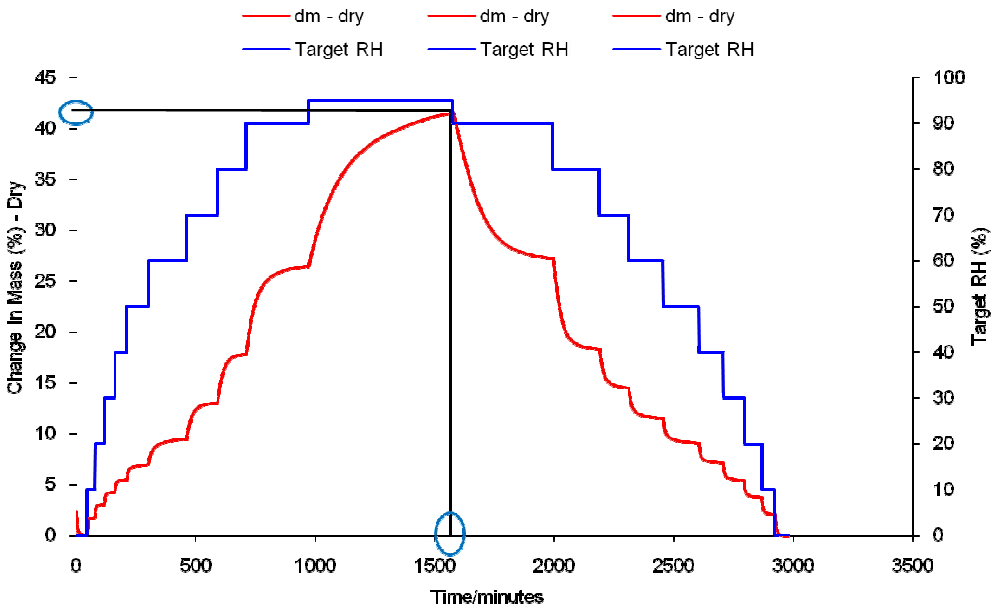

Figure 4.14 DVS curve of HPMC, using 0-95-0 %RH program (10% RH increased stepwise) at 25°C. The blue line shows target RH and red line shows percentage change in mass.

Two points have been used to study the differences in water sorption between formulations, (i) percentage of maximum humidity sorption (in relation to the dry weight) and (ii) time required to achieve that sorption, as illustrated in Figure 4.14. The numerical data obtained are shown in Table 4.8.

Table 4.8 DVS data of HPMC and VH:HPMC (1:1) microparticle formulations of concentrations 3% and 4%, precipitated by IPA (72 and 73) and acetone (74 and 75).

Formulation	Maximum change in mass (%, dry)	Time required to achieve maximum sorption (minutes)
HPMC	41.42	1570
72	30.92	2143
73	33.57	1851
74	28.02	2243
75	28.92	2168

HPMC powder absorbed more water, more rapidly than the VH:HPMC (1:1) microparticle formulations, using either IPA or acetone as a precipitating agent. This result may be attributed to the change of the polymer matrix after precipitation as evidenced by SEM.

It appeared that IPA precipitated microparticles absorbed more water than acetone precipitated microparticles, suggesting that the precipitating agent alters the water sorption capability of the polymer matrix. This will be discussed in more detail in later chapters.

4.4 Conclusion

- VH:HPMC (1:1) microparticles were obtained with the optimal particle size required for nasal delivery (less than 100μm), but low VH content in the microparticles, using a precipitation technique. This resulted from the solubility of VH in the precipitating agents (IPA and acetone).

- This technique produced a pronounced increase in the dynamic adhesion of precipitated HPMC microparticles using IPA or acetone as precipitating agents when compared to HPMC powder, due to the possible effects of differences in the surfaces of the material precipitated from IPA and acetone.

- VH:HPMC microparticles produced the same adhesion dynamic of blank HPMC microparticles due to the low drug content of microparticles.

- HPMC absorbed more water than microparticles precipitated by acetone or IPA processed microparticles. This result may be attributed to the change of the polymer matrix after precipitation.

Chapter 5

Preparation and evaluation of microparticles containing metformin

5.1. Introduction

Metformin hydrochloride (MH) is an imidodicarbonimidic diamide, N, N-dimethyl-monohydrochloride (Figure 5.1), with an empirical formula of $C_4H_{11}N_5$.HCl, and exists as white crystals. The molecular weight is 165.62, the pk_a is 12.4 and the pH of a 1% aqueous solution of MH is 6.68. It shows UV absorption at 233nm. MH is freely soluble in water, slightly soluble in alcohol, practically insoluble in acetone, ether, chloroform and methylene chloride (European Pharmacopoeia).

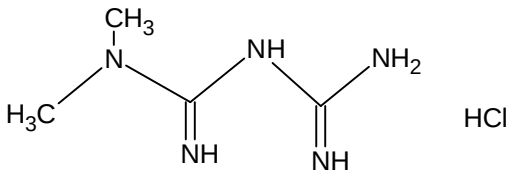

Figure 5.1 Chemical structure of metformin HCl (MH)

MH is used for hyperglycaemic patients (type II) by improving glucose tolerance and lowering plasma glucose levels. Its pharmacological mechanism of action is different from other classes of oral anti-hyperglycaemic agents. Metformin decreases hepatic glucose production, decreases intestinal absorption of glucose, and improves insulin sensitivity by increasing peripheral glucose uptake and utilisation. It is slowly and incompletely absorbed from the gastrointestinal tract, with its absolute bioavailability reported to be about 50 to 60% (Basak et al 2008). It is available in high dose tablets and capsules of 500-1000mg.

Although it is evident that this would not be a suitable molecule for nasal administration, because of the factors discussed above, it is nevertheless an acceptable water soluble model compound for formulation studies. Different analytical techniques were utilised to assess MH features as microparticles after processing such as DSC, XRPD, FT/IR, SEM, DVS and UV.

5.2 Materials and methods

The materials used in this chapter were MH, HPMC, IPA and acetone, previously discussed in Section 2.2.

5.2.1 Determination of MH solubility and UV absorbance

The solubility of MH in distilled water, IPA and acetone were studied using the method described in Section 2.5.2. The standard calibration curve of MH in distilled water was obtained using the UV spectrophotometric method mentioned in the same Section 2.5.2.

5.2.2 Determination of percent yield and metformin content of microparticles

Microparticles were prepared from MH:HPMC (1:1) aqueous systems 3% w/w (formulations 80 and 82) and 4% w/w (formulations 81 and 83) using the precipitation technique described in Section 2.5.3.2, with a stirring speed of 8000 rpm and a temperature of 4 ±0.5°C. IPA and acetone were used as precipitating agents respectively, and the compositions of the formulations are shown in Table 5.1 below.

Percent yield and drug content were determined using the method detailed in Section 2.5.4.1 (Equation 2.7 and 2.8).

Table 5.1 Composition and process parameters of MH:HPMC (1:1) microparticles

Formulation	MH concentration (%w/w)	HPMC concentration (%w/w)	Temperature (±0.5°C)	Stirring speed (rpm)	Precipitating agent
80	3	3	4	8000	IPA
81	4	4	4	8000	IPA
82	3	3	4	8000	Acetone
83	4	4	4	8000	Acetone

5.2.3 Preparation of physical mixtures

Physical mixtures corresponding to the final composition of the microparticles (assessed using the methods in Section 2.5.4.1) were prepared, and the corresponding formulation numbers are shown in Table 5.2.

Table 5.2 Physical mixtures of MH:HPMC in ratios similar to the prepared microparticles.

Physical mixture formulations	MH: HPMC microparticle
84	80
85	81
86	82
87	83

5.2.4 Physiochemical properties of prepared microparticles

5.2.4.1 Measurement of microparticle size using laser diffraction

The mean size of the microparticle formulations detailed in Table 5.1 was assessed using the laser diffraction technique described in Section 2.5.4.3.

5.2.4.2 Scanning electron microscopy

The SEM images of microparticle formulations and their unprocessed components were obtained using the technique described in Section 2.5.4.4.

5.2.4.3 X-ray powder diffraction

The crystalline and amorphous properties of MH:HPMC (1:1) microparticles in Table 5.1 were studied in comparison to unprocessed components and physical mixtures (Table 5.2) using XRPD (described in Section 2.5.4.8).

5.2.4.4 Differential scanning calorimetry

DSC thermograms of different concentrations of MH:HPMC (1:1) microparticles (formulations of Table 5.1), their physical mixtures (formulations of Table 5.2), blank HPMC microparticles (formulations 68-71 prepared in Chapter 4) and their unprocessed components were obtained using the specific method for MH described in Section 2.5.4.9.

5.2.4.5 Fourier transform infrared spectroscopy

The IR spectra of the microparticle formulations and their unprocessed components were obtained using the technique described in Section 2.5.4.7.

5.2.4.6 *In-vitro* dynamic adhesion

In-vitro dynamic adhesion of all formulations and blank HPMC microparticles (formulations 68-71) were studied using mucin-agar plates. The preparation of adhesion media and samples for this test was described in Section 2.5.4.11. The

effect of drug loading, contact time (15 seconds and 1 minute), compression of the powder into discs (using punch and die with 4 kg compression force) and temperature of the adhesion environment (for compressed discs at ambient laboratory temperature and 37 ±0.5°C) were assessed using the techniques mentioned in the same Section 2.5.4.11.

5.2.4.7 Dynamic vapour sorption

Water vapour sorption of microparticle formulations, blank HPMC microparticles (formulations in Table 4.1 of Chapter 4) and formulation 87 (physical mixture of unprocessed components MH:HPMC) were measured using the technique described in Section 2.5.4.12.

5.2.4.8 Metformin release

The release of metformin from MH:HPMC (1:1) microparticles (formulations 80, 81, 82 and 83), and their physical mixtures (formulations 84, 85, 86 and 87) were studied using the Franz-cell diffusion apparatus (described in detail in Section 2.1.13). Samples were analysed for MH content using UV spectrophotometry at 233nm (Section 2.5.4.14).

5.3 Results and discussion

5.3.1 Determination of MH solubility

It was found that MH has slight solubility in IPA (1 g/141 ml) and was practically insoluble in acetone (1 g/11,111 ml) (USP solubility definition). Figure 5.2 shows the standard calibration curve of MH in water using UV spectrophotometry at λ 233nm.

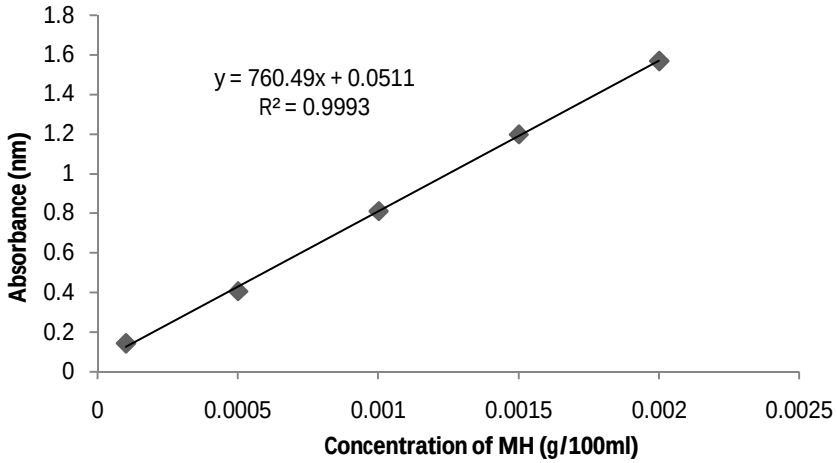

Figure 5.2 Standard calibration curve of metformin HCl (MH) determined in distilled water at 233 nm using 1 cm cell path length, using UV spectrophotometry.

5.3.2 Particle size and physiochemical properties of microparticles

The required microparticle size for nasal administration should be lower than 100µm (De Ascentiis et al 1996; Wermeling & Miller 2003). MH:HPMC (1:1) microparticles of all formulations (80-83) showed an acceptable range of particle size as shown in Table 5.3.

Table 5.3 Physical properties of MH:HPMC (1:1) microparticles, n=6.

Formulation	Mean size of microparticles (μm)	% Yield	Metformin content in microparticles (%)
3% MH:HPMC precipitated by IPA (80)	36.86 ±14.1	47.5 ± 3.5	8.0 ±1.1
4% MH:HPMC precipitated by IPA (81)	58.31 ±15.8	53.1 ± 4.4	8.2 ±0.8
3% MH:HPMC precipitated by acetone (82)	45.29 ±28.9	55.5 ± 14.8	45.0 ±3.2
4% MH:HPMC precipitated by acetone (83)	51.53 ±24.9	63.2 ± 0.4	53.0 ±1.2

A lower drug content was obtained for MH:HPMC (1:1) microparticles precipitated in IPA, while 45-53% drug content was obtained for acetone precipitated MH:HPMC (1:1) microparticles. This arose because of the slight solubility of MH in IPA, whereas MH and HPMC in were virtually insoluble in acetone.

5.3.2.1 Scanning electron microscopy

The SEM images of HPMC, MH, and microparticle formulations are shown in Figure 5.3. MH appears as an irregular crystalline solid, with a particle size of up to 500 μm, while the morphology of microparticle formulations varied depending on the precipitating solvent used. Formulations precipitated using IPA (80 and 81) showed discrete, well formed cubic drug crystals of around 2μm in size on a structureless surface. Microparticles precipitated by acetone (formulations 82 and 83) showed MH crystals of 1-2 μm enveloped within an amorphous HPMC matrix. This effect was more obvious from the micrographs of the 3% microparticles than for the 4% formulation. The co-precipitation technique therefore produced microcrystals of drug adsorbed on the surface or entrapped within the HPMC matrix, depending on the choice of solvent. The decreased in size of MH crystals following precipitation is attributed to the previously reported influence of HPMC inhibiting the crystal growth process of MH crystals (Chang & Gray 1978).

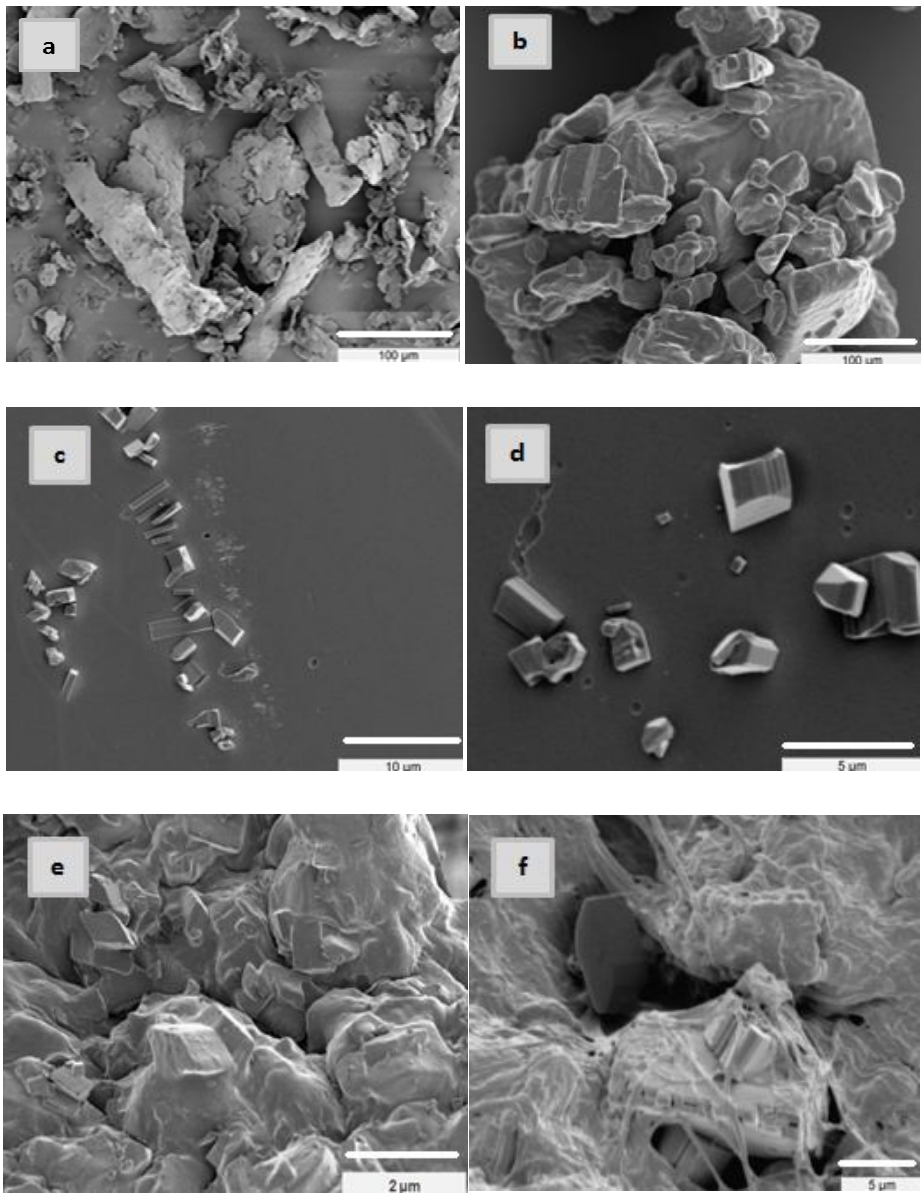

Figure 5.3 SEM images of a) HPMC, b) MH, c) formulation 80 (3% MH:HPMC (1:1) microparticle precipitated by IPA), d) formulation 81 (4% MH:HPMC (1:1) microparticle precipitated by IPA), e) formulation 82 (3% MH:HPMC (1:1) microparticle precipitated by acetone) and f) formulation 83 (4% MH:HPMC (1:1) microparticle precipitated by acetone).

5.3.2.2 X-ray powder diffraction

The XRPD spectra of MH, HPMC and their formulations are shown in Figure 5.4.

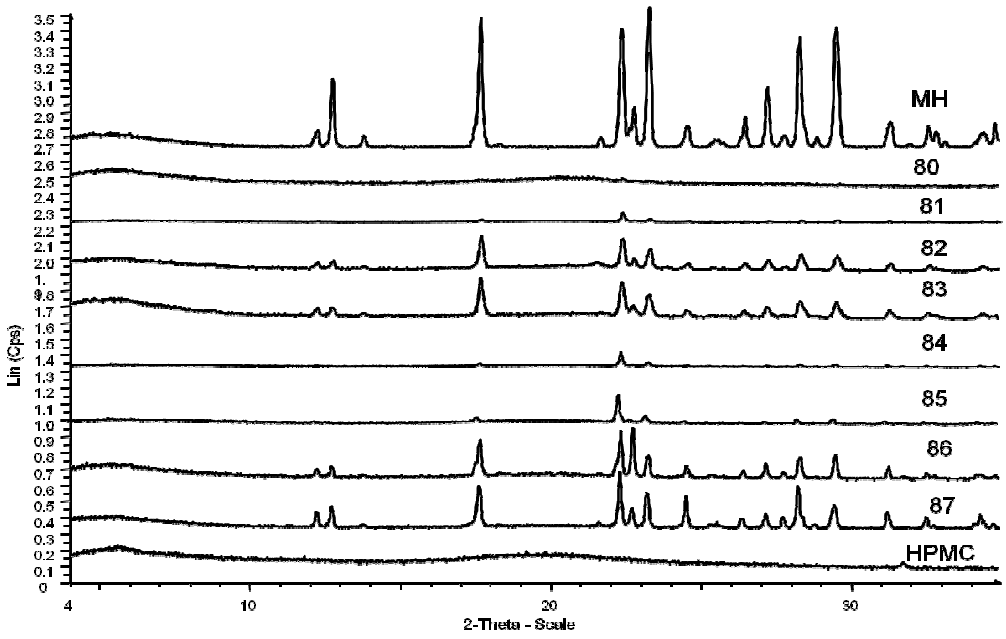

Figure 5.4 X-ray spectrums of MH, formulation 80 (3% MH:HPMC (1:1) precipitated by IPA), formulation 81 (4% MH:HPMC (1:1) precipitated by IPA), formulation 82 (3% MH:HPMC (1:1) precipitated by acetone), formulation 83 (4% MH:HPMC (1:1) precipitated by acetone), formulation 84 (physical mixture of formulation 80), formulation 85 (physical mixture of formulation 81), formulation 86 (physical mixture of formulation 82), formulation 87 (physical mixture of formulation 83) and HPMC.

Microparticles precipitated using IPA only retained a trace of the distinctive peaks of MH. This was also observed with the corresponding physical mixture, indicating that this was due to the low drug content. However for microparticle formulations precipitated in acetone, the distinctive pattern of crystalline MH was retained, and

was also present in the corresponding physical mixture. This confirms the morphological evidence from the SEM images.

5.3.2.3 Differential scanning calorimetry

As shown in Figure 5.5, MH has an endothermic peak of its melting point at 235°C which was also observed in the physical mixtures (formulation 84-87).

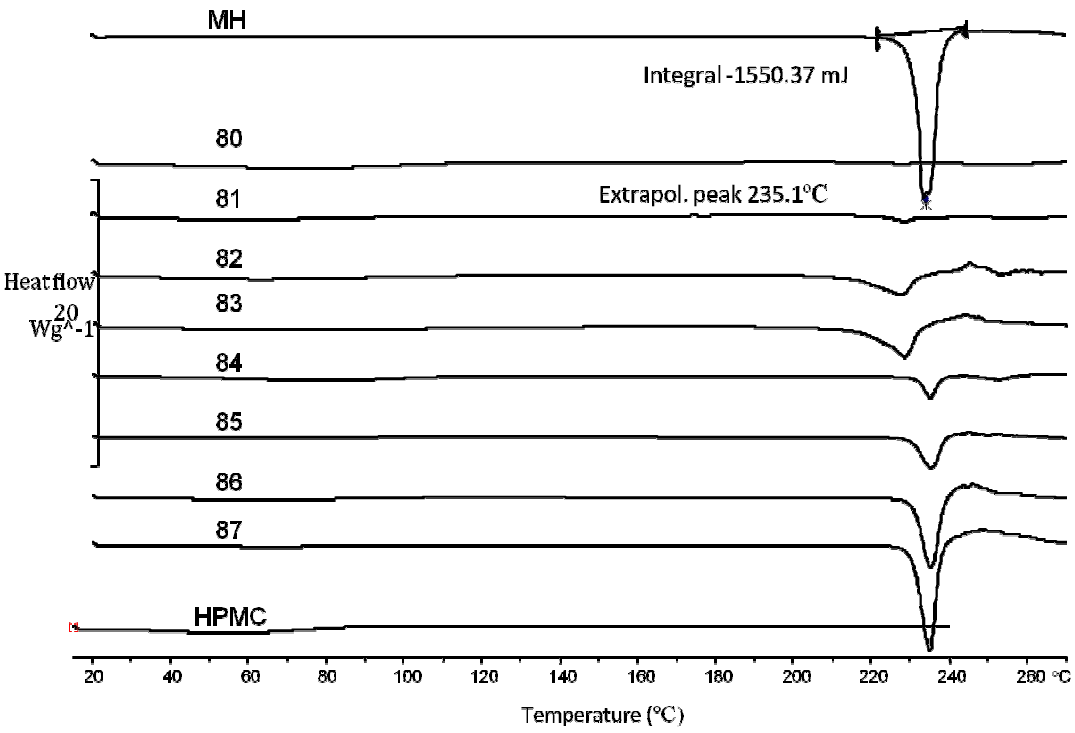

Figure 5.5 DSC thermograms of MH, formulation 80 (3% MH:HPMC (1:1) precipitated by IPA), formulation 81 (4% MH:HPMC (1:1) precipitated by IPA), formulation 82 (3% MH:HPMC (1:1) precipitated by acetone), formulation 83 (4% MH:HPMC (1:1) precipitated by acetone), formulation 84 (physical mixture of formulation 80), formulation 85 (physical mixture of formulation 81), formulation 86 (physical mixture of formulation 82), formulation 87 (physical mixture of formulation 83) and HPMC.

Microparticles precipitated using IPA did not show the MH endothermic peak, although this was present in the corresponding physical mixtures. The reason for this was unexplained, but may possibly be due to sampling difficulties associated with low drug contents. The microparticle formulations precipitated in acetone showed the distinctive endothermic peak for MH, although the peak occurred at a slightly lower temperature, thought to be due to an intra-molecular H-bonding interaction with HPMC in the matrix structure (Zhou 1993). The corresponding physical mixture revealed the expected MH endotherm. These findings further support the SEM and XRPD analyses. The integration of melting point peaks of MH is shown in Table 5.4.

Table 5.4 Quantification the endothermic peak of MH melting point in different formulations.

Formulation	Integration of endothermic peak of MH melting point (mJ)	Melting point of MH (°C)
MH	1550.37	235.1
3% MH:HPMC precipitated by IPA (80)	10.52	229.2
4% MH:HPMC precipitated by IPA (81)	38.47	230.0
3% MH:HPMC precipitated by acetone (82)	702.98	231.1
4% MH:HPMC precipitated by acetone (83)	935.26	231.3
physical mixture of formulation 80 (84)	104.75	234.6
physical mixture of formulation 81 (85)	118.69	234.5
physical mixture of formulation 82 (86)	1068.66	235.0
physical mixture of formulation 83 (87)	1072.63	234.9

5.3.2.4 Fourier transform infrared spectroscopy

Figure 5.6 shows the IR spectra of MH, HPMC and microparticle formulations.

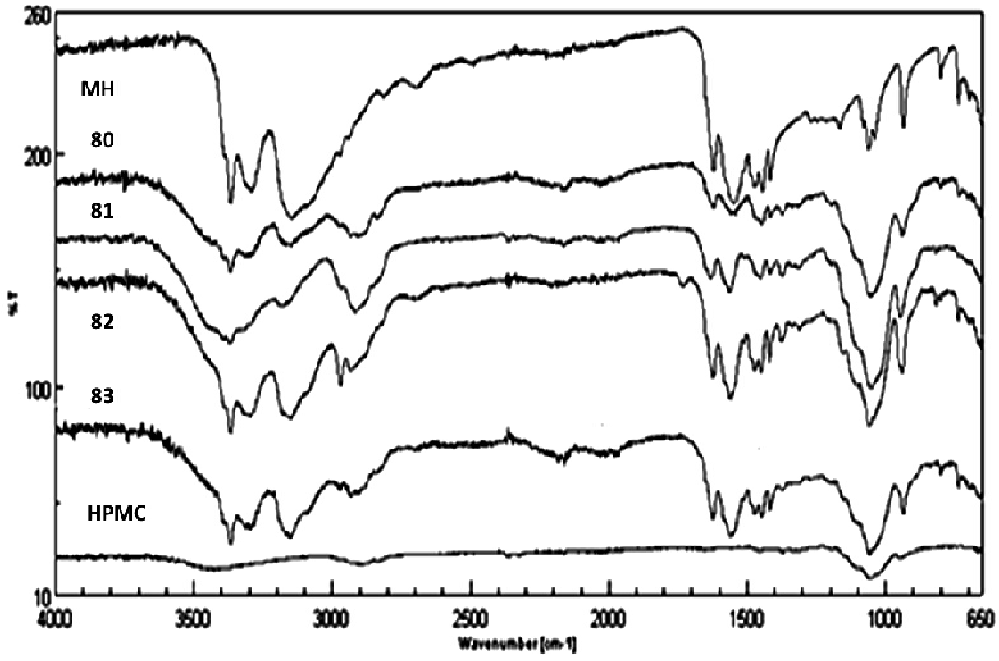

Figure 5.6 FT/IR spectra of MH, formulation 80 (3% MH:HPMC (1:1) precipitated by IPA), formulation 81 (4% MH:HPMC (1:1) precipitated by IPA), formulation 82 (3% MH:HPMC (1:1) precipitated by acetone), formulation 83 (4% MH:HPMC (1:1) precipitated by acetone) and HPMC.

HPMC displays two broad peaks between 3700-3000 cm^{-1} and 3000-2700 cm^{-1}, and MH displays a broad peak at 3400-2700 cm^{-1}. All microparticle formulations showed a spectrum reflecting a mixture of MH and HPMC, although the peak around 2900 cm^{-1} is more prominent in the processed materials than in the individual components. Acetone processed formulations (82 and 83) showed a more predominant MH pattern than IPA processed formulations, due to their higher drug content.

5.3.2.5 *In-vitro* dynamic adhesion

The bioadhesion of HPMC was less than precipitated HPMC microparticles using IPA or acetone as precipitating agents as discussed in Chapter 4 (Section 4.3.2.5).

Figure 5.7 shows the effect of IPA processing in the presence of MH on the adhesion properties of the microparticles and physical mixture.

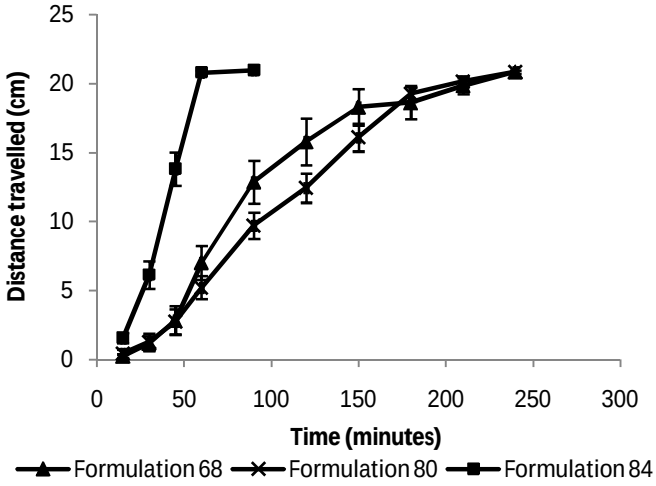

Figure 5.7 Effect of drug loading on the dynamic adhesion profiles of 3% blank HPMC microparticles precipitated by IPA (formulation 68), 3% MH:HPMC (1:1) microparticles precipitated by IPA (formulation 80) and corresponding physical mixture (formulation 84), n=6. Showing the non significant difference between the dynamic adhesion profiles of blank HPMC and microparticles loaded with MH, and the significant difference between the dynamic adhesions profiles of processed MH:HPMC microparticles and corresponding physical mixture of unprocessed MH and HPMC powders.

Microparticles containing MH precipitated in IPA (formulation 80) showed a similar dynamic adhesion profile to blank HPMC microparticles (formulation 68), while both were significantly more adhesive than the corresponding physical mixture (formulation 84). Similar effects were observed for 4% formulations, as shown in Figure 5.8.

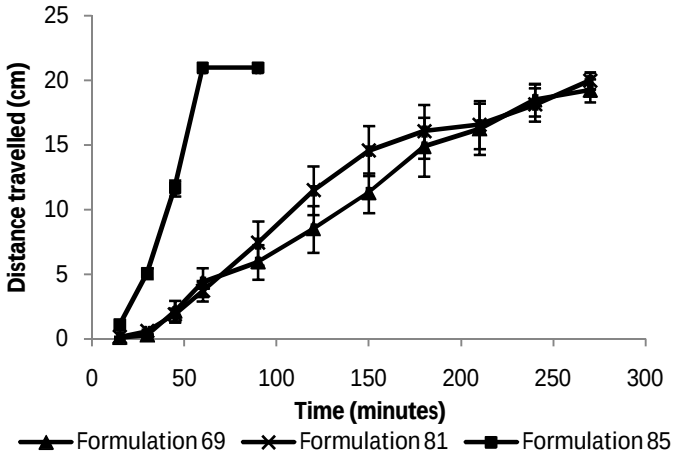

Figure 5.8 Effect of drug loading on the dynamic adhesion profiles of 4% blank HPMC microparticles precipitated by IPA (formulation 69), 4% MH:HPMC (1:1) microparticles precipitated by IPA (formulation 81) and corresponding physical mixture (formulation 85), n=6.

Figures 5.9 and 5.10 show the effect of acetone processing in the presence of MH on the adhesion properties of the microparticles and physical mixtures.

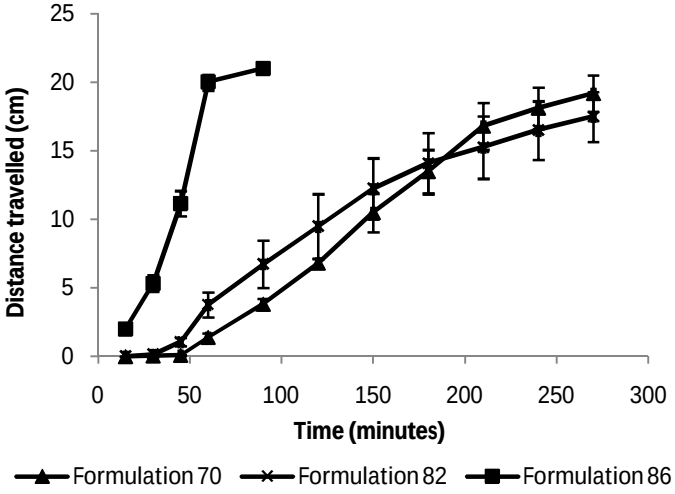

Figure 5.9 Effect of drug loading on the dynamic adhesion of 3% blank HPMC microparticles precipitated by acetone (formulation 70), 3% MH:HPMC (1:1) microparticles precipitated by acetone (formulation 82) and corresponding physical mixture (formulation 86), n=6.

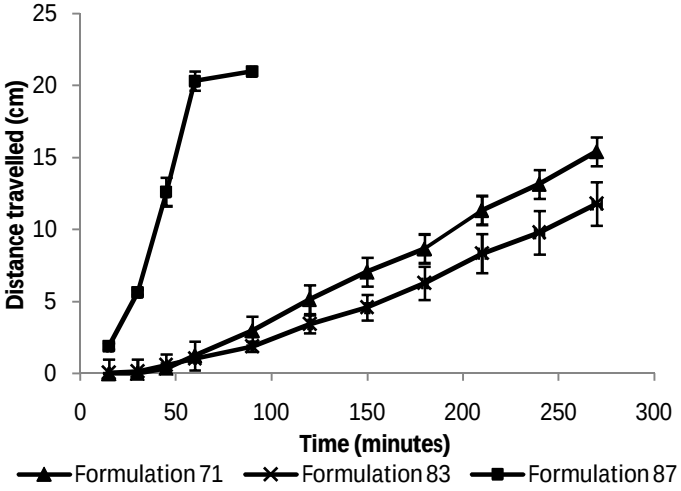

Figure 5.10 Effect of drug loading on the dynamic adhesion of 4% blank HPMC microparticles precipitated by acetone (formulation 71), 4% MH:HPMC (1:1) microparticles precipitated by acetone (formulation 83) and corresponding physical mixture (formulation 87), n=6. No significant difference was observed between blank HPMC and MH:HPMC microparticles, while a significant difference was observed between the dynamic adhesions profiles of processed MH:HPMC microparticles and corresponding physical mixture of unprocessed MH and HPMC powders.

Microparticles containing MH precipitated in acetone (formulations 82 and 83) generally show a similarity to the blank HPMC microparticles (formulations 70 and 71), while all were significantly more adhesive than the corresponding physical mixtures (formulations 86 and 87).

From the above data, it is evident that the bioadhesion of MH:HPMC microparticles is highly solvent dependant, as shown in Figure 5.11 below. The significance of the solvent effect on water uptake will be discussed in Section 5.3.2.6 and Chapter 6.

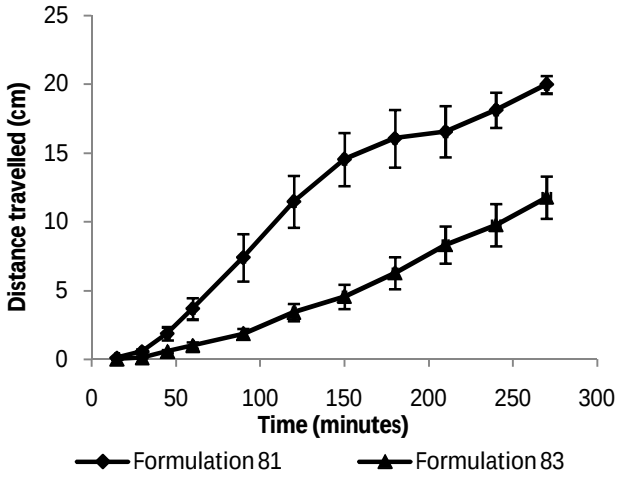

Figure 5.11 Dynamic adhesion of 4% MH:HPMC (1:1) microparticles precipitated by IPA (formulation 81) and acetone (formulation 83), n=6. Showing the enhanced bioadhesion obtained with acetone precipitated microparticles (formulation 83) in comparison to IPA precipitated microparticles (formulation 81).

As shown in the previous Figure 5.11, MH:HPMC microparticles precipitated by acetone showed better adhesion to the mucin-agar support in comparison to IPA precipitated microparticles ($P \leq 0.05$). It is suggested that IPA processing resulted in MH crystals adsorbed to the structureless surface of HPMC, while acetone precipitated microparticles contained MH crystals enveloped within HPMC matrix as evidenced by SEM images. This may result in rapid water uptake by IPA formulations, which then swell and slide down the adhesion media faster than acetone precipitated formulations. This hypothesis requires further study of water uptake by formulations as a result of different precipitating agents (see later Section 5.3.2.6 and Chapter 6).

The statistical comparison of these data is shown in Tables 5.5 and 5.6 below, using T-test for two samples of equal variances.

Table 5.5 Statistical analysis the dynamic adhesion of MH:HPMC (1:1) microparticles in comparison to the corresponding blanks and physical mixtures, n=6.

Composition	Mean of distance travelled at 90 minutes (cm)	Statistical T-test analysis (Probability*)
3% blank HPMC precipitated by IPA (68)	12.9 ±1.5	0.06
3% MH:HPMC precipitated by IPA (80)	9.7 ±0.9	
3% MH:HPMC precipitated by IPA (80)	9.7 ±0.9	0.00002
Corresponding physical mixture (84)	21±0.0	
4% blank HPMC precipitated by IPA (69)	5.9 ±1.3	0.2
4% MH:HPMC precipitated by IPA (81)	7.4 ±1.7	
4% MH:HPMC precipitated by IPA (81)	7.4 ±1.7	0.0006
Corresponding physical mixture (85)	21 ±0.0	
3% blank HPMC precipitated by acetone (70)	3.8 ±0.4	0.1
3% MH:HPMC precipitated by acetone (82)	6.7 ±1.7	
3% MH:HPMC precipitated by acetone (82)	6.7 ±1.7	0.00001
Corresponding physical mixture (86)	21 ±0.0	
4% blank HPMC precipitated by acetone (71)	3 ±0.3	0.2
4% MH:HPMC precipitated by acetone (83)	1.9 ±0.3	
4% MH:HPMC precipitated by acetone (83)	1.9 ±0.3	0.00005
Corresponding physical mixture (87)	21 ±0.0	

* The differences were significant when the probability was $P \leq 0.05$.

Table 5.6 Statistical analysis the effect of precipitating agents (IPA and acetone) on the dynamic adhesion of blank HPMC and MH:HPMC (1:1) microparticles, n=6.

Composition	Mean of distance travelled at 90 minutes (cm)	Statistical T-test analysis (Probability)*
3% blank HPMC precipitated by IPA (68)	12.9 ±1.5	0.00003
3% blank HPMC precipitated by acetone (70)	3.8 ±0.4	
3% MH:HPMC precipitated by IPA (80)	9.7 ±0.9	0.05
3% MH:HPMC precipitated by acetone (82)	6.7 ±1.7	
4% blank HPMC precipitated by IPA (69)	5.9 ±1.3	0.06
4% blank HPMC precipitated by acetone (71)	3 ±0.3	
4% MH:HPMC precipitated by IPA (81)	7.4 ±1.7	0.009
4% MH:HPMC precipitated by acetone (83)	1.9 ±0.3	

* The differences were significant when the probability was $P \leq 0.05$.

The effect of initial contact time of the sample to the adhesion medium was also studied and is shown in Table 5.7 (using T-test). Increasing contact time from 15 seconds to 1 minute resulted in an increase in measured adhesion, similar to results explained previously for verapamil formulations in Section 4.3.2.5.

Table 5.7 Statistical analysis the effect of the contact time (15 seconds and 1 minute) on the dynamic adhesion of MH:HPMC (1:1) formulations, n=6.

Composition	**Mean of the distance travelled at 90 minutes (cm)**		**Statistical T-test analysis (Probability)***
	15 seconds	**1 minutes**	
3% MH:HPMC precipitated by IPA (80)	16.5 ±1.9	9.7 ±0.9	0.05
4% MH:HPMC precipitated by IPA (81)	13.4 ±1.3	7.4 ±1.7	0.0001
3% MH:HPMC precipitated by acetone (82)	12.1 ±2.6	6.7 ±1.7	0.04
4% MH:HPMC precipitated by acetone (83)	10.5 ±2.7	1.9 ±0.3	0.03

* The differences were significant when the probability was $P \leq 0.05$.

The effect of compacting a physical mixture formulation into a disc on the adhesion profile is shown in Figure 5.12. It was found that when compressed into a disc the dynamic adhesion of formulation 87 decreased and became more variable, suggesting that compression reduced the porosity, impeding ingress of water required to form an adhesive bond.

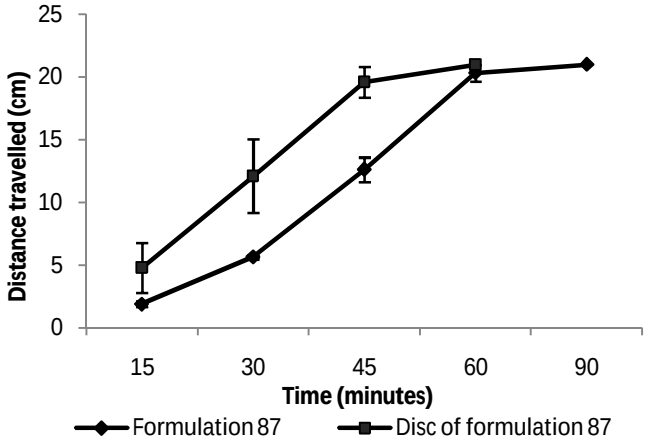

Figure 5.12 Effect of compression (discs) on the dynamic adhesion of formulation 87 (physical mixture of MH:HPMC), n=6. Showing the dynamic adhesion of formulation 87 decreased and became more variable when applied in disc form.

Comparison of MH:HPMC microparticles precipitated by IPA and acetone revealed interesting adhesion profiles when compressed into discs as shown in Figure 5.13.

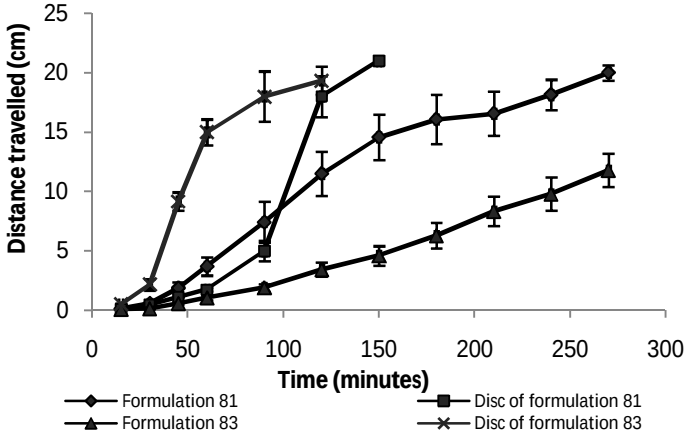

Figure 5.13 Effect of compression (discs) on the dynamic adhesion of 4% MH:HPMC (1:1) microparticle formulations 81 (precipitated by IPA) and 83 (precipitated by acetone), n=6. Showing the dynamic adhesion of formulation 81 and 83 decreased when applied in discs form.

Compression into discs completely altered the adhesion profiles of microparticle formulations precipitated from both solvents. The discs exhibited an initial lag period, followed by a phase of rapid transit which was not observed with the uncompressed materials. This is thought to be a result of complex interplay between porosity, rate of hydration, mass and adhesion. With acetone formulations the differences between the disc and loose microparticles were very pronounced. It is suggested that compression into a disc ruptured the continuous enveloping HPMC film around the particles (see SEM Figure 5.3e and f), exposing the high content of MH crystals to the moist mucin surface. Conversely, the uncompressed acetone microparticles present only HPMC to the mucin surface, whereby MH was unable to interfere with the adhesive process. Due to the low MH content of the IPA microparticles, the influence of compression on adhesion was much less significant.

The effect of temperature on the performance of the adhesion test with MH formulations (Figure 5.14) is similar to that previously reported for verapamil formualtions (Section 4.3.2.5).

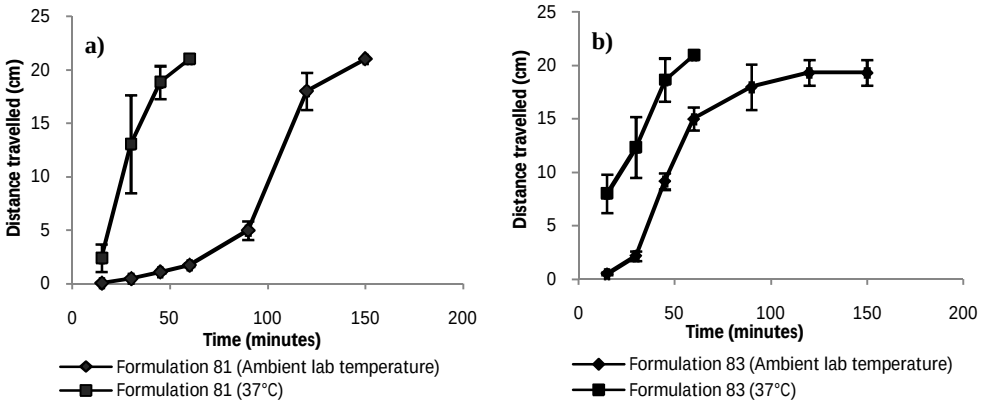

Figure 5.14 Effect of temperature (ambient laboratory temperature and 37°C) on the dynamic adhesion of a) formulation 81 (4% MH:HPMC (1:1) microparticles precipitated by IPA) and b) formulation 83 (4% MH:HPMC (1:1) microparticles precipitated by acetone), n=6. Elevated temperature (37°C) caused a decrease in the dynamic adhesion of all formulations.

5.3.2.6 Dynamic vapour sorption

The DVS uptake curve for MH alone is shown in Figure 5.15, and reveals that MH does not pick up significant quantities of water in response to exposure to humidity. The Moisture uptake measurements for MH:HPMC microparticles, their corresponding physical mixtures, and individual components are shown in Table 5.8 below.

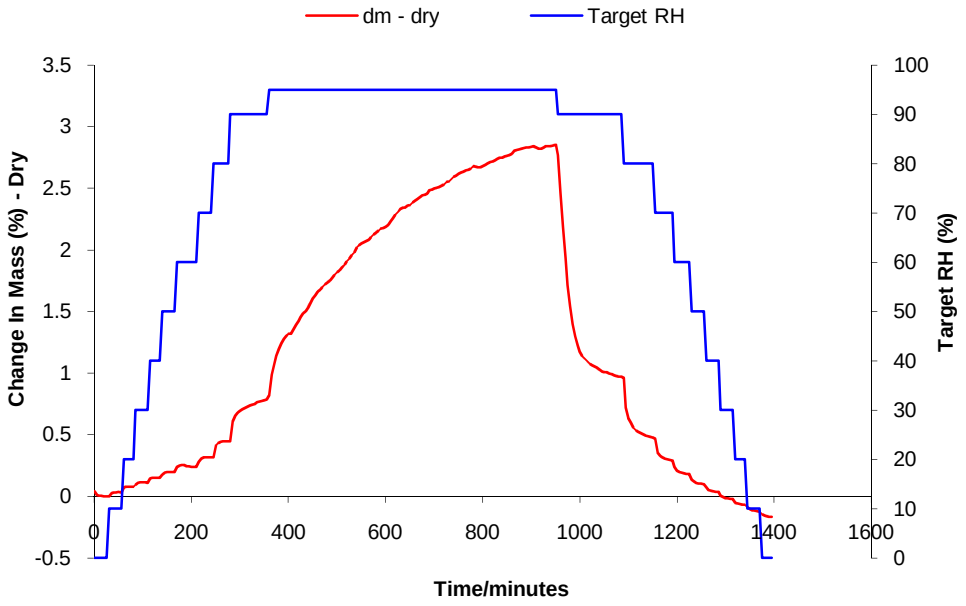

Figure 5.15 DVS curve of metformin HCl (MH), using 0-95-0 %RH program (10% RH increased and then decreased stepwise) at 25°C. The blue line shows target RH and red line shows percentage change in mass.

Table 5.8 DVS data of HPMC, MH, processed blank HPMC, MH:HPMC (1:1) microparticles and physical mixtures

Formulation	HPMC Content (%)	Mass increased at 95% RH (%, dry)	Time required to achieve maximum sorption (minutes)
HPMC	100	41.42	1570
MH	-	2.85	950
3% HPMC precipitated by IPA (68)	100	25.54	1603
4% HPMC precipitated by IPA (69)	100	21.21	1468
3% HPMC precipitated by acetone (70)	100	33.98	2115
4% HPMC precipitated by acetone (71)	100	30.47	1639
3% MH:HPMC precipitated by IPA (80)	92	38.39	1826
4% MH:HPMC precipitated by IPA (81)	92	45.92	2611
3%MH:HPMC precipitated by acetone (82)	55	107.90	3983
4%MH:HPMC precipitated by acetone (83)	47	115.50	3968
Physical mixture of MH:HPMC (87)	47	86.38	2857

Processing HPMC with IPA and acetone appears to decrease the total moisture uptake, and this effect appeared to be more pronounced with IPA samples (n=2). Inclusion of a small amount of MH (~8%) in the IPA processed materials had a significant effect on overall moisture uptake. This effect was even more pronounced with acetone processed materials, which contained approximately 50% MH. It is tempting to compare the DVS performance of 4% MH:HPMC (1:1) acetone processed microparticles with the corresponding physical mixture. However, while the MH in the physical mixture is totally exposed to the pervading atmosphere, in the acetone precipitated materials it is enveloped within the HPMC matrix (as observed previously in SEM, Figure 5.3e and f), and there is no obvious rational explanation for the observed data, which are most likely due to sampling difficulties with the physical mixture.

5.3.2.7 Metformin release

Figure 5.16 shows the release profile of MH in comparison to IPA precipitated microparticles (formulations 80 and 81) and corresponding physical mixtures (formulations 84 and 85).

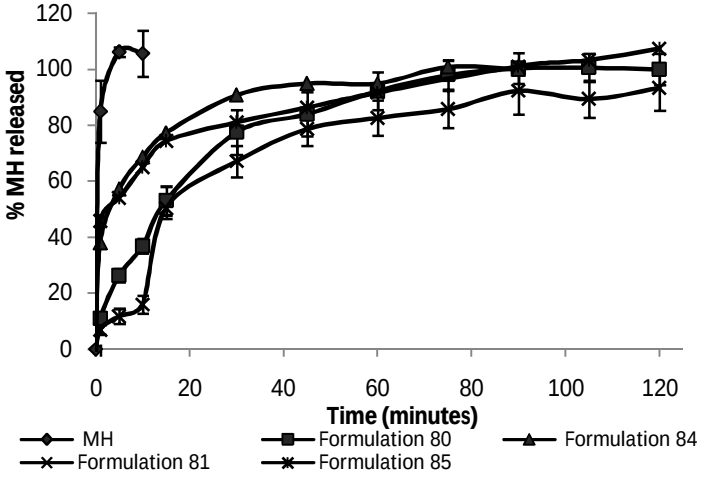

Figure 5.16 The release profile of MH from unprocessed MH, MH:HPMC (1:1) microparticles precipitated by IPA (formulations 80 and 81, 3% and 4% MH:HPMC respectively) and corresponding physical mixtures (formulations 84 and 85), n=6. The release profile of unprocessed MH was much more rapid than either microparticle or physical mixture preparations.

The release profile of unprocessed MH was much more rapid than either microparticle or physical mixture preparations. Comparison of MH to IPA precipitated microparticle formulations 80 and 81, and corresponding physical mixtures 84 and 85, is shown in Table 5.9, and revealed non-similarity in the release profiles.

Table 5.9 The similarity factor of MH release profiles by comparing MH powder to IPA precipitated microparticles and corresponding physical mixtures, n=6.

Formulation	Similarity factor (f_2)*
MH 3%MH:HPMC precipitated by IPA (80)	10.32
MH 4%MH:HPMC precipitated by IPA (81)	6.87
MH Physical mixture of formulation 80 (84)	21.88
MH Physical mixture of formulation 81 (85)	21.43

The differences were significant when f_2 similarity values were less than 50.

This suggests that the high ratio of HPMC to MH in the formulations (92:8) resulted in slower release of MH. The release of MH from the physical mixtures appeared more rapid in the initial stages, when compared to the processed microparticles. This suggests that in the physical mixture, MH is available for rapid dissolution and release prior to the hydration and gel formation of HPMC. However, in the processed microparticles, SEM images (Figure 5.3) appeared to indicate that one of the surfaces of the MH particles was embedded in the HPMC matrix, which may account for the slightly reduced rate of release.

Figure 5.17 shows the release of MH from acetone precipitated microparticles in comparison to the corresponding physical mixtures and MH.

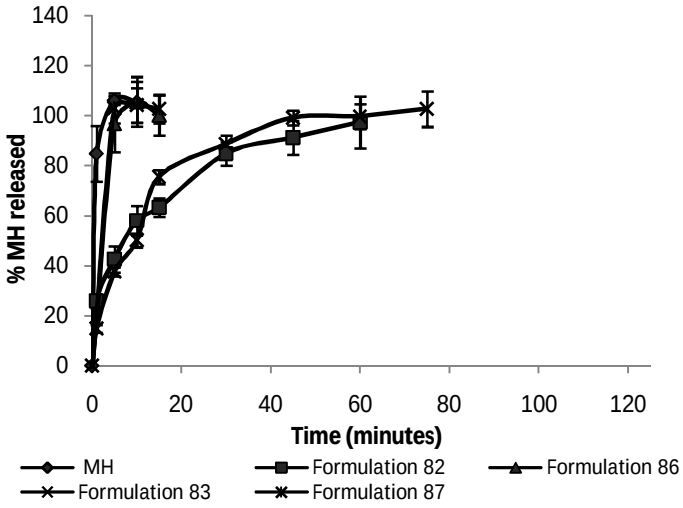

Figure 5.17 The release profile of MH from unprocessed MH, MH:HPMC (1:1) microparticles precipitated by acetone (formulations 82 and 83) and respective physical mixture (formulations 86 and 87), n=6. Showing the similarity in the release profiles of MH from unprocessed MH powder and physical mixture formulation, and the dissimilarity between these and the MH release profile of processed MH:HPMC microparticles.

In contrast to the results previously observed with physical mixtures containing approximately 8% MH (Figure 5.16), physical mixtures containing approximately 50% MH (formulation 86 and 87) achieved 100% after 5 minutes, similar to MH alone. It is suggested that this is due to the application technique, where the powder was sprinkled across the membrane surface. Both microparticle formulations (formulations 82 and 83) demonstrated controlled release up to one hour, demonstrating profiles which were different to the corresponding physical mixtures (f_2 19.959 and 20.55 respectively), and reflects the matrix nature of the precipitated material (Figure 5.3e and f).

5.4 Conclusion

- Small microparticles were obtained (lower than 100 μm) using high shearing mixer. A lower drug content (~8%) was obtained for MH:HPMC (1:1) microparticles precipitated in IPA, while 45-53% drug content was obtained for acetone precipitated MH:HPMC (1:1) microparticles. This correlates with the slight solubility of MH in IPA, whereas MH and HPMC were virtually insoluble in acetone.

- Processed microparticles using IPA as a precipitating agent produced formulations with discrete, well formed cubic drug crystals of around 2μm in size on a structureless HPMC surface, whereas microparticles precipitated by acetone showed MH crystals of 1-2 μm enveloped within an amorphous HPMC matrix. The co-precipitation technique therefore produced microcrystals of drug adsorbed on the surface or entrapped within the HPMC matrix, depending on the choice of solvent.

- Greater bioadhesion was achieved with processed microparticles when compared to the unprocessed components. However acetone precipitated microparticles demonstrated higher dynamic adhesion than IPA precipitated microparticles.

- Different water sorption uptake profiles were obtained for MH:HPMC microparticle formulations and physical mixtures, reflecting the morphological differences seen in SEM.

- Sustained release MH:HPMC (1:1) microparticles were produced using a co-precipitation technique, and achieved controlled release of MH.

- The acetone processed microparticles achieved high drug loading, uniform (small) particle size, significant bioadhesion and afforded prolonged drug release. These attributes indicate that such a product may have potential for nasal drug delivery.

Chapter 6

Physiochemical properties of HPMC microparticles precipitated by acetone

6.1 Introduction

Previous chapters have examined the formation of HPMC microparticles with lactose, verapamil hydrochloride (VH) and metformin hydrochloride (MH). Acetone processed microparticles appeared to offer particular advantage (Chapter 5 last conclusion). In order to further study the characteristics of HPMC precipitated by acetone, the properties of HPMC microparticles without drug were examined, in order to provide further elucidation of the mechanisms underlying the interactions with water.

6.2 Materials and methods

The chemicals used in this chapter were HPMC and acetone, which were discussed in Section 2.2.

6.2.1 Effect of water sorption on the physiochemical properties of HPMC microparticles precipitated by acetone

Blank 4% HPMC microparticles precipitated by acetone (formulation 71), using the same method described in Section 2.5.3.2, and unprocessed HPMC were chosen to study the effect of water sorption on the physiochemical properties of these formulations.

6.2.1.1 Dynamic vapour sorption

Water vapour sorption of 4% blank HPMC microparticles precipitated by acetone (formulation 71), and unprocessed HPMC were measured using the technique described in Section 2.5.4.12.

6.2.1.2 Saturated salts method

A saturated salt method was used as described in Section 2.5.4.13, in order to examine the effect of humidity on 4% blank HPMC microparticles precipitated by acetone (formulations 71) and HPMC powder. The effect of moisture on their physiochemical properties was assessed using DSC (specific for blank HPMC microparticles in Section 2.5.4.9), TGA (Section 2.5.4.10) and FT/IR (Section 2.5.4.7).

The samples were weighed at 4 day intervals to identify the weight gain with time for each relative humidity. Curves of percent humidity uptake with times were determined for all relative humidities.

6.3 Effect of processing variables on the physiochemical properties of HPMC microparticles precipitated by acetone

3% and 4% blank HPMC microparticles (formulations 70 and 71) were prepared using the technique described in Section 2.5.3.2, were used in the following sections.

6.3.1 Preparation of microparticles using different precipitation techniques

A Silverson SL 2T mixer or magnetic stirrer were used to prepare HPMC microparticles, either by dropping the aqueous gels (3% or 4% w/w) in acetone (dropping method using Silverson mixer, DS) or by direct mixing of that gel with precipitating agent (non-dropping method) using either Silverson (NDS) or magnetic stirrer (NDM), as shown in Scheme 6.1 and Table 6.1.

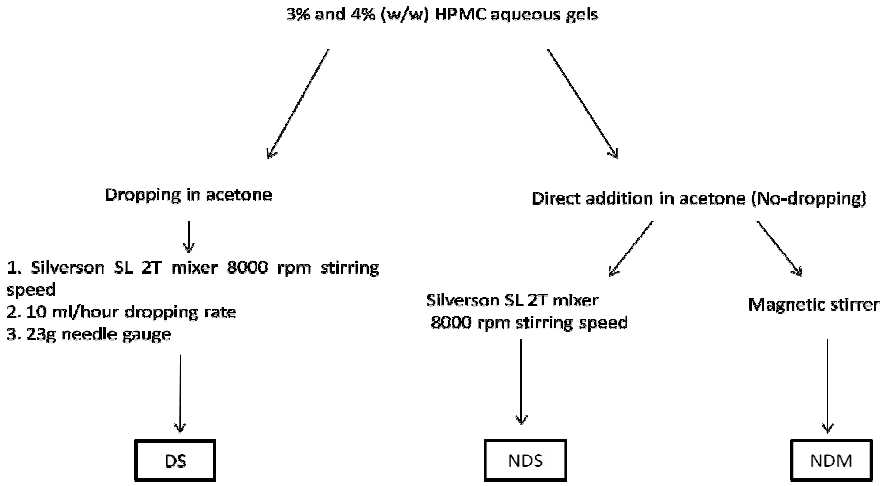

Scheme 6.1 Different techniques to prepare HPMC microparticles using acetone as a precipitating agent.

Table 6.1 Processing technique variables for preparation of HPMC microparticles using acetone as a precipitating agent.

Formulation	Concentration of HPMC (%w/w)	Volume of acetone (ml)	Technique used
70	3	200	DS
88	3	200	NDM
89	3	200	NDS
71	4	200	DS
90	4	100	DS
91	4	50	DS
92	4	200	NDM
93	4	100	NDM
94	4	50	NDM
95	4	200	NDS
96	4	100	NDS
97	4	50	NDS

DS dropping method using Siverson SL 2T
NDS non-dropping method using Silverson SL 2T mixer
NDM non-dropping method using magnetic stirrer

6.3.1.1 Acetone volume

A 10 ml volume of 4% aqueous HPMC gels were dropped into or mixed directly with, different volumes of acetone (50, 100 and 200 ml) to evaluate the effect on the physical properties of HPMC microparticles (as shown in Table 6.1).

6.3.1.2 Order of water and acetone addition

In order to explore the effect of water on the inter- and intra-molecular H-bonding orientation in the HPMC polymer, the modality of water and acetone addition was studied. HPMC powder was treated by direct addition to acetone (formulations 98 and 101, Table 6.2), while for formulation 100, there was a further addition of 10 mls of water. Formulations 99 and 102 were prepared by immediate addition of acetone to HPMC powder sprinkled on water. Mixtures were stirred for one hour using a magnetic stirrer.

Table 6.2 Processing technique variables of magnetic stirrer method for preparation of HPMC microparticles.

Formulation	HPMC weight (mg)	Volume of acetone (ml)	Order of mixing
98	300	200	HPMC powder to acetone
99	300	200	Acetone to (HPMC powder+10 ml DW)
100	300	200	10 ml DW to (HPMC + acetone powder)
101	400	200	HPMC powder to acetone
102	400	200	Acetone to (HPMC powder+10 ml DW)

DW=Distilled water

6.3.2 *In-vitro* dynamic adhesion

The distance travelled with time was measured using the method described in Section 2.5.4.11. The data were manipulated and the inverse of the slope of the resultant distance vs time curve was used as an indicative value of the extent of bioadhesion of all formulations in Table 6.1 and 6.2 as described by McInnes et al (2007a).

6.3.3 Scanning electron microscope

SEM images were obtained for microparticle formulations (71, 92, 95 and 102) and HPMC powder using the technique described in Section 2.5.4.4.

6.3.4 Differential scanning calorimetry

DSC was used to study the effect of process and formulation variables on the physical state of HPMC microparticles (Table 6.1 and 6.2) in comparison to HPMC powder. Samples were exposed to the heating programme described in Section 2.5.4.9 to calculate the glass transition temperature (Tg) and integration of endothermic peak between 20-125°C of all formulations in Table 6.1 and 6.2.

6.3.5 Water uptake measurement

A simple water uptake method (Section 2.5.4.13) was used to study the water uptake of the formulations in Table 6.1. AUC of water uptake curves was calculated to differentiate between tested formulations.

6.3.6 Dynamic vapour sorption

Vapour sorption of the formulations in Table 6.1 were studied using the method described in Section 2.5.4.12. Percentage of mass increase at 95% RH was calculated to assess the amount of moisture sorption by the sample.

6.3.7 Chemical study using nuclear magnetic resonance spectroscopy

All microparticle formulations in Table 6.1, and formulation 101 in Table 6.2 were examined using the technique described in Section 2.5.4.6 to elucidate any spectral changes in comparison to unprocessed HPMC powder.

6.4 Results and discussion

6.4.1 Moisture content of HPMC microparticles precipitated by acetone using DVS

Table 6.3 shows the percent of weight lost from each formulation in comparison to HPMC after the DVS drying phase (0% RH).

Table 6.3 Percent of weight lost during initial drying for HPMC powder and 4% HPMC microparticles precipitated by acetone.

Formulation	Change in mass (%)
HPMC	-2.3
4% HPMC precipitated by acetone (71)	-5.6

The decline in mass of HPMC after desorption cycle was 2.3%, suggesting that unprocessed HPMC powder contains few water molecules. However, the blank microparticles precipitated by acetone of formulation 71 contained 5.6% water. Interestingly, the dryness of blank microparticles precipitated by acetone was greater than that achieved by IPA (data not shown).

6.4.2 Moisture uptake measurements

HPMC microparticles precipitated by acetone (formulation 71) and HPMC powder were stored at different relative humidities (RH) for 16 days, in order to quantify the percent of water sorption by each formulation. This may clarify the effect of acetone on the physiochemical properties of precipitated microparticles and their water uptake and dynamic adhesion as a consequence.

6.4.2.1 Weight change in response to RH

The weight change of the samples in response to increasing RH is shown in Figure 6.1.

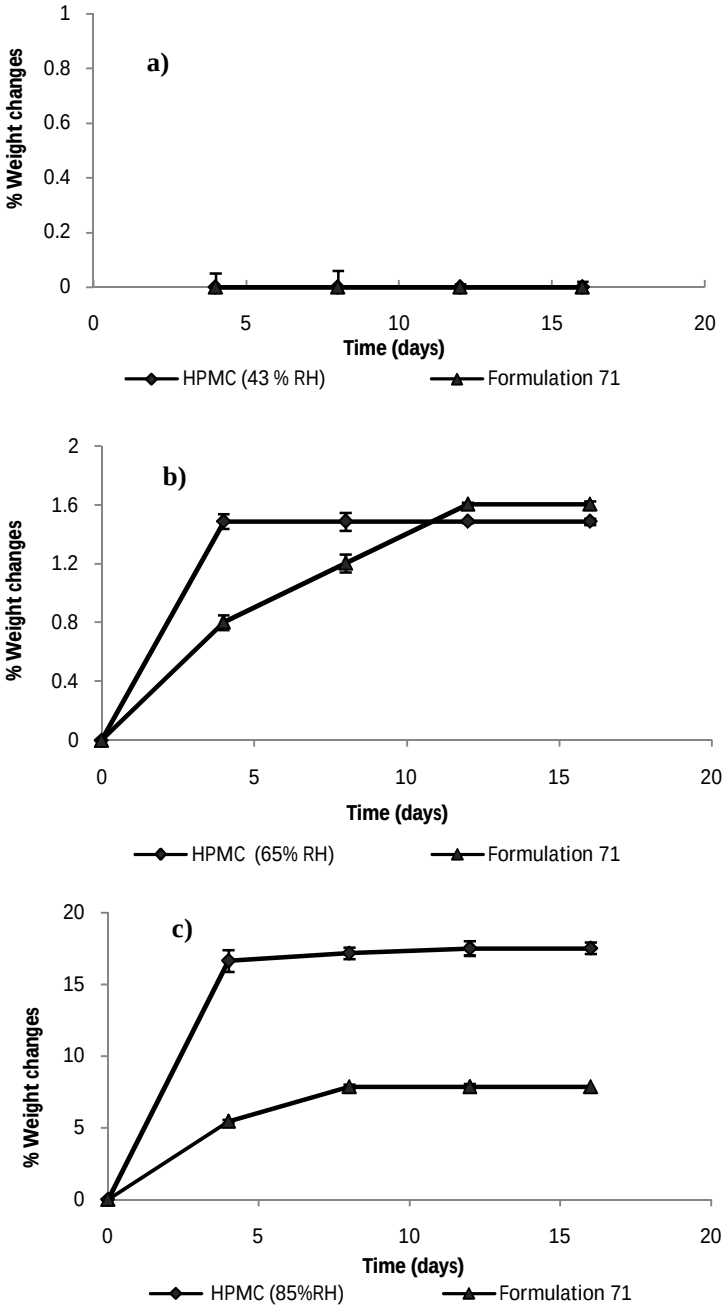

Figure 6.1 Effect of moisture sorption on the weights of HPMC powder and 4% blank HPMC microparticle formulation 71 (precipitated by acetone) stored at a) 43% RH, b) 65% RH and c) 85% RH, n=3. AT 85% RH, HPMC powder absorbed moisture higher than HPMC microparticles.

The samples showed no increase in weight when exposed to 43% RH over the 16 day period. At 65% RH, all samples increased in weight by approximately 1.5%. Whereas at 85% RH, significant increases in weight were observed, with HPMC powder absorbing more moisture (~15%) in comparison to the microparticles (~5%).

SEM images shown previously (Figure 4.3), revealed the loose particulate nature of HPMC powder alone, while HPMC precipitated in acetone showed a continuous surface. It is therefore suggested that the moisture uptake data reflects this alteration in morphology.

6.4.2.2 FT/IR spectroscopy of stored formulations

The FT/IR spectra of HPMC powder and acetone processed formulation stored at 85% RH are shown in Figure 6.2. In each case, the same individual sample was analysed at a particular time point, and then returned to storage. As previously noted, the spectrum of HPMC shows broad peaks in the region of 3700-2700 cm^{-1}, which is the area of O-H stretching vibrations of water (Section 3.3.5.2). Another area is in the range 1450-1650 cm^{-1} that arises from the bending vibration of water molecule (Anuar et al 2007).

The peak area between 3700-2700 cm^{-1} increased with storage time. A similar effect was observed for all samples with increasing humidity (data not shown). In this respect, both samples behaved similarly, although at 43% RH, FT/IR analysis suggested there was some uptake of water (data not shown), that was not previously detected in the gravimetric analysis (Section 6.4.2.1).

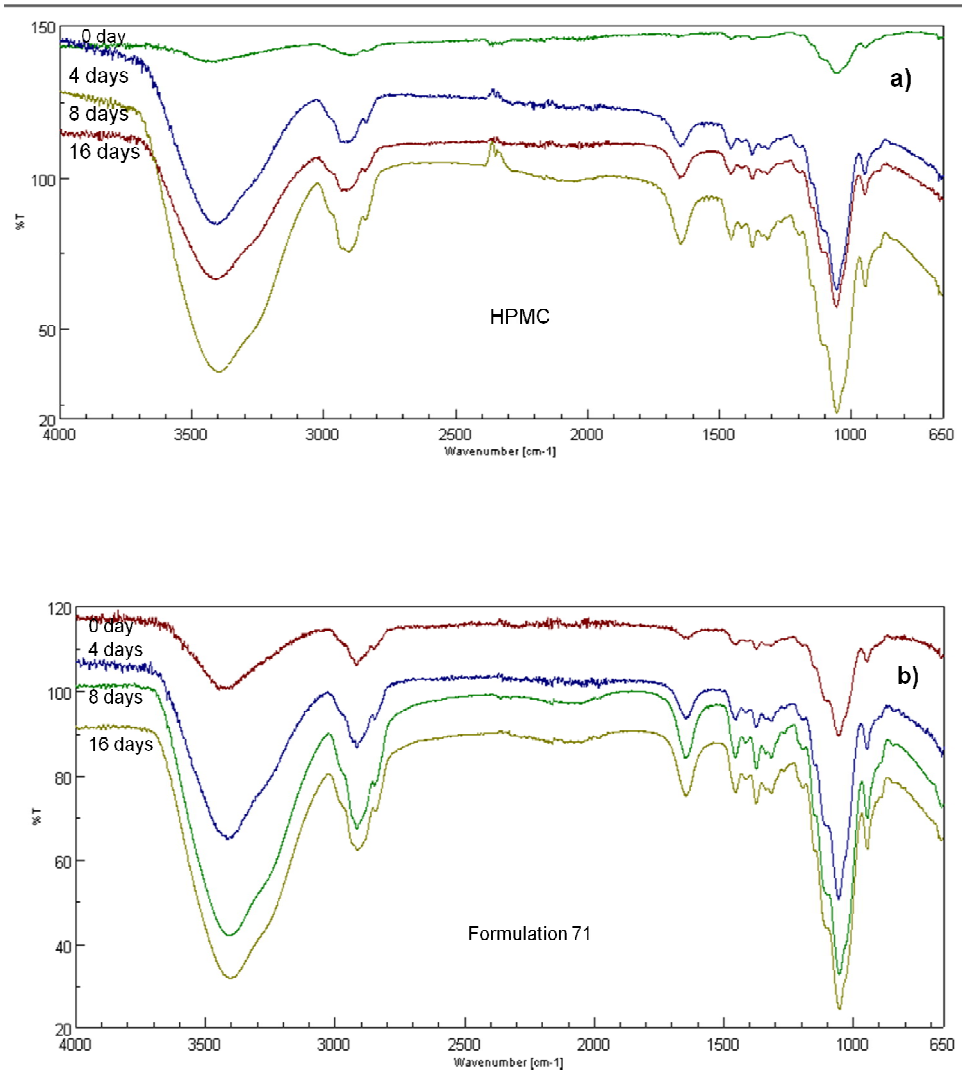

Figure 6.2 FT/IR spectra of a) HPMC and b) 4% HPMC microparticles precipitated by acetone (formulation 71), stored at 85% RH for 0, 4, 8 and 16 days at 25°C.

6.4.2.3 Differential scanning calorimetry

The effect of humidity on DSC thermograms of blank HPMC stored for 16 days is presented in Figure 6.3, and shows an increase in the integrated peak indicative of the presence of water.

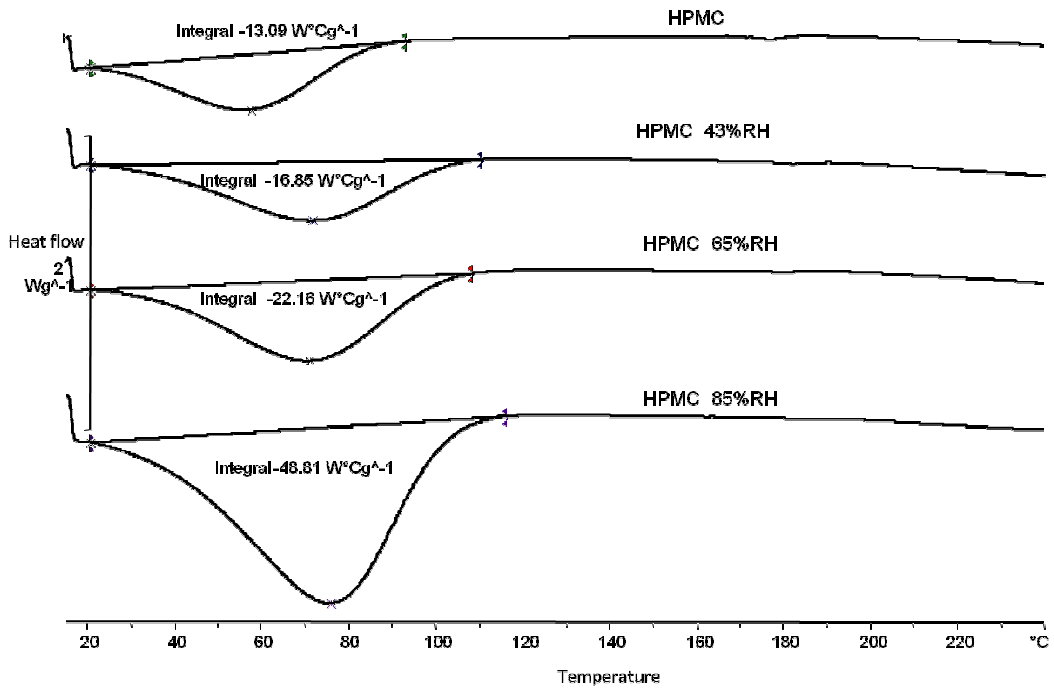

Figure 6.3 Integrated peaks of water contained within HPMC powder stored at different humidities for 16 days, compared with original HPMC. As the humidity increased, high moisture sorption achieved by HPMC powder. This was indicated by increasing the value of the integrated peak between 20-125°C.

Figure 6.4 shows the development of the endothermic peak following 16 days storage at different RH values, for HPMC in comparison to processed microparticles.

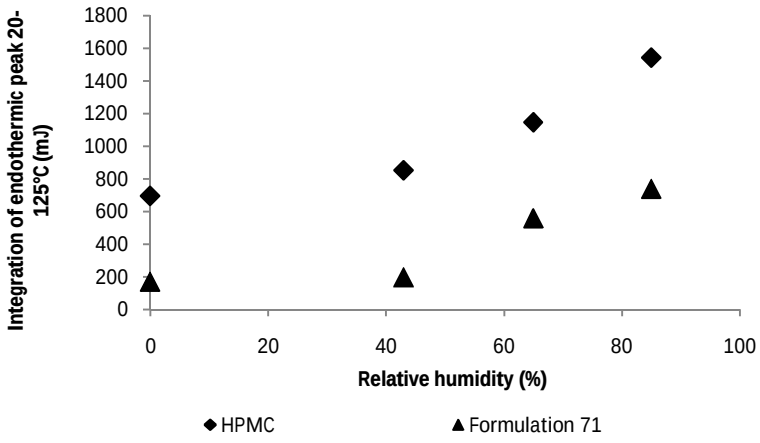

Figure 6.4 Effect of humidity on the DSC endothermic peaks of HPMC and formulation 71 (4% HPMC blank microparticles precipitated by acetone) after 16 days storage.

In both cases, as the humidity increased the area of this peak (20-125°C) increased which indicated an increase in moisture sorption by the stored sample. However, HPMC processed in acetone demonstrates a reduction in moisture uptake potential.

McPhillips et al (1999) reported that the Tg of HPMC was in the region of 162°C. Figure 6.5 shows the determination of this Tg for samples of HPMC powder stored at different RHs for 16 days, in comparison to original HPMC using the method described by Okhamafe & York (1985), as described in Section 2.5.4.9. Table 6.4 shows the glass transition temperature (Tg) determined for all formulations.

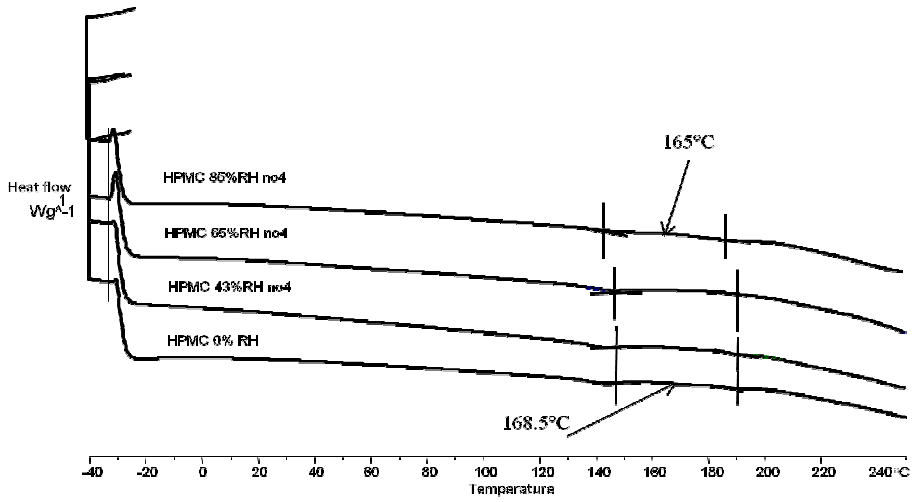

Figure 6.5 Determination the Tg of HPMC after 16 days storage at three different relative humidities. As the humidity increased, a slight decrease in the Tg of HPMC powder was produced.

Table 6.4 Glass transition temperature (Tg) of HPMC and acetone precipitated microparticles stored at different relative humidities for 16 days.

Formulation	Tg (°C)			
	0% RH	43% RH	65% RH	85%RH
HPMC	168.5	168	167	165
4% HPMC precipitated by acetone (71)	187.7	186.5	186	186

Tg of microparticle formulation 71 (precipitated by acetone) was higher than that of HPMC powder, suggesting that acetone penetrate the aqueous gel of HPMC and displace the water molecules efficiently because of its aprotic nature. Storing of these formulations in the different relative humidity produced a slight decrease in the Tg after 16 days as a consequence of re-establishing water molecules which acted as a plasticiser.

6.4.2.4 Thermo-gravimetric analysis

The results of TGA studies for precipitated microparticles shown in Figure 6.6 were unexpected, and did not display the correlation between RH storage and moisture uptake, as previously observed in Section 6.4.2.3. The samples all displayed similar weight losses, whereas gravimetric studies of moisture uptake suggested an approximate 7% difference between the moisture content of the 16 day sample stored at 85% RH compared to that stored at 43% RH. The reasons for this are unknown, and unfortunately it was not possible to repeat this series of experiments due to instrument failure. Table 6.5 summarises the results of these measurements, in comparison to HPMC powder, which are more consistent with expected behaviour.

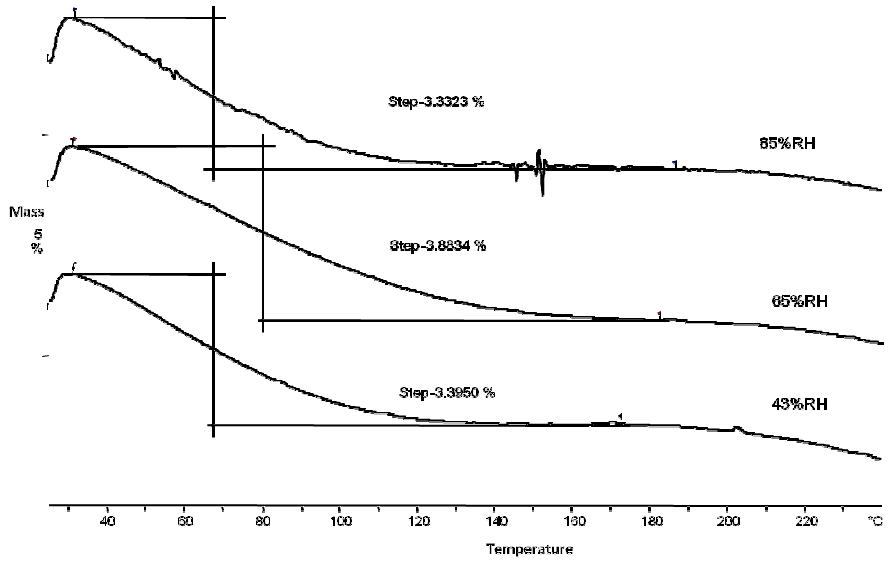

Figure 6.6 Calculation the weight lost with heating of formulation 71 (4% HPMC microparticles precipitated by acetone) as an indication of humidity uptake measurement, determined by TGA.

Table 6.5 Percentage of moisture uptake at different relative humidities, determined by TGA

Formulation	Moisture uptake (%)		
	43%RH	**65%RH**	**85%RH**
HPMC	2.10	2.69	5.73
4% HPMC precipitated by acetone (71)	3.39	3.88	3.33

It is concluded that HPMC microparticle precipitated by acetone demonstrated lower moisture sorption than HPMC powder, due to the matrix structure formed during the precipitation process. This effect on water uptake potential, may help to explain the dynamic adhesion results in the previous chapters (Sections 4.3.2.5 and 5.3.2.5), where formulations precipitated by acetone displayed significantly improved bioadhesion when compared to unprocessed material. Good bioadhesion appears to result from low water content in this instance, therefore further examination of effects of acetone processing was required.

6.5 Physiochemical properties of HPMC microparticles precipitated by acetone using different processing variables of precipitation techniques

Physically different products were obtained depending on the processing method used as shown in Figure 6.7.

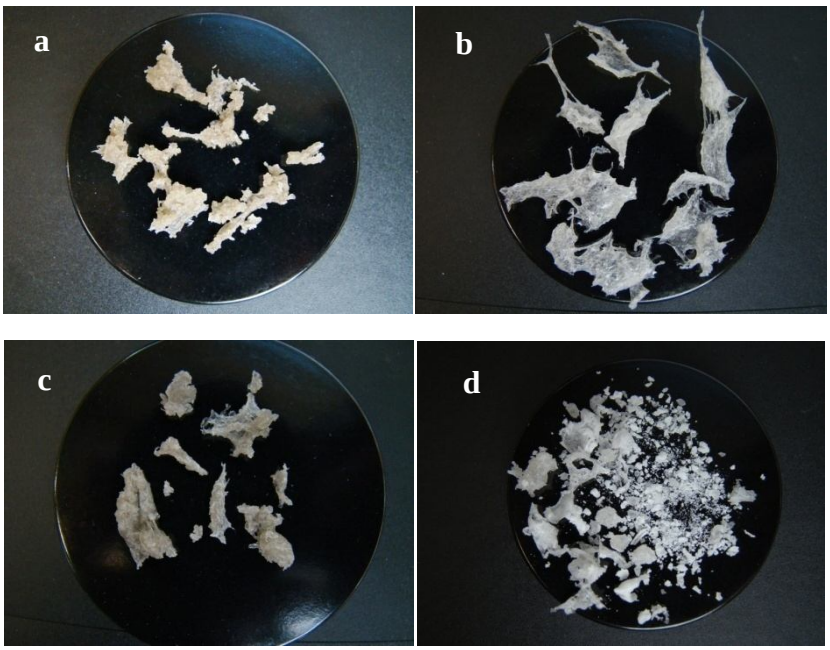

Figure 6.7 Different morphologies of a) DS (formulation 71), b) NDM (formulation 92), c) NDS (formulation 95) and d) formulation 102 (using magnetic stirrer without dropping and aqueous gel formation).

DS method, (Figure 6.7a) resulted in hard microparticles that attached to each other as macroparticle (clump). The image reveals material that is highly aggregated which forms on drying, whereas the acetone suspension reveals discrete microparticles (image not shown). The NDM method produced film like structures of aggregated macroparticles both in the acetone suspension, and after drying, as shown in Figure 6.7b. The NDS technique produced material with characteristics of both of the previous samples (Figure 6.7c). For the process where HPMC only had transient contact with water prior to addition of acetone (non-dropping, magnetic stirrer), resulted in a mixture of fine particles and sheet like structures, as shown in Figure 6.7d.

The percent yield of all formulations was high (80-90%) when using 10 mls of HPMC solution precipitated in acetone (200 ml), however, the yield decreased progressively (60-70%) when lower volumes of acetone (50 and 100 ml) were used.

This suggests that part of the HPMC remained soluble in the aqueous-organic mixtures in solvent ratios less than 1:20.

6.5.1 *In-vitro* dynamic adhesion

The dynamic adhesion profiles of blank NDM HPMC microparticle formulations 92, 93 and 94 (using different volumes of acetone), and HPMC with time are illustrated in Figure 6.8, along with the linearisation of the curves for bioadhesion quantification.

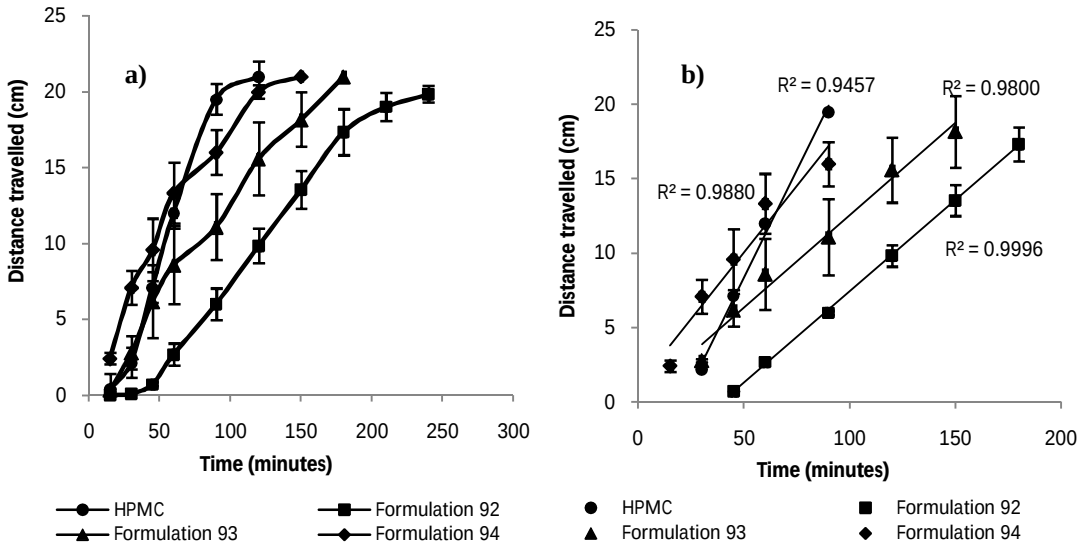

Figure 6.8 Effect of acetone volume on a) the *in-vitro* dynamic adhesion of HPMC and formulations 92 (4% HPMC precipitated by 200 ml acetone), 93 (4% HPMC precipitated by 100 ml acetone) and 94 (4% HPMC precipitated by 50 ml acetone) all using NDM technique, and b) the analysis of the linear parts of the curve, n=6. As the volume of acetone increased longer adhesion of the precipitated formulation on the mucin-agar medium was observed.

As the volume of precipitating agent increased, the bioadhesion increased *(P≤0.05)*. The explanation to this may be due to the efficiency of the dehydration effect on the HPMC matrix caused by different volumes of acetone. This suggests that the hygroscopic or water loving nature of acetone caused rapid dehydration of water molecules from HPMC aqueous gel according to its volume as shown in Figure 6.9 (Shukla 1973).

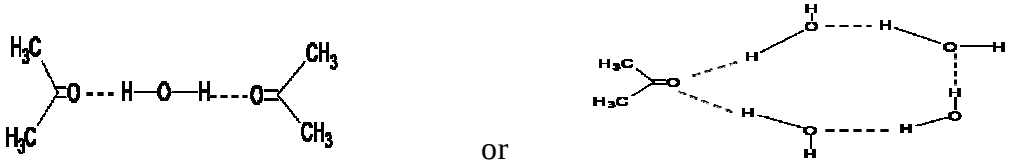

Figure 6.9 Mechanism of water interaction with acetone, reproduced from Shukla (1973).

The effect of preparation method (DS, NDM or NDS) on the dynamic adhesion of the processed polymer is shown in Figure 6.10, along with the linearisation of the curves for bioadhesion quantification.

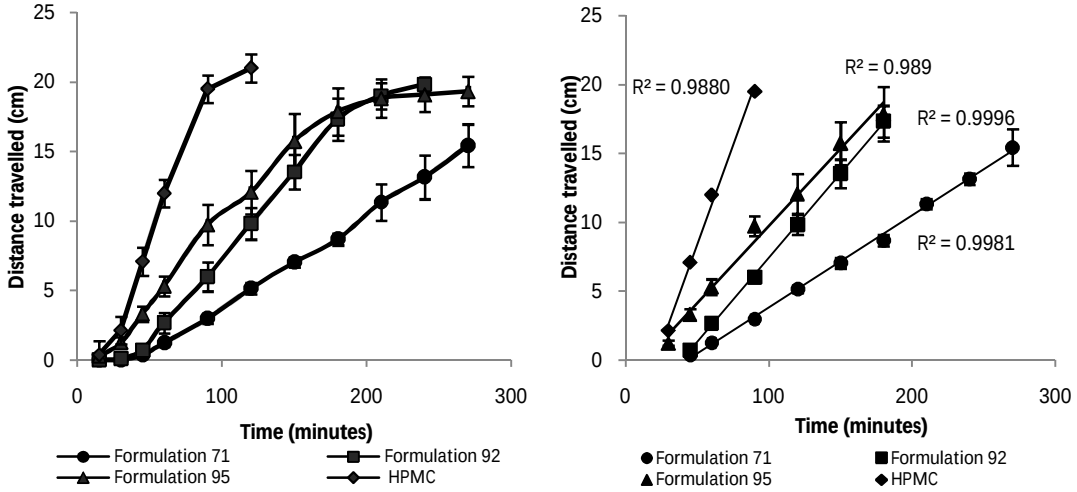

Figure 6.10 Effect of different precipitation techniques on a) the *in-vitro* dynamic adhesion of formulations 71 (4% HPMC precipitated by 200 ml acetone using DS), 92 (4% HPMC precipitated by 200 ml acetone using NDM) and 95 (4% HPMC precipitated by 200 ml acetone using NDS) and HPMC and b) the analysis of the linear parts of the curve, n=6. DS method produced microparticles with longer adhesion to the mucin-agar medium in comparison to the adhesion of microparticles precipitated by either NDM or NDS methods.

The dropping technique applied in formulation (71) resulted in higher *in-vitro* bioadhesion (*P≤0.05)* in comparison to the other two methods of precipitation (formulation 92, NDM and formulation 95, NDS), suggesting a more efficient dehydration process, as previously discussed.

The inverse slope of the linear phase of adhesion (Figure 6.8b and 6.10b) was used for quantification of the bioadhesive potential. Figure 6.11 summarises the effect of the different processing variables on the bioadhesion of all blank formulations (as the bioadhesion increases the 1/slope value increases).

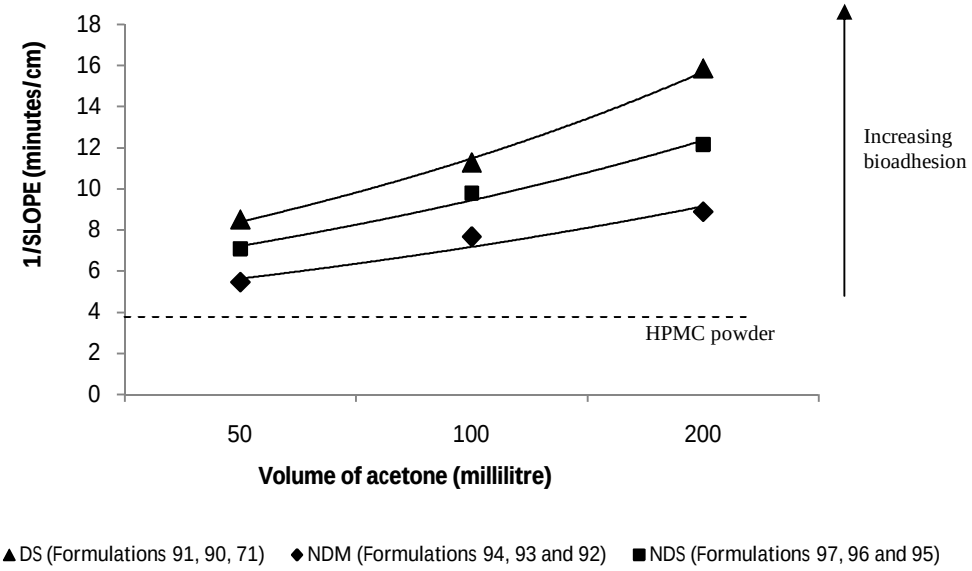

Figure 6.11 Effect of the precipitating agent volume on the *in-vitro* bioadhesion of 4% HPMC blank microparticles using three different preparation techniques, n=6.

The dynamic adhesion of processed blank HPMC microparticles was higher than HPMC powder. This suggests that dropping or mixing HPMC aqueous gel directly into acetone produced this increased the bioadhesive effect. However, particle size and morphology may play a role, since the above studies compare discrete particles of HPMC powder, with aggregated materials produced on processing.

As a further process variable, HPMC powder was treated with acetone in the absence of water, and also in a process allowing partial hydration by sprinkling HPMC onto water followed by rapid quenching with acetone (as described in Section 6.3.1.2). The bioadhesion data for these variables are shown in Table 6.6.

Table 6.6 *In-vitro* bioadhesion variables of HPMC, processed HPMC microparticles using NDM technique (formulation 101 and 102) and DS (formulation 71) and lyophilised 4%HPMC formulation, n=6.

Formulations	1/Slope (min/cm)	Regression (r^2)
HPMC	3.91 ± 0.4	0.9880
400mg HPMC powder+200 ml acetone (101)	4.60 ±0.06	0.9401
400mg HPMC powder +10 ml DW+200 ml acetone (102)	9.35 ±1.3	0.9862
4% HPMC precipitated by acetone (71)	15.85 ± 4.1	0.9912
(4%HPMC lyophilised formulation	14.81 ±5.6	0.9788)

Treating HPMC with acetone afforded a modest enhancement in adhesion properties, while transient contact with water (formulation 102) produced a significant increase over HPMC powder *($P \leq 0.05$)*, although not of the magnitude of material from the preferred process (formulation 71). It is hypothesised that the presence of water initially with HPMC, before addition to acetone was important to modify the bioadhesion. HPMC molecules have the ability to absorb water due to the OH groups in its structure (as previously discussed). With the completely gelled HPMC, there is a complete network of water surrounding the polymer. In such network, a water molecule may concurrently form hydrogen bonds with two or more polar groups on the polymer surface, in that way becoming highly immobilised (Katzhendler et al 2000). Precipitation with acetone causes complete and rapid dehydration of this system, effectively immobilising the expanded steric structure of the HPMC, leaving hydrogen bond forming moieties exposed for subsequent interaction with water. As a means of challenging this hypothesis, a further experiment was performed using lyophilised gels using a method previously studied in this group (McInnes et al 2007a). With lyophilisation, the expanded hydrated gel structure is also immobilised in a similar manner. Interestingly, when subjected to the same dynamic adhesion test, the lyophilised sample appeared to have approximately the same bioadhesion (*$P > 0.05$)*.

The effects of these processing parameters and resultant dehydration by acetone will be studied using SEM, DSC, DVS, TGA and NMR analysis in order to confirm these hypotheses.

6.5.2 Scanning electron microscopy

The SEM images of HPMC, blank HPMC microparticles precipitated by acetone using different processing variables and a lyophilised formulation (McInnes et al 2007a) are shown in Figure 6.12. The blank HPMC microparticles were morphologically dissimilar, depending on the method of preparation employed.

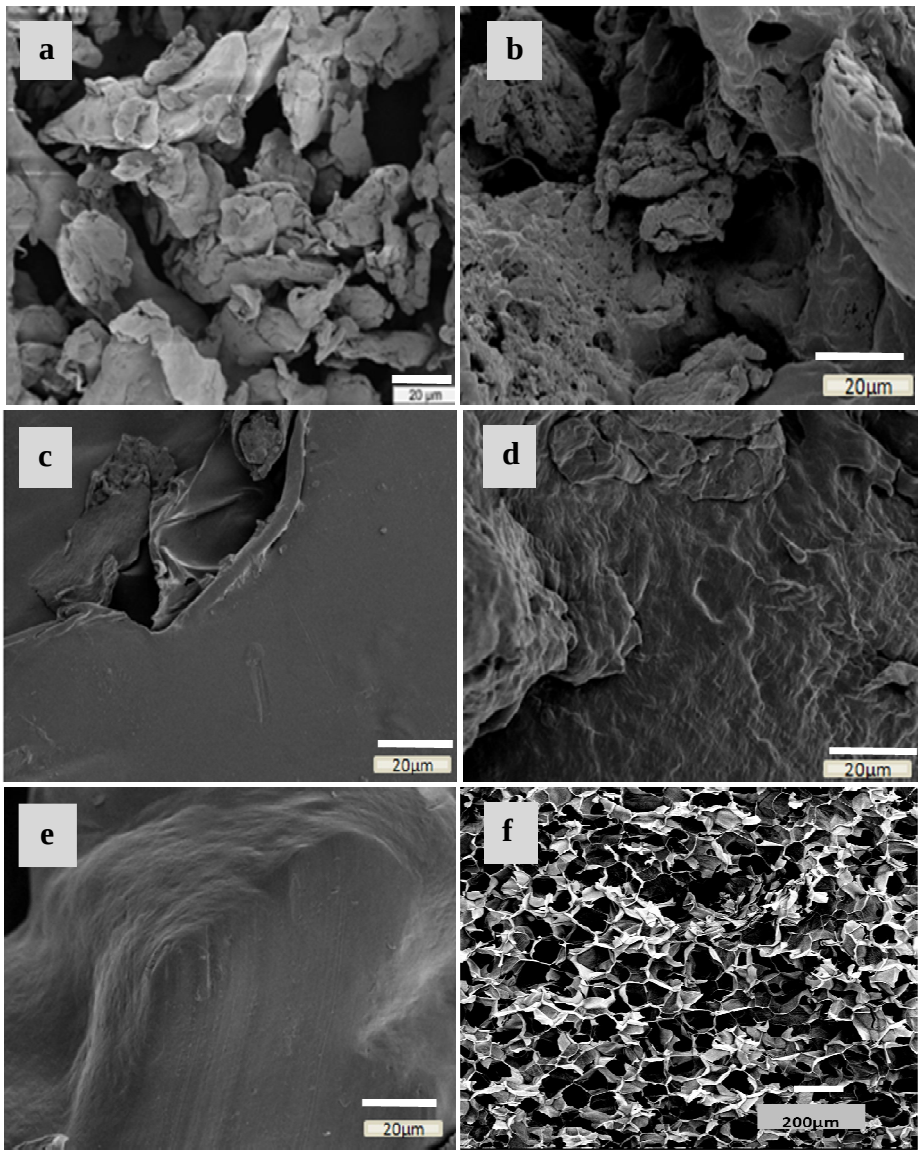

Figure 6.12 SEM images of a) HPMC, b) formulations 102 (NDM by addition of acetone to 400mg HPMC powder+ water), c) formulation 92 (NDM method for 4% HPMC aqueous gel), d) formulation 71 (DS method for 4% HPMC aqueous gel), e) formulation 95 (NDS method for 4% HPMC aqueous gel and f) 4%HPMC lyophilised formulation.

HPMC microparticles (formulation 102) which involved the addition of acetone directly to HPMC and water (without aqueous gel formation) formed a mixed structure of a semi-porous matrix, surrounded by unaffected HPMC particles. A smooth sheet like structure was produced when aqueous gel was stirred with acetone

using NDM method (formulation 92). A continuous structure resulted from the DS method as shown for formulation 71 (DS method), and a similar structure was observed for formulation 95, although slightly smoother in appearance (NDS method). The lyophilised material showed an open porous structure, previously described.

6.5.3 Differential scanning calorimetry

To quantify the water uptake by all formulations, the same method described previously in Section 6.4.2.3 was used. Table 6.7 summarises the integrated peak between 20-125°C and Tg data.

Table 6.7 Integrated peaks of water contained within HPMC powder and processed 4%HPMC microparticles, and glass transition temperature of each formulation.

Formulation	Integrated peak of DSC (20-125°C) (mJ)	Glass transition temperature (Tg °C)
HPMC	697.81	168.5
4%HPMC precipitated using DS and 200 ml acetone (71)	169.88	187.7
4%HPMC precipitated using DS and 100 ml acetone (90)	230.00	182.6
4%HPMC precipitated using DS and 50 ml acetone (91)	279.00	179.0
4%HPMC precipitated using NDM and 200 ml acetone (92)	300.81	179.0
4%HPMC precipitated using NDM and 100 ml acetone (93)	344.64	176.0
4%HPMC precipitated using NDM and 50 ml acetone (94)	350.12	172.0
4%HPMC precipitated using NDS and 200 ml acetone (95)	233.53	185.1
4%HPMC precipitated using NDS and 100 ml acetone (96)	233.76	182..4
4%HPMC precipitated using NDS and 50 ml acetone (97)	305.66	181.0
400mg HPMC powder+200 ml acetone (101)	692.01	168.6
400mg HPMC powder + 10 ml DW+200 ml acetone (102)	496.66	176.7

Any increase in the depth of the endothermic peak at 20-125°C can be helpful in determination the level of hydration or dehydration of the processed polymer (Bruni et al 2007). Also, the glass transition temperature (Tg) of the polymer was used for the same purpose given that the presence of water molecules acts as a plasticiser that decreases Tg of polymer (Laksmana et al 2008). So, two variables were measured to recognize the dehydration effect of acetone on the processed HPMC.

The smallest quantity of water was detected in microparticles formed by the DS method, where it was noted that as the volume of acetone used increased, the efficiency of water removal also increased. A similar trend for acetone volume was observed for both the NDM and NDS methods, although neither was as efficient as the DS method. Direct addition of HPMC powder to acetone, produced no significant change in water content over the results observed with untreated HPMC powder, while the technique employing transient exposure to water followed by acetone, revealed a modest decrease in water content when compared to HPMC alone.

As the volume of acetone increased, the integrated peak decreased and Tg of the polymer increased, for example, formulations 71, 90 and 91 prepared by DS method using 200 ml, 100 ml and 50 ml acetone respectively, produced an AUC of 169.88mJ, 230mJ and 279mJ, and Tg values of 187.74°C, 182.66°C and 179°C respectively. This is may be a result of the dehydration effect of acetone causing a decrease in the water content and high Tg of the HPMC matrix. Also the preparation of aqueous gel prior to acetone dehydration was important to get enhanced polymer dehydration.

6.5.4 Water uptake measurements

Water uptake is an important factor which should be studied in order to understand the behaviour of processed microparticle formulations. Figure 6.13 shows the area under the curve (AUC) of all hydration profiles at 90 minutes of processed formulations and HPMC powder.

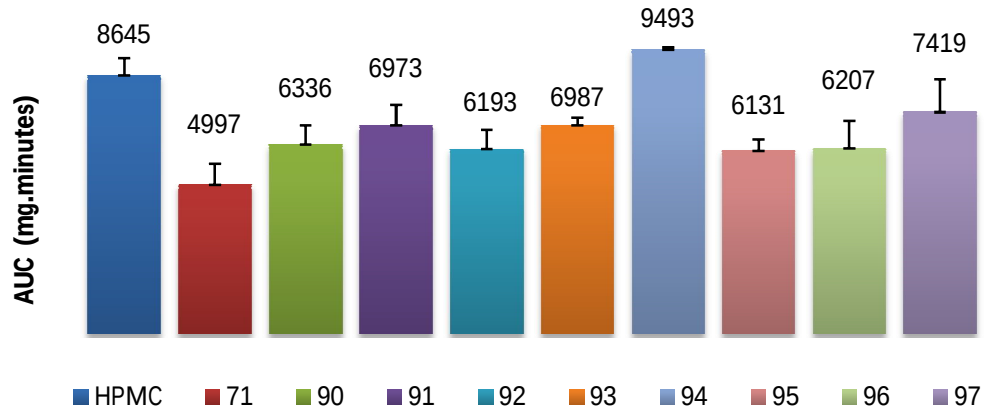

Figure 6.13 The AUC of water uptake curve for HPMC, formulation 71 (4%HPMC precipitated using DS and 200 ml acetone), formulation 90 (4%HPMC precipitated using DS and 100 ml acetone), formulation 91 (4%HPMC precipitated using DS and 50 ml acetone), formulation 92 (4%HPMC precipitated using NDM and 200 ml acetone), formulation 93 (4%HPMC precipitated using NDM and 100 ml acetone), formulation 94 (4%HPMC precipitated using NDM and 50 ml acetone), formulation 95 (4%HPMC precipitated using NDS and 200 ml acetone), formulation 96 (4%HPMC precipitated using NDS and 100 ml acetone) and formulation 97 (4%HPMC precipitated using NDS and 50 ml acetone), n=6.

Decreasing the acetone volume during preparation of the samples resulted in a significant increase in the extent of water uptake for DS, NDM and NDS methods. This suggests that water molecules remaining associated with the polymer as a result of the processing method, facilitated further uptake of water.

6.5.5 Dynamic vapour sorption

Figure 6.14 shows the correlation between acetone volume, processing method and resultant maximum vapour sorption at 95% RH.

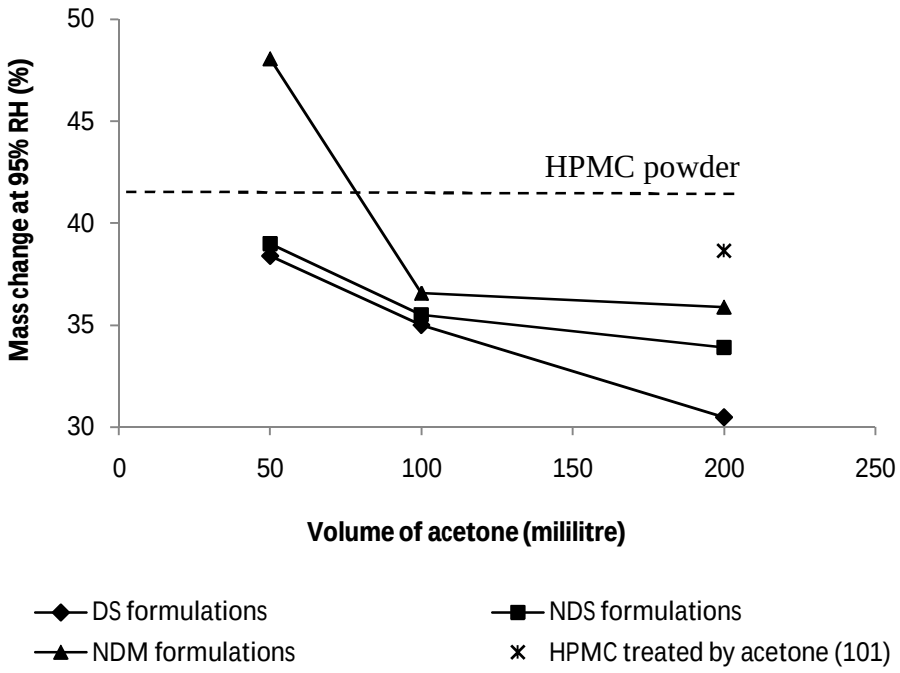

Figure 6.14 Mass change in response to vapour sorption (DVS) of HPMC processed formulations (using different volume of acetone), in comparison to HPMC powder.

The general trends observed from these data correlated with those obtained from the simple water uptake method described in Section 6.5.4. Again, it is observed that the sample containing the least water following processing (formulation 71), demonstrated the lowest capacity for water uptake during the study, suggesting that presence of water within the HPMC before precipitation in acetone subsequently decreased the vapour sorption due to the change in the orientation of inter and intra-molecular H-bonding groups on dehydration (Ghonasgi et al 1995; Simon & Eriksson 1996). This finding requires further study using NMR which will be performed in the following Section 6.5.6. Equally important are the data points at 200 ml acetone where the effect of processing on vapour sorption capability of the particles are striking, where the previous "water history" of HPMC appears to dictate the capability to uptake moisture. For example, washing HPMC with acetone directly reduces the vapour sorption potential of that material, in comparison to unprocessed

HPMC powder. If HPMC is fully hydrated as a gel, then the future vapour sorption capability is further reduced, and is dependent on the efficiency of the dehydration process with acetone. Mixing, and method of addition of components therefore has a pronounced effect.

6.5.6 Nuclear magnetic resonance

In order to elucidate the effect of processing method on the results previously observed, the NMR spectra of these formulations was obtained. Figure 6.15 shows the method used to identify these changes using ^{1}H-NMR spectrum of HPMC powder as a standard.

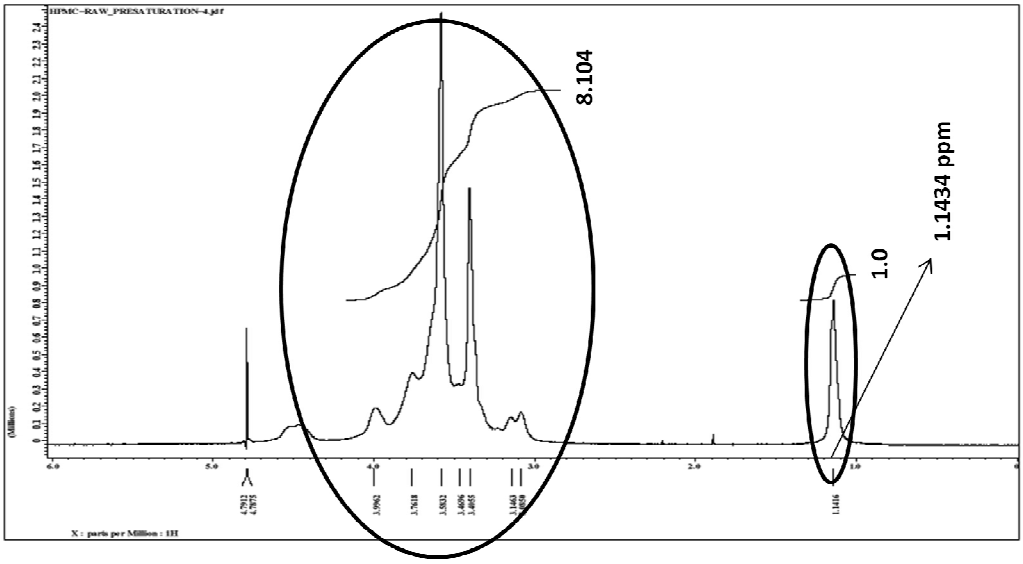

Figure 6.15 ^{1}H-NMR spectrum of HPMC showing the integration of peak area between 3 – 4.5 ± 0.25 ppm in relation to the area of peak at approximately 1.14 ppm.

The value between 4-5 ppm represents the number of protons or hydrogens of HPMC (H-bonding groups), as the solvent peak (D_2O) substituted the protons of water. So

any increase or decrease in the integration of the area between 3-5 ppm indicates a change in the water content. The standard spectrum of HPMC shown in Figure 6.15 was compared with processed microparticle formulations. Integration of peak area between 3 – 4.5 ± 0.25 ppm was calculated in relation to the area of peak at approximately 1.14 ppm (singlet peak representing HPMC, with an integration value of 1), and for unprocessed HPMC, this value was 8.104. Furthermore, another reading of HPMC was taken at 1.1-1.2 ppm, and was used as an indication of any chemical shift in the HPMC spectrum for processed formulations. Table 6.8 summarises these data.

Table 6.8 The integrations of NMR spectrum peaks of all processed formulations in comparison to HPMC.

Formulation	Number of protons at 3-4.5 ± 0.25 ppm	Peak at 1.1-1.2 ppm
HPMC	8.104	1.143
4%HPMC precipitated using DS and 200 ml acetone (71)	7.532	1.151
4%HPMC precipitated using DS and 100 ml acetone (90)	7.748	1.152
4%HPMC precipitated using DS and 50 ml acetone (91)	8.098	1.152
4%HPMC precipitated using NDM and 200 ml acetone (92)	8.043	1.145
4%HPMC precipitated using NDM and 100 ml acetone (93)	8.603	1.145
4%HPMC precipitated using NDM and 50 ml acetone (94)	9.613	1.152
4%HPMC precipitated using NDS and 200 ml acetone (95)	7.832	1.146
4%HPMC precipitated using NDS and 100 ml acetone (96)	8.167	1.145
4%HPMC precipitated using NDS and 50 ml acetone (97)	8.311	1.152
400mg HPMC powder+200 ml acetone (101)	8.031	1.151

As seen in values of the peak between 1.1-1.2ppm, no chemical changes were introduced as a result of processing HPMC. There were however changes observed in the integration values of the area between 3-4.5ppm (representing water content), which showed a similar trend to that discussed in the previous sections.

6.6 General discussion

Formulation 71 represents the exposure of a gelled HPMC to acetone, using the most efficient mixing process, and the slowest (dropwise) rate of addition of the gel to the acetone. It would be expected therefore, that the interaction of acetone and water would be instantaneous and complete, resulting in an extremely efficient dehydration process. Surprisingly, despite this state of dehydration (as evidenced by DSC), formulation 71 demonstrated the lowest affinity for moisture following processing (as evidenced by DVS and simpler water uptake studies). Interestingly this formulation also afforded the highest bioadhesion score in the test employed, which was designed to represent the dynamic interplay of hydration, entanglement of polymer and mucin, and rheological flow which a formulation would experience on the nasal mucosal surface. In the current work, it is hypothesised that the rapid dehydration of the HPMC gel resulted in a collapse of the matrix structure, forming a physical barrier to subsequent rehydration. With the other formulations and processes employed, less efficient interaction with acetone resulted in higher residual water content after processing, which allowed maintenance of a more open polymer structure, thereby facilitating future moisture uptake. Further support for this theory may arise from the DVS data presented in Chapter 5 (Table 5.8) for MH:HPMC processed in the same way as formulation 71, where the presence of metformin greatly enhanced the water uptake capacity, despite the very low water uptake of the drug alone (~3%). This may have been due to the physical presence of entrapped drug maintaining an open and more porous structure of the preparation, in contrast to the collapsed structure of formulation 71. Confirmation of such a hypothesis would require further study in the future by others.

To some extent, these findings are of a similar nature to previous studies within this group with HPMC/lactose direct compression or wet granulated tablet formulations, where the latter demonstrated significantly reduced erosion potential, reflecting differences in the interaction between the formulation and a dissolution medium (McConville et al 2004) and with the rehydration behaviour of lyophilised HPMC formulations when examined using confocal microscopy (McInnes et al 2007a).

6.7 Conclusion

- The presence of the solvent, acetone, caused dehydration of the HPMC polymer, and the degree of dehydration depended on the volume of acetone used as a precipitating medium. As the volume of precipitating agent increased (in order of 50 < 100 < 200 ml), its dehydration effect on the water molecules of HPMC aqueous gel increased.
- This effect was most noticeable with the dehydration of HPMC gel formulations, but was also observed to a slight extent when HPMC was treated as powder with acetone.
- The processing method employed for preparation of particles was also found to significantly affect the properties. The dehydration of the aqueous gel was most efficient when the gel was added dropwise to a highly agitated system. Less efficient mixing and/or lower volumes resulted in less efficient dehydration.
- Surprisingly, the most efficient dehydration resulted in the lowest potential for subsequent uptake of moisture, and the highest bioadhesive performance in the dynamic test employed.
- A hypothesis has been developed to explain the counter-intuitive behaviour in response to efficiency of dehydration, residual moisture and future affinity for moisture.

Chapter 7

Physiochemical properties of metformin HCl formulations

7.1 Introduction

The previous chapter discussed experiments demonstrating that processed HPMC using the DS method produced the greatest bioadhesion. While Chapter 5 demonstrated that DS processed 4% MH:HPMC microparticles lead to the formation of MH crystals enveloped by a continuous HPMC matrix, resulting in a prolongation of the release profile of MH in comparison to the corresponding physical mixture. In this chapter, the properties of a physical mixture of MH powder with processed HPMC microparticles were compared with the above materials.

7.2 Materials and methods

The materials used in this chapter were MH, HPMC and acetone, which were previously discussed in Section 2.2.

7.2.1 Preparation of three formulations of MH and HPMC

The three formulations defined in Table 7.1 were prepared as described in Section 2.5.3.2.

Table 7.1 MH and HPMC formulations

Formulation	Composition
83	4% MH:HPMC (1:1) microparticles
87	Physical mixture of MH and HPMC powder
103	Physical mixture of MH powder and blank 4%HPMC microparticles

The above formulations were prepared at a MH:HPMC ratio of 53:47, previously determined as the MH content of the microparticle formulation 83, Chapter 5.

7.2.2 Water uptake measurement

A simple water uptake method (Section 2.5.4.13) was used to study the water uptake of the formulations in Table 7.1.

7.2.3 *In-vitro* dynamic adhesion

Dynamic adhesion was measured using the method described in Section 2.5.4.11.

7.2.4 Metformin release

The release profiles of MH from the three formulations were studied (Section 2.5.4.14), using the Franz-cell diffusion apparatus (described in Section 2.1.13).

7.3 Results and discussion

7.3.1 Water uptake measurements

Figure 7.1 shows the water uptake profiles of the three formulations in Table 7.1.

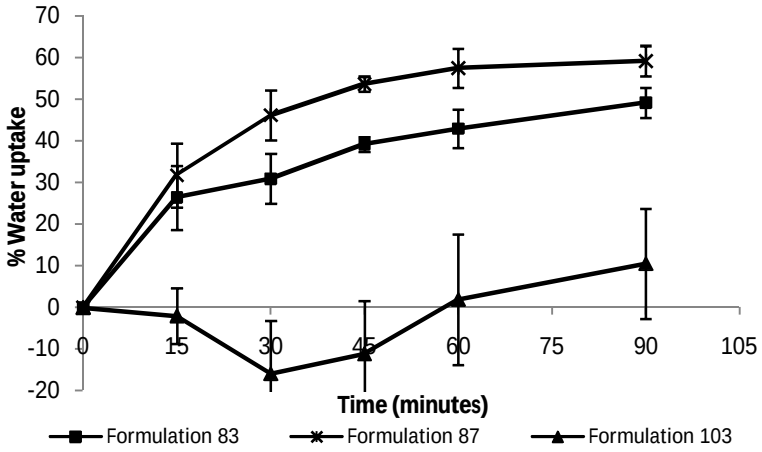

Figure 7.1 Water uptake of formulation 83 (4% MH:HPMC (1:1) microparticles), formulation 87 (physical mixture of MH and HPMC powder) and formulation 103 (physical mixture of MH powder and blank 4% HPMC microparticles), n=6.

The physical mixture of MH with HPMC powder (formulation 87) demonstrated the greatest moisture uptake during the study, followed closely by formulation 83 (the processed MH containing microparticles). This is due to the difference in the physical state of the HPMC, in fine powder in formulation 87 and in a continuous matrix structure in formulation 83. Formulation 103 however, demonstrated an initial weight loss in this test, followed by a gradual increase in weight. It is suggested that this effect arises from a combination of the freely available MH in this mixture which may dissolve and diffuse out of the sample, and the collapsed state of the HPMC blank microparticles, which have a reduced affinity for water (previously

discussed in Chapter 6). The resultant profile (weight loss followed by weight gain), is a combination of these two factors.

7.3.2 *In-vitro* dynamic adhesion

Figure 7.2 shows the dynamic adhesion profiles of the three formulations.

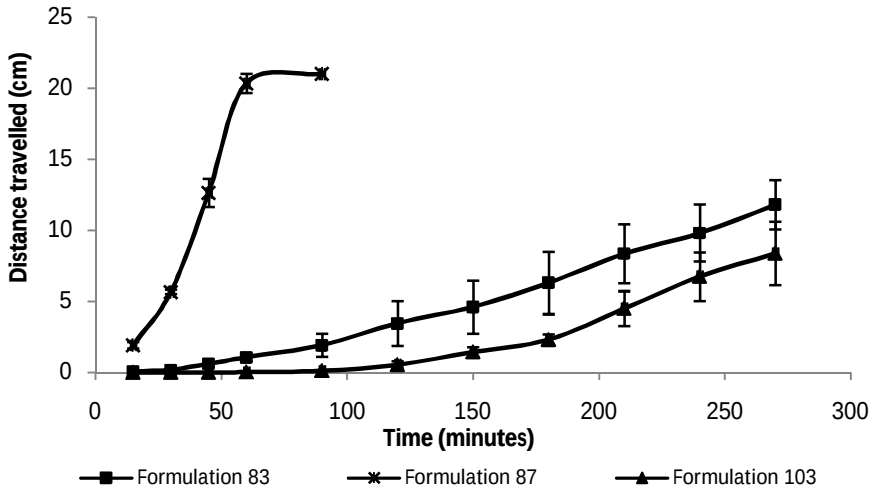

Figure 7.2 Dynamic adhesion of formulation 83 (4% MH:HPMC (1:1) microparticles), formulation 87 (physical mixture of MH and HPMC powder) and formulation 103 (physical mixture of MH powder and blank 4% HPMC microparticles), n=6.

The physical mixture of MH and HPMC powder (formulation 87) showed low bioadhesion in comparison to the microparticle formulations. It differs from formulation 83 due to the matrix nature of the latter formulation altering the rate of water uptake and gel formation which are critical parameters in this dynamic test. Formulation 103, containing blank HPMC microparticles in a collapsed structure, demonstrates the greatest dynamic adhesion due to the resultant low affinity for water, previously described in Section 7.3.1. Formulation 83 contains HPMC in a less collapsed structure following dehydration, due to the presence of MH within the

matrix, and this facilitates greater and more rapid water uptake for hydration of the polymer compared to blank microparticles, as discussed in DVS Section 5.3.2.6.

It is suggested that MH has little impact on the results of the bioadhesion study due to its low affinity for water, as previously determined using DVS (Figure 5.15). This is in contrast to the results of the water uptake study (Section 7.3.1), where rapid dissolution of MH and diffusion from formulation 103 was suggested to account for initial weight loss observed in that system.

7.3.3 Metformin release

Figure 7.3 shows the release profiles of MH from the three formulations.

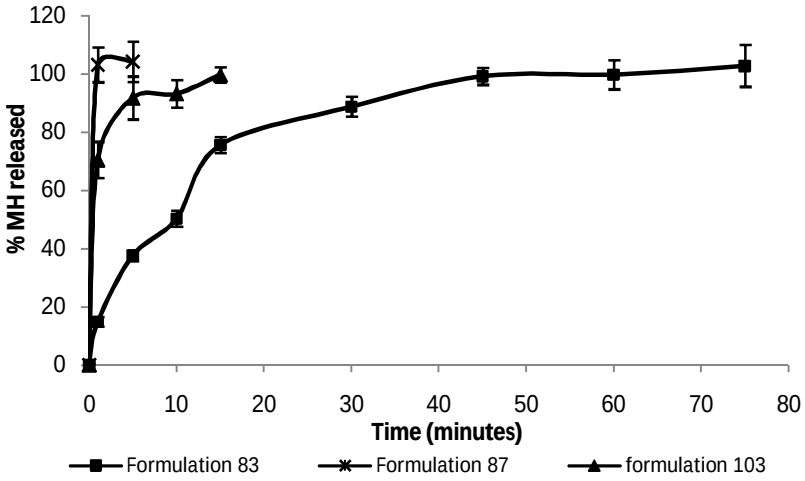

Figure 7.3 The release profile of formulation 83 (4% MH:HPMC (1:1) microparticles), formulation 87 (physical mixture of MH and HPMC powder) and formulation 103 (physical mixture of MH powder and blank 4% HPMC microparticles), n=6.

Release of MH from the physical mixture of MH and HPMC powder (formulation 87) was rapid, due to the availability of loose MH powder with no HPMC matrix.

The release of MH from formulation 103, which contained MH powder mixed with HPMC microparticles was again rapid, although statistically different (f_2 33.96), for similar reasons. With these formulations, the HPMC is having little or no effect on release of MH. However, the MH:HPMC microparticle formulation containing MH enveloped in an HPMC matrix demonstrated the expected slow release of drug from such a system. This release is statistically different from formulation 103 (f_2 16.86).

7.4 General discussion

The data from the experiments described in this chapter illustrate the complex interplay between drug and HPMC in different environments in the formulations studied. The release study showed that MH was rapidly released from formulation 103, where MH was mixed with blank HPMC microparticles, which confirms the hypothesis explaining the initial weight loss observed for this formulation in the simple water uptake studies. The rapid loss of MH from formulation 103 further confirms the supposition that MH in this formulations would have had little influence on the bioadhesive performance of the system, permitting the strongly bioadhesive nature of the blank HPMC microparticles to dominate the dynamic result, as previously discussed in Chapter 6.

7.5 Conclusion

- A physical mixture of HPMC powder with MH permits both constituents to interact separately with the surrounding environment.
- A physical mixture of MH with processed HPMC results in similar behaviour, with the collapsed HPMC structure dominating performance in this case.
- The behaviour of the MH:HPMC processed microparticles is dictated by the matrix nature of the formulation, where both components influence performance.
- The matrix formulations demonstrate bioadhesion and sustained release, and are therefore suitable candidates for nasal formulations as identified in the objectives of this thesis.

Chapter 8

Accelerated stability studies of MH formulations

8.1 Introduction

Stability studies are important during the pharmaceutical development of new dosage forms to provide evidence about the quality of a pharmaceutical substance after a time of storage under the effect of different environmental stresses such as temperature and humidity. In this chapter, an accelerated stability study is performed in which the storage conditions were 50°C ±2°C/ 75% RH±5%RH for six months, with testing at 0, 2, 4 and 6 months. This follows the suggestions of Lin & Chen (2009). The degradation of a drug included in a solid dosage form generally happens very slowly. For this reason, it is common to choose stressed storage conditions, in order to obtain rapid stability prediction data (Gil-Alegre et al 2001).

In the literature, different analytical studies have been reported on pharmaceutical products stored under accelerated stress conditions, such as potency, dissolution and water content (Khan 2009). Surface analysis technique such as SEM can identify the effect of stress conditions on the morphology of the products (Padala et al 2009).

In this chapter, the effect of stress conditions on the stability of MH and HPMC in each formulation was studied through analysis of SEM images (at 0 and 6 months) and MH release rate (at 0, 2 and 6 months).

8.2 Materials and methods

The materials used in this chapter were MH, HPMC and acetone, which were previously discussed in Section 2.2.

8.2.1 Stability study of the MH formulations

The formulations detailed in Table 8.1 were used for the stability studies.

Table 8.1 Formulations used for accelerated stability.

Formulation	Scanning electron microscopy (SEM)	MH release
HPMC	√	
MH	√	√
71 (4% blank HPMC microparticles)	√	
83 (4% MH:HPMC (1:1) microparticles)	√	√
87 (Physical mixture of MH and HPMC powder)	√	√
103 (Physical mixture of MH and 4% blank HPMC microparticles)	√	√

The most promising formulations, the physicochemical properties of which were described in Chapter 7 were chosen for these stability studies, along with the powder components and blank HPMC microparticles. The formulations were stored at 50 ±2°C/ 75% RH for 6 months to provide accelerated stress storage conditions. A RH of 75% was created using a saturated solution of sodium chloride salt (Greenspan 1977), with samples stored as described in Section 2.5.4.13.

8.2.2 Scanning electron microscopy

SEM images were obtained for all formulations in Table 8.1, using the method described in Section 2.5.4.4. Images were obtained of freshly prepared samples, and those stored for 6 months under accelerated conditions, in order to identify the changes in the morphology of the formulations.

8.2.3 Metformin release

The release of MH from the formulations in Table 8.1 were studied (Section 2.5.4.14) following storage for 0, 2 and 6 month intervals in order to examine any changes in the formulations after storing in stress conditions.

8.3 Results and discussion

In general, formulations stored under accelerated stress conditions did not change in visual appearance or colour, aside from HPMC powder which formed an agglomerated mass after 6 months storage.

8.3.1 Scanning electron microscopy

Figure 8.1 shows formulation 83 (4% MH:HPMC (1:1) microparticles precipitated in acetone), before and after 6 months storage under accelerated stress conditions. The sharp edges of MH crystals embedded within the HPMC matrix can clearly be observed in both images, indicating that the morphology of MH was not altered. The continuous HPMC matrix within which the MH crystals are embedded is also clearly visible in both images, and does not appear to have changed significantly.

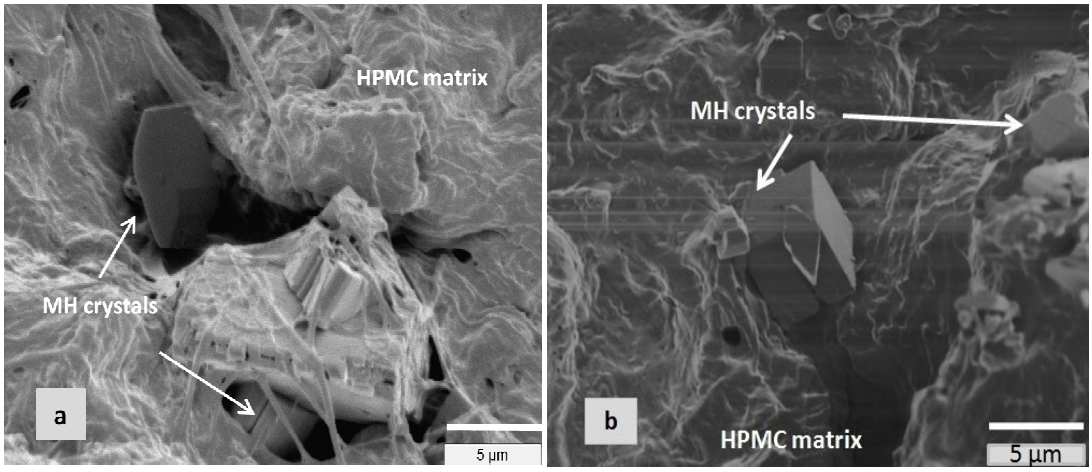

Figure 8.1 SEM images of, a) formulation 83 (4% MH:HPMC (1:1) microparticles) before storage and b) formulation 83 following 6 months storage at 75% RH and 50°C. The morphology of MH crystals was not altered following 6 month storage under stressed conditions.

Figure 8.2 shows formulation 71 (4% blank HPMC microparticles) before and after 6 months storage under accelerated stress conditions. The HPMC matrix appeared similar before and after storage, suggesting stability under stressed conditions. This is attributed to the collapsed structure suggested to be formed in blank HPMC microparticles following precipitation in acetone, resulting in low affinity for moisture uptake (as discussed previously in Chapter 6).

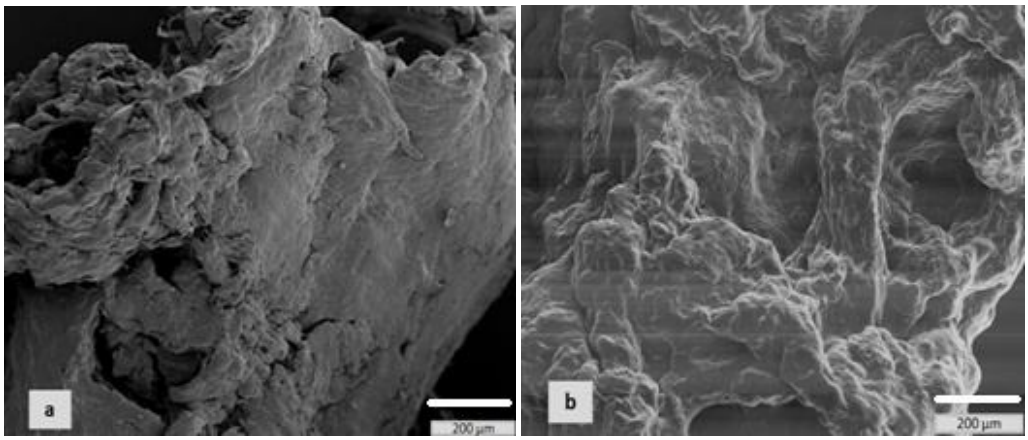

Figure 8.2 SEM images of, a) formulation 71 (4% blank HPMC microparticles) before storage and b) formulation 71 following 6 months storage at 75% RH and 50°C . The morphology of HPMC matrix appeared similar before and after storage.

Figure 8.3a-c shows MH powder at different magnifications, before and after 6 months storage under stressed conditions, and a physical mixture of MH powder with blank HPMC microparticles following storage under stressed conditions for 6 months (Figure 8.3d).

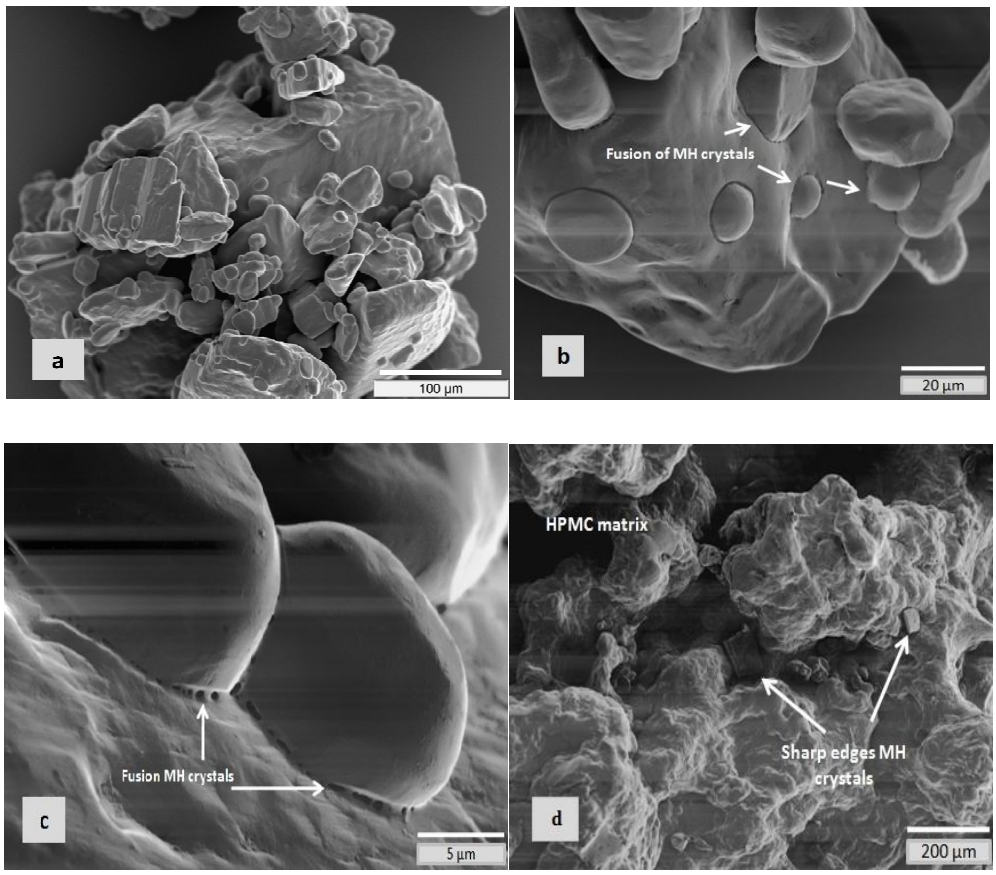

Figure 8.3 SEM images of a) MH powder before storage, b) and c) MH powder following 6 months storage at 75% RH and 50°C, and d) the physical mixture of MH powder with 4% blank HPMC microparticles (formulation 103) following 6 months storage at 75% RH and 50°C. The loss of the sharp MH crystal morphology and fusion of small and large particles were observed with MH powder following 6 months storage under stressed conditions, while sharp edged MH crystals with a similar morphology to the starting material were observed in formulation 103 following 6 months storage.

Storage of MH alone under stressed conditions showed loss of the sharp MH crystal morphology (Figure 8.3b and c), and fusion of small and large particles. Storage at high humidity can cause adsorption of water to the surface of a crystal lattice (Ahlneck & Zografi 1990), resulting in surface solubilisation of the compound, and the observation of particle fusion and rounded morphology following storage at

stressed conditions in this study, suggests that such a process occurred in the MH powder under these conditions.

This was not the case however, for MH when present as a physical mixture with blank HPMC microparticles (Figure 8.3d). Following storage under accelerated conditions, sharp edged MH crystals with a similar morphology to the starting material were observed in the sample, suggesting crystal stability of MH in this formulation (formulation 103). While blank HPMC microparticles were shown to have low moisture content following processing (Chapter 6), and a lower capacity for moisture uptake in comparison to most other formulations (Chapter 5), the vapour sorption capacity of blank HPMC microparticles determined using DVS (Section 5.3.2.6) was still significant at ~30%. It is hypothesised that this resulted in HPMC acting as a 'sponge' for the high moisture content of the surrounding environment, protecting the MH crystals from adsorbing water to their surface, and therefore maintaining the crystal morphology.

Figure 8.4 shows unprocessed HPMC before and after storage at 6 months.

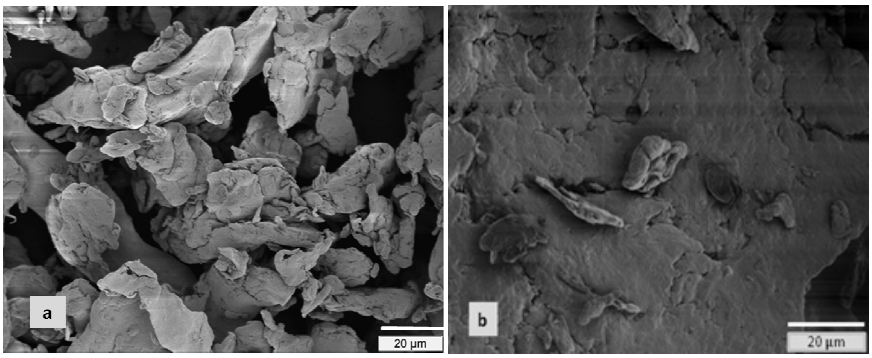

Figure 8.4 SEM images of a) HPMC powder before storage and b) HPMC powder following 6 months storage at 75% RH and 50°C. The fusion of HPMC particles was observed following 6 months storage under stressed conditions.

It is known that HPMC powder has a high capacity to absorb moisture (~41%), as evidenced from DVS studies in Chapter 5. The 75% RH storage conditions used here resulted in fusion of the particles at a microscopic level, and at a macroscopic level agglomeration of the material was also observed after 6 months storage.

Figure 8.5 shows the physical mixture of MH and HPMC powder (formulation 87) following 6 months under accelerated storage conditions.

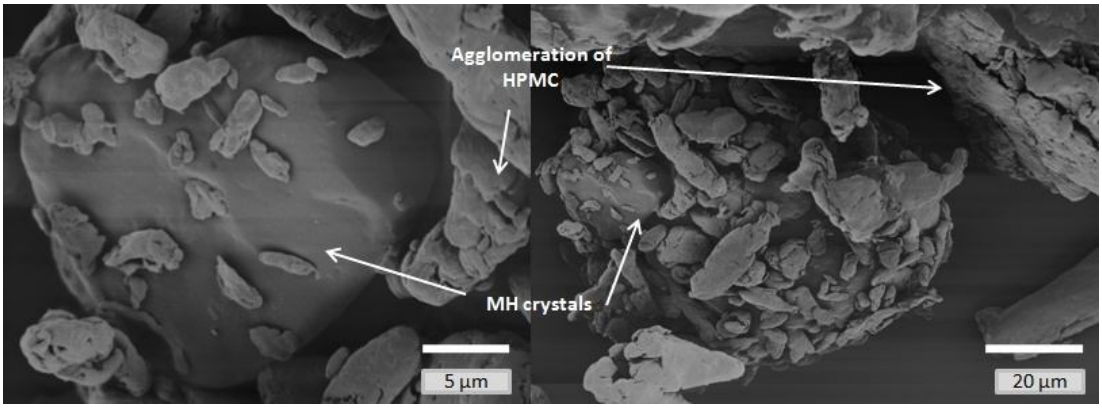

Figure 8.5 SEM images of the physical mixture of MH and HPMC powder (formulation 87) following 6 months storage at 75% RH and 50°C. The large rounded particles of MH, with some evidence for agglomeration of HPMC particles matched the observations for the drug and polymer powders when stored individually.

Under these storage conditions, MH presents as large rounded particles, with some evidence for agglomeration of HPMC particles, matching observations for the drug and polymer powders when stored individually (Figures 8.3b and 8.4b). In this physical mixture, the MH and HPMC particles are in intimate contact and the high affinity of unprocessed HPMC particles for water vapour (~41%), which it is suggested results in the hydration of the local environment surrounding the individual MH crystals, resulting in similar fusion phenomena previously observed for MH alone under the same storage conditions.

This contrasts with the behaviour of MH mixed with HMPC microparticles shown in Figure 8.3d where no changes in MH morphology were evident. In the wider context this supports the proposition that admixture of a drug with processed HMPC microparticles could present an environment where the drug will be shielded from humidity effects. This is a similar situation where MH was processed with HMPC (1:1) (Figure 8.1) where MH appeared protected from physical transformations as a result of exposure to high RH. The relatively low affinity of processed HMPC microparticles for moisture uptake appears responsible for these beneficial properties.

8.3.2 Metformin release

Figure 8.6 shows the release profile of MH from 4% MH:HPMC (1:1) microparticles (formulation 83), following different periods of storage under accelerated stress conditions.

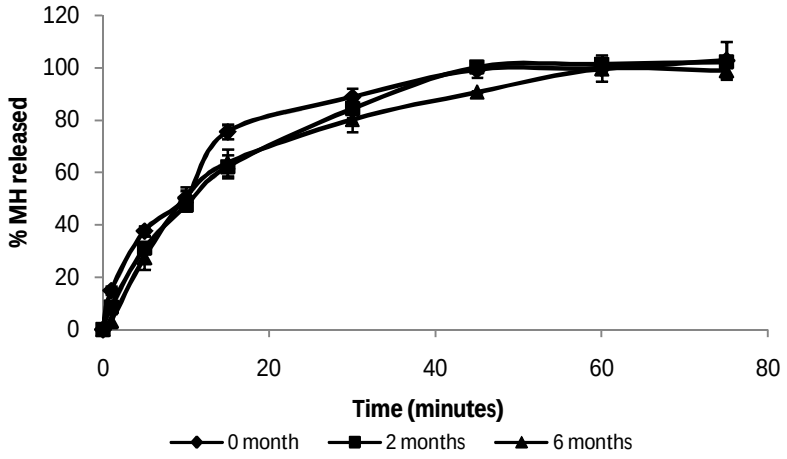

Figure 8.6 The release profile of MH from 4% MH:HPMC (1:1) microparticles (formulation 83) before storage and following 2 and 6 months storage at 75% RH and 50°C, n=6. No significant difference in the release profile of MH from formulation 83 was observed following 0, 2, and 6 months of storage.

No significant differences in the release profile of MH after 0, 2, and 6 months of storage was obtained, in which 100% release of MH was achieved in approximately 1 hour. This result can be explained by the observation that there were no changes in matrix or morphology of this formulation after storage, as evidenced by SEM images (Figure 8.1b).

Figure 8.7 shows the release profile of MH from the physical mixture of MH powder with blank HPMC microparticles (formulation 103), following different periods of storage under accelerated stress conditions.

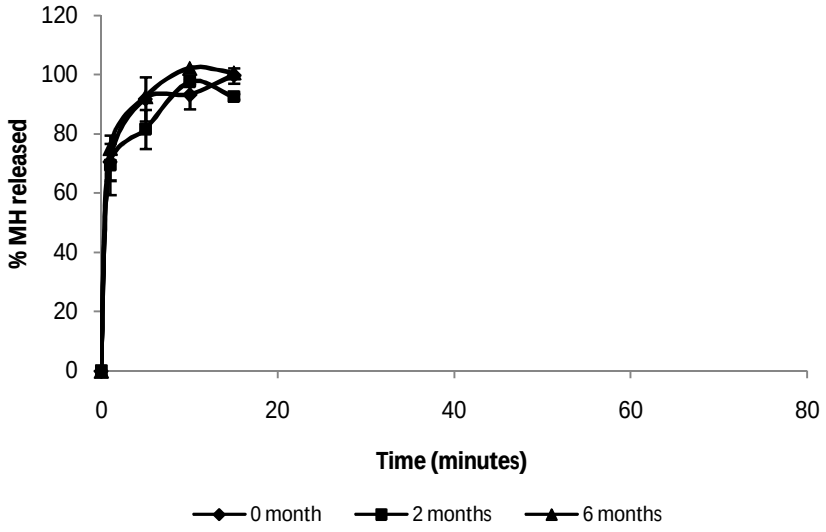

Figure 8.7 The release profile of MH from the physical mixture of MH powder and 4% HPMC blank microparticles (formulation 103) before storage and following 2 and 6 months storage at 75% RH and 50°C, n=6. No significant difference in the release profile of MH from formulation 103 was observed following 0, 2, and 6 months of storage.

The release rate of MH was not affected by storage, as might have been expected from SEM images (Figure 8.3d), where no changes were observed in either the HPMC matrix or MH crystal morphology.

Figure 8.8 shows the release rate of MH unprocessed powder alone.

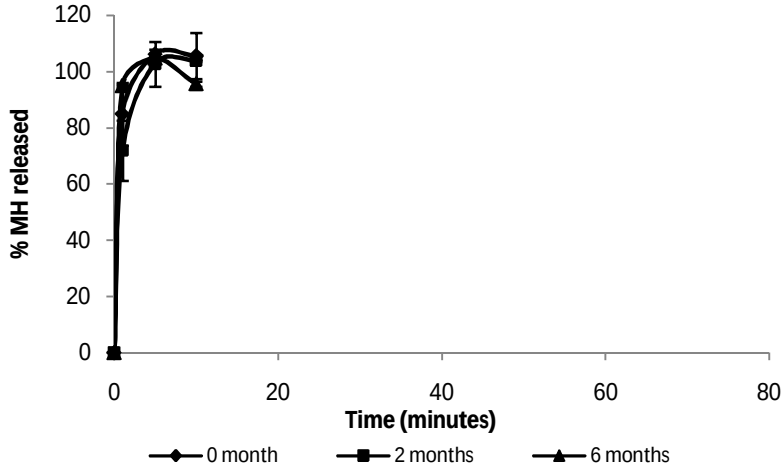

Figure 8.8 The release profile of MH before storage and following 2 and 6 months storage at 75% RH and 50°C, n=6. No significant difference in the release profile of MH was observed following 0, 2, and 6 months of storage.

The release rate of MH was unaffected by storage under stressed conditions, despite some changes in crystal morphology observed using SEM (Figure 8.3b and c).

Figure 8.9 shows the release profile of MH from the physical mixture of MH and HPMC powders, before and after storage under stressed conditions.

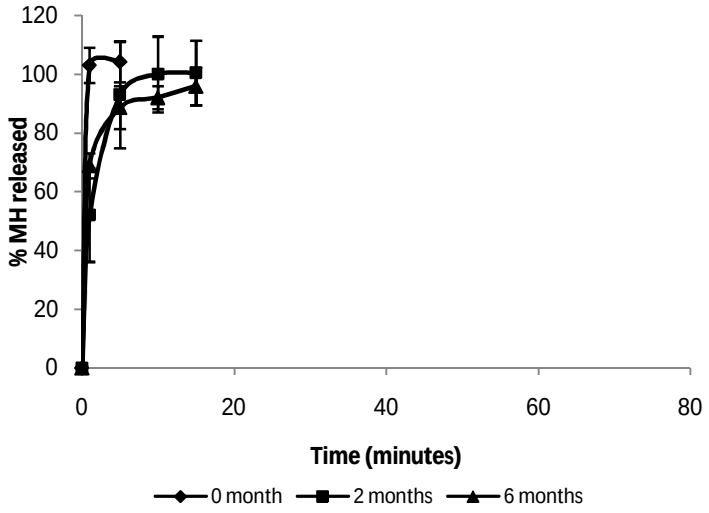

Figure 8.9 The release profile of MH from the physical mixture of MH and HPMC powder (formulation 87) before storage and following 2 and 6 months storage at 75% RH and 50°C, n=6. Storage under stressed conditions caused a significant delay in the release rate of MH from the physical mixture following 6 months storage under stressed conditions.

Storage under stressed conditions caused a slight delay in the release rate of MH from the physical mixture, which was significantly different at 6 months when compared to the initial mixture (f_2 35.4). The time taken to reach 100% release of MH was 1, 10 and 15 minutes for the initial formulation, storage for 2 months, and storage for 6 months respectively.

While the surface area and particle size of a drug is known to affect dissolution rate (Banker & Rhodes 2002), it was observed that the fusion and increase of crystal size of MH alone did not affect the release rate (Figure 8.3b). It is therefore suggested that the effect observed for the physical mixture is more likely to be a result of the agglomeration of HPMC powder (Figure 8.5), forming a semi-continuous matrix structure and offering partial control of MH release and diffusion.

8.4 Conclusion

- MH and HPMC powders were morphologically unstable under the accelerated stress conditions used in this study.
- MH:HPMC (1:1) processed microparticles and the physical mixture of MH powder with processed blank HPMC microparticles were the most stable formulations following 6 months storage under stressed conditions.
- MH release profiles obtained for the formulations reflected the observations on physical structure obtained from SEM images.
- The use of the precipitation technique employed in these studies appears to confer stability on MH included in these formulations.

Chapter 9

Overall conclusion and future work

α-lactose monohydrate was used as a model compound to optimise the manufacturing conditions of bioadhesive HPMC microparticles for nasal delivery. The preparation technique involved the addition of aqueous gels of lactose:HPMC (1:1) into a precipitating agent (1:20 DW:IPA or acetone). Different processing parameters were evaluated, such as effect of stirring speed (1000-2000 rpm), needle gauge (19g, 21g and 23g), and dropping rate (5 ml/hour and 10 ml /hour), to control the mean particle size. Two layers of precipitate (upper and lower) were obtained with a low shear stirrer when the concentration of HPMC increased above 3% w/w. The presence of HPMC resulted in a smaller particle size (upper layer) in comparison to only lactose microparticles. The precipitate contained unequal proportions of lactose and HPMC in each layer (evident by NMR results), despite a lactose:HPMC ratio of 1:1 being used as the initial aqueous gel (before processing in the precipitating agent).

A high shearing rate eliminated the problem of two layers. Effect of stirring speed 7500-8000 rpm, temperature of the precipitating media (4°C and 25°C) and precipitating agents (IPA and acetone) were studied on three concentrations; 3%, 4% and 5% w/w lactose:HPMC (1:1). The optimal particle size required for nasal delivery (less than 100 μm) was obtained using a stirring speed of 8000 rpm, a temperature of 4°C, a dropping rate of 10 ml/ hour, using a 23g needle.

FT/IR spectra and DSC thermograms of 1-5% w/w lactose:HPMC (1:1) formulations precipitated in IPA using the low shear stirrer showed lactose polymorphism as a result of HPMC concentration changing the habit of lactose crystals by H-bonding. At 1% lactose:HPMC, anhydrous α-lactose was obtained, while at 2-3% lactose:HPMC, a mixture of α- and β-lactose was observed. Whereas at 4 and 5% concentrations, the α- form progressively disappeared, with a corresponding increase in the presence of a β-form. In the absence of HPMC, particles precipitated from

lower lactose concentrations (1-4%) in IPA resulted predominantly in the β-form of lactose, however as the lactose concentration increased, the presence of the monohydrate also increased.

The replacement of lactose with drug molecules (verapamil HCl and metformin HCl) was studied using the optimised processing methods.

VH:HPMC (1:1) microparticles were obtained with the optimal particle size required for nasal delivery (less than 100μm), but with low VH content in the microparticles resulting from the sparingly solubility of VH in the precipitating agents (IPA and acetone). This technique produced a pronounced increase in the dynamic adhesion of precipitated HPMC microparticles using IPA or acetone as precipitating agents when compared to HPMC powder, due to the possible effects of differences in the surfaces of the material precipitated from IPA and acetone. VH:HPMC (1:1) microparticles produced the same adhesion dynamic of blank HPMC microparticles due to the low drug content of microparticles. HPMC absorbed more water than microparticles precipitated by acetone powder or IPA processed microparticles. This result may be attributed to the change of the polymer matrix after precipitation.

Small MH:HPMC (1:1) microparticles were obtained (less than 100 μm) using a high shearing mixer. A low drug content (~8%) was obtained for MH:HPMC microparticles precipitated in IPA, while 45-53% drug content was obtained for acetone precipitated MH:HPMC (1:1) microparticles. This correlates with the slight solubility of MH in IPA, whereas MH and HPMC were virtually insoluble in acetone.

Processed microparticles using IPA as a precipitating agent produced formulations with discrete, well formed cubic drug crystals of around 2μm in size on a structureless HPMC surface, whereas microparticles precipitated by acetone showed MH crystals of 1-2 μm enveloped within an amorphous HPMC matrix. The co-precipitation technique therefore produced microcrystals of drug on the surface or entrapped within the HPMC matrix, depending on the choice of solvent. Greater bioadhesion was achieved with processed microparticles when compared to the

unprocessed components, and acetone precipitated microparticles afforded greater dynamic adhesion than IPA precipitated microparticles.

Different water sorption uptake profiles were obtained for MH:HPMC microparticle formulations and physical mixtures, reflecting the morphological differences seen in SEM. Sustained release MH:HPMC (1:1) microparticles were produced using a co-precipitation technique, and achieved controlled release of MH**.** The acetone processed microparticles achieved high drug loading, uniform (small) particle size, significant bioadhesion and afforded prolonged drug release. These attributes indicate that such a product may have potential for nasal drug delivery.

Further studies were performed on acetone precipitated HPMC microparticles in the absence of drug. The presence of the solvent acetone, caused dehydration of the HPMC polymer, and the degree of dehydration depended on the volume of acetone used as a precipitating medium. As the volume of precipitating agent increased (in order of 50 < 100 < 200 ml), its dehydration effect on the water molecules of HPMC aqueous gel increased. This effect was most noticeable with the dehydration of HPMC gel formulations, but was also observed to a slight extent when HPMC was treated as powder with acetone. The processing method employed for preparation of particles was also found to significantly affect the properties. The dehydration of the aqueous gel was most efficient when the gel was added dropwise to highly agitated acetone. Less efficient mixing and/or lower volumes resulted in less efficient dehydration. Surprisingly, the most efficient dehydration resulted in the lowest potential for subsequent uptake of moisture, but the highest bioadhesive performance in the dynamic test employed. A hypothesis has been developed to explain the counter-intuitive behaviour in response to efficiency of dehydration, residual moisture and future affinity for moisture.

A physical mixture of HPMC powder with MH permits both constituents to interact separately with the surrounding environment. A physical mixture of MH with processed HPMC blank microparticles results in similar behaviour, with the collapsed HPMC structure dominating performance in this case. The behaviour of the MH:HPMC (1:1) processed microparticles is dictated by the matrix nature of the formulation, where both components influence performance. The matrix formulation

demonstrates bioadhesion and sustained release, and is therefore a suitable candidate for nasal drug delivery, as identified in the objectives of this thesis.

MH:HPMC (1:1) processed microparticles and physical mixture of MH with processed HPMC were the most stable formulations, in which MH crystals were unchanged after 6 month storage under stressed conditions. This technique is therefore a promising method for the formation of stable bioadhesive microparticles using low molecular weight HPMC (K100LV).

Future Work

In-vivo studies are ultimately essential for newly developed formulations such as MH:HPMC (1:1) processed microparticles and physical mixture of MH with processed HPMC. While those formulations achieved good adhesion dynamic (up to 4-5 hours) and controlled MH release up to 1 hour and 15 minutes respectively, correlation of *in-vitro* and *in-vivo* bioadhesion and drug release are essential to confirm the effectiveness of prepared microparticles.

Using gamma scintigraphy, McInnes and co-authors found that while increasing HPMC concentration resulted in greater *in-vitro* bioadhesion, this did not necessarily lead to increased nasal residence time *in-vivo*. This was hypothesised to be a result of inadequate hydration of the formulation leading to little or no spreading of gel, and rapid elimination (McInnes et al 2007a). Similar techniques could be applied to the formulation described in this thesis.

To broaden the applicability of the technique described in this thesis, a wider range of drugs, polymers and precipitation solvents could be investigated. The process of efficiently mixing gel with the dehydrating solvent could also be further studied.

References

ADHIYAMAN, R., BASU, S. K. (2006) Crystal modification of dipyridamole using different solvents and crystallization conditions. Int J Pharm 321: 27-34

AHLNECK, C., ZOGRAFI, G. (1990) The molecular basis of moisture effects on the physical and chemical stability of drugs in the solid state. Int J Pharm 62: 87-95

AHMED, S., SILENO, A. P., DEMEIRELES, J. C., DUA, R., PIMPLASKAR, H. K., XIA, W. J., MARINARO, J., LANGENBACK, E., MATOS, F. J., PUTCHA, L., ROMEO, V. D., BEHL, C. R. (2000) Effects of pH and dose on nasal absorption of scopolamine hydrobromide in human subjects. Pharm Res 17: 974-7

AMIDI, M., PELLIKAAN, H. C., HIRSCHBERG, H., DE BOER, A. H., CROMMELIN, D. J., HENNINK, W. E., KERSTEN, G., JISKOOT, W. (2007) Diphtheria toxoid-containing microparticulate powder formulations for pulmonary vaccination: preparation, characterization and evaluation in guinea pigs. Vaccine 25: 6818-29

ANDERSON, N. H., BAUER, M., BOUSSAC, N., KHAN-MALEK, R., MUNDEN, P., SARDARO, M. (1998) An evaluation of fit factors and dissolution efficiency for the comparison of in vitro dissolution profiles. J Pharm Biomed Anal 17: 811-22

ANDREWS, G. P., LAVERTY, T. P., JONES, D. S. (2009) Mucoadhesive polymeric platforms for controlled drug delivery. Eur J Pharm Biopharm 71: 505-18

ANUAR, N. K., WUI, W. T., GHODGAONKAR, D. K., TAIB, M. N. (2007) Characterization of hydroxypropylmethylcellulose films using microwave non-destructive testing technique. J Pharm Biomed Anal 43: 549-57

ARORA, P., SHARMA, S., GARG, S. (2002) Permeability issues in nasal drug delivery. Drug Discov Today 7: 967-75

BANKER, G. S., RHODES, C. T. (2002) Getting the drug into solution: factors affecting the rate of dissolution. In: *Modern Pharmaceutics*. 4th ed., rev. and expanded. edn. M. Dekker, New York, pp 156

BASAK, S. C., KUMAR, K. S., RAMALINGAM, M. (2008) Design and release characteristics of sustained release tablet containing metformin HCl. Braz J Pharm Sci 44: 477-483

BECKETT, A. H., STENLAKE, J. B. (1988) X-ray powder diffraction. In: *Practical Pharmaceutical Chemistry*. 4th edn. Athlone Pr, pp 78-84

BERTRAM, U., BODMEIER, R. (2006) In situ gelling, bioadhesive nasal inserts for extended drug delivery: in vitro characterization of a new nasal dosage form. Eur J Pharm Sci 27: 62-71

BLAGDEN, N., DAVEY, R. J., LIEBERMAN, H. F., WILLIAMS, L., PAYNE, R., ROBERTS, R., R., R., DOCHERTY, R. (1998) Crystal chemistry and solvent effects in polymorphic systems Sulfathiazole. J Chem Soc 94: 1035-1044

BRITTAIN, H. G., BOGDANOWICH, S. J., BUGAY, D. E., DEVINCENTIS, J., LEWEN, G., NEWMAN, A. W. (1991) Physical characterization of pharmaceutical solids. Pharm Res 8: 963-73

BROGLY, M., FAHS, A., BISTAC, S. (2010) Assessment of nanoadhesion and nanofriction properties of formulated cellulose-based biopolymers by AFM. In: *Scanning Probe Microscopy in Nanoscience and Nanotechnology*. In: Bhushan, B. (ed.). Springer, Berlin ; London, pp 473-504

BRUNI, G., MILANESE, C., BELLAZZI, G., BERBENNI, V., COFRANCESCO, P., MARINI, A., VILLA, M. (2007) Quntification of drug amorphous fraction by DSC. J Therm Anal Cal 89: 761–766

CALLENS, C., PRINGELS, E., REMON, J. P. (2003) Influence of multiple nasal administrations of bioadhesive powders on the insulin bioavailability. Int J Pharm 250: 415-22

CHANG, S. A., GRAY, D. G. (1978) The surface tension of aqueous hydroxylpropyl cellulose solutions. J Colloid Sci 67: 255-265

CHAYEN, J. (1983) Polarised light microscopy: principles and practice for the rheumatologist. Ann Rheum Dis 42 Suppl 1: 64-7

CHIEN, Y. W. (1992) Novel Drug Delivery Systems. M. Dekker, New York

COSTA, P., SOUSA LOBO, J. M. (2001) Modeling and comparison of dissolution profiles. Eur J Pharm Sci 13: 123-33

CRISP, J. L., DANN, S. E., EDGAR, M., BLATCHFORD, C. G. (2010) The effect of particle size on the dehydration/rehydration behaviour of lactose. Int J Pharm 391: 38-47

CUNNINGHAM, V. L. (2004) Special characteristics of pharmaceuticals related to environmental Fate. In: *Pharmaceuticals in The Environment : Sources, Fate, Effects and Risks.* In: Kümmerer, K. (ed.). 2nd ed. edn. Springer, Berlin ; London, pp 13-14

DANDAGI, P. M., MASTIHOLIMATH, V. S., PATIL, M. B., GUPTA, M. K. (2006) Biodegradable microparticulate system of captopril. Int J Pharm 307: 83-8

DE ASCENTIIS, A., BETTINI, R., CAPONETTI, G., CATELLANI, P. L., PERACCHIA, M. T., SANTI, P., COLOMBO, P. (1996) Delivery of nasal powders of beta-cyclodextrin by insufflation. Pharm Res 13: 734-8

DONDETI, P., ZIA, H., NEEDHAM, T. E. (1996) Bioadhesive and formulation parameters affecting nasal absorption. Int J Pharm 127: 115-133

DOUROUMIS, D., FAHR, A. (2007) Enhanced dissolution of oxcarbazepine microcrystals using a static mixer process. Colloids Surf B Biointerfaces 59: 208-14

DRAPIER-BECHE, N., FANNI, J., PARMENTIER, M. (1999) Physical and chemical properties of molecular compounds of lactose. J Dairy Sci 82: 2558-63

DYVIK, K., GRAFFNER, C. (1992) Investigation of the applicability of a tensile testing machine for measuring mucoadhesive strength. Acta Pharm Nord 4: 79-84

FORD, J. L., TIMMINS, P. (1989) Instrumentation for thermal analysis: In: *Pharmaceutical Thermal Analysis : techniques and applications.* Ellis Horwood, Chichester, pp 9-24

FU, J., FIEGEL, J., KRAULAND, E., HANES, J. (2002) New polymeric carriers for controlled drug delivery following inhalation or injection. Biomaterials 23: 4425-33

FUCHIGAMI, M., TERAMOTO, A., JIBU, Y. (2006) Texture and structure of pressure-shift-frozen agar gel with high visco-elasticity. Food Hydrocolloids 20: 160-169

FURUBAYASHI, T., INOUE, D., KAMAGUCHI, A., HIGASHI, Y., SAKANE, T. (2007) Influence of formulation viscosity on drug absorption following nasal application in rats. Drug Metab Pharmacokinet 22: 206-11

GARCIA, A. A., BONEN, M. R., RAMIREZ-VICK, J., SADAKA, M., VUPPU, A. (1999) Crystallization and precipitation. In: *Bioseparation Process Science*. Blackwell Science, Malden, Mass. ; Abingdon, pp 136

GHIMIRE, M., HODGES, L. A., BAND, J., O'MAHONY, B., MCINNES, F. J., MULLEN, A. B., STEVENS, H. N. (2010) In-vitro and in-vivo erosion profiles of hydroxypropylmethylcellulose (HPMC) matrix tablets. J Control Release 147: 70-5

GHONASGI, D., PEREZ, V., CHAPMAN, W. G. (1995) Prediction of the thermodynamic properties of complex polyatomic hydrogen bonding fluids. Int J Thermophys 6: 715-722

GIL-ALEGRE, M. E., BERNABEU, J. A., CAMACHO, M. A., TORRES-SUAREZ, A. I. (2001) Statistical evaluation for stability studies under stress storage conditions. Farmaco 56: 877-83

GIRON, D. (1998) Contribution of thermal methods and related techniques to the rational development of pharmaceuticals -Part 1. Res Focus 1: 206-211

GLICKSMAN, M. (1987) Utilization of seaweed hydrocolloids in the food industry. Hydrobiologia 151/152: 31-47

GOLDSTEIN, J., NEWBURY, D. E., JOY, D., LYMAN, C., ECHLIN, P., LIFSHIN, E., SAWYER, P., MICHAEL, J. (2003) The SEM and its modes of operation. In: *Scanning Electron Microscopy and X-Ray Microanalysis*. 3rd ed. edn. Plenum Press, New York, pp 24

GOMBAS, A., SZABO-REVESZ, P., KATA, M., REGDON, G., EROS, I. (2002) Quantitative determination of crystallinity of alpha lactose monohydrate by DSC. Journal of Thermal Analysis and Calorimetry 68: 503-510

GREENSPAN, L. (1977) Humidity fixed points of binary saturated aqueous solutions. J Research of the National Bureau of Standard 18A: 89-96

GREIMEL, A., WERLE, M., BERNKOP-SCHNURCH, A. (2007) Oral peptide delivery: in-vitro evaluation of thiolated alginate/poly(acrylic acid) microparticles. J Pharm Pharmacol 59: 1191-8

GUSTAFSSON, C., LENNHOLM, H., IVERSEN, T., NYSTRO¨M, C. (1998) Comparison of solid-state NMR and isothermal microcalorimetry in the assessment of the amorphous component of lactose. Int J Pharm 174: 243-252

HARSHA, S., R, C., RANI, S. (2009) Ofloxacin targeting to lungs by way of microspheres. Int J Pharm 380: 127-32

HASCICEK, C., GONUL, N., ERK, N. (2003) Mucoadhesive microspheres containing gentamicin sulfate for nasal administration: preparation and in vitro characterization. Farmaco 58: 11-6

HINCHCLIFFE, M., ILLUM, L. (1999) Intranasal insulin delivery and therapy. Adv Drug Deliv Rev 35: 199-234

HIRAI, S., YASHIKI, T., MATSUZAWA, T., MIMA, H. (1981) Absorption of drugs from the nasal mucosa of rat. Int J Pharm 7: 317-325

HOU, Q., CHAU, D. Y., PRATOOMSOOT, C., TIGHE, P. J., DUA, H. S., SHAKESHEFF, K. M., ROSE, F. R. (2008) In situ gelling hydrogels incorporating microparticles as drug delivery carriers for regenerative medicine. J Pharm Sci 97: 3972-80

HOUTMEYERS, E., GOSSELINK, R., GAYAN-RAMIREZ, G., DECRAMER, M. (1999) Regulation of mucociliary clearance in health and disease. Eur Respir J 13: 1177-88

HUO, D., DENG, S., LI, L., JI, J. (2005) Studies on the poly(lactic-co-glycolic) acid microspheres of cisplatin for lung-targeting. Int J Pharm 289: 63-7

HUSSAIN, A., FARAJ, J., ARAMAKI, Y., TRUELOVE, J. E. (1985) Hydrolysis of leucine enkephalin in the nasal cavity of the rat--a possible factor in the low bioavailability of nasally administered peptides. Biochem Biophys Res Commun 133: 923-8

HUSSAIN, A., FOSTER, T., HIRAI, S., KASHIHARA, T., BATENHORST, R., JONES, M. (1980) Nasal absorption of propranolol in humans. J Pharm Sci 69: 1240

ILIGER, S. R., DEMAPPA, T., JOSHI, V. G., KARIGAR, A. A., SIKARWAR, M. S. (2010) Formulation and characterization of mucoadhesive microspheres of verapamil hydrochloride in blends of gelatin A /chitosan for nasal delivery. J Pharm Res 3: 2463-2465

ILLUM, L. (2003) Nasal drug delivery--possibilities, problems and solutions. J Control Release 87: 187-98

ILLUM, L., JORGENSEN, H., BISGAARD, H., KROGSGAARD, O., ROSSING, N. (1987) Bioadhesive microspheres as a potential nasal drug delivery system. Int J Pharm 39: 189-199

ITOH, T., SATOH, M., ADACHI, S. (1977) Differential thermal analysis of alpha-lactose hydrate. J Dairy Sci 60: 1230-1235

JADHAV, K. R., GAMBHIRE, M. N., SHAIKH, I. M., KADAM, V. J., PISAL, S. S. (2007) Nasal Drug Delivery System-Factors Affecting and Applications. Cur Drug Therapy 2: 27-38

JAIN, K. K. (2008) Particulate drug delivery systems. In: *Drug Delivery Systems*. Humana ; [London : Springer, distributor], Totowa, N.J., pp 29-31

JONES, D. S., WOOLFSON, A. D., BROWN, A. F. (1997) Textural, viscoelastic and mucoadhesive properties of pharmaceutical gels composed of cellulose polymers. Int J Pharm 151: 223-233

JORGENSEN, L., BECHGAARD, E. (1994) Intranasal permeation of thyrotropin-releasing hormone: in vitro study of permeation and enzymatic degradation. Int J Pharm 107: 231-237

KALINER, M., MAROM, Z., PATOW, C., SHELHAMER, J. (1984) Human respiratory mucus. J Allergy Clin Immunol 73: 318-23

KAMATH, K. R., PARK, K. (1994) Mucosal adhesive preparations. In: *Encyclopedia of Pharmaceutical Technology*. In: Swarbrick, J., Boylan, J. C. (eds). Marcel Dekker, New York, pp 133-163

KAO, H. D., TRABOULSI, A., ITOH, S., DITTERT, L., HUSSAIN, A. (2000) Enhancement of the systemic and CNS specific delivery of L-dopa by the nasal administration of its water soluble prodrugs. Pharm Res 17: 978-84

KATZHENDLER, I., AZOURY, R., FRIEDMAN, M. (1998) Crystalline properties of carbamazepine in sustained release hydrophilic matrix tablets based on hydroxypropyl methylcellulose. J Control Release 54: 69-85

KATZHENDLER, I., KARSTEN, M., FRIEDMAN, M. (2000) Structure and hydration properties of hydroxypropyl methylcellulose matrices containing naproxen and naproxen sodium. Int J Pharm 200: 161-179

KEELER, J., CLOWES, R. T., DAVIS, A. L., LAUE, E. D. (1994) Pulsed-field gradients: theory and practice. Methods Enzymol 239: 145-207

KEELY, S., RULLAY, A., WILSON, C., CARMICHAEL, A., CARRINGTON, S., CORFIELD, A., HADDLETON, D. M., BRAYDEN, D. J. (2005) In vitro and ex vivo intestinal tissue models to measure mucoadhesion of poly (methacrylate) and N-trimethylated chitosan polymers. Pharm Res 22: 38-49

KHAN, M. A. (2009) Stability of repackaged products. In: *Pharmaceutical Stability Testing To Support Global Markets*. In: Huynh-Ba, K. (ed.). Springer, New York, pp 130

KHANDPUR, R. S. (2006) Nuclear magnetic resonance spectrometer. In: *Handbook of Analytical Instruments*. McGRAW-HILL, New Delhi, pp 273

KILICARSLAN, M., BAYKARA, T. (2003) The effect of the drug/polymer ratio on the properties of the verapamil HCl loaded microspheres. Int J Pharm 252: 99-109

KIRK, J. H., DANN, S. E., BLATCHFORD, C. G. (2007) Lactose: a definitive guide to polymorph determination. Int J Pharm 334: 103-14

KRAULAND, A. H., GUGGI, D., BERNKOP-SCHNURCH, A. (2006) Thiolated chitosan microparticles: a vehicle for nasal peptide drug delivery. Int J Pharm 307: 270-7

KREINER, M., PARKER, M. C. (2005) Protein-coated microcrystals for use in organic solvents: application to oxidoreductases. Biotechnol Lett 27: 1571-7

KREINER, M., MOORE, B. D., PARKER, M. C. (2001) Enzyme –coated micro –crystals: a 1-step method for high activity biocatalyst preparation. Chem Commun (Camb) 12: 1096-1097

KREINER, M., FUGLEVAND, G., MOORE, B. D., PARKER, M. C. (2005) DNA-coated microcrystals. Chem Commun (Camb) 21: 2675-6

LAHAYE, M., ROCHAS, C. (1991) Chemical structure and physico-chemical properties of agar. Hydrobiologia 221: 137-148

LAKSMANA, F. L., HARTMAN KOK, P. J. A., FRIJLINK, H. W., VROMANS, H., MAARSCHALK, K.V. (2008) Using the internal stress concept to assess the importance of moisture sorption-induced swelling on the moisture transport through the glassy HPMC films. American Association of Pharmaceutical Scientists 9: 891-898

LANSLEY, A. B., MARTIN, G. P. (2001) Nasal drug delivery. In: *Drug Delivery and Targeting for Pharmacists and Pharmaceutical Scientists.* In: Hillery, A. M., Lloyd, A. W., Swarbrick, J. (eds). Taylor & Francis, London, pp 215-243

LARHRIB, H., MARTIN, G. P., PRIME, D., MARRIOTT, C. (2003) Characterisation and deposition studies of engineered lactose crystals with potential for use as a carrier for aerosolised salbutamol sulfate from dry powder inhalers. Eur J Pharm Sci 19: 211-21

LATTIN, D. L., FIFER, E. K. (2002) Drug affecting cholinergic neurotransmission. In: *Foye's Principles of Medicinal Chemistry.* In: Williams, D. A., Lemke, T. L. (eds). 5th ed. edn. Lippincott Williams & Wilkins, Baltimore, MD, pp 282

LEE, J. W., PARK, J. H., ROBINSON, J. R. (2000) Bioadhesive-based dosage forms: the next generation. J Pharm Sci 89: 850-66

LEITNER, V. M., GUGGI, D., KRAULAND, A. H., BERNKOP-SCHNURCH, A. (2004) Nasal delivery of human growth hormone: in vitro and in vivo evaluation of a thiomer/glutathione microparticulate delivery system. J Control Release 100: 87-95

LERK, C. F., ANDREAE, A. C., DE BOER, A. H., DE HOOG, P., KUSSINDRAGER, K., VAN LEVERINK, J. (1984) Alterations of alpha-lactose during differential scanning calorimetry. J Pharm Sci 73: 856-7

LEVOGUER, C. L., WILLIAMS, D. R. (1997) Moisture sorption properties of foods products and packaging materials studied by dynamic vapor sorption. Food Technol Europe: 28-30

LI, X. S., WANG, J. X., SHEN, Z. G., ZHANG, P. Y., CHEN, J. F., YUN, J. (2007) Preparation of uniform prednisolone microcrystals by a controlled microprecipitation method. Int J Pharm 342: 26-32

LIM, S. T., FORBES, B., BERRY, D. J., MARTIN, G. P., BROWN, M. B. (2002) In vivo evaluation of novel hyaluronan/chitosan microparticulate delivery systems for the nasal delivery of gentamicin in rabbits. Int J Pharm 231: 73-82

LIN, T. Y. D., CHEN, C. W. (2009) Stability study designs. In: *Methods and Applications of Statistics in The Life and Health Sciences.* In: Balakrishnan, N. (ed.). Wiley-Blackwell, Oxford, pp 782

LIU, Q., FASSIHI, R. (2009) Application of a novel symmetrical shape factor to gastroretentive matrices as a measure of swelling synchronization and its impact on drug release kinetics under standard and modified dissolution conditions. J Pharm Pharmacol 61: 861-7

LUESSEN, H. L., LEHR, C. M., RENTEL, C. O., NOACH, A. B. J., DE BOER, A. G., VERHOEF, J. C., JUNGINGER, H. E. (1994) Bio-adhesive polymers for the peroral delivery of peptide drugs. J Control Release 29: 329-338

MACHADO, J. J. B., COUTINHO, J. A., MACEDO, E. A. (2000) Solid–liquid equilibrium of a-lactose in ethanol/water. Fluid Phase Equilibr 173: 121-134

MALVERN, I. (2004) Zeta potential theory Zetasizer nano series user manual. Malvern Instruments Ltd, England, UK

MARTTIN, E., VERHOEF, J. C., SCHIPPER, N. G., MERKUS, F. W. (1998) Nasal mucociliary clearance as a factor in nasal drug delivery. Adv Drug Deliv Rev 29: 13-38

MARUYAMA, S., OOSHIMA, H. (2000) Crystallization behavior of taltirelin polymorphs in a mixture of water and methanol. J Crystal Growth 212: 239-245

MARUYAMA, S., OOSHIMA, H. (2001) Mechanism of the solvent-mediated transformation of taltirelin polymorphs promoted by methanol. Chem Eng J 81: 1-7

MATHISON, S., NAGILLA, R., KOMPELLA, U. B. (1998) Nasal route for direct delivery of solutes to the central nervous system: fact or fiction? J Drug Target 5: 415-41

MCCONVILLE, J. T., ROSS, A. C., CHAMBERS, A. R., SMITH, G., FLORENCE, A. J., STEVENS, H. N. (2004) The effect of wet granulation on the erosion behaviour of an HPMC-lactose tablet, used as a rate-controlling component in a pulsatile drug delivery capsule formulation. Eur J Pharm Biopharm 57: 541-9

MCINNES, F., BAILLIE, A. J., STEVENS, H. N. E. (2001) Quantification of adhesion of lyophilised HPMC formulations using a novel dynamic adhesion test, AAPSPharmSci, 3(S1), s1708

MCINNES, F., THAPA, P., STEVENS, H. N. E., BAILLIE, A. J., WATSON, D. G., NOLAN, A., GIBSON, I. (2000) Nasal absorption of nicotine in sheep from a lyophilised insert formulation, AAPS PharmSci, 2 (4), s2121

MCINNES, F. J., BAILLIE, A. J., STEVENS, H. N. E. (2007a) The use of simple dynamic mucosal models and confocal microscopy for the evaluation of lyophilised nasal formulations. J Pharm Pharmacol 59: 759-767

MCINNES, F. J., O'MAHONY, B., LINDSAY, B., BAND, J., WILSON, C. G., HODGES, L. A., STEVENS, H. N. (2007b) Nasal residence of insulin containing lyophilised nasal insert formulations, using gamma scintigraphy. Eur J Pharm Sci 31: 25-31

MCMAHON, G. (2007) Thermogravimetric analysis. In: *Analytical Instrumentation : A Guide to Laboratory, Portable and Miniaturized Instruments.* 1st ed. edn. J. Wiley, Chichester, pp 163-164

MISHRA, A. K., VACHON, M. G., GUIVARC'H, P.-H., SNOW, R. A., PACE, G. W. (2003) IDD Technology: Oral Delivery of Water-Insoluble Drugs Using Phospholipid-Stabilized Microparticulate IDD Formulations. In: *Modified-Release Drug Delivery Technology*. In: Rathbone, M. J., Hadgraft, J., Roberts, M. S. (eds). Marcel Dekker, New York, pp 154

MOORE, J. W., FLANNER, H. H. (1996) Mathematical comparison of dissolution profiles. Pharm Tech 20: 64-74

MORTAZAVI, A. S., SMART, J. D. (1993) An investigation into the role of water movement and mucus gel dehydration in mucoadhesion. J Control Release 25: 197-203

MURDAN, S., SOMAVARAPU, S., ROSS, A. C., ALPAR, H. O., PARKER, M. C. (2005) Immobilisation of vaccines onto micro-crystals for enhanced thermal stability. Int J Pharm 296: 117-21

MURUGESAN, M., CUNNINGHAM, D., MARTINEZ-ALBERTOS, J. L., VRCELJ, R. M., MOORE, B. D. (2005) Nanoparticle-coated microcrystals. Chem Commun (Camb) 21: 2677-9

NAKAMURA, F., OHTA, R., MACHIDA, Y., NAGAI, T. (1996) In vitro and in vivo nasal mucoadhesion of some water-soluble polymers. Int J Pharm 134: 173-181

NAKAMURA, K., MAITANI, Y., LOWMAN, A. M., TAKAYAMA, K., PEPPAS, N. A., NAGAI, T. (1999) Uptake and release of budesonide from mucoadhesive, pH-sensitive copolymers and their application to nasal delivery. J Control Release 61: 329-35

NOKHODCHI, A., BOLOURTCHIAN, N., DINARVAND, R. (2003) Crystal modification of phenytoin using different solvents and crystallization conditions. Int J Pharm 250: 85-97

NUNES, R. S., SEMMAN, F. S., RIGA, A. T., CAVALHEIRO, T. G. (2009) Thermal behavior of verapamil hydrochloride and its association with excipients. J Therm Anal Calorim 97: 349-353

OFIR, E., OREN, Y., ADIN, A. (2007) Electroflocculation: the effect of zeta-potential on particle size. Desalination 204: 33-38

OHWAKI, T., ANDO, H., KAKIMOTO, F., UESUGI, K., WATANABE, S., MIYAKE, Y., KAYANO, M. (1987) Effects of dose, pH, and osmolarity on nasal absorption of secretin in rats. II: Histological aspects of the nasal mucosa in relation to the absorption variation due to the effects of pH and osmolarity. J Pharm Sci 76: 695-8

OKHAMAFE, A. O., YORK, P. (1985) Interaction phenomena in some aqueous-based tablet coating polymer systems. Pharm Res 2: 19-23

OLDFIELD, R. J. (1994) Polarisation microscopy. In: *Light Microscopy: An Illustrated Guide* M Wolfe, England, pp 119-120

PADALA, N. R., K., P., REDDY BONEPALLY, C. S., B., K., K., S., M., L. N. (2009) Stavudine loaded microcapsules using various cellulose polymers: preparation and in-vitro evaluation. IJPSN 2: 551-556

PARK, H., ROBINSON, J. R. (1987) Mechanisms of mucoadhesion of poly(acrylic acid) hydrogels. Pharm Res 4: 457-64

PATNAIK, P., DEAN, J. A. A. C. H. (2004) Applications of TGA. In: *Dean's Analytical Chemistry Handbook*. 2nd ed. edn. McGraw-Hill Professional ; London : McGraw-Hill, New York, pp 15.6

PECHKOVA, E., NICOLINI, C. (2003) Protein solubility and supersaturation. Nucleation and crystal growth. In: *Proteomics and Nanocrystallography*. Kluwer Academic/Plenum, Dordrecht ; London, pp 22-24

PENNINGTON, A. K., RATCLIFFE, J. H., WILSON, C. G., HARDY, J. G. (1988) The influence of solution viscosity on nasal spray deposition and clearance. Int J Pharm 43: 221-224

PERESWETOFF, L., EDMAN, P. (1995) Infleunce of osmolarity on nasal absorption of insulin from the thermogelling polymer ethyl(hydroxyethyl)cellulose. Int J Pharm 125: 205-213

PILLAY, V., FASSIHI, R. (1998) Evaluation and comparison of dissolution data derived from different modified release dosage forms: an alternative method. J Control Release 55: 45-55

PRIESTLE, J. P., PARIS, C. G. (1996) Nuclear magnetic resonance. In: *Expermimental Techniques and Data Banks*. In: Cohen, N. C. (ed.) Guidebook on Molecular Modeling in Drug Design. Academic, San Diego ; London, pp 150-152

PYGALL, S. R., TIMMINS, P., MELIA, C. D. (2008) Detailed Microscopic Visualisation of Hydration and Swelling in a Rapidly Hydrating Particle Bed Containing a Cellulose Ether. In: Williams, P. A., Phillips, G. O. (eds) Gums and stabilisers for the food industry 14 RCS (Great Britain) pp 40-45

PYGALL, S. R., KUJAWINSKI, S., TIMMINS, P., MELIA, C. D. (2009) Mechanisms of drug release in citrate buffered HPMC matrices. Int J Pharm 370: 110-20

RAJABI-SIAHBOOMI, A. R., BOWTELL, R. W., MANSFIELD, P., DAVIES, M. C., MELIA, C. D. (1996) Structure and behavior in hydrophilic matrix sustained release dosage forms: 4. Studies of water mobility and diffusion coefficients in the gel layer of HPMC tablets using NMR imaging. Pharm Res 13: 376-80

RANADE, V. V., HOLLINGER, M. A. (1996) Microcapsules and microencapsulation. In: Miscellaneous Forms of Drug Delivery: Drug delivery systems. CRC Press, Boca Raton, Fla. ; London, pp 345-348

RASENACK, N., STECKEL, H., MULLER, B. W. (2003) Micronization of anti-inflammatory drugs for pulmonary delivery by a controlled crystallization process. J Pharm Sci 92: 35-44

RAWLINS, D. J. (1992) *Light Microscopy*. Bios Scientific Publishers in association with the Biochemical Society, Oxford, pp v

REED, S. J. B. (2005) Sample preparation. In: *Electron Microprobe Analysis and Scanning Electron Microscopy in Geology*. 2nd ed. edn. Cambridge University Press, Cambridge, pp 156-160

REEKMANS, S. (1998) Novel surfactants and adjuvants for agrochemicals. In: *Chemistry and Technology of Agrochemical Formulations*. In: Knowles, D. A. (ed.). Kluwer Academic, Dordrecht ; London, pp 189

REMUNAN-LOPEZ, C., LORENZO-LAMOSA, M. L., VILA-JATO, J. L., ALONSO, M. J. (1998) Development of new chitosan-cellulose multicore microparticles for controlled drug delivery. Eur J Pharm Biopharm 45: 49-56

REUTZEL-EDENS, S. M., NEWMAN, A. W. (2006) Physical characterisation of hygroscopicity in pharmaceutical solids. In: *Polymorphism In The Pharmaceutical Industry*. In: Hilfiker, R. (ed.). Wiley-VCH, Weinheim, pp 239-240

ROBINSON, J. R., LONGER, M. A., VEILLARD, M. (1987) Bioadhesive polymers for controlled drug delivery. Ann N Y Acad Sci 507: 307-14

ROSS, A. C., PARTRIDGE, J., FLORES, M. V., MOORE, B. D., PARKER, M. C., STEVENS, H. N. E. (2002) Peptide and protein drug delivery using protein coated microcrystals. Symp Comtrol. Rel. Bioact. Mater. Symp Comtrol. Rel. Bioact. Mater. Int Proc. 29th Int, pp 53

ROSS, A. C., PARTRIDGE, J., VOS, J., GANESAN, A., STEVENS, H. N. E., MOORE, B. D., PARKER, M. C. (2004) Engineering the morphology of protein-coated amino acid crystals J Pharm Pharma, pp S45.

ROSS, K. D. (1978) Effects of methanol on physical properties of alpha- and beta-lactose. J Dairy Sci 61: 152--158

ROWE, R. C., SHESKEY, P. J., P.J., W. (2003a) Hypromellose. In: *Handbook of Pharmaceutical Excepients* Pharmaceutical Press and American Pharmaceutical Association, London, pp 326-329

ROWE, R. C., SHESKEY, P. J., P.J., W. (2003b) Lactose, Monohydrate. In: *Handbook of Pharmaceutical Excepients* Pharmaceutical Press and American Pharmaceutical Association, London, pp 364-369

SAHOO, J., MURTHY, P. N., BISWAL, S., MANIK. (2009) Formulation of sustained-release dosage form of verapamil hydrochloride by solid dispersion technique using Eudragit RLPO or Kollidon SR. AAPS PharmSciTech 10: 27-33

SARKAR, M. A. (1992) Drug metabolism in the nasal mucosa. Pharm Res 9: 1-9

SHAH, V. P., ELKINS, J., LAM, S., SKELLY, J. P. (1989) Determination of in vitro drug release from hydrocortisone creams. Int J Pharm 53: 53-59

SHAHIWALA, A., MISRA, A. (2004) Nasal delivery of levonorgestrel for contraception: an experimental study in rats. Fertil Steril 81: 893-8

SHENOY, A. V. (1999) Other relationships for shear viscosity functions. In: *Rheology of Filled Polymer Systems.* Kluwer, Dordrecht ; London, pp 103

SHUKLA, S. K. (1973) Study of Solvent-Solvent Interaction by Paper Chromatography II. Acetone - Water System. Chromatographia 6(11): 463-467

SIEPMANN, J., SIEPMANN, F. (2006) Microparticles Used as Drug Delivery Systems. Prog Colloid Polym Sci 133: 15-21

SIMON, J. P., ERIKSSON, K.-E. L. (1996) The significance of intra-molecular hydrogen bonding in the B-O-4 linkage of lignin. J Mol Str 384: 1-7

SIPAHIGIL, O., DORTUNC, B. (2001) Preparation and in vitro evaluation of verapamil HCl and ibuprofen containing carrageenan beads. Int J Pharm 228: 119-28

SIVADAS, N., O'ROURKE, D., TOBIN, A., BUCKLEY, V., RAMTOOLA, Z., KELLY, J. G., HICKEY, A. J., CRYAN, S. A. (2008) A comparative study of a range of polymeric microspheres as potential carriers for the inhalation of proteins. Int J Pharm 358: 159-67

SMART, J. D., KELLAWAY, I. W., WORTHINGTON, H. E. (1984) An in-vitro investigation of mucosa-adhesive materials for use in controlled drug delivery. J Pharm Pharmacol 36: 295-9

SOUZA, R., MUTALIK, S., VENKATESH, M., VIDYASAGAR, S., UDUPA, N. (2005) Nasal Insulin Gel as an Alternate to Parenteral Insulin: Formulation, Preclinical, and Clinical Studies. AAPS PharmSciTech. 6(2): E184-E189

STRICKLAND, W. A., JR. (1962) Study of water vapor sorption by pharmaceutical powders. J Pharm Sci 51: 310-4

STRIEBEL, H. W., POMMERENING, J., RIEGER, A. (1993) Intranasal fentanyl titration for postoperative pain management in an unselected population. Anaesthesia 48: 753-7

STUART, B. (2004) *Infrared Spectroscopy: Fundamentals and Applications*. Wiley, Chichester, pp 2-18

SURYANARAYANA, C., NORTON, M. G. (1998) X-rays and diffraction. In: *X-Ray Diffraction : A Practical Approach*. Plenum Press, New York ; London, pp 3-18

SUZUKI, Y., MAKINO, Y. (1999) Mucosal drug delivery using cellulose derivatives as a functional polymer. J Control Release 62: 101-7

TAKKA, S., ACARTURK, F. (1999) Calcium alginate microparticles for oral administration: I: Effect of sodium alginate type on drug release and drug entrapment efficiency. J Microencapsul 16: 275-90

TANWAR, Y. S., NARUKA, P. S., OJHA, G. R. (2007) Development and evaluation of floating microspheres of verapamil hydrochloride. Braz J Pharm Sci 43: 529-534

THOMAS, C., AHSAN, F. (2008) Nasal Delivery of Peptide and Non Peptide drugs. In: Gad, S. C. (ed.) Pharmaceutical manufacturing handbook : production and processes. Wiley-Interscience, Hoboken, N.J., pp 591-649

TIWARY, A. K. (2007) Crystal habit changes and dosage form performance. In: *Encyclopedia of Pharmaceutical Technology*. In: Swarbrick, J. (ed.). 3rd edn. Informa Healthcare, New York ; London, pp 820-828

TOS, M. (1983) Distribution of mucus producing elements in the respiratory tract. Differences between upper and lower airway. Eur J Respir Dis Suppl 128 269-79

UGWOKE, M. I., VERBEKE, N., KINGET, R. (2001) The biopharmaceutical aspects of nasal mucoadhesive drug delivery. J Pharm Pharmacol 53: 3-21

UGWOKE, M. I., AGU, R. U., VERBEKE, N., KINGET, R. (2005) Nasal mucoadhesive drug delivery: background, applications, trends and future perspectives. Adv Drug Deliv Rev 57: 1640-65

VAUGHAN, A. S. (1993) Polymer microscopy. In: *Polymer Characterisation*. In: Hunt, B. J., James, M. I. (eds). Blackie Academic & Professional, pp 297-303

VON BONSDORFF-NIKANDER, A., RANTANEN, J., CHRISTIANSEN, L., YLIRUUSI, J. (2003) Optimizing the crystal size and habit of beta-sitosterol in suspension. AAPS PharmSciTech 4: E44

VYAS, T. K., BABBAR, A. K., SHARMA, R. K., SINGH, S., MISRA, A. (2006) Preliminary brain-targeting studies on intranasal mucoadhesive microemulsions of sumatriptan. AAPS PharmSciTech 7: E8

WANNER, A., SALATHE, M., O'RIORDAN, T. G. (1996) Mucociliary clearance in the airways. Am J Respir Crit Care Med 154: 1868-902

WATSON, D. G. (1999) Nuclear magnetic resonance spectroscopy. In: *Pharmaceutical Analysis: A Textbook For Pharmacy Students and Pharmaceutical Chemists*. Churchill Livingstone, Edinburgh, pp 145-155

WEBB, S. D., PAGE, R. C., JAY, M., BUMMER, P. M. (2002) Characterization and validation of the gamma-scintigraphic method for determining liquid holdup in foam. Appl Radiat Isot 57: 243-55

WERMELING, D. P., MILLER, J. L. (2003) Intranasal drug delivery. In: *Modified-Release Drug Delivery Technology*. In: Rathbone, M. J., Hadgraft, J., Roberts, M. S. (eds). M. Dekker, New York, pp 727-748

WEST, A. R. (1984) Optical microscopy. In: *Solid State Chemistry and Its Applications*. Wiley, Chichester [West Sussex] ; New York, pp 60-62

WILLIAMS, H. D., WARD, R., HARDY, I. J., MELIA, C. D. (2009) The extended release properties of HPMC matrices in the presence of dietary sugars. J Control Release 138: 251-9

WISHART, D. (2005) Nuclear magnetic resonance spectroscopy. In: *Methods for Structural Analysis of Protein Pharmaceuticals*. In: Jiskoot, W., Crommelin, D. J. A. (eds). AAPS Press, New York, pp 219-220

YAMASHITA, K., NAKATE, T., OKIMOTO, K., OHIKE, A., TOKUNAGA, Y., IBUKI, R., HIGAKI, K., KIMURA, T. (2003) Establishment of new preparation method for solid dispersion formulation of tacrolimus. Int J Pharm 267: 79-91

YEO, Y., BAEK, N., PARK, K. (2001) Microencapsulation methods for delivery of protein drugs. Biotechnol Bioprocess Eng 6: 213-230

YOKOI, Y., YONEMOCHI, E., TERADA, K. (2005) Effects of sugar ester and hydroxypropyl methylcellulose on the physicochemical stability of amorphous cefditoren pivoxil in aqueous suspension. Int J Pharm 290: 91-9

YOSHIDA, M. I., GOMES, E. C., SOARES, C. D., CUNHA, A. F., OLIVEIRA, M. A. (2010) Thermal analysis applied to verapamil hydrochloride characterization in pharmaceutical formulations. Molecules 15: 2439-52

YUDIN, B. A., KOLESNIKOV, V. N., KORNIENKO, V. P. (1974) Effects of precipitation conditions on the crystal size of silver oxalatenickel oxalate salt mixtures Part I. Powder Metallurgy and Metal Ceramics 7: 531-533

ZAKI, N. M., AWAD, G. A., MORTADA, N. D., ABD ELHADY, S. S. (2006) Rapid-onset intranasal delivery of metoclopramide hydrochloride. Part I. Influence of formulation variables on drug absorption in anesthetized rats. Int J Pharm 327: 89-96

ZHANG, Y., WEI, W., LV, P., WANG, L., MA, G. (2011) Preparation and evaluation of alginate-chitosan microspheres for oral delivery of insulin. Eur J Pharm Biopharm 77: 11-9

ZHOU, G.-D. (1993) Structural chemistry of hydrogen and the hydrogen bond. In: *Fundamentals of structural chemistry*. World Scientific, Singapore ; London, pp 447-449

ZIMMER, A., KREUTER, J. (1995) Microspheres and nanoparticles used in ocular delivery systems. Adv Drug Deli Rev 16: 61-73